Modeling the Thermal Performance of Windows Using a Two-Dimensional Finite Volume Model

by

Pedro Felipe de Abreu

A thesis

presented to the University of Waterloo

in fulfillment of the thesis requirement for the degree of

Doctor of Philosophy

in

Mechanical Engineering

Waterloo, Ontario, 1996

The University of Waterloo requires the signatures of all persons using or photocopying this thesis. Please sign below, and give address and date.

ABSTRACT

The objective of this research is the numerical determination of overall heat transfer coefficients (*U-Factor*), solar heat gain factors (*SHGF*), and surface temperature profiles of windows. The program used takes account of the presence of the natural convection, the radiation between panes, and the thermal effects of the frame. Temperature profiles are useful for the calculation of thermal stresses in glazings and the prediction of condensation problems.

Results are compared with measurements and the numerical calculations of others. In benchmark solution comparisons errors, are less than 10^{-2} %. Comparisons with the numerically determined heat flux through a cavity bounded by two sheets of glass and spacer bars, i.e., a simple window, differed by less than 1 %. In a comparison between simulated solar heat gain factors and solar calorimeter experimental results very good agreement is obtained for nine samples, with errors of 2.5% or less for seven samples, and errors of 12% and 5% for the other two.

From the simulation of more realistic windows, both geometrically and with respect to boundary conditions, this work yielded the following observations: In modeling an entire wood frame window the error in *U-factor* is 0.38% while the maximum surface temperature difference is less than 0.5%; A quantitative comparison with a set of thermographic measurements for a flush mounted insulated glazing unit (IGU) yielded satisfactory results for clear double glazed units with the center glass temperature differing by about 1°C, and very good agreement for the triple glazed units and the double low-E unit with the center glass temperature differing by less than 0.25°C; And, the effects of heat transfer coefficients in flush and recessed mounted IGU's clearly reveal the importance of modeling a locally varying heat transfer coefficient.

ACKNOWLEDGEMENTS

I wish to express my sincere gratitude to my supervisors. Professors H.F. Sullivan and R.A. Fraser whose advise and guidance have greatly benefited me in the course of this study.

Especial thanks is offered to Dr. J.L. Wright for the helpful discussions and suggestions in the course of this work.

Also, I wish to thank my friends for they help and support: Antônio Carlos and Marli de Souza, Sebastião and Lilian Gobbi, Marcelo and Beatriz Bessa, Otto and Luciah Rotunno, Jessé and Cristiane Thé, Augusto and Maria Alice Jacques, Cecílio and Giselle Pimentel and Fernando Sasse.

My deepest appreciation is extended to my mother Nagibe and my mother-in-law Wilma. Their support and encouragement was, and remains, invaluable. The memory of my father Ademi have inspired and encouraged me in my studies.

I also wish to thank my brothers and sisters, especially my sisters Vânia and Rosane, for their support.

The financial support of the Conselho Nacional de Desenvolvimento Científico e Tecnológico of Brazil and the Natural Sciences and Engineering Research Council of Canada is gratefully acknowledged.

DEDICATION

To my wife Aline and my children, Cláudia, Marina and Júlia. I am forever indebted for their understanding and who deserve much more attention than I could devote to them while working on this thesis.

For the greater that would be your idealism or pragmatism and,

your desire, will, commitment, perfection, ...

to accomplish your goal, never let them destroy your family,

yourself, ...

anybody's life.

TABLE OF CONTENTS

LIST OF FIGURES

LIST OF TABLES

NOMENCLATURE

A_c	center-glass area, m^2
A_e	edge-glass area, m^2
A_f	frame area, m^2
A	aspect ratio h/l or area
$[A]$	coefficient matrix
AAMA	American Architectural Manufacturers Association
AGSL	Advanced Glazing System Laboratory
ASHRAE	American Society of Heating, Refrigerating and Air Conditioning
ASTM	American Society for Testing and Materials
BJ2ST	2-D computer program for the analysis of heat loss through window frames
CDS	central differencing scheme
c_p	specific heat at constant pressure, kJ/(kg°C)
CSA	Canadian Standards Association
CV	control volume
DSA	reference glazing with 3 mm double-strength sheet glass
EDS	exponential differencing scheme
E_{jk}	especular exchange factor from j^{th} surface to k^{th} surface
ER	annual energy rating
F_{jk}	radiative view factor from j^{th} surface to k^{th} surface
$F(...)$	dimensionless ratio of the solar heat gain to the incident solar radiation.
FRAME	2-D computer program for the analysis of heat loss through window frames
g	acceleration due to gravity, m/s^2
Gr	Grashof number $Gr_l = \frac{g\beta l^3 \Delta T}{\nu^2}$.
h	cavity height, m

h_c	convective heat transfer coefficient, m^2K/W
h_r	radiative heat transfer coefficient, m^2K/W
HEAT2	2-D computer program for the analysis of heat loss through window frames
HVAC	heating ventilating and air conditioning
IGU	insulated glazing unit
IR	infrared
ISO	International Standardization Organization
J	fluxes (mass, heat)
J_j	radiosity at j^{th} surface
k	thermal conductivity, W/(mK)
KOBRU86	2-D computer program for the analysis of heat loss through window frames
l	cavity width, m
l_c	height of a single secondary cell, m
l_{cn}	new height of a single secondary cell, m
l_t	height of the tertiary cell, m
LBL	Lawrence Berkeley Laboratory
low-E	low emissivity
LTP	linear temperature profile
$\dot{m}$	mass flux
$\vec{n}$	outward normal vector
n_c	number of secondary cells
n_t	number of tertiary cells
n_{ts}	number of times that secondary cells are generated
n_{tt}	number of times that tertiary cells are generated
n	number of times that secondary cells and tertiary cells are generated: $n=n_{ts}+n_{tt}$
NFRC	National Fenestration Rating Council
NRC	National Research Council Canada

Nu	Nusselt Number, $Nu = \frac{h_c l}{k}$
$Nu(...)$	local Nusselt Number
P	control volume node
p	pressure, Pascal
p_k	kinematic pressure, Pascal
PC	personal computer
Pr	Prandtl number, $Pr=\nu/\alpha$
q	irradiance, W/m^2
q_{sg}	solar heat gain, W/m^2
q_{hl}	heat loss, W/m^2
Q_{net}	total heat gain or loss, W
R	thermal resistance, m^{2}K/W
	R-n, n m^{2}K/W of thermal resistance
Ra	Rayleigh number
Ra_l	Rayleigh number based on width l, $Ra_l = \frac{g\beta l^3 \Delta T}{\alpha\nu}$
Ra_c	critical Rayleigh number
$\dot{S}$	volumetric source term
SC	shading coefficient
SGU	sealed glazing units
$SHGF$	solar heat gain factor
t	time, s
T	temperature, °C or K
$\overline{T}$	reference temperature, °C or K
T_c	temperature in the cold wall, °C
T_h	temperature in the hot wall, °C
u	horizontal velocity component, m/s
$\hat{u}$	horizontal velocity component, m/s
u_c	horizontal velocity component of secondary cell, m/s

u_{max}	maximum velocity of the base flow, m/s
u_t	horizontal velocity component of tertiary cell, m/s
U, U-factor	heat transfer coefficient, W/(m^{2}K)
U_o	overall heat transfer coefficient, W/(m^{2}K)
UDS	upwind differencig scheme
US	United States
UV	ultraviolet
v	vertical velocity component, m/s
$\hat{v}$	vertical velocity component, m/s
v_c	vertical velocity component of secondary cell, m/s
v_t	vertical velocity component of tertiary cell, m/s
VISION	1-D computer program for the analysis of heat loss through centre glass
x	horizontal cartesian coordinate
y	vertical cartesian coordinate
ZHF	zero heat flux
WINDOW	1-D computer program for the analysis of heat loss through centre glass
W_{tw}	total window width, m
2-D	two dimensional
3-D	three dimensional

Greek Sybols

α	thermal diffusivity, m^2/s
αr	hemispheric absortivity
α_c	secondary cell wavenumber
β	coefficient of thermal expansion, K^{-1}
Γ	diffusion coefficient

ΔT	temperature difference, °C
Δx	distance between two nodal points in x direction, m
Δy	distance between two nodal points in y direction, m
ε	hemispheric emissivity
μ	dynamic viscosity, kg/(m·s)
ν	kinematic viscosity, m^2/s
Φ	general variable, it may represent any conserved quantity
ρ	density, kg/m^3
ρr	hemispheric reflectivity
σ	Stefan-Boltzman constant, 5.729×10^{-8} $W/(m^2K^4)$
τ	hemispheric transmissivity
ψ_c	perturbation stream function

Subscripts

e	edge-glass
eff	effective
E,W,N,S	east, west, north, south, respectively
e,w,n,s	east, west, north, south, respectively
c	centre-glass
f	frame
i	inside
in	indoor
o	outside
out	outdoor
P	nodal point
surf	surface

Superscript

Φ	general variable
l	long wave, thermal radiation
s	short wave, solar radiation
c	convective
D	diffusive

1 INTRODUCTION

The many benefits provided by windows in a building have been recognized and appreciated for hundreds of years. These benefits include daylighting, visual contact with the outdoors, and a potential for ventilation and natural cooling. In addition, proper orientation and sizing can enable windows to positively impact a building's heating and cooling loads and to assist in energy load management. However, windows have traditionally been "energy losers" because of their low thermal resistance relative to the other building envelope elements. In the early 1980's approximately five per cent of total United States (US) energy consumption was attributable to undesired heat gains or heat losses through windows (Sabatiuk, 1983; Selkowitz *et al.*, 1982). Also, in countries with cold winters, low window thermal resistance can cause discomfort for occupants adjacent to large window areas, low allowable humidity levels, and damaging accumulations of condensation, thus increasing the need for windows with high thermal resistance (Wright, 1989).

In the past windows were typically constructed of single or insulating (double) glass and wood or aluminum frames. Calculating heat transfer through the glass and frame was relatively simple, because the heat transfer coefficients, *U-Factors*[1], of these two components were not too different. The window thermal performance was estimated simply by counting

[1] The *U-factor* is defined in Sub-Section 2.1.4.1

the number of glazing panes where each pane of glass in a conventional glazing system provided approximately *R*-1 (1 hr•ft^{2}F/BTU) of thermal resistance (e.g., double glazing was *R*-2). However, evolving window designs (Arasteh and Wolfe, 1989; Wright, 1989; Hutchins, 1995; Lampert, 1995; Platzer and Braun, 1995; Simko *et al.*, 1995; and Smith *et al.*, 1995) are reducing heat transfer, improving solar gain control, and improving thermal and visual comfort conditions in residential and commercial buildings. Spectrally selective low emissivity (low-E) coatings, angular selective coatings, solar control coatings, infrared (IR) transparent glazing, optically switchable glazing, and anti-reflective surface treatments, to reduce radiative heat transfer; low-conductivity gas fills, to reduce conductive heat transfer; and honeycombs, silica aerogels and evacuated enclosures to suppress or avoid convection are being designed into many state-of-the-art window products. Therefore, advanced glazing materials offer a wide range of options for enhancing the optical and thermal performance of windows and the building envelope.

Given these advances, researchers and manufacturers are focusing their attention on reducing heat transfer through window edges. Metal spacers and frames greatly detract from the performance of a low-E, gas filled unit (Arasteh and Wolfe, 1989). Wood frames, which once improved the overall thermal performance of insulated glass, now slightly lower overall performance. To solve these problems new designs and new materials are being studied. For instance, the Lawrence Berkeley Laboratory (LBL) High-R window has achieved a thermal

resistance of *R*-6 to *R*-10 (1.1-1.7 *RSI*) for the center glass heat transfer (Arasteh *et al.*, 1988).

These changes in window design and the vast array of products on the market create a need for accurate and consistent information about all aspects of window heat transfer, and means that a window cannot be judged by its appearance alone anymore (Carpenter, 1991).

According to Ballinger and Lyons (1993),

> *"glazing performance parameters are required to define the exact nature and quality of a glazing system, to provide product selection information for engineers and building designers and to provide descriptive information for use in computer-based thermal performance simulation programs for buildings. The three uses each have their own requirements and levels of accuracy.*
>
> *The development of computer design tools and simulation programs has created the need for more sophisticated glazing performance data to input into such programs. Most of the computer programs developed to date have very crude descriptions for the glazing materials and in today's situation are quite inadequate. The Materials Scientist on the other hand, working from a 'pure physics' base where all materials must be properly and fully defined in physical terms, has developed a wide range of parameters to fully identify every aspect of glazing systems. New products and materials present the scientist with additional and exciting challenges in the field of measurement. The two positions must meet so that engineers and building designers can fully utilize the new technologies to produce energy efficient, comfortable, people-responsive buildings".*

Twenty years ago most engineers used various hand calculation methods based on the so called *steady-state methods* to design for peak-load conditions in a building. The most important design consideration then was to ensure that any HVAC plant could meet the worst design peak load for heating and cooling. These conditions could be satisfactorily designed for using a *U-factor* for the thermal conductance and a Solar Heat Gain Factor[2], *SHGF*, for peak solar gain. Nowadays engineers are interested in the optimization of a building's energy efficiency and thermal performance. Therefore, such approximations alone are no longer adequate. Also, with the development of new window technologies and materials, given the rise of so called *super windows* (Gilmore, 1986), even the determination of these parameters cannot be handled by current calculation procedures. The design of super windows or their elements, such as edge-seals, frames and glazing systems, cannot be done experimentally alone because experiments are quite expensive and time consuming, and the type and accuracy of measurement are limited by experimental capabilities. In addition, the development of measures for energy labeling schemes require that more detailed parameters be determined, e.g., shading coefficient, condensation resistance, solar heat gain. These needs, mentioned above, are leading to the development of new tools, both experimental and numerical, to quantify the heat transfer, to design new elements, and to develop new parameters in addition to the *U-factor* and *SHGF* for fenestration systems.

[2] The *SHGF* is defined in Sub-Section 2.1.4.2

The objective of this research is the numerical determination of the overall heat transfer coefficient (*U-Factor*) and the solar heat gain factor (*SHGF*) to evaluate the thermal performance, and surface temperature profiles to assist in the prediction of condensation on windows. The program takes account of the presence of the natural convection, the radiation between panes and, the thermal effects of the frame. The in-house developed numerical model, a non-orthogonal finite-volume code, provides information regarding energy flows within the window and temperature distributions in individual glazings and frame. The latter is useful for the calculation of thermal stresses in glazings and the prediction of condensation problems. The results are compared with measurements and numerical calculations of others (ElSherbiny *et al.*, 1982a; Lee and Korpela, 1983; Shewen, 1986; Wright, 1989; Curcija, 1992; ASHRAE, 1993; Fraser *et al.*, 1993; Harrison and Wonderen, 1994; AGSL, 1995; and Enermodal, 1995). Also, the code used is designed to run on a PC or compatible platform to permit portability and access by the research community and window manufacturers.

At present there is no computer program capable of providing data for the thermal analysis of a whole window (glazing systems and frames) with two or more panes in the presence of radiation (solar and thermal) with either the generation of secondary cells near the critical Rayleigh number, or with deflected glazings, or bar grills. Also, the code is used to investigate the existence of tertiary cells in windows which is an improvement in the analysis of natural convection in tall cavities. Therefore, the code provides a unique instrument for the thermal analysis and design of new windows.

Instead of modifying an existing commercial code in order to provide all the features above, an in-house code is developed because most commercial codes:

- were too expensive (considering the economic resources available),
- are a "black box", that for some problem could only be modified by the software house, and regardless, would not be easy to modify, while the learning curve to the modifications would be steep,
- do not run on a PC platform, and
- the author is most familiar with a control volume formulation.

Also, the code development is part of an effort by the University of Waterloo Advanced Glazing System Laboratory to expand its capabilities to analyze aspects of the window problem systematically and, at the same time, solve a whole fenestration system, with the features aforementioned. By working systematically the Laboratory can see how to improve the solution of the entire problem and understand better fenestration system physical phenomena. Moreover, an in-house code provides continuity to ongoing research.

This work is divided into seven parts: Chapter 2 presents the background information on window heat transfer together with a review of natural convection in a vertical cavity; in Chapter 3 the problem formulation is laid out; Chapter 4 describes the 2-D computational model employed for thermal analysis of windows; Chapter 5 shows the procedures carried out to validate the code; Chapter 6 presents comparisons between simulations and experiments as

well as additional simulations of selected problems of interest, e.g., deflected windows, and Chapter 7 outlines the conclusions, the contributions, and gives suggestions for future work.

2 LITERATURE REVIEW AND BACKGROUND

The primary objective of this chapter is to present a literature review and some basic information on the physics of the heat transfer in windows. The contents of this chapter complement several well known and excellent reviews that have appeared in the literature concerning *U-Factor* calculation procedures (McCabe and Goss, 1987) and natural convection in enclosures (Ostrach, 1972; Catton, 1978; Raithby and Hollands, 1985; Yang, 1986; Yang, 1987; Ostrach, 1988; Wright and Sullivan, 1989a; Fusegi and Hyun, 1994). Especially note worthy is the work of Wright and Sullivan (1989a) that presents a review in natural convection in sealed glazing units (SGU).

This chapter is organized into 3 sections as follows: in Section 2.1, the parameters that are used to evaluate thermal performance are defined and a review of the thermal performance of windows is presented; in Section 2.2, a review of the mechanisms of heat transfer with emphasis on natural convection in enclosures is given. It describes, in particular, a tall vertical cavity with its various flow regimes, instabilities of the flow, and details concerning effective modeling; Section 2.3 provides a summary.

2.1 Thermal Performance

In the following sections a overview and basic definitions of the parameters used in Canada and United States to calculate heat transfer performance are given. Section 2.1.1 gives a bit of window history; Section 2.1.2 describes the window components; Section 2.1.3 outlines the factors that affect windows performance, Section 2.1.4, lays out calculation procedures for the overall coefficient of heat transfer, the shading coefficient, the solar heat gain factor and the net energy gain or loss. Also presented are the design conditions used by the American Society of Heating, Refrigerating and Air Conditioning (ASHRAE, 1993) to simulate windows thermally.

2.1.1 A Little History of Window

According to Rousseau (1988) based on the book of Schmidt (1976):

"Windows are just about as old as civilization itself. The Assyrians several centuries before Christ had long, narrow windows divided by little columns. The Egyptians depicted windows in their early wall paintings, and there are windows in the temple built by Pharaohs Seti I and Ramses II at Karnak. In just about every case, the windows were only openings in walls, covered occasionally with hides, drapes, or matting. Not until the height of Roman architecture did windows actually start looking like windows. Ordinarily, the Romans glazed their windows with sheets of mica, panels of seashell, even thin sheets of translucent marble. By the tenth century, there was fairly high production of window glass in northern Europe, probably encouraged by the dictates of the climate."

2.1.2 Components of a Window

The basic parts of a windows are the lights, the glazing, the sash, the frame, the sealants and the weatherstrippings, and the hardware (Figure 2.1). The lights are the transparent portion of the window, made of glass or plastic. The glazing is the assembly of multiple lights and their connections. The sash holds the glazing and is the operable portion of the window. The frame holds the sash and is mechanically connected to the wall or the roof. The weatherstrippings and sealants ensure some tightness against air, rain, snow, vapor flow and sound transmission at the interface between materials, while the hardware ensures the operation and locking of the sash.

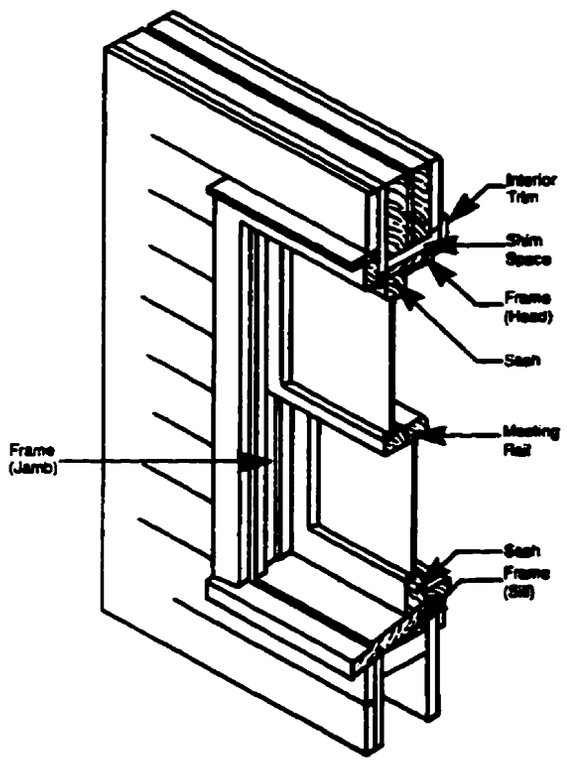

Figure 2.1: Components of a Window[1] .

[1] taken from NRC, 1988 "Window Performance and New Technology," in Proceedings of Building Science Insight '88, National Research Council Canada.

A double-glazed window is typically constructed as shown in Figure 2.2. Windows with more than two glazing layers are constructed similarly. Glazing layers are separated by a spacer (usually metallic) and then sealed (i.e., SGU) to form an insulated glass unit. The SGU is then sealed inside a wood, aluminum, vinyl, or fiberglass frame.

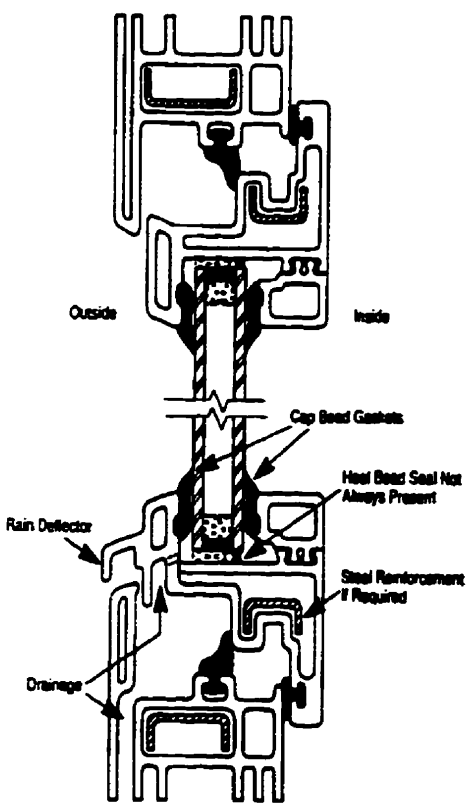

Vertical cross-section of PVC window

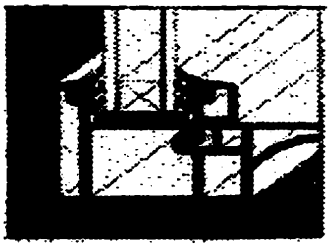

Aluminum (thermally broken)

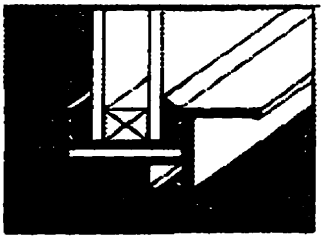

Vinyl (PVC)

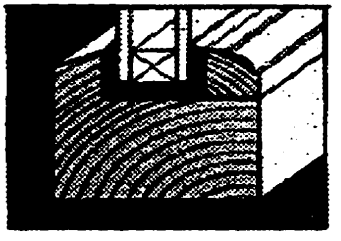

Wood

Frame Sections

Figure 2.2: Double Glazed Window[2].

[2] taken from information brochure distributed by AEC - Aluminum Extruders Council, and NRC, "Window Performance and New Technology," in Proceedings of Building Science Insight '88, National Research Council Canada, 1988.

2.1.3 Window Performance Factors

Window performance parameters are required to define the exact nature and quality of a glazing system, to provide product selection information for engineers, building designers and consumers, and to provide descriptive information for use in computer-based thermal performance simulation programs (Ballinger and Lyons, 1993).

Three important aspects of the window performance are the physical characteristics of the window as an assembly of building (the physical interface with the enclosure which it becomes part of), the effect of the windows on the quality of the indoor space and the comfort of the occupants (Rousseau, 1988 and, Brown and Ruberg, 1988), i.e.,

- windows as energy filters for the space:
  - light transmission and access view;
  - thermal performance;
  - sound transmission;
- windows as part of the building envelope:
  - structural strength;
  - fire performance;
  - airtightness and water penetration;
- windows as building component:
  - operation and natural ventilation strategies;
  - security;
  - long term durability;

Performance levels may be set by standards, or, if standards do not exist, they are implicitly decided by the building designer or specifier. Thermal performance and sound transmittance are examples of issues not covered by standards.

The choice of windows for a building depends on the owner's or occupant's requirements, the architect's vision of the facade and form of the building, and the environmental demands to be met by the building envelope. A formidable array of issues, including those mandated by building codes, must be addressed when selecting windows.

This thesis is concerned only with those requirements linked to thermal performance, that, after light and view, is the most commonly used performance criteria (Brown and Ruberg, 1988). It involves both heat transmission through the window and surface temperature of the window. Heat transmission includes either, heat loss from a heated interior to the colder exterior and heat gain by solar radiation or heat gain from outside to the inside during sunny and warm days which increases inside temperature (or air conditioning costs, if applicable). Surface temperature performance relates to moisture condensation and its effect on the durability of the system. Both aspects of thermal performance can have an impact on the thermal comfort of the space.

2.1.4 Heat Transmission

Heat is transferred from high temperature areas to low temperature areas by conduction, convection, and radiation. All three mechanisms of heat transfer are important to the thermal performance of windows. The basic definition of the common parameters used to evaluate thermal performance are presented in the next paragraphs.

2.1.4.1 Overall Heat Transfer Coefficient (*U-Factor*), *Uo*

Thermal transmittance or *U-factor* is normally used to rate the heat transmission of windows. The amount of heat transferred through a window is directly proportional to the *U-factor* of the window. Overall thermal resistance, the reciprocal of *U-factor*, is the arithmetic sum of the thermal resistance of the window, both glazing and frame, plus the surface resistance on the inside and outside of the window.

In the absence of sunlight, air infiltration, and moisture condensation, the rate of heat transfer through a window system is proportional to the indoor/outdoor (dry bulb) air temperature difference, as given by Equation 2.1.

$$q_{hl} = U_o \bullet (T_{in} - T_{out}) \qquad (2.1)$$

where,

q_{hl} is the indoor to outdoor heat flux (or heat loss), and T_{in}, T_{out} are the indoor and outdoor air temperatures, respectively.

In the center of a sealed glazing unit a one-dimensional analysis accurately quantifies the heat transfer. However, since a spacer's conductivity is generally much higher than the effective conductivity of the air space it bridges, the spacer acts as a thermal bridge between the edge areas of the glazing layers it separates. Consequently, two-dimensional heat transfer in these areas must be considered. The edge area is defined to be that area of the glass within 63.5 mm of the window's sight line (ASHRAE, 1993; Peterson, 1987).

The total heat flux through a fenestration system can be calculated by knowing separately the heat transfer contributions from the center glass, edge-glass and frame. The overall *U-Factor*, U_o, is estimated by weighting the center glass, edge-glass, and frame *U-Factors* according to their corresponding areas (Peterson, 1987).

$$U_o = \frac{(U_c A_c + U_e A_e + U_f A_f)}{(A_c + A_e + A_f)} \tag{2.2}$$

U-Factors for a variety of windows designs, are given in table 5 of chapter 27 of the ASHRAE Fundamentals Handbook (ASHRAE, 1993).

The areas for the purpose of calculating heat loss are: 1) the edge-glass area, *Ae*, consisting of a band of glazing area that is less than 65 mm from the sight line; 2) the center glass area, *Ac*, which is the remaining visible area of the glazing system; and 3) the frame area, *Af*, which is defined as the projected area of a band of width, *Wtw*, lying outside the sight

line. The value of *Wtw* is a function of frame type and material. Details can be found in Figure 2.3.

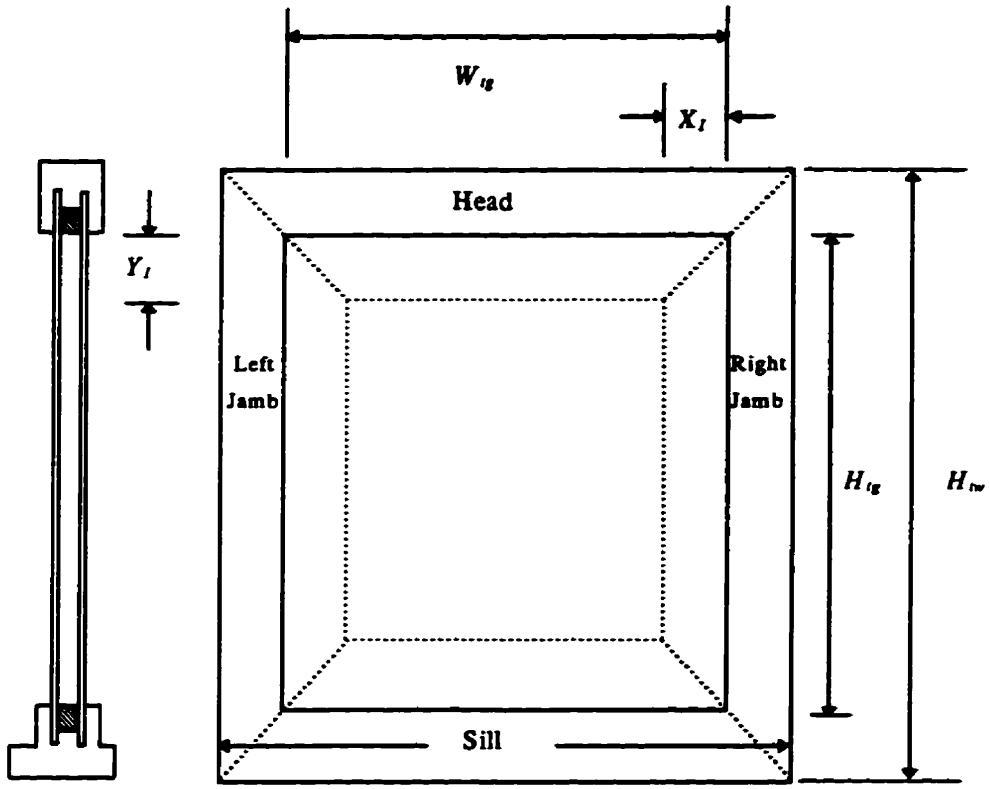

$A_f=H_{tw}W_{tw}-H_{tg}W_{tg}$ $A_e=2X_1H_{tg}+2Y_1W_{tg}-4X_1Y_1$ $A_c=(W_{tg}-2X_1)x(H_{tg}-2Y_1)$

Figure 2.3: Typical Window Areas for U_o Calculation.

2.1.4.2 Shading Coefficient and Solar Heat Gain Factors

The shading coefficient (*SC*) is the ratio of incident solar radiation that ends up inside a building, under a specific set of conditions, to the solar heat gain through a single reference

glass under the same conditions. This quantity includes solar radiation that is directly transmitted through the glazing, plus the amount that is absorbed by the window and is redirected into the building (ASHRAE, 1993). The reference glazing is 3 mm double-strength sheet glass (*DSA*). Denoting the ratio of solar heat gain to total incident solar radiation by *F*, the *SC* is given by

$$SC = \frac{F(glazing\ system)}{F(DSA)} \tag{2.3}$$

where *F(...)* = dimensionless ratio of the solar heat gain to the incident solar radiation[3].

Values of solar heat gain for the reference glazing are called solar heat gain factor (*SHGF*) and they are tabulated in the ASHRAE Fundamentals Handbook (ASHRAE, 1993). For a given orientation and existing conditions (a particular location, time, etc.) the solar heat gain for any glazing system, q_{sg}, will be

$$q_{sg} = SC \bullet SHGF \tag{2.4}$$

Windows, as a transparent part of the building envelope, act as "energy filters". By changing the characteristics of the glazing, or the transparent portion of a window, energy can be selectively transmitted or reflected.

[3] For the standard summer condition, the value of *F* for the reference glazing, *F(DSA)*, is 0.87.

Figure 2.4 illustrates the "spectrum" of energy, i.e., energy as a function of the wavelengths, emitted by the sun and transmitted by several glass types (Brown and Ruberg, 1988). The ultraviolet (UV) wavelengths are shorter than the visible radiation wavelength range (400 to 760 nm). The visible radiation wavelength range coincides with the sun's peak power wavelengths, and the thermal radiation has longer wavelengths.

Most of the solar radiation, or short wavelength energy, falling on surface of clear glass is transmitted. The rest is absorbed and reflected. The transmitted energy provide heat to a room and light. Also, this property permit us to see through it. The choice of glazing can affect both the amount of natural light and its color. The thermal performance of windows and the comfort of building occupants can be improved by properly specifying the wavelengths that the glazing should reflect, transmit and absorb.

About 3% of the solar spectrum is UV and half is near infrared (short-wave). Clear glass transmits 80% to 90% of this radiation. It must be selectively absorbed or reflected if solar heat gain and UV is to be reduced. Clear glass absorbs about 80% to 90% of the far infrared (long-wave) radiation emitted by the bodies at terrestrial temperatures, but re-emits the heat at the same rate.

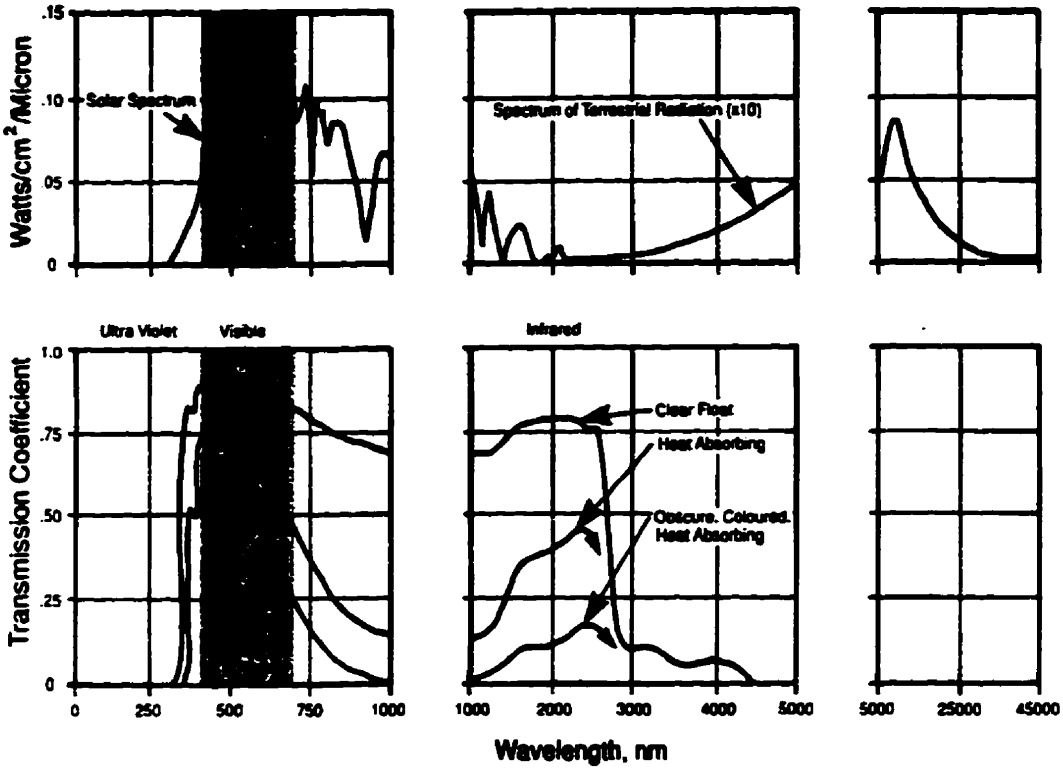

Figure 2.4: Solar Radiation and Spectral Transmittance for Typical Architectural Glass[4].

2.1.4.3 Total Heat Gain or Loss

The total heat gain experienced by a window, Q_A, is the solar gain (see Equation 2.4) less losses (using the total window *U-factor* in Equation 2.2).

$$Q_A = SC \bullet SHGF - U_o \bullet (T_{in} - T_{out}) \qquad (2.5)$$

[4] NRC, 1988. "Window Performance and New Technology", in Proceedings of Building Science Insight '88, National Research Council Canada.

2.1.4.4 Design Conditions

The ASHRAE Fundamentals Handbook (1993) standard summer and winter design conditions, which represent extreme cases and are used for the window simulations, are listed in Table 2.1.

	Indoor Temperature (°C)	Outdoor Temperature (°C)	Wind Speed (m/sec)	Solar Radiation (W/m^2)
Summer	24.0	32.0	3.3	783.3
Winter	21.0	-18.0	6.7	0.0

Table 2.1: ASHRAE Design Conditions (ASHRAE, 1993)

2.1.5 Procedures to Calculate the Heat Transfer in Windows

Due to the necessity of comparing windows against each other and evaluating their overall impact in buildings (Arasteh and Reilly, 1989), an accurate and unbiased analytical procedure to calculate window heat transfer performance indices is required.

The heat loss characteristic of the window is represented by its *U-Factor* (which is the inverse of the *R-value* commonly used for insulation). According to McCabe (1989) the earliest known research on window thermal transmission coefficients, *or U-Factors*, is

attributed to E. Peclet a French experimenter who measured thermal conductivity for a wide range of materials including glass. About 1860 Peclet proposed that the *U-Factor* of multiple-glazed windows could be determined by simply multiplying the single-glazed *U-Factor* by the factor 2/(1+n), where n is the number of glazing layers. This gives reasonable results for units with small (3 to 4 mm) air spaces, but is inaccurate otherwise.

In 1947, Parmalee (1947) published an exhaustive compilation of window heat transfer data extending back 40 years. That work described the guarded hot box, calibrated hot box, and hot plate measurement techniques, and commented on their potential sources of error. According to Wright (1989)

> *"a calculation procedure was developed but was hindered by a lack of knowledge about natural convection and/or forced convection at the exposed window surfaces and natural convection in the window cavity. Edge effects were neglected. It is interesting to note that the importance of radiant heat exchange with the clear sky was recognized. The emissivity of glass was thought to be 0.937 in contrast to the value of 0.84 that is currently considered valid."*

A report written by McCabe and Goss (1987) presents a review of the current sources of information on calculation procedures for *U-Factors* and describes the state of thermal performance testing methods for fenestration systems. It provides a discussion of the standards followed by hot-box methods in United States, Norway, Sweden, and Belgium. Unlike the standards reviewed by McCabe and Goss the new Belgian Standard (NBN B62-004, 1986) for calculating thermal transmission coefficients (*U-Factors*) for windows includes

the effect of edge-glass heat transfer and is being prepared in support of the draft ISO Standard *U-Factor* Calculations.

In 1993 the Canadian Standard Association approved a standard, "Energy Performance Evaluation of Windows and Sliding Glass Doors", CAN/CSA-A440.2-M 93 (CSA, 1993), describing the procedures to evaluate the thermal performance of windows. This document describes the procedure for determining a window's *U-Factor*, solar heat gain factor (*SHGF*), and annual energy rating (*ER*)[5].

The window *U-Factor* can be determined by either National Research Council (NRC) testing or by computer simulation (Carpenter, 1991). The CSA procedure treats these two options as equal based on the results of a joint Canada-US research project which showed very little difference between experimental and computational results. Computer simulation, however, offers the advantages of low cost and shorter turn-around time. In addition computer programs are useful in designing more thermally efficient windows, minimizing condensation, and comparing components (e.g., low-E coatings, spacer assemblies). A window solar heat gain factor (*SHGF*) can also be evaluated by either test or computer simulation. This quantity includes solar radiation that is directly transmitted through the glazing plus the amount that is absorbed by the window and is conducted into the building (ASHRAE, 1993).

[5] the *SHGF* is defined in subsection 2.1.4.2 and the *ER* is a combination of *SHGF*, *U-Factor* and air leakage (CSA 1993), i.e., $ER = Q_A$ - *air leakage heat loss*. The Q_A is defined in subsection 2.1.4.3.

There are two hand calculation methods for estimating *U-Factor* that take into account the effects of edge-glass heat transfer. The first method has been adopted in Belgium, France, and England. It proposes a set of edge-seal conductance or "linear" conductance values (McCabe and Goss, 1987; Thomas and Mühlebach, 1987; IEA, 1987) based on measurements and finite-element calculations. The center glass *U-Factor* is applied over the sight area of the glazing system and additional heat loss caused by the edge-seal is calculated as the product of the linear conductance, length of edge-seal, and the temperature difference between the outside air and the interior space of the building. The ISO working group on Thermal Transmission Properties of Windows is considering a similar procedure categorizing edge-seals as being metal or non-metal (IEA, 1987). The second method of *U-Factor* calculation is the ASHRAE procedure (ASHRAE, 1993). This procedure uses prescribed area ratios of frame, edge-glass and center glass with the edge-glass *U-Factor* being determined as a function of the center glass *U-Factor* and seal type.

Others procedures, i.e., *U-Factor* calculation procedures, were documented in Rubin (1982), revised by Arasteh *et al.*(1995), Ferguson and Wright (1984), and revised by Wright (AGSL, 1995). These procedures, as compared to that presented in the ASHRAE Fundamentals (1993), offer added flexibility. They are PC-compatible computer programs, WINDOW (LBL, 1994) and VISION (AGSL, 1995), and have been distributed to the glass and window industries.

The *U-Factor* procedures outlined above give no information about variations in heat flux and cannot provide temperature profiles for individual glazings. They are only useful for estimating the total thermal losses of a window. Characterization of frame heat transfer coefficients is complicated by the variety of frame configurations in existence: operable windows, different materials, and different product sizes. Simple methods for measuring frame heat flux are not generally available. Also, calculations are difficult because of the two and three-dimensional nature of the heat conduction path and because of uncertainties associated with contact resistance at moving joints.

Recently, substantial progress has been made in analyzing edge-glass and frame heat conduction. The quantification of, and the mechanisms governing heat transfer in the edge-seals have been extensively studied by Wright and Sullivan (1989b), Fraser *et al.* (1993) and Wright *et al.* (1994). However, none of the four two dimensional programs in widespread use that are specifically designed for the analysis of heat loss through window frames and edge-glass account for the two dimensional nature of gas convection or radiative heat transfer (BJ2ST , Jonsson, 1985; KOBRU86 , Standaert, 1986; FRAME, Enermodal, 1995; Heat2, Blomberg, 1995). To account for the increased local heat transfer due to convection and radiation these programs use an "effective" thermal conductivity, i.e., they treat the sealed cavity as though it were filled with a solid material that is opaque to thermal radiation. The minimum temperature near the bottom of the indoor glazing will be consistently over predicted as a result of this simplified fill gas model (Wright, 1989).

Although in the last five years more advanced models that incorporate convection and radiation heat transfer have appeared in the literature (Wright, 1989; Curcija, 1992; Smith *et al.*, 1993; Curcija and Goss, 1994; Wright and Sullivan, 1995), they still lack some capabilities in modeling fenestration system heat transfer. The drawbacks of these models are briefly described below:

- Wright and Sullivan's code is only able to model a double pane IGU unit including the effect of secondary cells. To model the whole window it needs to be re-coded. It only accepts constant temperatures as boundary conditions for the two sheets of glass.
- Curcija and Goss on the other hand present a model that permits the numerical calculation of heat transfer for the whole window, but it lacks the capability to model even simple solar radiation, secondary cells (near the critical Rayleigh number), more then two cavities (inside glazing or frame), and solid materials inside the glazing unit.
- Despite a versatile and refined radiation heat transfer model, which can simulate radiation with blocking surfaces, Smith *et al.*'s numerical code, can only model flush mounted windows with orthogonal grids. Also, it does not account for either the effect of secondary cells near the critical Rayleigh number or for solar radiation.

One attempt to model three dimensional heat transfer in windows was made by Curcija and Goss (1995a), but due to computational storage capabilities they could only model one

quarter of the window at a time, thus they needed to make the assumption of a symmetrical vertical center line, and still a coarse grid was needed.

The following statement made by Goss and Curcija (1989) is still valid. They pointed out that there are many available computer programs which might be adapted to model window heat transfer including edge and frame effects. These programs are capable of modeling 2-D or 3-D conduction and convection heat transfer. They require expertise in computational fluid dynamics to do the necessary modifications to model radiation and to apply the boundary conditions. The major drawback of these programs is their lack of flexibility to model convection and radiation together, making these programs unsuitable for modeling and for designing windows. There are some fenestration system configurations that were modeled using commercials codes, but they can only model the types of fenestration systems for which the program was designed, i.e. they seriously lack flexibility

To better understand the heat transfer process and the fluid flow structure in fenestration systems, a review of the mechanisms of heat transfer that occur will be discussed in the next section.

2.2 Heat Transfer Mechanisms in Windows

All three main mechanisms of heat transfer appear in windows, i.e.,

- Convection:
  - between room air and internal window surface;
  - between outside air and external window surface;
  - inside the IGU unit (air space); and
  - inside existing cavities in seals and frame;
- Radiation:
  - between room and surroundings, and the internal window surface;
  - between surroundings, and external window surface;
  - direct and diffuse solar radiation;
  - inside the IGU unit (air space); and
  - inside existing cavities in seals and frame; and,
- Conduction:
  - inside glazing, seals and frame.

Although there exists a great amount of research on convection, radiation, and conduction, there is no work which deals with all the mechanisms together resulting in a tool capable of simulating or designing windows subjected to real conditions. In the next section a literature review of the natural convection in slender vertical cavities is given. Convective heat transfer coefficients, solar heat gain and short-wave radiation are discussed. Surface radiation, long-wave radiation inside cavities and from the surroundings is reviewed. Also, the interaction between natural convection and radiation is presented.

Due to the impact of convection fill gas on the heat transfer in windows, with particular respect to the surface temperature, emphasis in the literature review will be on

natural convection in tall cavities. This review extends the excellent review by Wright and Sullivan (1989)

2.2.1 Natural Convection in a Vertical Slot

Natural convection heat transfer in cavities is closely tied with the fluid mechanics because the rate of the heat transport depends on flow structure. Until now, most of the studies in cavity natural convection dealt with a fixed temperature difference between the side walls while the others boundary conditions have been either a specified zero heat flux (ZHF) or a linear temperature profile (LTP).

In practice, the temperatures of either of the sidewalls is not uniform and all walls can be made either of high or low conducting materials. As pointed out by Wright and Sullivan (1989a), despite a great amount of research in cavities, no single work deals with all the heat transfer mechanisms and boundary conditions that appear in windows and few papers deal with conditions of interest in glazing units, i.e., for air and argon fill gases, a Rayleigh number based on width of $Ra_l<1.2\times10^4$, Prandtl number, $Pr\approx0.71$, and an aspect ratio, $A\geq40$.

While the determination of overall heat transfer rates across such enclosures does not necessarily depend on *a prior* knowledge of the flows, it is still essential that the details of the flow field be obtained. Only then can one gain physical insight into the interactions among the various mechanisms involved in natural convection, such as are important in windows where

the flow must be controlled. Consequently, it is not surprising that much of the emphasis in enclosure natural-convection studies is placed not only on the overall heat transfer rates, but also on the flow field and related phenomena such as stability and transition.

In subsequent subsections the variables that affect fill gas flow and its various flow regimes, instability, and modeling efforts are reviewed.

2.2.1.1 Two-Dimensional Buoyant Enclosure Flow: Analyses

In the past eighty years natural convection in vertical cavities has been under study. Laminar buoyant flows in two-dimensional enclosures are the most studied of all buoyant enclosure flows. Two-dimensionality greatly simplifies the analyses, and yet, most of the physics involved in general buoyant enclosure flows is still retained.

For rectangular enclosures with aspect ratios $A \geq 1$ and differentially heated vertical side walls, Eckert and Carlson (1961) and Elder (1965a) measured the temperature and velocity fields. On the basis of these observations and the early theoretical ideas of Batchelor (1954) refined by Elder (1965a), Gill (1966), Bejan (1979), and Graebel (1981), resulted in the main features of this flow are understood today. Many more solutions, dealing with both insulated and perfectly conducting end walls for the vertical slot problem, have been studied by numerical methods. Earlier studies reviewed by Wright and Sullivan (1989a), and more recent

studies by Chait and Korpela (1989) and by Le Queré (1990) are also available. Window cavity geometry and useful information are depicted in Figure 2.5.

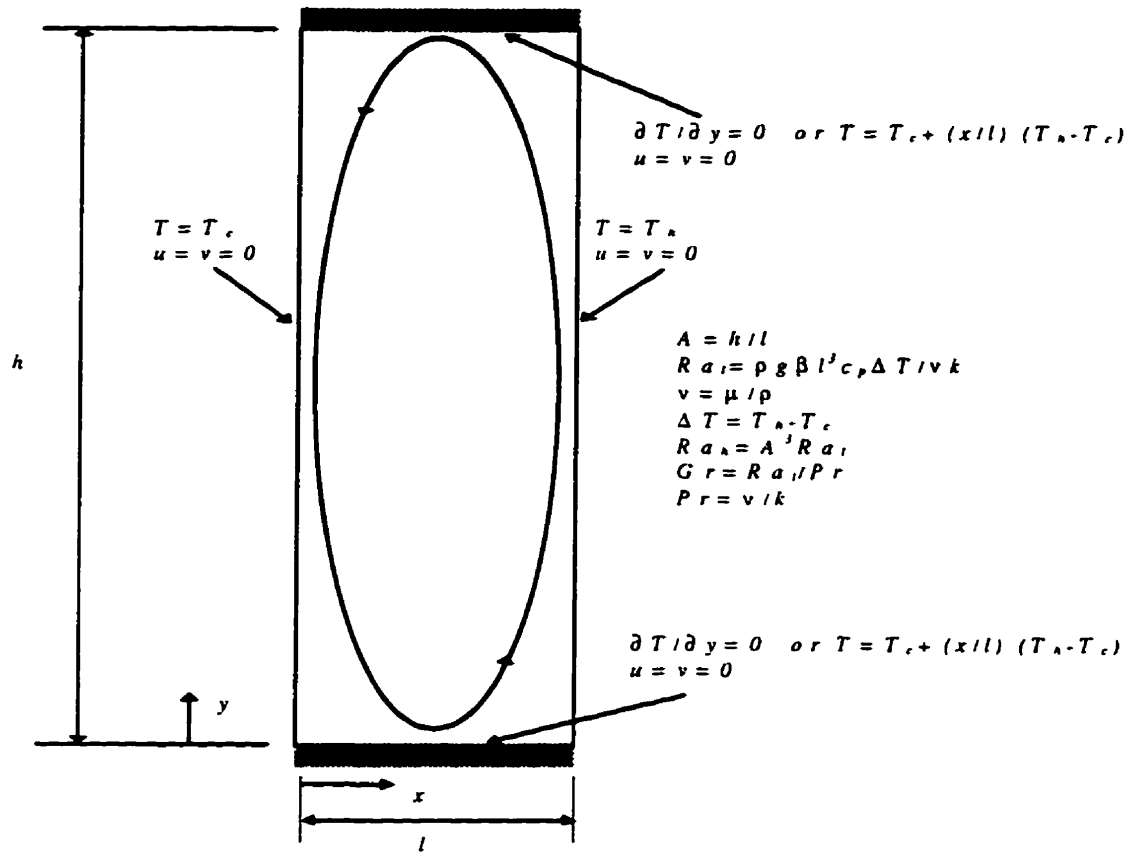

Figure 2.5: Problem Domain for the Analysis of Natural Convection in a Vertical Slot.

If the governing equations for natural convection in a cavity are cast in non-dimensional form, it becomes clear that there are only three parameters that describe the flow. These are the Rayleigh Number, $Ra_l=g\beta\Delta Tl^3/\alpha\nu$ (l, based on width of cavity), the Prandtl Number, $Pr=\nu/\alpha$, and the aspect ratio, $A=h/l$. Batchelor (1954) analyzed laminar natural convection and was the first to define the conduction and boundary layer flow regimes. In

accordance with the classification proposed by Eckert and Carlson (1961), refining Batchelor's work, three flow regimes can be defined with Pr and A held constant:

- **Conduction regime:** if Ra_l is small, the end regions where the flow turns around are of limited extent and a parallel flow exists in the central portion of the slot. In this region the isotherms are parallel to the vertical walls (there is little variation of the fluid temperature with height) and the heat is transferred mainly by conduction from the hot wall to the cold wall.
- **Boundary Layer Regime:** if the Ra_l is large enough it leads to the emergence of boundary layers on the vertical sidewalls and a core in the center. In this regime, heat is transferred primarily by horizontal convection across the ends. The flow in the ends is, however, sufficiently complex that the analysis of the flow in the boundary-layer regime is still incomplete today (Lee and Korpela, 1983; Fant and Jarman, 1991).
- **Transition Regime:** for moderate values of Ra_l, between the conduction and boundary layer regimes, the flow is said to be in the transition regime. A stable vertical temperature gradient develops in the core region of the flow.

There is another distinct flow regime lying between the conduction regime and transition regime for a given aspect ratio. It is characterized by regularly spaced multicellular flow in the core region caused by a hydrodynamic instability, i.e., a steady secondary flow (see Figure 2.6) as reported by several researchers (Elder, 1965a; Vesti and Arpaci, 1969; Korpela,

1974; and Seki *et al.*, 1978a and 1978b) who performed visualization experiments. These secondary cells gain their energy from the shear between the two counter-flowing streams.

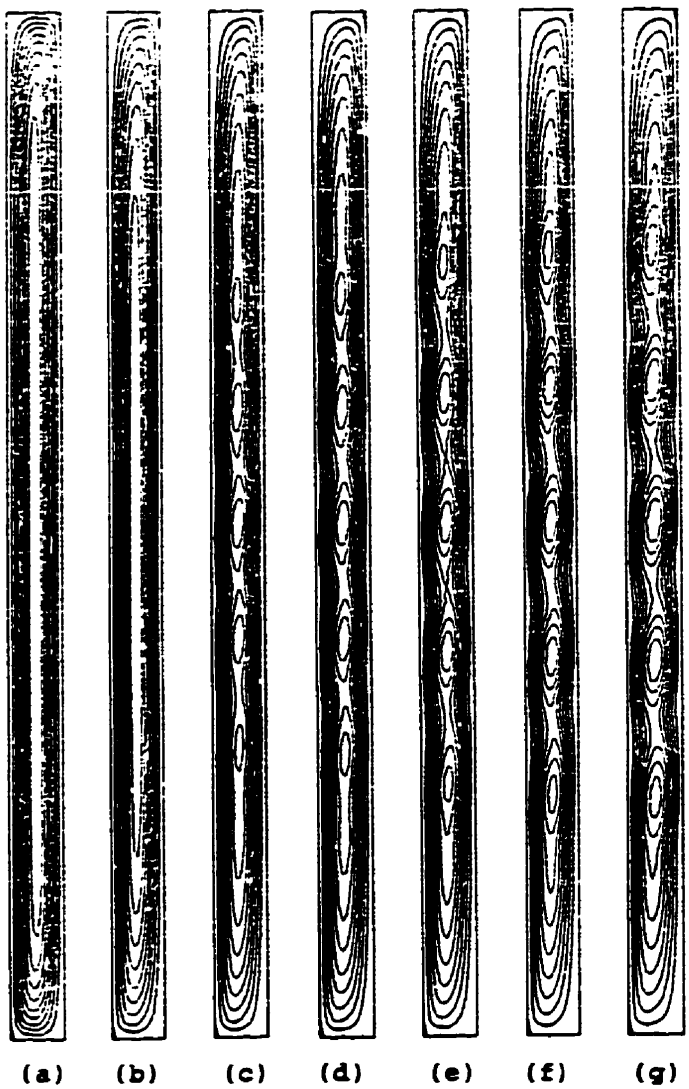

Figure 2.6: Secondary Cells in Air, $A = 20$. a) $Ra = 3.55 \times 10^3$, b) $Ra = 7.10 \times 10^3$, c) $Ra = 7.81 \times 10^3$, d) $Ra = 8.52 \times 10^3$, e) $Ra = 1.07 \times 10^4$, f) $Ra = 1.42 \times 10^4$, g) $Ra = 1.78 \times 10^4$. Based on data from Korpela *et al.* (1982).

This secondary flow consists of regular "cat's eye" pattern of transverse, stationary cells within the core of the base flow – with the flow in each cell rotating in the same direction

as the base flow. These cells do not affect the overall heat transfer much, since most of the energy is transferred in the end regions away from the cells. Figure 2.7 shows the local Nusselt Number (denoted *Nu(y)*) based on the heat flux at the warm vertical wall. In the conduction regime, when Ra_l is sufficiently small (see Ra=3.55x10^3), *Nu(y)*=1 except near the end walls. When *Ra* increases, the rate of heat transfer increases (except in the top of the cavity) and secondary cells appear in the middle portion of the cavity as indicated by the waves in the curves.

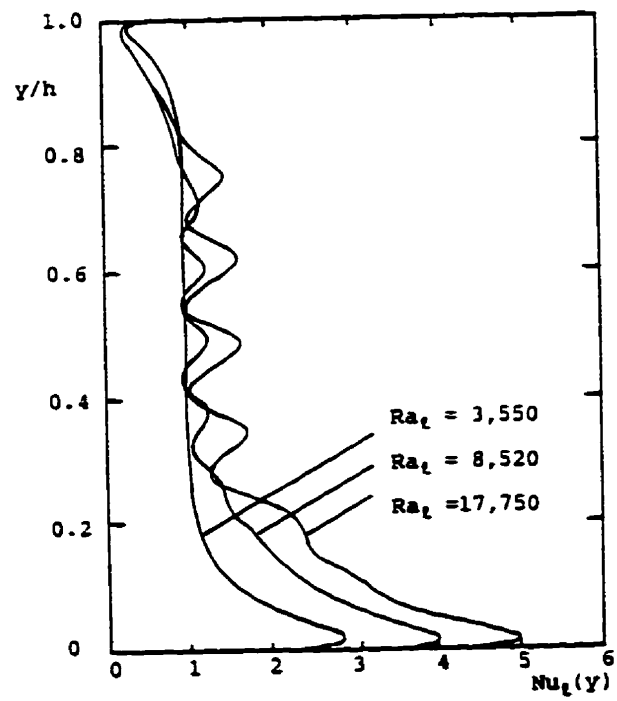

Figure 2.7: Local Nusselt Number[6], *Nu(y)*, for *A*=20, With and Without the Presence of Secondary Cells.

For oil at certain values of *Ra* counter-rotating cells (tertiary cells) were found in the regions between the secondary cells (Elder, 1965a; de Vahl Davis and Mallison, 1975; Seki *et*

[6] Based on Data from Korpela *et al.* (1982).

al., 1978a and b; Chen and Thangam, 1985; Wakitani, 1994). The tertiary cells are not expected for conventional windows in the range of the design conditions and are sketched in Figure 2.8.

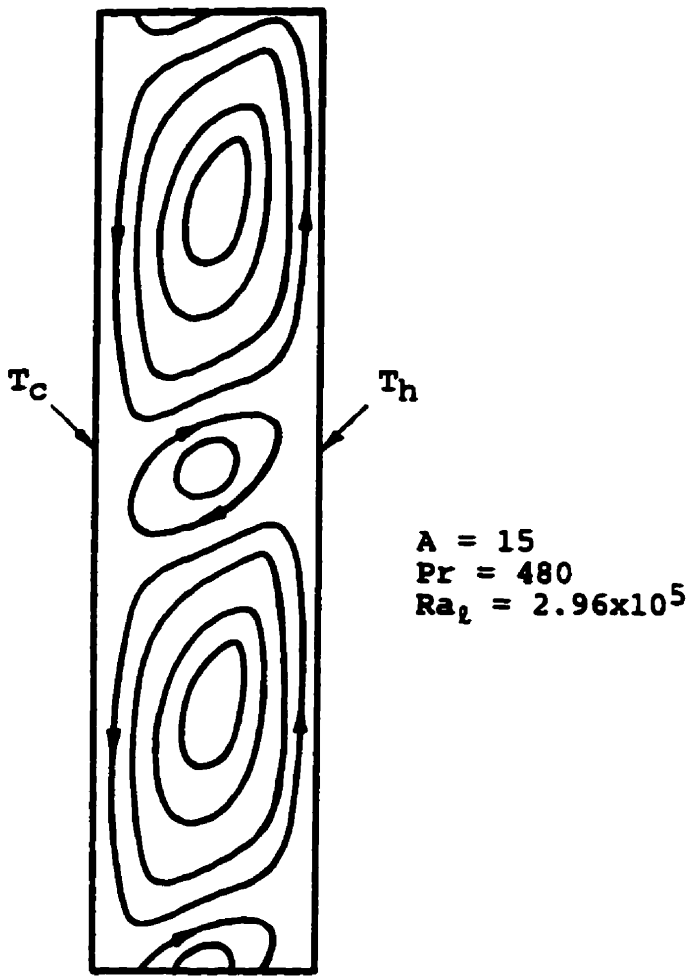

Figure 2.8: Sketch of Secondary and Tertiary Flows[7].

Several authors (Lee and Korpela, 1983; Roux *et al.*, 1979 and 1980; Lauriat, 1980; de Vahl Davis, 1986; Liakopoulos and Blythe, 1990) have shown that the cat's eye regime

[7] base on the work of Seki *et al.* (1978a)

can only be observed in air-filled cavities at aspect ratios larger than a critical value, between 11 and 15. In air, steady cat's eyes appear for small critical values of the Ra_t. These have been observed by many researchers, for instance, Vest and Arpaci (1969). However, as many people have noted, these cat's eyes become unsteady upon increasing Ra_t (Lauriat and Desrayaud, 1985a; Pignatel and Marcillat, 1986; Chikhaoui *et al.*, 1988a). This fact is not explained by linear stability theory for two-dimensional base flows, and has not been observed numerically either, except perhaps by Polezhev *et al.* (Le Queré, 1990) in a very tall cavity.

Furthermore, the existence of a reverse transition from a multicellular to monocellular flow when increasing the value of the Ra_t has been shown by Roux *et al.* (1979 and 1980) and Le Queré (1990) by numerical solutions. This is due to the increasing influence of the stabilizing temperature gradient in the core, which also leads to a boundary layer type flow structure. Experimental evidence is, however, still controversial. Some authors have reported the return to steady monocellular convection (Pignatel and Marcillat, 1986; Chikhaoui *et al.*, 1988a) while others, for instance Lauriat and Desrayaud (1985), never saw such a return and generally report an increasingly chaotic motion.

Lee and Korpela (1983) mention that, in some cases, the number of cells depends on the initial condition which suggests the possible existence of multiple solutions. Le Queré (1990) has shown that the return to the unicellular flow structure is more complex than previously analyzed. The number of cells decreases step by step, and each change in the

number of cells is characterized by hysteresis, which corroborates the findings of Lee and Korpela (1983).

In order to explain the appearance of unsteady cat's eyes, Thangam and Chen (1986) and Lauriat and Desrayaud (1985a), argued that steadiness exists only if the odd-symmetry of the problem is maintained. Any breaking of this odd-symmetry, such as that resulting from variation of the thermophysical properties with temperature, would inevitably result in unsteady perturbations. Others, such as Chikhaoui *et al.* (1988b) have invoked three-dimensional effects. Nagata and Busse (1983), Chait and Korpela (1989), and Le Queré (1990) have showed that two-dimensional secondary flows can became unstable when disturbed.

All these discrepancies between experimental observations, numerical computations, and results from linear and nonlinear stability theory indicate that the understanding of convection in tall cavities is not yet complete (Le Queré, 1990).

The nature of flow in the conduction and boundary layer regimes, with attempts to predict the critical Rayleigh number, Ra_c, at which hydrodynamic instability causes the onset of secondary flow have been studied by Birikh *et al.* (1968), Gill and Davey (1968), Vest and Arpaci (1969), Gill and Kirkhan (1970), Hart (1971), Unny (1972), Korpela *et al.* (1973), Hollands and Konick (1973), Korpela (1974), Clever and Busse (1977), Bergholz (1978), Seki *et al.* (1978a and b) and Choi and Korpela (1980). These predictions (for $Pr \approx 0.71$) fall

in a relatively narrow band, ranging from $Ra_c = 5{,}595$ (Vest and Arpaci, 1969) to $Ra_c = 7{,}827$ (Unny, 1972) for large aspect ratios. Vest and Arpaci (1969) made a visual measurement at $Ra_c = 6{,}177 \pm 618$ for $A = 33$. Hollands and Konick (1973) used a calorimetric method to determine Ra_c and reported $Ra_c = 7{,}860 \pm 363$ for $A = 44$.

From the stability analysis results of Bergholz (1978) it can be stated that in the conduction regime the heat transfer across the slot decreases as the aspect ratio is reduced, and achieves a minimum when multicellular flow first appears. Based on this same work a correlation was determined by Korpela *et al.* (1982) to relate aspect ratio to the critical Rayleigh number Ra_c when such a minimum occurs, and is given by

$$Ra_c = \frac{Pr(1 + \frac{5}{A})}{1.25 \times 10^{-4}} \tag{2.6}$$

When the Rayleigh number becomes sufficiently high, an enclosure flow undergoes transition to turbulent flow. The transition process has been documented experimentally by study of Elder (1965b) for natural convection in vertical enclosures with $10 < A < 30$ and high Pr fluids ($Pr = 1000$).

As pointed out by Wright (1989) for high aspect ratio window cavities the flow moves from the conduction regime directly into the secondary flow or the turbulent regime as Ra

increases. Neither laminar transition nor laminar boundary layer flows are unlikely to exist. Figure 2.9 gives a better understand of this character of the flow.

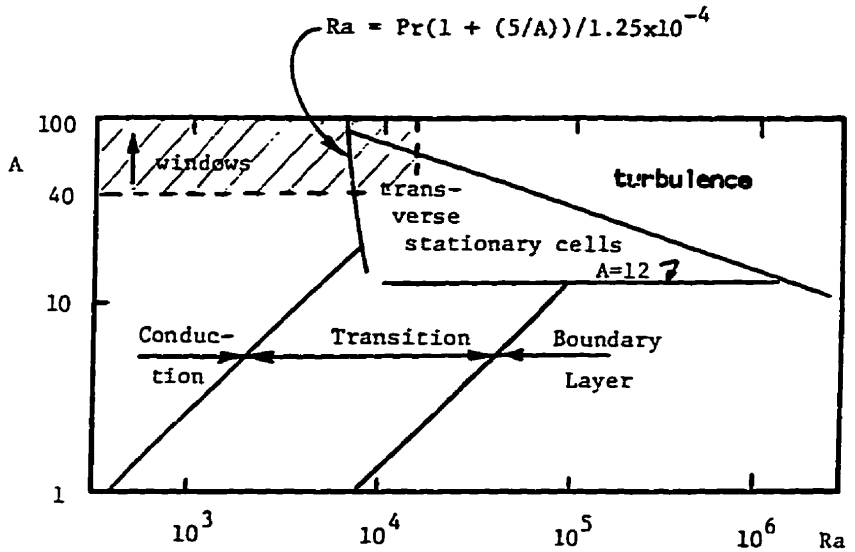

Figure 2.9: Convective Flow Regimes for Window Cavities[8].

The boundaries suggested by Yin *et al.* (1978) to delimit the laminar flow regimes are shown along with the line of slope = -1/3 above indicating the expected onset of turbulent flow. Also shown is that the region of aspect ratios applicable to windows ($A \geq 40$ and $Ra_l < 1.2 \times 10^4$) together with the line representing the onset of secondary cells, given by Korpela *et al.* (1982). According to Wright (1989), for conventional double glazed windows (12.7 mm edge-seals), when air ($Ra_l < 6.6 \times 10^3$) or argon ($Ra_l < 8.25 \times 10^3$) is used the motion of the

[8] from the work of Wright (1989)

fill gas will be laminar and free of secondary cells under most conditions. Also, window designers avoid the presence of turbulence because it only augments heat loss, therefore, it will be not considered in this work.

2.2.1.2 Two-Dimensional Buoyant Enclosure Flow: Experimental Studies

Ever since the work of Elder (1965a and 1965b) on the details of flow field in vertical rectangular enclosures, experimental studies on a variety of essentially two-dimensional enclosures have received much attention. These studies serve two important functions. One is to provide heat transfer data for pragmatically important enclosures, for example, correlations as functions of Rayleigh and Prandtl numbers and other geometrical parameters, etc.. The other is to serve as a complement to asymptotic, numerical, and stability analyses, either to provide a means to validate them or to furnish proper physical insight to guide them. It is clear that for the latter purpose, detailed velocity and temperature measurements are also needed.

Many experimental techniques are available to study buoyant enclosure flow. A review of these techniques has been given by Hoogendoorn (Yang, 1987). Known heat transfer data and their correlations for various two-dimensional enclosures, among others, have been compiled by Raithby and Hollands (1985). The extensiveness of this compilation attests to the recent interest in buoyant enclosure flows. Yang (1987) observes that there exists considerable scatter among the data. This scatter poses a problem in that these data

cannot appropriately be used to validate corresponding analytical and numerical solutions. Most of this problem can be traced to the difficulty of controlling the thermal boundary conditions at the enclosure walls (ElSherbiny *et al.*, 1982b; Zhong *et al.*, 1983). In the analysis, differentially heated rectangular enclosures are treated as having either adiabatic or perfectly conducting horizontal walls. Unfortunately, both of these conditions are very difficult to achieve in the laboratory, and the actual horizontal-wall conditions lie somewhere between adiabatic and perfectly conducting (Zhong *et al.*, 1983).

Only few correlations (Peck *et al.*, 1951; Batchlor, 1954; Eckert and Carlson, 1961; Emery, 1963; Raithby *et al.*, 1977; ElSherbiny *et al.*, 1982a) for the average heat flux over the vertical cavity wall (expressed as a Nusselt number, $Nu = Nu(Ra, Pr, A)$) can be applied to windows. The correlations proposed by ElSherbiny *et al.* (1982a) are the most used in window computational codes because these are based on a well established experimental procedure carried out over a very wide range of Rayleigh number, Ra, and aspect ratio, A.

2.2.1.3 Two-Dimensional Natural Convection in Enclosures with Partitions

Partitions in enclosures are used to modify the heat transfer by natural convection, conduction, or radiation and are used in the design of windows, and solar collectors. Despite their importance for windows design, little attention has been given to investigations of heat transfer within tall enclosures containing partitions. More attention has been given to square enclosures. Chung *et al.* (1995) provide a good review of partially divided square enclosures,

while Kangni *et al.* (1995) presents a review in enclosures completely divided with single and multiple diathermal partitions.

For completely partitioned slender vertical cavities where the aspect ratio of the cavity, A, is bigger than 10 there appears to be no references in the literature, and there are only a few for partially partitioned enclosures, for instance, the works of Nowak and Novak (1994) and Probert and Ward (1974). Also, there are only a few works for aspects ratios in the range 1 to 10: 1) for a partially divided cavity, Bejan (1982), Ciafalo and Karayiannis (1991); 2) for a single vertical partition: Nakamura *et al.* (1984), and Tong and Gerner (1986), Nishimura *et al.* (1987a), Ciafalo and Karayiannis (1991), Zhang *et al.* (1991), and *Kangni et al.* (1991) and, for inclined enclosure Tsang and Acharya (1984), and, Acharya and Tsang (1985); and, 3) for a vertical partition including double partition: Anderson and Bejan (1981) and including multiple partition, Jones (1980), Nishimura *et al.* (1987b, 1989, 1990), and, Kangni *et al.* (1995).

Table 2.2 gives an overview of the literature for completely partitioned enclosures. The results of the studies for completely divided vertical enclosure show that heat transfer rates through the system with partitions decreases with increasing number of partitions. The boundary conditions in these studies consisted of two isothermal vertical bounding walls and two adiabatic horizontal bounding walls and a partition equally spaced from the walls. Anderson and Bejan (1981) studied enclosures with a single partition analytically. Their study was in the boundary-layer regime and the effect of the conductance through the partition was

supposed to be negligible. They confirmed their results experimentally using an enclosure with a double partition. The experimental results were correlated to obtain a heat transfer relation between the two ends. This correlation was proportional to $(1+N)^{0.61}$ where N is the number of partitions. Acharya and Tsang (1985) have studied inclined enclosures with a centrally located partition using a finite difference procedure. The effect of an off-center partition on natural convection heat transfer has also been reported by Tsang and Acharya (1984), Nishimura *et al.* (1987b) and Kangni *et al.* (1991). Nishimura *et al.* (1987a, 1987b, 1988. 1990) have used a boundary-layer solution and confirmed their results experimentally for the case of an enclosure with an off-center partition as well as with equi-distant multiple partitions. They also extended their study to the non-boundary-layer regime numerically. Nishimura *et al.* (1988) showed that the isothermal partition model was not suitable for multiple partitions and they derived a correlation for heat transfer between the two ends. This correlation was proportional to $(1+N)^{-1}$ in the boundary-layer regime where the boundary-layer thickness is smaller than the half-width of each cell. The effects of heat transfer and conductivity have been studied numerically by Kangni *et al.* (1991, 1995) for vertical partitions with finite thickness operating in both the boundary-layer and the non-boundary-layer regimes. Although Kangni *et al.* (1995) derived a Nusselt number correlation as a function of the Rayleigh number Ra, aspect ratio A, conductivity k, wall thickness C, partition number N, and inclination angle Φ, it is valid only for aspect ratios between 1 to 5.

Authors		Working Fluid	A	Partitions				Type of work			Effects of				
				1		2	N	num	anal	exp	C	k	Φ	HT	CF
				center	off										
Anderson and Bejan	1981	air		X		X			X	X				X	X
Nakamura et al.	1984	air	3/8 - 5	X				X						X	X
Tsang and Acharya	1984	Note 1	1		X			X					X	X	X
Acharya and Tsang	1985	Note 1	1	X				X					X	X	X
Tong and Gerner	1986	air						X						X	X
Nishimura *et al.*	1987a	water	4 & 8	X				X	X	X				X	X
Nishimura *et al.*	1987b	water	4 & 8		X			X	X	X				X	X
Nishimura *et al.*	1988	water	4 & 10				1 - 4	X	X	X				X	X
Nishimura *et al.*	1990	water	4 & 10				1 - 4			X			X	X	X
Kangni et al.	1991	air					1 - 5	X			X	X		X	X
Zhang *et al.*	1991	air		X				X						X	X
Ciafalo and Karayiannis	1991	air	0.5 - 10	X				X				X		X	X
Kangni et al.	1995	air	1 - 5				1 - 5	X			X	X	X	X	X

Notation: HT = heat transfer; CF = convective flow; A = cavity aspect ratio;
k = conductivity; C = wall thickness; N = partition number; Φ = inclination angle.

Note 1: Fluids for which the Boussinesq approximation is valid

Table 2.2: A Overview of the Literature for Completely Partitioned Enclosures.

The works of Zhang *et al.*(1991) for a completely divided enclosure, and Probert and Ward (1974) and Nowak and Novak (1994), for partially divided enclosures, deserve a paragraph alone because they represent vertical partition applications in vertical cavities which can be directly applied to double glazed windows. Zhang *et al.* (1991) documented the thermal insulation effect of a screen installed inside a vertical rectangular enclosure. The screen is a venetian blind system made out of horizontal strips that can be rotated. Their focus was on the *closed* position, where the strips almost touch. The effect of this permeable screen

on convective flow and overall heat transfer was determined numerically. The study shows that there is a ceiling (critical) conductance for air leakage through the screen above which the screen does not cause a significant drop in overall heat transfer rate. Nowak and Novak (1994) studied numerically the nature of the convective flow and the heat transfer in a tall vertical air-filled enclosure with two small vertical partitions, with aspect ratios up to 45, located in the middle of the horizontal walls. They show that under certain conditions, a small glass partitions may appreciably suppress the peak of heat-transfer near the top and bottom walls. If the window is prone to condensation, this could lead to the possible elimination of condensation formation since the surface edge-seal (in the sash) temperature was greater than the temperature at the edge-glass. Probert and Ward (1974) reported experimental results in an assembly similar to that presented by Nowak and Novak (1994) for aspect ratios of 18 and 36. The heat transfer rate was reduced up 25% for H/h=6, were H is the height of the cavity and h is the height of the partition.

Table 2.3 shows a representative compilation of studies for partially divided enclosures.

Authors		Fluid	A	Partition									Method			Effects of					
				Inner		End Walls		Vert. Walls		Position			Num.	Exp.	Anal.	P	C	k	Φ	HT	CF
				center	off	top	bot	hot	cold	center	off	multi									
Emery	1969	water	1				X			X				X							X
Probert and Ward	1974	air	18 & 36			X	X			X				X			X	X		X	
Nansteel and Greif	1981	water	0.5			X				X				X			X	X		X	X
Chang *et al.*	1982	air	1			X	X				X		X			X	X			X	X
Bajoreck and Lloyd	1982	air	1			X	X			X				X						X	
Winters	1982	air	1				X			X			X					X		X	X
Nansteel and Greif	1983	f(*Pr*)	1			X				X				X			X			X	
Lin and Bejan	1983	water	0.5	X								X		X	X					X	
Nansteel and Greif	1984	water	1			X				X				X							
Bilski *et al.*	1986	air	1			X	X			X				X							X
Zimmerman and Acharya	1987	air	1			X	X			X			X							X	
Shaw	1987		1			X	X			X			X			X	X			X	X
Winters	1988	f(*Pr*)	1			X				X			X							X	X
Jetli and Acharya	1988	air	1		X								X			X	X				X
Frederick	1989	air	1&2						X	X			X				X		X	X	X
Frederick and Valencia	1989	air	1					X					X							X	X
Fu *et al.*	1989		1			X							X			X				X	X
Acharya and Jetli	1990	air	1				X				X		X			X	X			X	X
Ciafalo and Karayiannis	1990	air	0.5 - 10			X	X			X			X				X			X	X
Kelkar and Patankar	1990	air	1	X		X	X			X			X				X	X		X	X
Chen and Ko	1991	water	0.5			X							X			X		X		X	X
Chung *et al.*	1991	water	1				X							X					X		X
Caroutas and kirkpatrick	1991	air	1			X	X			X			X				X			X	X
Ciafalo and Karayiannis	1991	air	0.5 - 10			X	X			X			X				X			X	X
Kim *et al.*	1992	water	1										X			X				X	X
Chung *et al.*	1994	water	1										X			X			X	X	X
Nowak and Novak	1994	air	up 45			X	X			X			X				X			X	X
Chung *et al.*	1995	water	1				X			X			X						X	X	X

Note: HT = heat transfer; CF = convective flow; A = cavity aspect ratio;
k = conductivity; C = wall thickness; P = position; Φ = inclination angle.
f(Pr) means that a study of the effect of Prandtl number was done

Table 2.3: Summary of Studies for Partially Divided Enclosures.

2.2.1.4 Interaction Between Radiation and Natural Convection

In the previous section it was pointed out that buoyancy-driven natural convection in differentially heated upright cavities has been extensively studied experimentally, analytically, and numerically in order to gain a better understanding of the governing processes. Although the main focus of most studies has been on buoyancy driven flow and other modes of heat transfer, other interactions with the internal convection have usually not been considered, though there have been some studies for combined radiation and natural convection.

When an enclosure is filled with a gas (with or without absorbing and scattering particles), radiation effects become important even in the range of the window design temperature differences of order of 40°C. Radiation effects can be either passive (non-participating medium) or active (participating medium).

The calculation of radiative transfer in multidimensional enclosures is not a simple task and is often complicated by the use of realistic spectral models. A comprehensive review up to 1986 on the interaction between natural convection and an active gas medium for an enclosure flow has been given by Yang (1986). Most studies have been done for an active medium with black boundaries (Zhong *et al.*, 1987; Webb and Viskanta, 1987a and 1987b; Naraghi and Kassemi, 1988; Draoui *et al.*, 1988 and 1991; Yücel, 1989; Fusegi and Farouk 1989, 1990; Fusegi *et al.*, 1991; Yücel *et al.*, 1989; Behnia *et al.*, 1990; Tan and Howell; 1991; Zenouszi and Yener, 1992; Castellano *et al.*, 1992) and, as a limiting case, for a passive

medium, except for the works of Tan and Howell (1991), Zenouszi and Yener (1992) and Castellano *et al.* (1992), that treated the case of gray boundaries. An extensive review of methods used to solve the radiative transport equation (RTE) for multidimensional geometries in participating media is given by Viskanta and Menguc (1987) and Modest (1993). After the review of Modest (1993) new works have been published (Sánchez and Smith, 1992; Lobo and Emery, 1992 and 1993; Siegel and Spuckler, 1993; Menart and Lee, 1993; Menart *et al.*, 1993; Chai *et al.*, 1994a, 1994b, 1994c and 1994d; Fiveland and Jessee, 1994 and 1995; Haidekker *et al.*, 1994; Sánchez *et al.*, 1994; Ehlert and Smith, 1994; Shawn *et al.*, 1994; Maryama and Aihara, 1995).

In all these works radiation is found to play an important and sometimes major role in the heat transfer and fluid processes- directly through absorption and emission process within the fluid. This effect may be negligibly small, for example if the fluid is dry (or fairly dry) air or a monatomic gas. Radiation may also have an effect on the temperature field indirectly by affecting the solid boundaries. In a multi-pane window, radiation is transmitted and absorbed by the boundaries and may have a stronger influence on the convective flow patterns than expected because of the inherent coupling in natural convection between the thermal field and the flow field through buoyancy effects. The interaction between radiation and natural convection in vertical slots and enclosures filled with a non-participating fluid has not received as much attention as for a participating medium (Balaji and Venkateshan, 1994a). The effect of surface radiation exchange for gray boundaries with no heat sources (solar radiation), has

been treated by Larson and Viskanta (1976), Asako and Nakamura (1982), Kim and Viskanta (1984), Han *et al.* (1986), Wright (1989), Engelman and Jamnia (1991), Curcija (1992), Smith *et al.* (1993) and Balaji and Venkateshan (1993, 1994a and 1994b, and 1995). Cases with heat sources and semi-transparent surfaces have been investigated by Behnia and de Vahl Davis (1990), and Hutchinson and Stefurak (1995).

All of the aforementioned investigations treated the effects of radiation on a fluid bounded by differentially heated walls with a few including the effect of an external source. None of them deals with the effects for an external source with more than one cavity (e.g., windows with more the two glazing panes) and/or internal specular surfaces to solar radiation or long-wave radiation.

2.2.1.5 Indoor Convective Film Coefficient

Although indoor heat transfer coefficients are affected by the nature of the boundary layer, which in turn is strongly influenced by surface geometry, temperature gradient and the flow outside of the boundary layer, most solutions are based on simplified boundary conditions which are approximations for fenestration systems. This is also valid for the outside heat transfer coefficients.

Current correlations for the convective heat transfer coefficient come from studies of laminar natural convection over a short isothermal flat plate. They are used in all the

computational models for both energy calculation in buildings and heat transfer calculations through fenestration systems. These correlations are unsatisfactory when used to determine the surface temperatures, because they do not reflect the local heat transfer at the edge of glass and in the frame regions which are relevant for the prediction of condensation potential.

In spite of many works done in the past for flow over an isothermal flat plate, for example, the experimental work of Wilkes and Peterson (1938), the correlation of McAdams (1956), the analytical/numerical work of Ostrach (1952), the experimental work of Min *et al.* (1956), the simplified empirical correlation of Le Fevre (Ede, 1967), and the numerical solution of Martin (1984), only a few works have been done for non-isothermal flat plates, for instance, Raithby and Hollands (1975). Perhaps the only attempt to obtain correlations for isothermal walls with steps were made by Curcija and Goss (1993), who give a best guess correlation for realistic boundary conditions; at least it represents a better assumption than that of a vertical flat plate.

Studies that considered two-dimensional natural convective enclosure flow with natural convection at one or both of the outside surfaces of the cavity are as follows: Sparrow and Prakash (1981) modeled a square enclosure in which one surface is cooled by an external boundary layer flow and the other is maintained isothermal; Marballi *et al.* (1984) investigated a tall enclosure with uniform heat transfer coefficient on both outside surfaces; Varapaev (1987) also considered a uniform convective film coefficient; Yeoh *et al.* (1989)

reported a model which included a vertically varying convection coefficient on one surface; Curcija (1992) examined varying convection coefficients on both surfaces; and, Smith *et al.* (1993) described a model that uses a constant heat transfer coefficient on both external surfaces or a varying film coefficient on the indoor side. In all these studies the indoor film coefficient used was for a vertical flat plate, except the work of Curcija (1992), which used a heat transfer coefficient that takes in to account the steps at the window frame's sill and head.

To conclude, the flat plate assumption is fairly realistic for the glass outside the edge-glass region. For the case of frames, and for the edge-glass region, the flat plate assumption does not apply and care has to be taken when reaching conclusions concerning local heat fluxes, or surface temperatures. Also, there is some controversy about the nature of the flow inside a room; it is generally assumed laminar but it is in reality usually turbulent and unsteady. Unfortunately, there are no detailed works which could be used to characterize the air movement inside such rooms near fenestration systems under typical conditions.

2.2.1.6 Exterior Convective Film Coefficient

The exterior film coefficient is an important issue for window performance. Until the relatively recent emergence of high thermal resistance windows in the market the exterior film coefficient had an important role to play in nighttime *U-factor*. Even for the newer generation of windows the exterior film coefficient does not become unimportant until the window

reaches a thermal resistance smaller than the range 1.4 to 1.8 (m^2K)/W (Yazdanian and Klems, 1994).

Yazdanian and Klems (1994) pointed out from a careful survey of the literature on exterior film coefficients by Furler *et al.* (1988) that there exists as many as 14 sets of equations for predicting the external convective film coefficient, with wide variations between predictions. Exterior film coefficients have been based on laboratory measurements, computer simulations, or measurements on a medium-rise building. There is great ambiguity and disagreement in these studies, as well as inconsistency in their application, most notably in their definition of free-stream wind speed.

The methods used to estimate exterior convective film coefficients are technically unsatisfactory (Yazdanian and Klems 1994). For many years, ASHRAE, and most energy balance computational codes have adopted the standard film coefficient proposed by Rowley and Eckley (1932), of approximately 31 W/(m^2K) after radiative heat transfer is removed, and assuming a 6.7 m/s wind. This value is based on wind-tunnel measurements and this free-stream wind speed was interpreted by ASHRAE as *the ambient wind speed obtained from weather data*. Lokmanhekim (1975), as part of an ASHRAE committee, presented a set of equations based on Ito and Kimura (1972) "sixth floor" model. The equations come from measurements of a sixth floor medium-rise building. This model predicts a convective film coefficient value of 25 W/(m^2K) at a 6.7 m/s wind which is lower than the ASHRAE standard

from Rowley and Eckley (1932). In 1977 Kimura presented a set of equations summarizing Ito and Kimura's (1972) measurements made at the fourth floor of the same medium-rise building. Yazdanian and Klems (1994) arrived at an experimental model for windows in low-rise buildings which correlates the difference in temperatures between the exterior glass surface and the ambient in the natural convection region and with the site wind speed in the forced convection region. They have shown that the exterior film coefficient decreases, and has a weaker wind dependence, with the decreasing height of the building.

Although the new correlation of Yazdanian and Klems (1994) will allow a more accurate predictions of *U-factors* for low-rise buildings, contributing to a more precise calculation of window energy use in residential buildings and providing better information for developing window energy ratings, it will be inaccurate for predicting local surface temperatures in fenestration systems because the correlation predicts an average heat transfer coefficient. It is important to know the local heat transfer coefficient principally at the edge seals or steps in the window frame where it will differ greatly from the average film coefficient, as demonstrated by Curcija and Goss (1995b) in a numerical solution, for a typical wood casement window with constant temperature. Curcija and Goss (1995b) report a convective heat transfer correlation for outdoor surfaces (vertical and horizontal) for a laminar free-stream flow (perpendicular to the vertical surfaces). Therefore, care has to be taken when using their correlations since they might also be a function of Biot number (wall conductivity), surface temperature, and free-stream direction. To reinforce this point, Abu-

Mulaweh *et al.* (1993 and 1994) presented results for measurements and calculations in a buoyancy assisted and opposed laminar flow over a backward-facing step. This showed the effects of axial conduction in the recirculation region where the assumption of constant heat flow boundary condition was not valid, showing discrepancies between computational and experimental results when the axial conduction was not considered.

Only a few studies have considered the interaction between the two dimensional natural convective flow inside an enclosure formed by two glass panes with external convective boundary conditions. Behnia *et al.* (1985a, 1985b) examined the case of an isothermal indoor pane while the other pane had heat loss due to radiation and convection. Curcija (1992) examined varying convection coefficients on both surfaces using a heat transfer coefficient that takes into account the steps at the window frame's head and sill. Smith *et al.* (1993) described a model that used a constant heat transfer coefficient on the outside surface and either a uniform, or a varying, film coefficient on the indoor side.

The conclusion for outdoor fenestration system surfaces is similar to that for inside surfaces: the plate averaged correlations based on experimental results are fairly realistic for the glass outside of the edge-glass region and vertical frame surfaces, but do not apply for to the frame horizontal surfaces or the edge-glass region. This means that care has to taken when conclusions related to local heat fluxes, or surface temperatures, are made for these regions of fenestration system.

2.2.1.7 Condensation Potential: Prediction of Surface Temperatures

The control of condensation on windows is important because it not only impairs visibility but can also deteriorate sash, frame, and sill as well as the interior finish and the supporting wall (Rousseau 1988). When the temperature of a surface falls below the dew point of the inside air in its vicinity moisture will condense on the surface. Air leakage affects both the glass surface temperature and the local relative humidity. Air leakage can either make condensation worse, makes it better, or makes no difference, depending on the window design, the application, and the boundary conditions (air temperatures, humidity, wind speed, presence or absence of insolation, etc.). Knowing the surface temperature of the glazing, sash and frame is critical to condensation control. The surface temperature in all cases analyzed in this work, does not include air leakage effects.

Although condensation potential increases energy consumption (due to latent loads), reduces occupant comfort and indoor air quality (from presence of bacteria and mold), and produces structural damage, little work has been done to predict condensation potential using numerical methods (Curcija and Goss, 1994; McGowan, 1995; Wright, 1995).

2.2.1.8 Thermal Stresses in the Glass: Prediction of Surface Temperatures

Thermal stresses, leading to thermal breakage, are another source of concern in the design of glazing systems. They are caused by temperature differences between the edges and

middle of a light of glass. The condition of the glass pane will strongly influence the breaking stress of the pane (Brown and Ruberg, 1988). Barry (1995) points out that today's thermal performance glazings require more attention to maintain good glass edge quality. Thermal stress can be significant when the heated central area of a glass pane approaches about 30° C hotter than the edge.

2.3 Closure

As pointed out in previous sections, most fenestration thermal performance models are concerned with one-dimensional heat transfer through the central portion of the glazing with adjustments made to include the effects of the edge spacer and frame heat transfer. A limited number of two-dimensional models have been developed in the past several years to improve this analysis. These models, however, do not fully represent the two dimensional natural convection and gray body radiation heat transfer in the glazing cavity. The development of improved insulating glazing units has indicated the necessity for improvement in the frame and edge-glass thermal performances. Also, the development of a uniform system for rating window energy efficiency, resulting in a window labeling system, affects window design. As a result of advances in technology and the window labeling system two-dimensional and three-dimensional heat transfer models are needed to provide a more complete understanding of the

heat transfer processes in windows and provide a method to reduce the number of expensive experimental tests.

The next chapters will present the mathematical and numerical formulations for the development of a 2-D model capable of handling more realistic boundary conditions – e.g., solar radiation, long-wave radiation, and convection with variable temperatures at the walls and radiative heat transfer inside the cavities.

3 PROBLEM DEFINITION - MATHEMATICAL MODEL

The definition of the heat transfer problem in windows is presented in this chapter. At the external surfaces of the window, Figure 3.1, (both indoor and outdoor), convection and radiation heat transfer occur simultaneously, while in window cavities (frame and glazing cavities), depending on the intensity of the air movement, convection or radiation can prevail. In the solid portions of the window system (glazing layers, edge, and frame construction elements) and small enclosed air spaces, where air motion is suppressed, only conduction occurs.

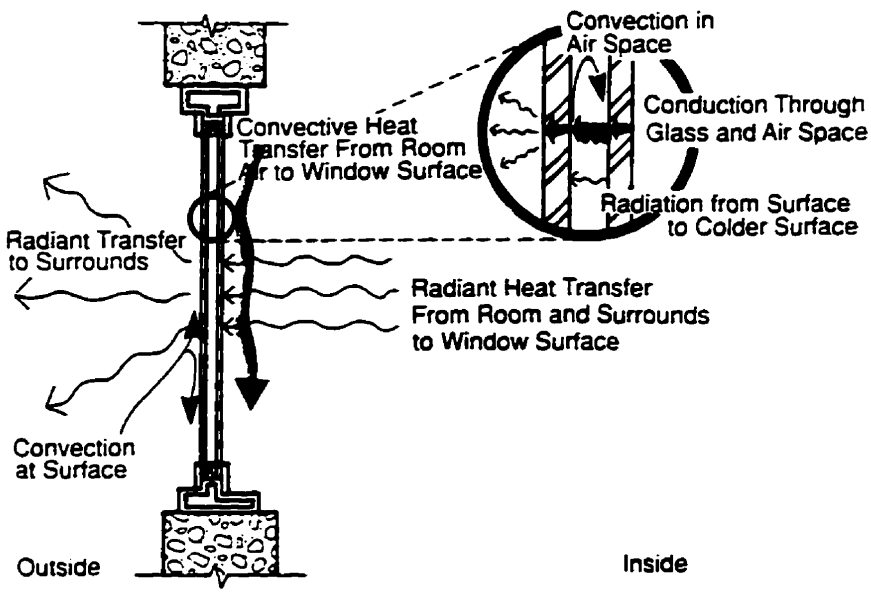

Figure 3.1: Representation of the Window System.[1]

[1] taken from NRC, 1988. "Windows Performance and New Technology", in Proceedings of Building Science Insight '88, National Research Council Canada.

3.1 Physical Model and Assumptions

The window system[2] shown in Fig. 3.1 consists of:

- double glazing;
- spacer;
- frame;
- portion of wall (necessary for the walls to be adiabatic).

These components form the region of interest. The heat transfer from the inside surroundings at temperature T_i, to outside surroundings at temperature T_o, will be analyzed.

The gas filled double pane window shown in Figure 3.1 has its third dimension (not shown in the figure) horizontal, normal to the plane of the paper, and much longer than the width of the cavity (spacer bar), so that a two-dimensional flow is assumed to exist in a high aspect ratio, rectangular cavity surrounded by a vertical glass wall and space bar (horizontal walls).

All the walls are stationary and impermeable; the no slip conditions exists at them. The glazing system is imperfectly transparent to radiation (i.e., some absorption of radiation may occur) and the frame components are opaque to radiation with convection, radiation and

2 Windows with more than two panes are constructed similarly and all the assumptions made here are still valid.

conduction energy exchanges with the surroundings occurring on window outside surfaces. The top and bottom walls are opaque to radiation.

Although one of the ultimate goals of the research is to predict the potential for condensation of a window the effects of condensation/evaporation and air infiltration are not considered in this work. Even though different mixed convective regimes on window surfaces are possible, natural convection on inside surfaces and forced convection on outside surfaces are generally assumed as the appropriate conditions. Therefore, both natural convection, on the indoor window surfaces and within the glazing cavity; and forced, wind driven, convection heat transfer on the outdoor window surfaces are used in all cases considered in the following chapters.

It is assumed that the confined fluid is Newtonian and that the Boussinesq approximation is valid (Leonard and Reizes, 1979). All surfaces are taken to be gray diffuse reflectors and emitters of long-wave radiation (may be specular in case of a closed rectangular cavity) and the confined gas is assumed to be radiatively passive.

The radiation model is a two-band model: short and long wave. This implies that emission from the surfaces of the cavity is "long-wave" radiation and that solar radiation is "short-wave". If one or more of the glass panes are spectrally selective a spectral solar radiation model (short wave) may be used to account for sharp changes in the radiation properties with the wave length.

3.2 Mathematical Model

In this section the governing differential equations and boundary conditions, for the window system as posed in section 3.1, are presented. The equations are written in terms of the primitive variables, namely, local velocity components, pressure and temperature.

When viscous dissipation in the energy equation is neglected the governing differential equations for Newtonian and incompressible fluid, with constant properties except in the formulation of the buoyancy term[3], can be written in Cartesian coordinates as:

- **continuity:**

$$\frac{\partial u}{\partial x} + \frac{\partial v}{\partial y} = 0 \tag{3.1}$$

- **momentum:**

in x:

$$\rho \frac{Du}{Dt} = -\frac{\partial p_k}{\partial x} + \mu\left(\frac{\partial^2 u}{\partial x^2} + \frac{\partial^2 u}{\partial y^2}\right) \tag{3.2}$$

in y:

$$\rho \frac{Dv}{Dt} = -\frac{\partial p_k}{\partial y} + \mu\left(\frac{\partial^2 v}{\partial x^2} + \frac{\partial^2 v}{\partial y^2}\right) + \rho g \beta (T - \overline{T}) \tag{3.3}$$

3 Leonard and Reizes (1979) examined the assumption of constant fluid properties and demonstrated its validity for cases where the temperature variation is less than 10% of the mean (absolute) temperature.

- **energy:**

$$\rho c_p \frac{DT}{Dt} = k\left(\frac{\partial^2 T}{\partial x^2} + \frac{\partial^2 T}{\partial y^2}\right) + \dot{S} \tag{3.4}$$

where, ρ, μ, β, g, c_p and k are the density, viscosity, coefficient of thermal expansion, gravity, constant-pressure specific heat and conductivity, respectively; t is the time; x, y are the Cartesian coordinates; u, v are the velocity components; T is the temperature; $\rho g \beta (T - \overline{T})$ is the buoyancy force/unit volume in the y direction where $\overline{T} = \frac{(T_h + T_c)}{2}$; T_h and T_c are the temperatures at the hot wall and cold wall, respectively; $\dot{S}$ is the source term, and the origin of the coordinates (x, y) is placed at the most lower left corner of the fenestration system with gravity in the -y direction. p_k, the kinematic pressure, drives the flow. It is obtained from the following expression $p(y) = p_o - \int_0^y \overline{\rho}(y) g dy + p_k$

The above set of equations and boundary conditions are applied to the portions inside of the frame and glazing cavities. The velocity boundary conditions are:

- *at all surfaces (fluid / solid interfaces)*

$$v = u = 0 \tag{3.5}$$

On the solid portions of the window system heat transfer is governed only by the modified energy equation since the velocity components are zero, and therefore momentum and continuity equations no longer needed to be solved. The energy equation becomes:

- **energy:**

$$\rho c_p \frac{\partial T}{\partial t} = k\left(\frac{\partial^2 T}{\partial x^2} + \frac{\partial^2 T}{\partial y^2}\right) + \dot{S} \tag{3.6}$$

The temperature boundary conditions are derived from the energy balance at the surfaces.

The top and bottom portion of the window are adiabatic, so the boundary conditions are:

$$\frac{\partial T}{\partial x_j}\vec{n}_j = 0 \tag{3.7}$$

The energy balance at the outside surfaces of the window may be written as:

$$-k\left(\frac{\partial T}{\partial x_j}\vec{n}_j\right)_{surf} - h_c(T_{surf} - T_o) + \alpha r^s q + h_r(T_{eff} - T_{surf}) = 0 \tag{3.8}$$

where, h_c is the convective heat transfer coefficient; h_r is the radiation heat transfer coefficient; αr is the absorptivity, and q is the radiative flux. The superscript s refer to short-wave, and the subscripts, *eff*, *o* and *surf*, refer effective, outside and surface, respectively.

A similar energy balance on the inside surface of the window leads to

$$-k\left(\frac{\partial T}{\partial x_j}\vec{n}_j\right)_{surf} - h_c\left(T_{surf} - T_{in}\right) + \alpha r^l \sigma T_{eff}^4 - \varepsilon\sigma T_{surf}^4 = 0 \qquad (3.9)$$

where, ε and σ are the emissivity and the Stefan-Boltzman constant, respectively. The superscript *l* and the subscript *in* refer to long-wave and inside, respectively.

The energy balance at the surface of the cavities between glazing panes yields

$$-k\left(\frac{\partial T}{\partial x_j}\vec{n}_j\right)_{surf} + \alpha r^l q^s + \alpha r^l q^l - \varepsilon\sigma T_{surf}^4 = 0 \qquad (3.10)$$

q^l is the long wave radiative flux incident on the surface.

For other cavities in the frame the energy balance is

$$-k\left(\frac{\partial T}{\partial x_j}\vec{n}_j\right)_{surf} + \alpha r^l q^l - \varepsilon\sigma T_{surf}^4 = 0 \qquad (3.11)$$

After the radiative fluxes have been determined, the temperatures of the boundaries can be calculated from equations (3.8) to (3.11) which couple the internal radiative and convective heat transfers. These equations also relate the internal convection and radiation transfers to the external convection and radiation energy transfers at the surroundings.

The long wave radiation heat transfer occurring in the glazing cavity can be described using the Radiosity Matrix Method for determining radiation exchange in an enclosure (Siegel and Howell, 1981). The incident long-wave radiative heat flux denoted by the superscript *l*, at any surface j of the cavity can be written as

$$q_j^l = \frac{(J_j^l - \varepsilon_j^l \sigma T_j^4)}{\rho r_j^l} \tag{3.12}$$

in which J_j^l is the radiosity:

$$J_k^l = \varepsilon_k^l \sigma T_k^4 + \rho r_k^l \sum_{j=1}^{N} J_k^l E_{j-k}^l \tag{3.13}$$

where the E_{j-k}^l is the specular exchange factor between j and k, which accounts for radiation going from surface j to surface k directly and by all possible specular (mirror-like) reflections and ρr_k^l is the diffuse reflectance of surface k. When the surfaces of the enclosure do not specularly reflect radiation, the specular exchange factors E_{j-k}^l reduce to the usual view factor (configuration factor) F_{j-k}^l . Methods for calculating E_{j-k}^l are given in advanced radiation texts, like Siegel and Howell, 1979. For a rectangular cavity (bounded by plane surfaces), the view factor between any two points on the same surface is zero; this substantially reduces the number of terms on the right hand side of equation (3.13).

Furthermore, since a two-band radiation model is assumed and all the emitted radiation is in the long-wave band, the short-wave component of radiosity, J^s, depends only on

the geometry and the solar radiation. The short-wave radiosity for a double pane window is therefore,

$$J_j^s = \tau_j^s q^s + \rho r_j^s \sum_{k=1}^{N} J_k^s E_{k-j}^s \tag{3.14}$$

and at the others surfaces

$$J_j^s = \rho r_j^s \sum_{k=1}^{N} J_k^s E_{k-j}^s \tag{3.15}$$

The Edward's embedding technique was chosen as the model to calculate the short wave radiosities because is a simple way to determine the fraction of solar radiation that strike and is absorbed by the surface directly or by multiple reflections, in multi-glazed windows.

It follows from Equations (3.14) and (3.15) that the short-wave radiosities need only to be calculated once for a given geometry. The long wave component J^l_j, however, needs to be evaluated at each stage of the calculation so that the radiosity

$$J_j = J_j^s + J_j^l \tag{3.16}$$

The incident radiative heat fluxes q^l and q^s in the Equations (3.8), (3.10) and (3.11) can then be calculated from the radiosity by

$$q_j^l = \frac{(J_j^l - \varepsilon_j^l \sigma T_j^4)}{\rho r_j^l}, \qquad q_j^s = \frac{J_j^s}{\rho r_j^s} \tag{3.17}$$

The incident short-wave radiation q_s is externally imposed (from the sun) and the incident long-wave radiation σT_{eff}^4 is calculated from the externally imposed radiation temperature, which depends on the surroundings.

3.3 Closure

The physical and mathematical model formulations were presented, as well as the assumptions which were made. In the next chapter the numerical model to solve the set of equations and boundary conditions established in this chapter will be discussed.

4 NUMERICAL MODEL

Despite recent advances in computer hardware, numerical simulation algorithms, and grid generation schemes, which have the potential capability to model the physical and geometrical complexities of windows, little work has been done to model a whole window, except for the works of Smith *et al.* (1993), Curcija and Goss (1994), and Wright and Sullivan (1994). Numerical modeling can provide detailed information (velocity and temperature distributions, stream line and heat flux fields, throughout an entire window) that is generally unavailable from experimental studies due to limitation in the experimental techniques currently available. A well defined comparison between numerical simulation and measurement can determine the level of numerical accuracy for a given calculation. Therefore, various aspects of the window performance that are not available from experimental measurements can be further studied. It is this unique capability of the computational tool that can most impact the design and thermal analysis of windows.

To advance the current state-of-the art of modeling windows two different approaches can be devised:

- the first approach is to conduct step by step, logically progressing research using simplified geometries to start. As soon as the basic features of the numerical algorithm and/or physical mechanism in a simpler case are known, complexity is added. As this

process progresses a satisfactory and complete knowledge of fluid flow and heat transfer mechanisms in windows would eventually be reached. The goal of these studies is to develop new prediction techniques and fundamental understanding based on idealized conditions; and,

- the second approach is to solve the complete fenestration system.

It is useful to address research at both levels since much window research is motivated by practical engineering needs. The gradual, and at times slow, pace of progress in the first approach cannot satisfy the demand for some approximate, though nevertheless useful, information before complete knowledge is attained. In addition, transport processes in windows are subject to multiple dependent variables with strong non-linearities. This implies that various physical mechanisms cannot be treated separately, as "modules", that can be added or deleted without affecting the characteristic of the other mechanisms in a quantitative way.

Obtaining solutions to the nonlinear Navier-Stokes equations has always been a challenge to fluid mechanicians and mathematicians alike. Even though exact solutions do exist (Schlichting, 1979), they are restricted to very specialized cases. Much of the effort has therefore been devoted to developing approximate solution techniques which can be applied to a much larger variety of problems.

For window cavities the natural-convection phenomena (in both frame and glazing, as described by Equations (3.1), (3.2), (3.3), and (3.4)), the momentum and energy equations are coupled through the body force term which depends on the temperature field. The solid portions (glazing layers, edge-seal, and frame), also depend on the temperature field as described by Equation (3.6). As a result, all the aforementioned equations must be solved simultaneously and hence represent an additional level of complexity to obtaining a solution.

All existing methods of analysis to solve the natural convection problem in cavities are approximate in nature, with restricted applicability to a variety of enclosure-flow problems. They can be broadly classified into three categories as follows (Yang, 1987):

1. Asymptotic analysis (analytical);
2. Discretization methods (numerical); and,
3. Hybrid and other numerical methods.

The discretization methods are the most suitable category among them for cavity buoyancy flow modeling (Yang, 1987) because, until today, they are the only class of methods that have yielded results for a complete range of parameters (*Pr*, *Ra* and *A*). There are several approaches to making a continuous problem discrete. One way is to give a point-wise approximation to the governing equations, e.g., the Finite Difference Method (FDM). This model is formed by replacing derivatives by difference approximations in the differential equations, and requiring that the resulting approximate equations be satisfied at each grid point. A second way is to give a piece-wise approximation to the governing equations, e.g.,

the Finite Element Method (FEM). In this approach, a finite number of functions are chosen, and a combination of those trial functions is used to approximate the exact solution. It is a variation of the first approach which will be used in this thesis, i.e., a Finite Volume Method (FVM) (Patankar, 1980) using a collocated pressure arrangement on a non-orthogonal grid (Rhie, 1981). In this formulation the approximate equations are obtained through conservation balances of the conserved property (mass, momentum, enthalpy, etc.) in the elemental control volume. In contrast to the FDM and the FEM, the FVM permits the observation of the physical character of each term of the differential equation allowing an association of the physical interpretation with the mathematical formulation. Nowadays, both methods (FVM and FEM) are solving highly convective problems, including shock-waves, in complex geometries, showing that they actually have more than a strong likeness in general terms (Maliska, 1995). From a mathematical view point the latter observation is confirmed, once all the numerical methods can be derived from a weighted residual method, by using different weighting functions. For more information on this subject see Oñate and Idelsohn (1992).

In fact, most of the considerations concerning the advantages of one method over another are immaterial, since they are derived from the same premise and differ only in the way that the weighting function is chosen. In practice the difference lies in the degree of experience gained with a particular method for a particular class of problems. Nevertheless, it is well known that because of the non-linearities of the equations (via convective terms), none

of the aforementioned methods give optimal results, and all approaches propose different ways to overcome this handicap. The numerical model employed in this thesis is an extension of Wright's model (Wright, 1989). The differences and extensions between them are shown in Table 4.1.

	Wright	This Work
Modeling	- only vertical cavities	- cavities with inclination less than 30° from the vertical
	- double glazing windows	- multi pane windows
	- model the cavity and seal with one solid element	- model cavity, seal and frame (several solid elements or cavities)
	- no solar radiation	- allow solar radiation
Grid	- orthogonal	- non-orthogonal
	- uniform everywhere	- uniform for glazing cavities and non uniform for solid sections, frame and seals cavities.
Formulation Method for Pressure	- staggered	- collocated
Radiation model	- diffuse gray and specular surfaces	- diffuse gray and specular surfaces
Boundary Conditions	- specified T	- specified T
		- specified h
		- specified heat flux

Table 4.1: Extensions and Differences Between the Proposed Model and Wright's Work (1989).

In the next Sections the methodology adopted is described. In Section 4.1 the numerical formulation is outlined. In Section 4.2 the procedure to solve the set of algebraic equations is posed. Finally, in Section 4.3 a closure is presented.

4.1 Numerical Formulation

The primary aim of this research is to solve numerically the natural-convection of fill gas (glazing cavity) simultaneously with the radiative exchange (solar and thermal) and the conduction in the solid portion (glazings, edge-seal and frame) in a window. This is a conjugate problem, as posed in Chapter 3, requiring a scheme capable of resolving secondary cells.

4.1.1 Equation Discretizations

Heat transfer and fluid flow problems require the solution of general conservation equations (Patankar, 1980) of the form

$$\frac{\partial}{\partial t}(\rho\Phi)+\frac{\partial}{\partial x}(\rho u\Phi)+\frac{\partial}{\partial y}(\rho v\Phi) = \frac{\partial}{\partial x}\left(\Gamma^{\Phi}\frac{\partial\Phi}{\partial x}\right)+\frac{\partial}{\partial y}\left(\Gamma^{\Phi}\frac{\partial\Phi}{\partial y}\right)+\dot{S}^{\Phi} \qquad (4.1)$$

over some specified problem domain and with the appropriate boundary conditions for the solution variable Φ, which may represent any conserved quantity. Equation (4.4) reverts to the mass conservation when Φ=1 and the volumetric source term, $\dot{S}^{\Phi}$=0. The momentum equation in the two-dimensional Cartesian coordinate system can be obtained replacing Φ, by u and v (the fluid velocities) in the x and y directions respectively, with the appropriate source term, $\dot{S}^{\Phi}$, that includes the pressure gradient. The energy equation is obtained by making $\Phi=T$, also with the appropriate source term. The variable t is the time coordinate and ρ is the fluid density. The quantity Γ^{Φ} is the diffusion coefficient: for the energy equation it is defined as the ratio of the fluid thermal conductivity to the fluid specific heat (k/c_p) and for Navier-Stokes equations, Γ^{Φ} is the effective fluid viscosity (μ_{eff}). Table 4.2 shows the values of Φ, $\dot{S}^{\Phi}$, Γ^{Φ} for the variables in a two dimensional case. This notation is well established in the literature (see for example, Patankar, 1980).

The first term on the left hand side of Equation (4.1) is the temporal term and describes the advance of the solution in time, following either a real transient or a distorted transient. Physically, it represents the variation of the property ,Φ, inside the control volume. The remaining terms on the left hand side of Equation (4.1) are the convective balance of the variable Φ. Numerically, they are the most delicate terms for treatment, due to their intrinsic non-linearities. The first three terms on the right hand side of the equation represent the

diffusive flux balances, whereas the source term is responsible to accommodate all terms that do not fit in the format of the Equation (4.1).

Conservation Equation	Φ	Γ^{Φ}	$\dot{S}^{\Phi}$
Mass	1	0	0
Momentum in x	u	μ	$-\frac{\partial p}{\partial x}$
Momentum in y	v	μ	$-\frac{\partial p}{\partial y}+\rho g\beta(T-\overline{T})$
Energy[1]	T	k/c_p	$\frac{1}{c_p}\frac{Dp}{Dt}$

Table 4.2: Values of Φ, $\dot{S}^{\Phi}$, Γ^{Φ} for the Variables in a Two-Dimensional Case.

Representing the source term, $\dot{S}^{\Phi}$, by its active and lagged components, Equation (4.1) is expressed in a general form:

$$\frac{\partial}{\partial t}(\rho\Phi)+\frac{\partial}{\partial x}(\rho u\Phi)+\frac{\partial}{\partial y}(\rho v\Phi) = \frac{\partial}{\partial x}\left(\Gamma^{\Phi}\frac{\partial\Phi}{\partial x}\right)+\frac{\partial}{\partial y}\left(\Gamma^{\Phi}\frac{\partial\Phi}{\partial y}\right)+R^{\Phi}\Phi+Q^{\Phi} \qquad (4.2)$$

[1] ϕ is the dissipation term. The equation for ϕ can be found in Bejan 1984.

where $R^{\Phi}\Phi$ and Q^{Φ} represent the active source term and the lagged source term, respectively. The integration for the two-dimensional case is then:

$$\int_t^{t+\Delta t}\iint_A \frac{\partial}{\partial t}(\rho\Phi)dAdt + \int_t^{t+\Delta t}\iint_A \frac{\partial}{\partial x}(\rho u\Phi)dAdt + \int_t^{t+\Delta t}\iint_A \frac{\partial}{\partial y}(\rho v\Phi)dAdt =$$

$$\int_t^{t+\Delta t}\iint_A \frac{\partial}{\partial x}\left(\Gamma^{\Phi}\frac{\partial\Phi}{\partial x}\right)dAdt + \int_t^{t+\Delta t}\iint_A \frac{\partial}{\partial y}\left(\Gamma^{\Phi}\frac{\partial\Phi}{\partial y}\right)dAdt + \int_t^{t+\Delta t}\iint_A R^{\Phi}\Phi dAdt + \int_t^{t+\Delta t}\iint_A Q^{\Phi}dAdt \quad (4.3)$$

where A is the surface area of the control volume having a depth of unity, and Δt is a time step.

The collocated grid formulation that was implemented (Rhie, 1981) is applied over each control volume, as depicted in Figure 4.1. Each rectangular control volume whose node is designated as P, has four neighboring nodes designated by their compass bearing from P, i.e., S, N, W and E; similarly, s, n, w and e refer to the location of the faces of the control volume of interest. Δx_w and Δx_e are the distances in the x direction from the node to the west and east faces of the control volume considered, respectively, while Δy_s and Δy_n are the distances to the south and north faces, respectively. The variables p, u, v and T are located and calculated at the center of the P control volumes.

For sake of simplicity, the integration of Equantion (4.2) in space is applyed to an orthogonal grid arranjement. The non-orthogonal terms are given in Appendix A. The transport equations are integrated over a finite number of control volumes (CVs), leading to

balance equations of fluxes J through the CV faces, and volumetric sources $\dot{S}^{\Phi}$. Thus (see Fig. 4.1 below, for the grid arrangement and notation)

$$J_e - J_w + J_n - J_s = 0 \tag{4.4}$$

Evaluation of the convection and diffusion contribution to the flux J will be described for the CV face "e". Analogous expressions follow for the others faces.

First the cell face mass flux is evaluated as

$$\dot{m}_e = \rho \hat{u} A_e \tag{4.5}$$

where $\hat{u}$ is the convecting velocity in the x direction. The mass fluxes are assumed to be known when solving the momentum and heat transport equations.

The convective flux of a variable Φ is evaluated as

$$J_e^c = \dot{m}_e \Phi_e \tag{4.6}$$

where Φ_e stands for the mean value of the transported variable (u, v *or* T) at CV face "e". The estimate for this value is expressed in terms of the nodal values by employing the upwind weighted scheme of Raithby and Torrance (1974), from now on called EDS (Exponential Differencing Scheme).

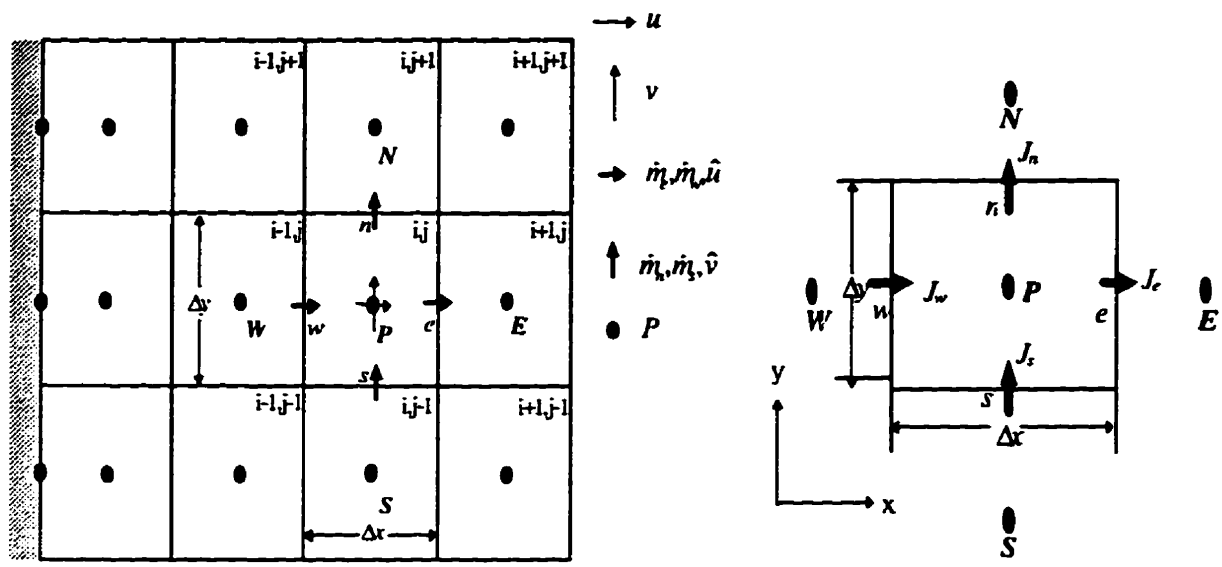

Figure 4.1: Computational Grid and Labeling Scheme.

The diffusion flux involves an estimate of the mean gradient of Φ at the CV face. Here again EDS is employed, leading to

$$J_e^D = -\Gamma \left.\frac{\partial \Phi}{\partial n}\right|_e A_e \tag{4.7}$$

To perform the integration, values of variables at the faces of the control volumes were related to the nodal values using EDS. Hence, to relate Φ_e to Φ_E and Φ_P, the following approximation is made:

$$\Phi_e = (0.5 + \alpha_e)\Phi_P + (0.5 - \alpha_e)\Phi_E \tag{4.8}$$

Furthermore, the diffusion at the east face is approximated by:

$$\Gamma_e \left.\frac{\partial \Phi}{\partial n}\right|_e = \beta_e \frac{\Gamma_e}{\Delta x}(\Phi_E - \Phi_P) \tag{4.9}$$

The convective and diffusive weights, α_e and β_e, are functions of the Peclet number, Pe, i.e.:

$$\alpha_e = 0.5\left(\frac{Pe^2}{5+Pe^2}\right)\frac{|\dot{m}_e|}{\dot{m}_e} \tag{4.10}$$

$$\beta_e = \frac{1+0.005Pe^2}{1+0.05Pe^2} \tag{4.11}$$

where $Pe = \frac{\dot{m}_e}{D_e}$, $D_e = \frac{\Gamma_e A_e}{\Delta x}$, $\dot{m}_e$ is the mass flux through the east face, A, is the surface area of the east face, and Δx is the distance in the x direction between nodes P and E.

After integration is performed using the EDS scheme, the resulting equation is an algebraic expression of the form:

$$A_p^{\Phi}\Phi_p = A_N^{\Phi}\Phi_N + A_S^{\Phi}\Phi_S + A_E^{\Phi}\Phi_E + A_W^{\Phi}\Phi_W + B^{\Phi} \tag{4.12}$$

Equation. (4.12) can be cast in a short form:

$$A_p^{\Phi}\Phi_p = \sum A_{nb}^{\Phi}\Phi_{nb} + B^{\Phi} \tag{4.13}$$

where the subscript *nb* refers to the nodes neighboring node P, i.e., W, E, S and N. In Equation. (4.12), the A's are the coefficients and B^{Φ} is the source term:

$$
\begin{aligned}
A_N^{\Phi} &= \beta_n D_n - \frac{\dot{m}_n}{2} + \alpha_n \dot{m}_n \\
A_S^{\Phi} &= \beta_s D_s + \frac{\dot{m}_s}{2} + \alpha_s \dot{m}_s \\
A_E^{\Phi} &= \beta_e D_e - \frac{\dot{m}_e}{2} + \alpha_e \dot{m}_e \\
A_W^{\Phi} &= \beta_w D_w + \frac{\dot{m}_w}{2} + \alpha_w \dot{m}_w \\
A_P^{\Phi} &= A_N^{\Phi} + A_S^{\Phi} + A_E^{\Phi} + A_W^{\Phi} - R^{\Phi}\forall + \frac{M_P}{\Delta t} \\
B^{\Phi} &= Q^{\Phi}\forall + \frac{M_P^0 \Phi_P^0}{\Delta t} \\
M_P &= \rho\forall
\end{aligned}
\tag{4.14}
$$

For a value of grid Peclet number greater than ten, $|Pe| \geq 10$, the exponential scheme (EDS) approaches the fully upwind differencing scheme (UDS). If the grid Peclet number is smaller than two, $|Pe| \leq 2$, it approaches the central difference scheme (CDS). So to use UDS, the values of the convective and diffusive weights should be set constant, say, α=0.5 and β=0.1, and to apply CDS , the values of the convective and diffusive weights should be fixed to, α=0 and β=1.

4.1.2 Grid Description

The aim of the finite volume method is to replace Equation (4.1) with a set of algebraic equations involving the values of Φ at a finite number of discrete control volumes and to preserve conservation throughout as noted in Section 4.1.1. The nodes are located inside the control volumes which collectively constitute the solution domain. For sake of

simplicity Figure 4.2 represents one example for a window system (glazing, seal and frame) with a straightforward geometry.

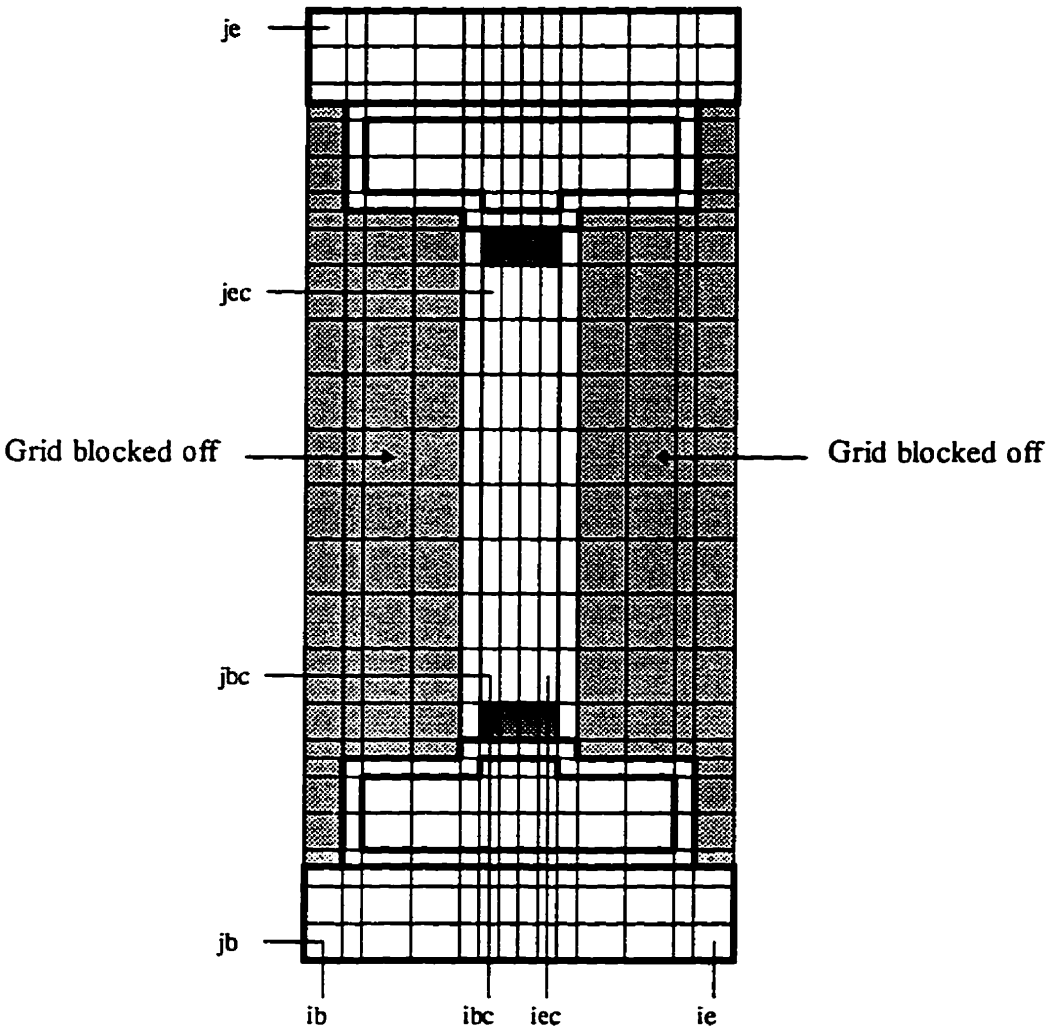

Figure 4.2: The Collocated Grid.

Note that the x-direction index, i, begins at i = ib and ends at i = ie. The cavity includes control volumes from i = ibc to i = iec. Similarly, the y-direction index runs from j =

jb to j = je over the entire problem domain, j = jbc to j = jec over the height of the cavity. To handle the irregular shape of the window system, as shown in Figure 4.2, some control volumes are blocked off, so that the remaining active control volumes form the desired shape.

Uniform grid spacings in both the x and y directions are used in the glazing cavities because secondary cells can be present in the flow and can be present everywhere. This precludes the use of a non-uniform grid. On the other hand, for the elements in the edge-seal and frame, either cavities or solid parts, any geometry might be expected, and the use of non-orthogonal, non-uniform grids would be suitable.

Since false diffusion depends on the control volume size, it is expected that different false diffusion levels would lead to different solutions (Markatos and Pericleous, 1984). To obtain high resolution in the computed results and ensure good accuracy without the contamination of false diffusion, the control volume sizes should be as small as possible, though not so small as to overtax the available computing facilities. As pointed out by Wright (1989) the grid aspect ratios (i.e., $A_{grid} = \Delta y/\Delta x$) used in the studies found in the literature (Raithby and Wong, 1981; Korpela *et al.*, 1982; Lee and Korpela, 1983; Ramanan and Korpela, 1989) ranged from 2.5 to 10. Throughout the current study the grid aspect ratio will depend on the insulated glazing unit (IGU) being simulated, varying between 5 to 20 (refer to section 5.1) and the number of control volumes will be determined by a grid independence study for each case studied.

4.1.3 Perturbation

At high Rayleigh numbers, $Ra > Ra_c$, transverse stationary cells may be expected. For $A = 40$, Wright (1989) has shown that if secondary cells are not present in the flow, the heat transfer across the cavity, for $Ra > Ra_c$, is lower than the measured values of ElSherbiny *et al.* (1982a) and Shewen (1986). When the secondary cells are generated the values for the heat transfer across the cavity agree with those measured within 1% to 5% (see Figure 4.3).

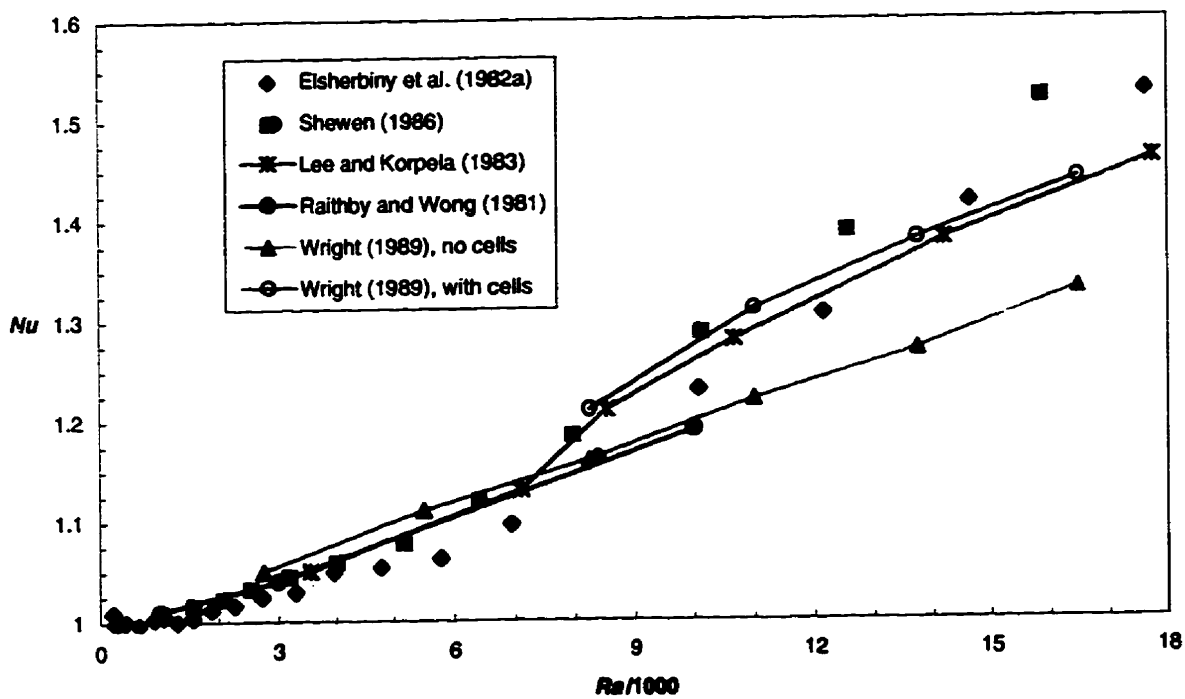

Figure 4.3: Comparison of Available Simulation and Measured *Nu vs. Ra* Results for the Vertical Cavity, A=40.

Several models have been able to resolve secondary cells in the vertical cavities (Roux *et al.*, 1979; Korpela *et al.*, 1982; Lee and Korpela, 1983; de Vahl Davis and Jones, 1984; Chait and Korpela, 1989; Ramanan and Korpela, 1989; Le Queré, 1990). It is well known (Patankar, 1980) that fully upwind differencing schemes (UDS) or hybrid schemes, as exponential differencing schemes, EDS, produce false diffusion in recirculating flows which may overwhelm the physical diffusion when convection effects are dominant. This effect can delay the onset of secondary instabilities

Most models capable of generating secondary cells are based on high order discretization schemes (Roux *et al.*, 1979; Korpela *et al.*, 1982; Ramanan and Korpela, 1989; Chait and Korpela, 1989; Le Queré, 1990). Due to the difficulty of applying boundary conditions and solving the conjugate problem they are not suitable to solve the window problem. Others claim to have avoided false diffusion by using a central differencing scheme (CDS) and uniform grids (Lauriat and Desrayaud, 1985a; de Vahl Davis and Jones, 1984; Wright, 1989), but only Wright (1989) could obtain secondary cells near the critical Rayleigh number. Although, from the results of the stability analysis of Bergholz (1978), applied to Equation (2.6), the secondary cells might be expected for Ra as low as 7,150 for $A = 20$, de Vahl Davis and Jones (1984) and Lauriat and Desrayraud (1985) have reported secondary cells for Ra as low as 2×10^4 and 2.2×10^4, respectively. However, Wright (1989) , perturbing the flow, has modeled secondary cells with Ra as low as the theoretical critical

value. The numerical model employed here uses the same approach used by Wright (1989), CDS when secondary cells are expected and EDS when secondary cells are not expected.

To model secondary cells, the same four step procedure used by Wright (1989) will be utilized, as follow:

1) establish the solution for a unicellular base flow using EDS, allowing large time step;
2) switch to CDS, reducing the time step to the maximum explicit time step;
3) perturb the flow by summing the existing flow field with a "perturbation" velocity field which resembles secondary cells alone and;
4) allow the iteration process to continue to convergence.

The perturbation field is generated following the steps below given by Wright (1989).

The height of a single secondary cell, l_c, expressed in terms of a wave-number, α_c, and width of the cavity, l, is

$$l_c = l\left(\frac{2\pi}{\alpha_c}\right) \tag{4.15}$$

where α_c is the interpolated value between the wave-numbers given in Lee and Korpela (1983). These are:

α_c=2.82	Gr=1.1x10^3
α_c=2.50	Gr=1.5x10^3
α_c=2.41	Gr=2.0x10^3
α_c=2.33	Gr=2.5x10^3

and $Ra = Pr \cdot Gr$. If $Gr < 1.1 \times 10^3$, α_c, is set to 2.82.

The number of cells, n_c, is

$$n_c = INT\left[(A - 10)\frac{\alpha_c}{2\pi}\right] + 2 \tag{4.16}$$

and the perturbation velocity components at the P point of the any control volume, u_c and v_c, are:

$$u_c = \frac{u_{max}}{\alpha_c A}(\Psi_S - \Psi_N) \bullet (je - jb + 1) \tag{4.17}$$

$$v_c = \frac{u_{max}}{\alpha_c}(\Psi_E - \Psi_W) \bullet (ie - ib + 1) \tag{4.18}$$

where the perturbation stream function, Ψ_c, is applied over the solution grid and scaled such that the maximum value of u_c would be half of the maximum value of u known in the unicellular base flow, u_{max}.. This scaling differs slightly from that presented by Wright (1989), where he used $u_c \leq u_{max}$.. The reason for this difference is that the secondary flow is weaker

than the unicellular base flow, so the velocities must be lower in the secondary flow than in the unicellular base flow which leads to a faster convergence.

The perturbation stream function (Wright, 1989) is given by

$$\Psi_c = -\frac{l}{2}\bullet\left(1 + \cos\left(2\pi\left(\frac{x}{l}-\frac{l}{2}\right)\right)\right)\bullet\left(1 - \cos\left(\alpha_c A\left(\frac{y}{h}-\frac{l}{2}\right)+n_o/e\pi\right)\right) \qquad (4.19)$$

where $n_{o/e}$=1 if n_c is odd, $n_{o/e}$=0 if n_c is even.

Equation (4.6) applies over the range

$$\frac{(h - n_c l_c)}{2} < y < \frac{(h + l_c n_c)}{2} \qquad (4.20)$$

Otherwise, near the ends of the cavity, $\Psi_c = 0$.

Wright (1989) pointed out that for Ra>1.4x10^4 the calculated values of Nusselt Numbers, Nu, are lower than those measured by ElSherbiny *et al.* (1982a) and Shewen(1986) (see Figure 4.2). Consequently, the simulation was not fully modeling all of the physical mechanisms of heat transfer. This discrepancy could be due to several factors as already seen in section 2.2.1. Among them the presence of tertiary cells, the appearance of unsteady cat's eyes and three dimensional effects would increase the heat transfer. Although, tertiary flows have only been visualized in oil by Elder (1965a), Seki *et al.* (1978a and 1978b), Chen and Thangam (1985) and Wakitani (1994) and numerically determined for Pr > 50 by de Vahl

Davis and Mallinson (1975), they are modeled in this work to verify whether they are present in the flow in range of the critical Rayleigh number. The reason for perturbing (modeling) the tertiary cells is because in that range neither the experiments of ElSherbiny *et al.* (1982a) nor Shewen (1986) have shown unsteady disturbance, and no work has been done to determine tertiary cells for *Pr* as low as for air. Also, the first appearance of the tertiary flow in the work of de Vahl Davis and Mallinson (1975) was far from the experimental critical *Ra*.

The procedure to generate the perturbation field for the tertiary flow will be similar to that producing the perturbation field for the secondary flow:

1) calculate l_c and n_c for the secondary flow;

2) find the number of tertiary cells , $n_t=n_c-1$. Here, the assumption is made that between two secondary cells there is one tertiary cell;

3) determine the new height of a single secondary cell, l_{cn}[2] and the height of the tertiary cell, l_t.

4) estimate the perturbation stream function,

where,

[2] the l_{cn} was thought to be 2.5 times l_t, because this was the scaling found by both Elder (54) and Seki *et al.* (58) in their visualization experiments.

$$l_{cn} = 2.5\,l_t \quad and \quad l_t = \frac{l_c}{\left(3.5+\frac{1}{n_c}\right)} \tag{4.21}$$

$$\Psi_c = -\left(1 + \cos\left(2\pi\left(\frac{x}{l}-\frac{1}{2}\right)\right)\right)\bullet\left(1 + \cos\left(2\pi\left(\frac{y^*}{l_{st}}-\frac{1}{2}\right)\right)\right)\bullet(-1)^n \tag{4.22}$$

and

$$y^* = y - \left(\frac{1}{2}(h - n_c l_c) + n_{ts} l_{cn} + n_{tt} l_t\right) \tag{4.23}$$

n_{ts}, n_{tt} are the number of times the secondary cells and tertiary cells were generated, $n=n_{ts}+n_{tt}$ and l_{st} is equal to l_{cn} or l_t depends on the cell that are being produced. The generation of the stream function for the secondary and tertiary cells alternates between the two. First a secondary, and then a tertiary cell is generated, then a secondary cell, and so on, until the last secondary cell is made;

5) evaluate the perturbation velocity components of the tertiary cells[3],

$$u_t = \frac{u_{max}}{5\alpha_c A}(\Psi_S - \Psi_N)\bullet(je - jb + 1) \tag{4.24}$$

$$v_t = \frac{u_{max}}{5\alpha_c}(\Psi_E - \Psi_W)\bullet(ie - ib + 1) \tag{4.25}$$

[3] the maximum velocities for the perturbation field of the tertiary flow were supposed to be 5 times less than that of the secondary flow, because the tertiary flow is weaker.

4.1.4 Boundary Condition Implementation

The numerical implementation of the boundary conditions presented in Section 3.3 is described here. The boundary conditions are approximated and expressed in the general form of Equation. (4.12), i.e.:

$$A_p^{\Phi}\Phi_p = A_N^{\Phi}\Phi_N + A_S^{\Phi}\Phi_S + A_E^{\Phi}\Phi_E + A_W^{\Phi}\Phi_W + B^{\Phi}$$

Fig. 4.4 shows a W Φ-control volume adjacent to the boundary of the problem domain. The boundary node P is situated on the boundary a distance one-half control volume dimension from node W. The n axis in the figure is the outward facing normal for the domain. The boundary conditions are expressed as algebraic equations for those control volumes. They are then "absorbed" in the algebraic equations for the adjacent control volumes within the boundaries. The same "absorption" process is also used to decouple the flow in each cavity from the solid boundaries, in which the momentum equations are only solved inside the cavity domain.

The boundary conditions for the governing partial differential equations of the problem are used to establish discrete equations for the boundary nodes. A general boundary condition at node P is:

$$C_{1P}\Phi_P + C_{2P}\left.\frac{\partial\Phi}{\partial n}\right|_P + C_{3P} = 0 \qquad (4.26)$$

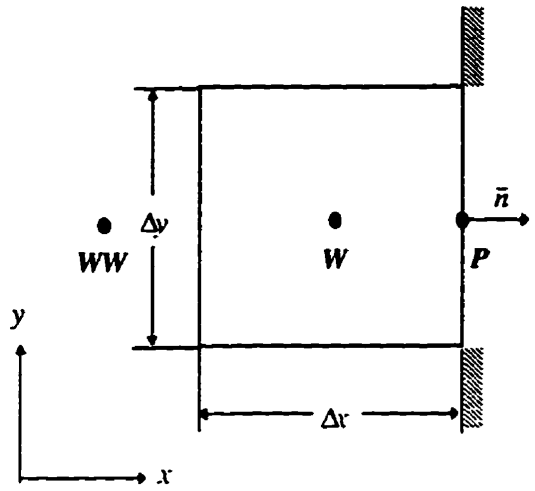

Figure 4.4: Boundary Control Volume.

This embodies all conditions for windows, as can be seen from table 4.3, where the subscript "*spec*" refers to boundary specified values.

Type	C_{1P}	C_{2P}	C_{3P}
Dirichlet	1	0	$-\Phi_{spec}$
Neumann	0	1	$-\left(\left.\frac{\partial\Phi}{\partial n}\right\|_{spec}\right)$
Robin	$-h$	$-\Gamma$	$h\Phi_{\infty}$
Flux	$-\frac{\rho u_w}{\Gamma}$	1	$\frac{J_{spec}}{\Gamma\Delta y}$

Table 4.3: Possible Window Boundary Conditions.

Using a backward difference approximation for the boundary gradient,

$$\left.\frac{\partial \Phi}{\partial n}\right|_P = \frac{2(\Phi_P - \Phi_W)}{\Delta r} \tag{4.27}$$

it is possible to cast Equation. (4.26) into the form of a discrete equation for the nodal value Φ_P in Fig. 4.1:

$$A_P^{\Phi}\Phi_P = A_W^{\Phi}\Phi_W + B^{\Phi} \tag{4.28}$$

where:

$$A_P^{\Phi} = C_{1P} + \frac{2C_{2P}}{\Delta r}$$
$$A_W^{\Phi} = \frac{2C_{2P}}{\Delta r}$$
$$B^{\Phi} = -C_{3P}$$

By formulating equations such as Equation (4.28) the boundary conditions may be stored along with the coefficients of the finite volume equations. To clarify the absorption at the boundaries, consider Fig. 4.4. The term Φ_E in the Equation (4.12) for the P node of the control volume within the domain adjacent to the boundary (W node in Fig. 4.4), is replaced by the boundary Equation (4.28).

Special treatment is needed for the radiation boundary conditions within cavities, since there are no discretization points *P* for temperature at the internal boundaries. This special treatment is presented in the next section.

4.1.4.1 Radiation Exchange

Due to the non-existence of discretization points *P* for temperature at the internal boundaries of the cavities, the long-wave radiation exchange will be included in the energy equation as a source term of the control volumes adjacent to the boundary. Equation (3.17) can be put in the matrix formulation

$$[A] \bullet [q] = [T] \tag{4.29}$$

and the irradiance q can be found by inverting the coefficient matrix A. The coefficient matrix depends only on the geometric configuration of the enclosure. Therefore the rate of energy generation per unit volume at any wall control volume is

$$\dot{S} = \frac{q}{\Delta x} \tag{4.30}$$

Also, the solar radiation transmitted to the cavities and absorbed by the walls is placed as a source term in Equation (4.30). The solar radiation absorbed by the outside surfaces of the window is placed as a source term for the semi-transparent medium in the centre control volume and for the opaque surfaces as flux in Table 4.3.

4.2 Solution Procedure

The numerical model can use three different schemes for modeling the convective and diffusive fluxes of energy and momentum at each control volume face (Patankar, 1980): first-order upwinding differencing scheme (UDS), central differencing scheme (CDS), and exponential differencing scheme (EDS). A non-staggered pressure grid arrangement was applied to the flow field. Several authors (Peric *et al.*, 1988; Yang *et al.*, 1990; Thé, 1993) note that this should not bring any disadvantage to methods using a staggered grid. In the presence of multicellular flows in a thermally driven cavity CDS is used, because EDS damps the appearance of these multicellular flows for a fairly wide range of parameters (Drummond *et al.*, 1991). Either EDS, CDS, UDS or a procedure that makes a smooth transition between UDS to CDS, or EDS to CDS, or UDS to EDS can be used. This permits the use of the more than one scheme in sequence to accelerate the rate of convergence. Also, it guarantees that the Courant condition for CDS, when generating multicellular flow, will be achieved at all iterations, i.e., after the formation of base flow is reached by using UDS or EDS, a transition scheme is used to get a smooth change, and then the flow is perturbed and CDS is used even for grid Peclet number greater than two, $|Pe| \geq 2$.

The numerical solution algorithm for obtaining a solution to the window problem is shown in Figure 4.5.

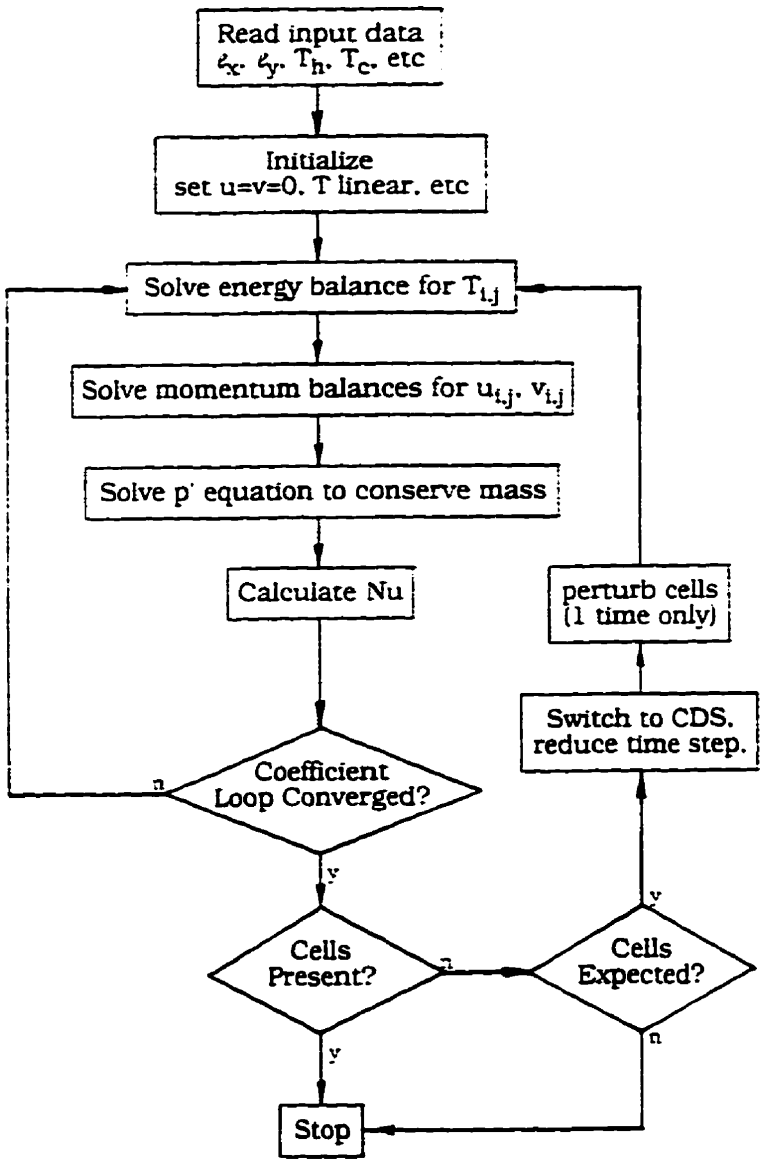

Figure 4.5: Solution Algorithm Flow Chart.

The numerical model consists of an algebraic equation for each variable and for each control volume. The coefficients and source terms of these equations depend on the other variables. This set of algebraic equations is non-linear, and a solution can therefore be obtained only through an iterative process. The iterative procedure marches implicitly through time using the false transient formulation (Mallinson and de Vahl Davis, 1973).

There are two iteration loops. In the main iteration (or coefficient update loop), outer loop, the coefficients are evaluated from the most recent solution fields and the set of linear equations for temperature (T) is solved iteratively, using a line by line solver based on an Alternating Direction Implicit (ADI) procedure, along with an over relaxation procedure due to Raithby (Stubley, 1990). Iterations are performed on the linear equations for T until a preset level of residual reduction (4 levels in all cases thereafter) or until a maximum number of iterations is reached. The residual, *rsd*, is calculated as:

$$rsd = \sum_{i=1}^{N_{cv}} \left| \sum A_{nb} \Phi_{nb} - A_P \Phi_P + B^{\Phi} \right|$$

where N_{cv} is the total number of control volumes. The residual, *rsd*, is a good indication of how well the linear equations are satisfied. When the residual criterion cannot be satisfied due to machine roundoff, a third criterion is used:

$$\Phi_P^{n+1} - \Phi_P^n \leq 10^{-4}$$

where the superscript $n+1$ refers to the current iteration, and n, to the previous one.

Within each coefficient update loop, an inner loop is called to solve the velocities equations, u and v, and the pressure equations, p, which corresponds directly to the SIMPLEC algorithm (Hutchinson and Raithby, 1986). The numerical solution of each of these variables is carried out using an ADI procedure, using the same criterion described for the temperature equations. An Additive Correction Method (Ramanan and Korpela, 1989; Hutchinson and Raithby, 1986), ACM, block correction is applied to speed the solution for p. Also, the ACM algorithm can be used to accelerate convergence for T, u, v when necessary.

The order of solution of the linear equations is:

Outer loop - Coefficient update loop

1. T equations

Inner loop - SIMPLEC

2. u and v equations

3. p equations

At the end of each outer loop iteration, steady state convergence is verified by comparing the relative maximum change T, u and v between two consecutive iterations:

$$\Phi_P^{n+1} - \Phi_P^n \leq 10^{-4}$$

Finally, the condition of steady state will only be satisfied if the error between the heat flow in and out of the window accomplish the following criteria:

$$\left| \frac{Q_{in} - Q_{out}}{Q_{out}} \right| \leq 10^{-5}$$

between two consecutive iterations and

$$Q_{in}^{n+1} - Q_{in}^n \leq 10^{-5}$$

for at least four consecutive iterations.

As stated before, to obtain steady state solutions a false transient method is employed. Large changes in coefficient update from on iteration to the next can lead to large oscillations in the evolution of the solution, resulting in convergence problems or even in failure to converge. To avoid this problem the time steps are selected small enough. It is worthwhile to mention that the time step for solving natural convection problems depends on the grid size and the Rayleigh number because of the weak coupling between momentum and energy equation due to buoyancy, that affects in turn the delicate u, v and p coupling. If the time step is too small the evolution of the solution is prone to oscillations due to decoupling between the energy and momentum equations, and consequently the decoupling in u, v and p

equations. The time step is obtained by multiplying the natural time scale (maximum time step allowed for numerical stability based on an explicit scheme) by a factor n, i.e.:

$$\Delta t = n\Delta t_{max}$$

The energy balance is applied over the entire problem domain with the thermal boundary conditions (See Figure 4.1) applied at the outer edges. This step in the coefficient update loop generates a temperature solution for all control volumes. However, all velocities at locations outside the cavity are set to zero and the velocity boundary conditions, used in solving balances to conserve momentum and mass, are applied at the walls of the cavity. Thus, the natural convection velocity field in the cavity is generated for non-uniform temperature distributions at the cavity walls.

Application of the energy balance across the composite problem domain required care to ensure that the heat flux is correctly calculated at the surfaces between materials of different thermal conductivities. The conductive heat flux at the bordering faces is calculated using the harmonic mean of the neighboring conductivities according to the procedure outlined by Patankar (1980).

4.3 Closure

A numerical model of a two-dimensional vertical or inclined window, filled with a radiatively non-participating gas, with internal and external radiative heat exchange, external convection and radiation has been described. The computer program will be structured such that all the radiative transfer can be bypassed enabling the significance of radiation to be determined. Also, for comparison purposes, isothermal walls, boundary conditions with no radiative effects, unicellular flow alone, among other cases will be simulated. The next chapter reports the assessment of the numerical model.

5 ASSESSMENT OF THE NUMERICAL METHOD

The purpose of this chapter is to examine the capabilities of the solution method described in the previous Chapters to model windows, with respect to accuracy, cost, and reliability. In order to fulfill this goal, code validation is divided into three stages, with increasing degree of complexity. Each stage is designed to examine and to validate a particular feature of the code. In Section 5.1 the pure natural convection problem is examined; then in Section 5.2 the conjugate problem (conduction coupled with natural convection); in Section 5.3 the interaction among surface radiation, natural convection and convection, which includes all modes of heat transfer present in a window system, is investigated; and finally, in Section 5.4 conclusions are given.

The numerical results are compared with experimental results where available. When an experimental method does not exist or results are inaccessible, the computed results are compared with numerical solutions obtained by other codes.

The model calls for a solution of the coupled two-dimensional equations of continuity, momentum, and energy. The solution method is the same as posed in Chapter 4 for an entire window system, along with the expression for the radiative flux. The addition of the boundary conditions for each case to these equations completes the mathematical formulation of the problem. The system of equations is solved numerically because a closed form analytical

solution is not possible. The control volume formulation for a collocated pressure grid arrangement is used to discretize the governing equations, with radiation as a source term. The SIMPLEC algorithm (Hutchinson and Raithby 1986) is employed to treat the coupling between pressure and momentum. The numerical code is named BRAVO, therefore, reference to the numerical model is by the name BRAVO.

5.1 Pure Natural Convection Problem in Enclosures

At this stage the code is required to solve the natural convection problem in enclosures for vertical isothermal walls, and either adiabatic or perfectly conducting horizontal walls. Also, the code capability to resolve secondary and tertiary cells is investigated.

5.1.1 Benchmark Solutions Comparison

To verify the accuracy, cost, and reliability of the convection model, two cases were chosen for comparison: an orthogonal grid - square cavity for the benchmark solutions of de Vahl Davis (1983), de Vahl Davis and Jones (1983) and Hortmann *et al.* (1990); and, a non-orthogonal grid - 45° inclined side walls for the benchmark solutions of Demirdzic *et al.* (1992).

Demirdzic *et. al.* (1992) point out that by assuming that the conservative equations for mass, momentum and energy, as given in Chapters 3 and 4, describe the laminar flow and heat transfer accurately, and that the Boussinesq approximation is valid, the numerical solutions are affected only by the following errors:

- discretizations errors (the difference between the exact solution of the correctly discretized equations on a given grid and the exact solution of the governing differential equations);
- convergence errors (the difference between the exact and the approximate solution of the discretized equations remaining after iterations are stopped); and,
- algorithmic and programming errors (errors due to incorrect discretization, erroneous implementation of boundary conditions, programming errors, etc.).

Both Hortmann *et al.* (1990) and Demirdzic *et al.* (1992), claim that their code was free of the third kind of error. The second is minimized in their calculations by iterating long enough for the variable values to be converged to six significant digits. Finally, as the first type of error depends on the discretization scheme and the grid used, they argue that by refining the grid enough they obtained an estimated error lower than 0.1%.

5.1.1.1 Orthogonal Grid - Square Cavity

In this section a test comparison with a benchmark problem proposed by de Vahl Davis (1983), de Vahl Davis and Jones (1983) and Hortmann *et al.* (1990) is presented. The

test case consists of a Boussinesq fluid of Prandtl number 0.71 (air) in an upright cavity flow with orthogonal grids (Figure 5.1).

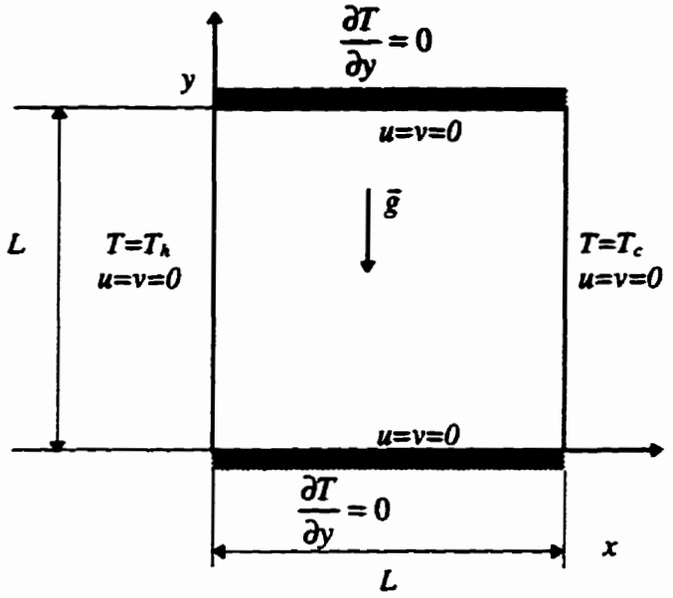

Figure 5.1: Geometry and Boundary Conditions for Square Cavity.

Both velocity components are zero on the boundaries. The horizontal walls are insulated, and the vertical side walls are kept at constant temperatures T_h and T_c, respectively. Gravity acts in the vertical direction.

In this comparison exercise, the following quantities are supplied:

u_{max} the maximum horizontal velocity on the vertical mid-plane of the cavity.

v_{max} the maximum vertical velocity on the horizontal mid-plane of the cavity.

Nu_{avg} the average Nusselt number throughout the cavity

The calculations start on a coarse grid and proceed to finer grids until the desired accuracy or maximum affordable storage is reached. They are performed in two sets of mesh refinements with consecutive grid refinement, i.e., the first set started with 10 x 10, than was refined to 20 x 20 , 40 x 40 until 80 x 80 control volumes and the second set started with 16 x 16 then was refined to 32 x 32 and 64 x 64 control volumes, totaling 7 different mesh refinements. This procedure of mesh refinement (doubling the number of control volumes in each direction) enables the use of Richardson extrapolation to obtain more accurate results, as done by de Vahl Davis (1983) and Hortmann *et al.* (1990). However, for this extrapolation to be accurate it is necessary that the two grids employed are fine enough to guarantee monotomic convergence with a known order, which is difficult to satisfy (see the discussion by de Vahl Davis about calculations for Rayleigh number 10^6).

The accuracy of solutions on various grids (i.e. grid dependence) is checked by comparing mean Nusselt Numbers defined as

$$Nu_{avg} = \frac{Q}{Q_c} \tag{5.1}$$

where Q is the actual heat flux across the cavity and Q_c is the heat flux that would result from pure conduction:

$$Q_c = \frac{\mu}{Pr}\frac{T_h - T_c}{L}L \tag{5.2}$$

The heat flux Q may be calculated by summing the convection and diffusion fluxes through the control volume faces along any grid line at x = constant.

The required results are furnished in Tables 5.1 to 5.4 and they are compared with the benchmark values. Only the results of the first set of mesh refinements (10 x 10, 20 x 20, 40 x 40 and 80 x 80) are presented for the benchmark comparison because they match the grid sizes reported by de Vahl Davis (1983) and Hortmann *et al.* (1990). The second set of grid refinement (16 x 16, 32 x 32, and 64 x 64) is used together with the first set to show the evolution of the number of iterations and time with grid size. In Tables 5.1 to 5.4 below BM is the grid independent value (or bench mark solution): 1) BM#0 for BRAVO; 2) BM#1 for de Vahl Davis (1983) and; 3) BM#2 for Hortmann *et al.* (1990). The grid independent value from this work was evaluated using the Equation (5.3) given by Hortmann *et al.* (1990), that corresponds to the Richardson extrapolation for second-order schemes. They clearly show the convergence to the benchmark solution for a more and more refined meshes. For Ra = 10^6, 10 x 10 and 16 x 16 control volumes, the mesh grid is too rough to reproduce - even qualitatively - the flow configuration.

$$\Phi = \Phi_k + \frac{1}{3}(\Phi_k - \Phi_{k-1}) \tag{5.3}$$

Grid	10 x 10	20 x 20	40 x 40	80 x 80	BM#0	BM #1	BM #2
u_{max}	3.6026	3.6392	3.6485	3.6455	3.6501	3.649	N/A
v_{max}	3.6875	3.6945	3.6897	3.6995	3.7028	3.697	N/A
Nu_{avg}	1.1329	1.1214	1.1187	1.1182	1.1181	1.118	N/A

Table 5.1: Calculated Values and Benchmark Results for $Ra = 10^3$.

Grid	10 x 10	20 x 20	40 x 40	80 x 80	BM#0	BM #1	BM #2
u_{max}	15.654	16.080	16.112	16.174	16.194	16.178	16.1802
v_{max}	17.876	19.493	19.594	19.634	19.647	19.617	19.6295
Nu_{avg}	2.4495	2.2957	2.2577	2.2490	2.2461	2.243	2.24475

Table 5.2: Calculated Values and Benchmark Results for $Ra = 10^4$.

Grid	10 x 10	20 x 20	40 x 40	80 x 80	BM#0	BM #1	BM #2
u_{max}	34.561	34.725	34.052	34.757	34.741	34.73	34.7399
v_{max}	76.003	66.793	68.856	68.665	68.601	68.59	68.6396
Nu_{avg}	5.5791	4.8929	4.6177	4.5457	4.5217	4.519	4.52164

Table 5.3: Calculated Values and Benchmark Results for $Ra = 10^5$.

Grid	10 x 10	20 x 20	40 x 40	80 x 80	BM#0	BM #1	BM #2
u_{max}	90.969	62.744	65.583	65.044	64.865	64.63	64.8367
v_{max}	198.26	214.35	223.95	218.38	218.05	219.36	220.461
Nu_{avg}	8.1830	9.5124	9.4301	8.9789	8.8285	8.800	8.82513

Table 5.4: Calculated Values and Benchmark Results for $Ra = 10^6$.

Complex flow predictions require the use of very fine grids if high numerical accuracy is demanded. However, standard iterative finite volume methods are known to converge

more and more slowly as the grid is refined; the number of iterations required for convergence increases, typically linearly, and the computing time therefore, typically increases quadratically. Computations on grids with more than 80 points in one space direction are hence extremely expensive, and are yet in many instances not accurate enough (Hortmann *et al.* 1990). The same trend for the evolution of the number of iterations and time with the increment of grid size as shown by Hortmann *et al.* (1990) is seen with BRAVO and is documented in Tables 5.5 and 5.6 running on a PC 486 DX4 100MHz.

Grid	10 x 10	16 x 16	20 x 20	32 x 32	40 x 40	64 x 64	80 x 80
iterations	124	128	134	135	163	311	532

Table 5.5: Evolution of Number of Iterations with Grid Size - Square Cavity.

Grid	10 x 10	16 x 16	20 x 20	32 x 32	40 x 40	64 x 64	80 x 80
time	24.56	59.43	1:47.43	6:55.79	14:36.39	1:12.6.02	5:18:54.40

Table 5.6: Evolution of Computational Time with Grid Size (h:m:s.1/100s) - Square Cavity.

5.1.1.2 Non-Orthogonal Grid - 45° Inclined Side Walls

A comparison with the benchmark solutions of Demirdzic *et al.* (1992) is presented in this section. The test case consists of a buoyancy-driven cavity flow with non-orthogonal grids designed by deforming the cavity to 45° (Figure 5.2). The inclined walls are kept at

constant temperatures T_h and T_c, respectively, while the horizontal walls are assumed adiabatic. Gravity acts in the vertical direction.

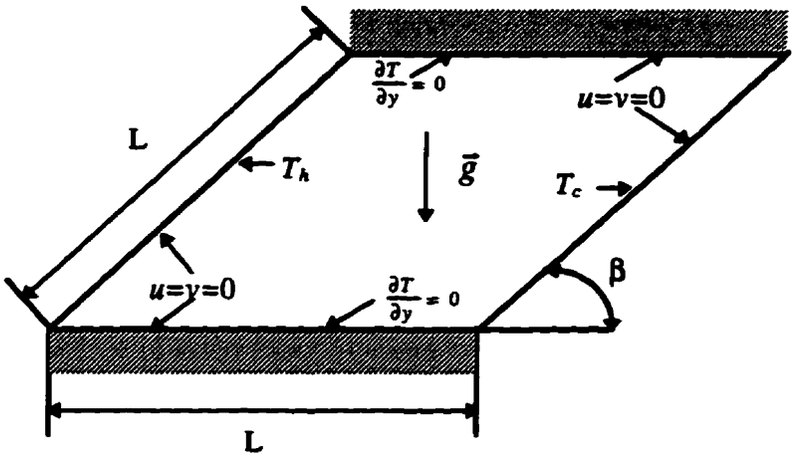

Figure 5.2: Geometry and Boundary Conditions for 45° Cavity.

The dimensions and fluid properties used are as follows: L=1, ρ=1, gravity constant g=1, expansion coefficient β=0.1, specific heat c_p=1, T_h=1 *and* T_c=0, so that the Rayleigh number is only a function of the viscosity and the Prandtl number:

$$Ra = \frac{\rho^2 g \beta L^3 \Delta T}{\mu^2} \qquad \Pr = \frac{0.1}{\mu^2}\Pr$$

Flows at $Ra=10^6$ are studied, for two values of the Prandtl number: Pr=0.1 and 10, corresponding to $\mu=10^{-4}$ and 10^{-3}, respectively.

Table 5.7 shows the calculated average Nusselt Number for the respective grids and benchmark results, showing convergence for more and more refined grids.

Grid	10 x 10	20 x 20	40 x 40	80 x 80	Benchmark
Pr=0.1	5.5660	6.4458	6.3919	6.0867	5.98493
Pr=10	6.2822	8.1107	8.0349	7.6938	7.58013

Table 5.7: Calculated Nu_{avg} and Benchmark Results for Pr=0.1 and Pr=10 - 45° Cavity.

5.1.2 Multicellular Flow

To examine the reliability of the code to generate secondary and tertiary cells near the critical Rayleigh number comparison with experiments and numerical results are presented

It is well known that second order schemes, like CDS, and first order schemes, like UDS, preclude the generation of secondary cells at the critical Rayleigh number, Ra_c (Chapter 2, Section 2.2.1). Higher order discretization schemes can generate cells naturally at Ra_c, but they are difficult to implement to solve complex configurations other than the natural convection problem due to the complexities in setting the boundary conditions as well as instabilities inherent in the discretization scheme. As pointed out by Wright (1989), knowing

that two or more solutions exist at lower *Ra*, it was thought that simulation might select a solution with secondary cells if it were given a "push", i.e., overriding the damping effect introduced by the discretization scheme. The procedures to generate secondary and tertiary cells are presented in Chapter 4, Section 4.1.3. These procedures allow the generation of secondary cells as low as the theoretical critical *Ra* using CDS, but the cells are damped when UDS or EDS schemes are used due to the upwind formulation in both schemes which introduces a higher numerical diffusion for recirculating flows.

A grid size study is conducted on computational meshes ranging from 10 to 40 control volumes in the horizontal direction, with grid (cell) aspect ratio 5, cavity aspect ratio 10, 20, 30 and 40, $Pr = 0.71$ for $Ra = 10^4$ and, $Pr = 100$ for $Ra = 10^5$. For these different grids the difference in total heat transfer to the warm wall and the maximum velocities and temperature is less than 1% for all case for a grid consisting of 30 and 40 control volumes. Therefore, the grid with 30 control volumes in the horizontal direction for any aspect ratio cavity was selected for the calculations unless otherwise noted. The nodes are regularly spaced in order to assist capturing the secondary cells when present. It is noticed that the grid is fine enough to resolve the thermal and velocity boundary layers near the wall when they are present.

5.1.2.1 Secondary Cells

The importance of secondary cells with respect to code validation is critical as they can lead to complex window surface temperature profiles. In effect, if a code can correctly capture these more complex temperature profiles then confidence in that code's ability to model windows is increased substantially. The validity of incorporating secondary cells has already been confirmed by comparison with measured heat transfer rates (Wright and Sullivan 1994).

In order to assess the accuracy of BRAVO, Nusselt Number results are compared against two sets of measured results (ElSherbiny *et al.*, 1982a and Shewen, 1986), Figure 5.3, and numerical results of Wright (1989), Table 5.8. Furthermore, a plot of Nu as a function of *Ra* including the results of ElSherbiny *et al.*(1982a), Shewen (1986), Raithby and Wong (1981) and Lee and Korpela (1983) is presented in Figure 5.4.

	Nu_{avg} without Cells		Nu_{avg} with Cells	
Ra	Wright	BRAVO	Wright	BRAVO
2,746	1.05	1.05	N/A*	N/A
5,493	1.11	1.11	N/A	N/A
6,413	1.12	1.12	N/A	N/A
6,800	1.13	1.13	1.15	1.14
8,239	1.16	1.16	1.21	1.19
10,102	1.20	1.20	1.28	1.24
10,986	1.22	1.22	1.31	1.27
13,732	1.27	1.28	1.38	1.34
16,479	1.33	1.33	1.44	1.40

*N/A = not applicable

Table 5.8: *Nu vs. Ra* Comparison for BRAVO and Wright's Results, A=40.

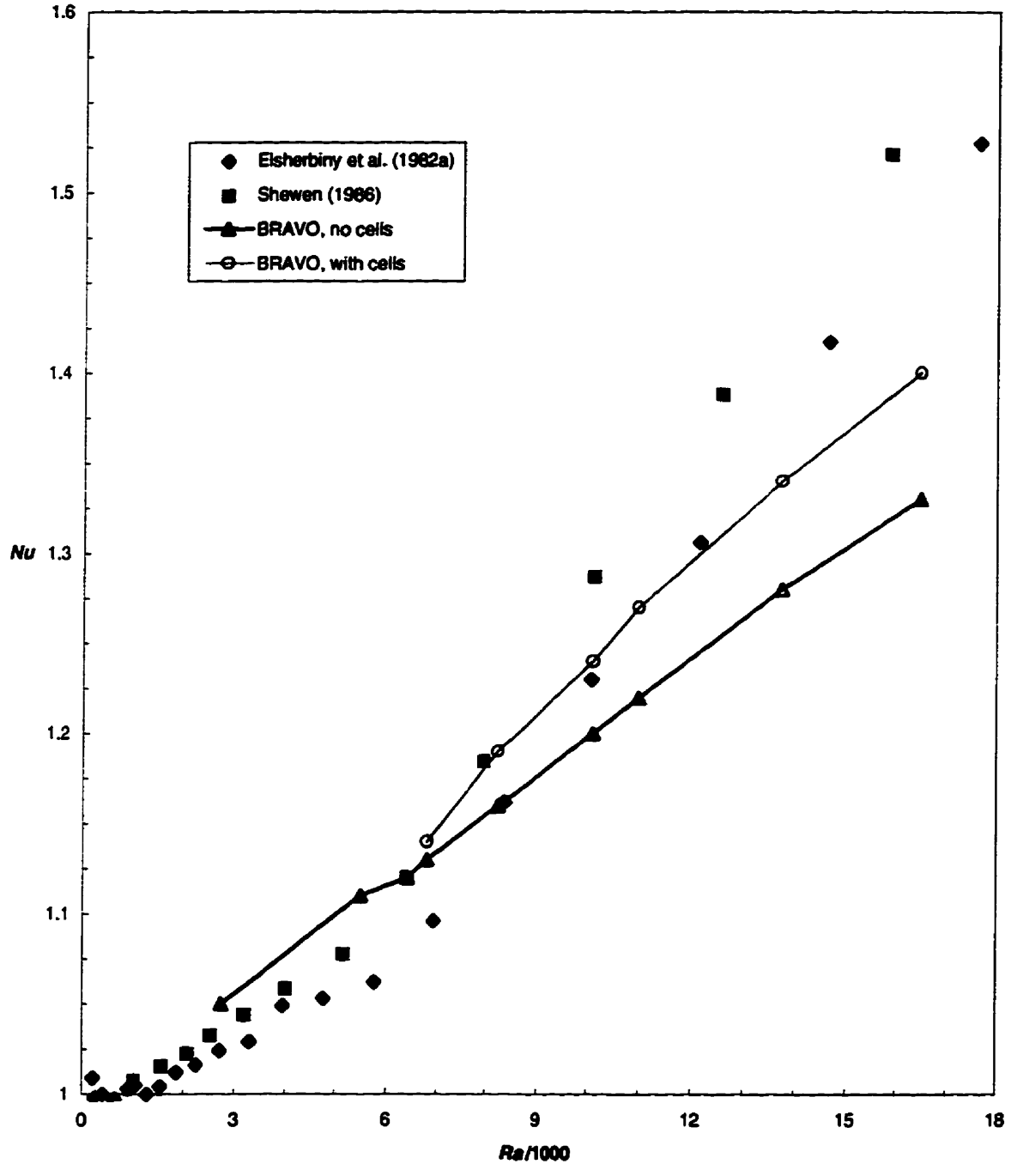

Figure 5.3: Comparison of BRAVO Results and Measured *Nu vs. Ra* , *A*=40.

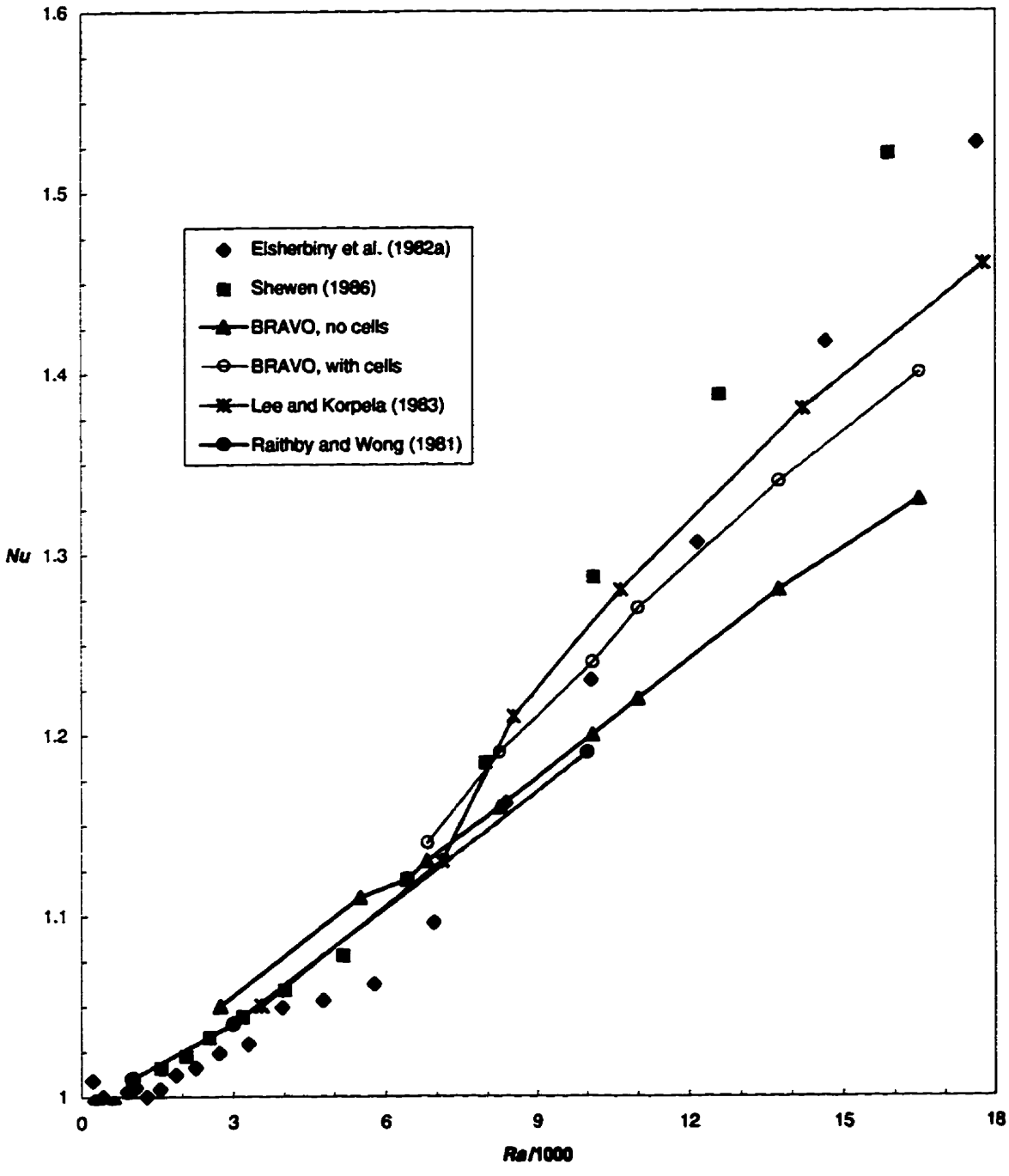

Figure 5.4: *Nu vs. Ra* Results of Available Simulations and Measurements for A=40.

Several observations can be made regarding the data shown in Figure 5.4 and they are fully discussed in Wright's 1989 work. Values of Nu_{avg} calculated with secondary cell generation agree with the numerical results of Raithby and Wong (1981) and Wright (1989) to about 1%. Also they agree to about 1% and 5% or less with the measured data of Shewen (1986) and ElSherbiny *et al.* (1982a) until the critical Rayleigh number, Ra_c is reached, at which point values about 6% and 10% lower than the data of ElSherbiny *et al.* (1982a) and Shewen (1986) for $Ra > Ra_c$ until $Ra > 10^4$ are seen. These three sets of results, Wright (1989) and BRAVO, closely follow the results of Lee and Korpela (1983) (also with cells) with discrepancy being 2% or less. At $Ra > 10^4$ these three sets of results begin to depart from the trend of the measured data, and fall bellow the measured data of ElSherbiny *et al.*(1982a). For $Ra > 10^4$ the numerical simulations are not fully modeling all the physical mechanisms of heat transfer. One reason could be the presence of tertiary cells as discussed in Section 5.1.2.2.

The agreement between the numerical simulations and experimental results indicates that the numerical simulations are capturing (modeling) all heat flow and heat transfer mechanisms for natural convection in cavities in the range of Ra that occur in windows, $Ra > 6 \times 10^3$ to $Ra < 10^4$ (Wright 1989). The ability to model secondary cells enables BRAVO to model accurately heat fluxes for $Ra > Ra_c$ until $Ra \approx 10^4$. It is concluded that the two-dimensional simulation of the natural convection flow in a cavity can be used to better understand, both qualitatively and quantitatively, the physical mechanisms involved.

5.1.2.2 Tertiary Cells

In the previous Section for $Ra > 1.4 \times 10^4$ the calculated values of Nusselt Numbers, Nu, are lower than those measured by ElSherbiny *et al.* (1982a) and Shewen(1986) (see Figure 5.4). Consequently, the simulation is not fully modeling all of the physical mechanisms of heat transfer. This discrepancy could be due to several factors as already seen in Section 2.2.1, among them the presence of tertiary cells, the appearance of unsteady cat's eyes and three dimensional effects could increase the heat transfer. Although tertiary flows have only been visualized in oil by Elder (1965a), Seki *et al.* (1978a and 1978b), Chen and Thangam (1985) and Wakitani (1994) and numerically determined for $Pr = 1000$ by de Vahl Davis and Mallinson (1975), they are modeled in this work to verify whether they are present in the Rayleigh number flow of windows and for air Pr. The reason tertiary cells are suspected is because in this range neither the experiments of ElSherbiny *et al.* (1982a) nor Shewen (1986) have shown unsteady disturbances, and no work has been done to determine the regime for tertiary cells for Pr number as low as that for air. Also, the first appearance of tertiary flow in the work of de Vahl Davis and Mallinson (1975) was far from the experimental critical Ra. Table 5.9 summarizes the aforementioned results and BRAVO calculations. It can be seen, that BRAVO can model tertiary cells near critical Rayleigh number, Ra_t, within experimental error, in contrast to de Vahl Davis and Mallinson (1975) in which tertiary cells are modeled far from the tertiary critical Rayleigh number (they did not use any provision to perturb the flow).

A flow in a cavity filled with air and aspect ratio 40 is perturbed by superimposing a tertiary flow, in the same fashion that was done for the secondary flow, in the following range of Rayleigh numbers, $1.5 \times 10^4 < Ra < 2.0 \times 10^4$. For this range of Ra the cells perturbed die out in the course of converging to a solution.

Works	Pr	A	Ra_t
Elder (1965a)	1000	10-20	3.0 Ra_c
Seki et al. (1978b)	480	15	3.0×10^5
Chen and Thangam (1985)	160	15	2.5 Ra_c
Wakitani (1994)	50	15	1.7×10^6
	125	10	1.0×10^6
	125	15	1.8×10^6
	900	10	8.5×10^6
de Vahl Davis and Mallinson (1975)	1000	10	9.4×10^6
BRAVO	55	15	1.8×10^6
	125	15	1.9×10^6
	793	10	8.9×10^5

Table 5.9: Summary of Values for Critical Rayleigh Number for Onset of Tertiary Flow.

Although BRAVO has been shown to be able to model tertiary cells for $Pr \geq 50$ near the critical Rayleigh number for tertiary cells, Ra_t, it is not able to do the same for $Pr = 0.71$ (air). Therefore, it can be concluded that tertiary flows does not exist for air Prandtl number ($Pr = 0.71$), or that any tertiary flow in the cavity is so weak that BRAVO is not able to reproduce it. It is more likely the flow is going to transition to turbulence. Seki *et al.* (1978b)

in their visualization experiments pointed out that when tertiary cells appear, which is created by shear stress between two secondary cells, does not increase substantially the heat flow between the two vertical walls in contrast to when the flow changes to transition type flow. Consequently, further work has to be done to determine the reasons for the existing discrepancies between numerical and experimental results for high *Ra*.

5.2 Conjugate Heat Transfer Problem - Natural Convection and Conduction Interaction

In the last section the ability of BRAVO to solve the natural convection problem was demonstrated. In this section one further step is performed, to show the capability of BRAVO in resolving the conjugate heat transfer problems, the solution of conduction and natural convection simultaneously. In other words, to verify the ability of BRAVO to calculate the heat transfer in an entire window system taking into account the natural convection in cavities (multi-pane windows, with/without cavities in the frame) and the conduction in solid components.

5.2.1 Pure Conduction

Before solving the conjugate heat transfer problem, the ability of BRAVO to solve pure conduction is examined in this section. The heat transfer in two different edge-seal systems using foam and aluminum spacers are calculated and compared with experimental results (Fraser *et al.*, 1993). The experimental data are obtained in a guarded heater plate apparatus (Wright, 1989) and the numerical results calculated using FRAME 3.0 (Enermodal, 1992), a commercial conduction code used to evaluate frame and edge-glass heat transfer. These two spacers, foam and aluminum, are chosen for comparison because in all cases presented in the next sections of this chapter and Chapter 6 either one or the other of these spacers is used.

The purpose of this section is two-fold, first to examine the accuracy of the code for pure conduction, and second to show the capability of the code to model new edge-seal designs. The calculation of the heat flux through the spacer by itself could be misleading (Fraser *et al.*, 1993 and Wright *et al.*, 1994) due to the two-dimensional nature of the heat transfer path when the spacers are integrated into window systems. A sketch of a foam and an aluminum spacer are shown in Figure 5.5.

As pointed out by Wright (1989), thermal resistance testing is carried out using a guarded heater plate apparatus. The numerical calculations are performed using the edge-seal configuration shown in Figure 5.6 for the foam spacer, which is similar to that for the

aluminum spacer. The configuration consists of two neoprene mats, two glass sheets, a spacer, and sealant.

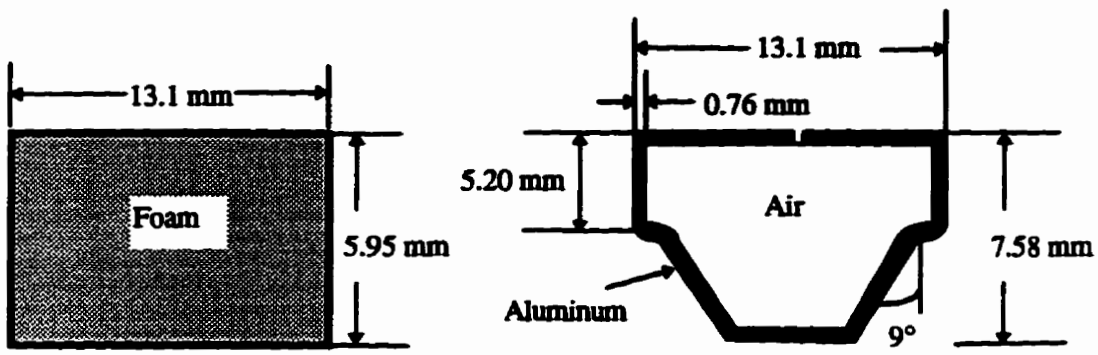

Figure 5.5: Typical Edge-Seal Design for Aluminum and Foam Spacers.

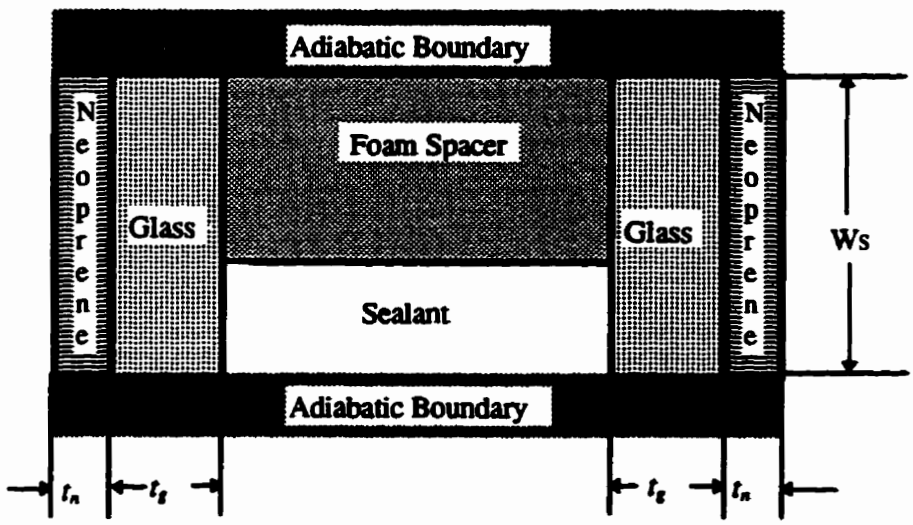

	Foam	Aluminum
Ws [mm]	12.30	12.70
t_g [mm]	4.75	3.96
t_n [mm]	1.59	3.18

Figure 5.6: Foam Edge-Seal Configuration.

As a preliminary calculation a sensitivity analysis for the aluminum spacer is made. The original geometry of the spacer is modeled and compared with a spacer of rectangular shape. The difference in heat flux is in the third decimal place. Consequently, the rectangular shape is used for remaining comparisons.

A second set of calculations are made modeling only conduction in the cavity, then conduction and convection without radiation and finally, conduction, convection and radiation (Table 5.10). Table 5.10 presents a comparison of the two numerical codes, BRAVO and FRAME 3.0, and the measured results for the heat transfer in foam and aluminum spacers. It reveals that the BRAVO results are in better agreement with experimental results than for FRAME 3.0 calculations, but the calculation error of both programs relative to the experimental results is only marginal. The grid size used in BRAVO was fine and the convergence criteria was tight, thus leading to a better agreement with the experimental results.

First the spacer is modeled for conduction only either without (sample #1), or with (sample #2) contact resistance between the glass sheet and the aluminum spacer. An effective conductivity obtained in FRAME 3.0 is used to account for convection and radiation effects. It is found that with no contact resistance the error is 7% and with a contact resistance the error is around 1% compared with the experimental result. The same finding was reported by Fraser *et al.* 1993, hence for all other simulations the contact resistance is modeled. In sample

#3 only pure conduction is modeled in the cavity of the aluminum spacer. The actual air conductivity is taken without accounting for the radiation and convection effects. The difference between samples #2 and #3 is in the second decimal place with a relative error of 0.00515% (see table 5.10). Thereafter, samples #4 - conduction, convection and no radiation and #5 - conduction, radiation, and convection are simulated. The greatest error found is between sample #3 and #4, and is only 0.02%. It can be concluded that a small cavity in the vicinity of highly conductive spacers can be simulated using conduction only without considering an effective conductivity.

Spacers	ΔT [°C]	q [W/m^2] Exper	q [W/m^2] FRAME 3.0	q [W/m^2] BRAVO
Aluminum	18.70	372.2	376.1	368.71
sample #1①	18.70			398.73
sample #2②	18.70			368.66
sample #3③	18.70			368.64
sample #4④	18.70			368.64
sample #5⑤	18.70			368.71
Foam	18.69	187.9	190.0	186.10

① sample #1 - conduction only with effective conductivity and no contact resistance;
② sample #2 - conduction only with effective conductivity and contact resistance;
③ sample #3 - conduction only with air conductivity and contact resistance;
④ sample #4 - conduction, convection with no radiation and contact resistance;
⑤ sample #5 - conduction, convection, radiation and contact resistance.

Table 5.10: Results of BRAVO, FRAME 3.0 and Guarded Heater Plate Apparatus.

5.2.2 Conjugate Problem

Although in the previous section natural convection and conduction are solved simultaneously (samples #4 and #5) the ability of BRAVO to solve the conjugate problem has not yet been shown. In this section the ability to model the conjugate problem is proven. The conjugate problem, as demonstrated by ElSherbiny *et al.* (1982b) and Kim and Viskanta (1985), is important in the thermal analysis in windows. They have shown that all resistances (thermal boundary conditions) throughout the enclosure are relevant to natural convection heat transfer in the cavity.

A set of five runs is made with BRAVO and compared with Wright's work (1989) for cavity aspect ratio, A=40, width 0.0127 mm and $6 \times 10^3 \leq Ra \leq 1.2 \times 10^4$. The same grid, same numerical scheme (CDS), and same convergence criteria are used by both programs. The results are compared and for all runs the errors are less than 1% for heat flux through the hot wall.

5.3 Interaction of Conduction, Natural Convection, and Radiation

In the previous two sections the ability of BRAVO to solve pure natural convection, Section 5.1, and the conjugate heat transfer problem, Section 5.2, was verified. In this section a third degree of complexity is added to the numerical method, non-participating radiative heat transfer. Therefore, BRAVO is now able to tackle the window system heat transfer problem predicting thermal and solar radiative heat transfer together with viscous fluid flow and conduction heat transfer. Radiation, convection, and conduction interact at fluid boundaries only, hence, the working fluid is non-participating. Hottel's crossed string rule (Siegel and Howell, 1981) is used for the automatic generation of the geometric exchange factors.

The purpose of this section is to assess and present numerical results concerning buoyancy-driven flow due to differential wall temperatures and radiant energy deposition in a window's solid media.

Radiative heat transfer is in general quite complex. Fortunately, there are many situations where complete generality is not required, and simplifying assumptions can be introduced:

1. The method employed here for thermal radiation is limited to non-participating fluids, to diffuse gray radiation exchange between surfaces in all cavities, and to specular reflections between surfaces when the glazing cavities are rectangular. The radiosity method presented in Siegel and Howell (1981) is used to solve the radiation interchange.

2. Solar radiation is considered in the analysis method by making the approximation that the spectral wavelengths of the diffuse and beam radiation are mutually exclusive. The solar beam radiation absorbed by any surface is determined by either Edwards' embedding technique (Edwards 1972) or by a ray tracing technique for normal or off-normal beam radiation. When diffuse radiation is considered and the ray tracing technique for beam solar radiation is being used the radiosity method is employed to solve the radiation interchange. The model is limited to either a double or a triple glazed unit for off-normal radiation if the ray tracing technique is being used, and diffuse gray radiation exchange between surfaces for diffuse solar radiation.

3. In addition, the models (solar and thermal radiation) do not account for full or partial blockage of surfaces, except for the case of a window with blockage in the center of the cavity when only thermal radiation is present.

Although the problem of radiation-natural convection interaction in enclosures, filled with a radiative participating medium, has been the subject of considerable research effort (Chapter 2, Section 2.5), only a few studies deal with the effect of radiation exchange between surfaces of an enclosure containing a non-participating fluid exposed to solar radiation. None

of them, to the knowledge of the author, deals with the interaction of radiation-conduction-natural convection in a narrow enclosure with more than one subsequent semi-transparent wall, for either normal or off-normal solar radiation.

A grid size study is conducted on computational meshes ranging from 15 to 40 control volumes in the horizontal direction, for cavity aspect ratios ranging from 20 to 100, with grid aspect ratios 5 and 10, and width 12.7 mm. The difference in total heat transfer (also Nusselt number) on the warm wall and, the maximum velocities and temperature are less than 1% between 30 and 40 meshes (as seen before, Section 5.1.1.1) for cell aspect ratio 5. Therefore, a grid with 30 control volumes in the horizontal direction with any cavity aspect ratio and cell aspect ratio 5 is selected for the calculations. The nodes are regularly spaced in order to capture the secondary flow when present. The iterations are terminated when the heat gain matches the heat loss to within 1×10^{-4} % and the velocities and temperature fields did not change in the fourth decimal place, or when a pre-determined number of iterations was reached and yet the convergence is considered satisfactory (the error between heat gain and heat loss is less than 10^{-2}%).

5.3.1 Thermal Radiation Interaction

The purpose of this section is to show that BRAVO can model surface to surface thermal radiation. BRAVO simulations are compared with Wright's (1989) numerical and

experimental results. The seven glazing systems tested by Wright (1989) were simulated in order to assess BRAVO. The samples cover a wide range of thermal resistances for seals, from highly insulating foam, an intermediate thermal resistance corrugated strip edge-seals, and finally, a highly conductive aluminum spacer bar. All but one had low-e coatings and two units had argon as a fill gas. Details of the sample sets are given in Table 5.11.

Sample	ΔT [°C]	lx [mm]	W_{seal} [mm]	k_{seal} [W/mK]	t_n [mm]	t_g [mm]	ε_{le}	ε_{seal}	Aspect Ratio	Fill gas
#1	18.88	12.13	9.53	0.520	3.175	3.94	0.840	0.827	50.8	air
#2	19.39	12.41	9.53	0.530	3.175	2.84	0.096	0.827	49.6	air
#3	19.12	14.12	11.05	2.560	1.524	3.30	0.047	0.054	43.4	argon
#4	11.38	11.96	11.30	2.120	3.175	3.91	0.094	0.054	51.2	argon
#5	27.42	16.00	25.40	0.035	1.524	5.59	0.070	0.054	36.5	air
#6	27.34	13.00	25.40	0.035	1.524	5.59	0.070	0.054	44.9	air
#7	14.86	13.00	25.40	0.035	1.524	5.59	0.070	0.054	44.9	air

Table 5.11: Details of Samples - Thermal Radiation Interaction.

Further details are reported by Wright (1989). Table 5.12 shows the results of the measured heat flux, for the top, middle, and bottom of the glazing systems corresponding to the location of the three guarded heater plates where the heat flux is experimentally metered. The experimental results and the two sets of calculated results are presented.

Although, both codes use the same discretization scheme to simulate the samples and the radiation models of both code produce similar results for an evacuated cavity (0.1%), BRAVO is found to agree slightly better than Wright's code with the guarded heater plate measurements, i.e. the heat flux is evenly distributed over the three heater plates, falling near the experimental error of 10%, except for the units with argon fill gas (units #3 and #4). The differences between the two calculations can only be explained by differences in better grid refinement for the neoprene mats and glass sheets (the grid size is the same for the cavity) and the tighter convergence criteria used in BRAVO. The discrepancies in units #3 and #4 could be due to small difference in the calculated physical properties for the argon, or by the choice of reference temperature which in turn alters the heat transfer results. To verify the magnitude of the error introduced by the non-adiabatic boundary conditions at the ends of the cavity an extra piece of foam is placed on the bottom and top of the glazing system along the total width of the neoprene mats, for the glass sheets and the edge seals of unit #7; the unit is called unit #7b. This modification gives a little improvement in the calculated heat of the cavity, yielding 28.4 W/m^2 (-12.07%) in the top and to 38.7 W/m^2 (0.00%) in the bottom of the cavity. The heat flux at the center of the cavity remains the same. Although there is a slight change in the bottom and top heat fluxes when more insulation is added to the ends of the cavity, it is insufficient to explain the discrepancies between the measured values and calculated results.

Sample	Position	Measured [W/m^2]	BRAVO [W/m^2]	Error [%]	Cells	Wright 1989 [W/m^2]	Error [%]	Cells
#1	top	96.9	96.4	-0.51	0	90.1	-7.02	0
	middle	95.3	96.5	1.26		89.4	-6.19	
	bottom	105.7	104.5	1.13		96.7	-8.51	
#2	top	49.0	46.1	-5.91	0	45.1	-7.96	0
	middle	47.0	46.4	-1.27		44.1	-6.17	
	bottom	58.9	56.4	-4.24		55.0	-6.62	
#3	top	32.1	31.0	-3.43	16	33.5	4.36	16
	middle	28.7	30.7	6.97		28.0	-2.44	
	bottom	45.7	43.5	-4.81		45.6	-0.22	
#4	top	24.4	22.9	-6.14	0	24.5	0.41	0
	middle	19.7	20.1	2.03		19.9	1.02	
	bottom	27.7	25.0	-9.74		27.1	-2.17	
#5	top	56.5	48.1	-14.86	10	44.9	-20.53	10
	middle	62.7	56.4	-10.05		56.1	-10.53	
	bottom	89.0	82.3	-7.52		87.2	-2.02	
#6	top	60.8	53.1	-12.66	16	50.2	-17.43	17
	middle	61.2	59.0	-3.59		59.6	-2.61	
	bottom	83.7	77.5	-7.40		82.6	-1.31	
#7	top	32.3	28.0	-13.31	0	26.6	-17.65	0
	middle	30.6	30.0	-1.96		30.2	-1.31	
	bottom	38.7	36.5	-5.68		38.7	0.00	
#7b	top	32.3	28.4	-12.07	0			
	middle	30.6	30.0	-1.96				
	bottom	38.7	38.7	0.00				

Table 5.12: Calculated and Measured Glazing System Heat Flux Results.

5.3.2 Solar Radiation Interaction

To validate BRAVO in relation to the interaction of radiation, conduction and natural convection when solar radiation is present, no data was found in the literature showing local effects in the fluid flow and in the heat transfer mechanisms (see Section 2.2.1.4). Experimental and numerical results of solar heat gain factor (*SHGF*), an averaged quantity, for a set of nine window samples (Harrison and Wonderen, 1994) are therefore used to verify BRAVO. The *SHGF* used together with the window's thermal transmittance (*U-factor*) permits comparative ranking of fenestration systems, calculating Energy Rating (ER) numbers, and determining the annual energy performance.

The nine window samples selected represent a broad range of insulating glazing systems that include clear and heat absorbing glass, reflective and spectrally selective coatings. All samples are specified to be double-glazed air-filled sash units fitting in a common wood casement frame, see Figure 5.7. Details of the nine glazing systems are given in Table 5.13.

Sash No.	Glazing System
S1	Clear / Clear
S2	Clear / Pyrolytic low-E, ε=0.2
S3	Clear / LoE-178, ε=0.08
S4	Clear / LoE Sun, ε=0.1
S5	LoE Sun-145, ε=0.1 / Clear
S6	Evergreen Tinted / Clear
S7	Reflective Metal SS-114 / Clear
S8	Clear / Low-E^2-171, ε=0.04,
S9	Evergreen Tinted / Pyrolytic Low-E, ε=0.2

Table 5.13: Description of Test Glazing Systems.

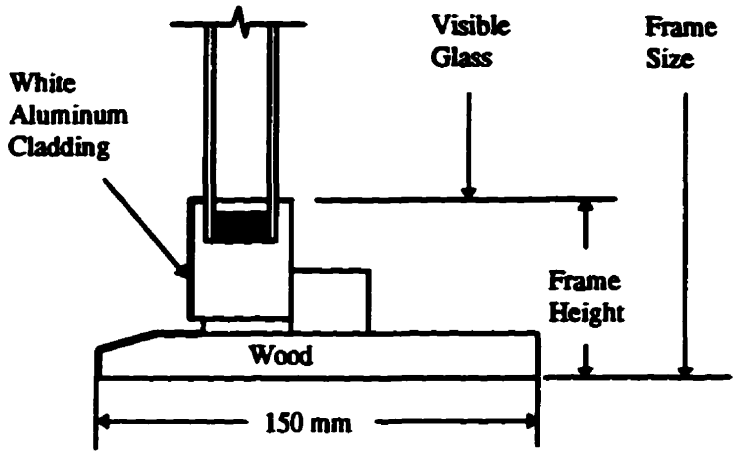

Figure 5.7: Test Frame Sash Cross Section.

The *SHGF* measurements were performed at the CANMET Window Test Facility (Harrison and Wonderen, 1994) and the average measurement uncertainty was ± 4.9%. They did numerical simulations using the VISION/FRAME computer program package (for a description of these programs see Section 2.1.5). Results for the nine windows are presented in Table 5.14.

The results shown in Table 5.14 indicate good agreement among measured results and those calculated values using FRAME/VISION and BRAVO. They agree to about 2.5% or less for samples S1 to S5 and S9, 5.3% for S6, 19% for S7, and 12% for S8. The BRAVO results are consistently higher than those from FRAME/VISION. This can be explained by the approximation used by FRAME to calculate the *SHGF* (see Harrison and Wonderen,

1994). The values of center-glass *SHGF* calculated by BRAVO are nearly the same as those calculated by VISION as expected because both programs use the Edwards' embedding technique to calculate *SHGF*.

Sash No.	Solar Heat Gain Factor		
	Measured	VISION/FRAME	BRAVO
S1	0.50 ± 0.02	0.49	0.495
S2	0.48 ± 0.02	0.46	0.468
S3	0.41 ± 0.02	0.40	0.404
S4	0.36 ± 0.02	0.35	0.356
S5	0.21 ± 0.02	0.21	0.212
S6	0.34 ± 0.02	0.31	0.322
S7	0.12 ± 0.02	0.09	0.097
S8	0.29 ± 0.02	0.32	0.325
S9	0.30 ± 0.02	0.29	0.296

Table 5.14: Summary of Results of Solar Heat Gain Factors.

5.4 Closure

The solution method described in Chapters 3 and 4 and coded in BRAVO proves satisfactory to model the heat transfer and fluid dynamics in fenestration systems. The following conclusions about BRAVO's performance in modeling glazing systems can be drawn from the results of this chapter:

- the accuracy and reliability is satisfactory to model natural convection alone in orthogonal and non-orthogonal grids, as shown in the comparison with bench mark solutions, where errors are lower than 10^{-2}%;
- the ability to correctly model secondary and tertiary cells by perturbing the flow is demonstrated;
- although the capability to model tertiary flows for $Pr \geq 50$ is proven, tertiary cells cannot be sustained for $Pr = 0.71$ (i.e. air), aspect ratio 40, and $Ra > 10^4$. This fact needs further investigation to prove whether tertiary cells are present in a cavity filled with air for aspect ratio 40 and $Ra > 10^4$;
- in modeling aluminum spacers, fine geometric details, convection, and radiation all are not major factors in controlling the net heat flux. On the other hand, contact resistance between the aluminum and glass is found to be important;
- the ability to model the conjugate heat transfer problem is demonstrated;
- surface-to-surface radiation exchange is shown to be accurately modeled. Differences are found in the third decimal place for the radiation heat flux when compared to Wright's code (Wright 1989);
- in spite of accurate calculations for the total heat transfer (averaged values), the model results showed discrepancies with measured results when modeling the heat flow at the top and bottom of insulated glazing units. These differences from the measured values do

not represent a major concern because they are within measurement error. Also, there is an uncertainty in getting the proper physical properties of materials for simulation purposes. Therefore, this observation does not invalidate the ability of the code to locally simulate the heat transfer in windows as presented in Chapter 6;

- the solar heat gain for normal radiation is simulated, with errors for the solar heat gain factor lower than 2.5% for samples S1-S5 and S9, 5.3% for S6, 19% for S7 and 12% for S8;
- Finally, it is concluded that two-dimensional simulations of conduction, convection, and radiation inter-change can be accurately calculated and used to better understand, both qualitatively and quantitatively, the heat transfer and fluid flow mechanisms within a window.

In Chapter 6 surface temperature profiles are compared with thermographic measurements and results from a modified commercial code. A sensitivity analysis of the boundary conditions that exist in windows is also given.

6 APPLICATION OF THE NUMERICAL CODE

This chapter describes the application of the present numerical code, BRAVO, to simulate more realistic window problems, both geometrically and physically. Unfortunately, experimental data for full temperature profiles in a real window configuration does not exist (de Abreu *et al.*, 1996).

Therefore, a compromise is necessary. To test BRAVO, comparisons are made with the reported surface temperature simulations of Curcija (1992) (Pella Window) and with preliminary experimental IR thermographic data for four IGU's (Sargent, 1992). For this last set, the indoor (warm side) heat transfer coefficient, h_i, and the outdoor (cold side) heat transfer coefficient, h_o, although reproducible, were unknown.

As this work neared completion, two additional thermographic data sets became available from a planned set of tests that included IR measurements by Griffith *et al.* (1996) and Elmahdy (1996). In addition, a single set of IR measured temperature data for a deflected glazing unit was also recently reported in the literature (Beck *et al.*, 1995). Comparison of BRAVO results with this recent data is also reported in this Chapter.

Before comparisons between the calculations and experiments are made, efforts are made to obtain results that are grid independent. Sample grid refinement results are presented in Section 6.1.

Following in Section 6.2, simulations of the four insulated glazing units (IGU's) of Sargent (1992) are compared qualitatively with Sargent's (1992) experimental results. In Section 6.3 some calculations in a wood frame window are presented as well as a comparison with a modified commercial CFD code (Curcija, 1992). In Section 6.4 a comparison is made between a set of simulated temperature profiles and heat fluxes with the most recent set of experimental results (Griffith *et al.*, 1996; Elmahdy, 1996) for relatively simple geometrical configurations (de Abreu *et al.*, 1996; Sullivan *et al.*, 1996). This set includes seven insulated glass units (IGU's) with a variety of parameter variations: different gap widths, two different spacer types, a low-E coating and, double and triple glazing units. In Section 6.5 BRAVO is applied to deflected windows where a sensitivity analysis study is done. Results are compared qualitatively with the experimental results from Beck *et al.* (1995). In Section 6.6 a sensitivity analysis is performed to investigate the impact from boundary conditions. Finally, in Section 6.7, the conclusions are summarized.

6.1 Grid Refinement

Before any production runs are undertaken, the question of grid independence is studied using a uniform grid for three representative insulated glazing units (IGU's), with spacers' widths of 6.40 mm, 12.70 mm, and 19.05 mm and a glazing height of 508 mm with clear glass of 3 mm thickness. All windows studied in this Chapter will use one of these IGU's to compose the fenestration system, except in Section 6.3, where a study in a whole window with a IGU 1.05 m high and a spacer of 12.70 mm thick is used. Details of the IGU's and boundary conditions are given in Figure 6.1.

6.1.1 Grid Size

Only a single cavity of the IGU, without a spacer, is tested for grid independence since the spacer and frame are dependent upon the material conductivity and geometry. The number of control volumes in x direction, conforming to the definition given in Chapter 3, is varied from 10 to 45 in increments of five, for cell aspect ratios of 5, 10, 20 and 40. The heat flux for the cell aspect ratio *vs.* number of control volumes in the x direction is given in Tables 6.1, 6.2 and 6.3 for cavity widths of 6.40 mm, 12.70 mm and 19.05 mm, respectively. Also, these tables show the error between heat flux calculated for each grid size in relation to the heat flux obtained for the most refined grid studied for the IGU under consideration.

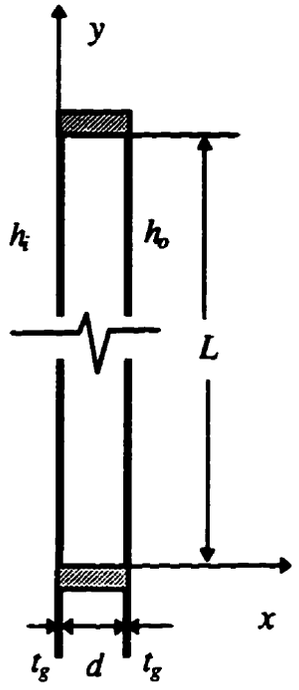

Boundary Conditions:

$T_i = 21.1$ °C

$T_o = -17.8$ °C

$h_i = h_{ci} + h_{ri} = 7.65$ W/(m^2°C)

$h_o = h_{co} + h_{ro} = 30.0$ W/(m^2°C)

Dimensions:

$d =$ 6.40 mm	$A_c = 80$
$d = 12.70$ mm	$A_c = 40$
$d = 19.05$ mm	$A_c = 26.67$

$L = 508$ mm

$t_g = 3$ mm

Figure 6.1: Glazing Unit Geometry and Boundary Conditions.

The grids with 30 control volumes in the x direction and grid aspect ratios 5 and 10 are used to simulate natural convective flow throughout subsequent simulations. The errors for these grids in comparison to the most refined grid were about 0.5%, fine enough to pick up the secondary flow.

Cell Aspect Ratio	Number of c.v.'s	10	15	20	25	30	35	40	45
40	heat flux	105.35	106.61	107.25	107.64	107.89	108.07	108.21	108.31
	error	2.74	1.58	0.99	0.63	0.40	0.23	0.10	0.01
	number of cells	0	0	0	0	0	0	0	0
20	heat flux	105.64	106.78	107.36	107.70	107.94	108.10	108.22	108.32
	error	2.47	1.42	0.88	0.57	0.35	0.20	0.09	0.00
	number of cells	0	0	0	0	0	0	0	0
10	heat flux	105.76	106.82	107.38	107.71	107.94	108.11	108.24	not
	error	2.36	1.38	0.87	0.56	0.35	0.19	0.07	enough
	number of cells	0	0	0	0	6	6	6	storage
5	heat flux	105.78	106.83	107.39	107.71	107.95	108.12	not	not
	error	2.34	1.37	0.86	0.56	0.34	0.18	enough	enough
	number of cells	0	0	0	6	6	6	storage	storage

note: heat flux [W/(m^2°C)]
error [%]
number of cell = the number of secondary cells found
the available memory was 32 Mb

Table 6.1: Heat Flux for Aspect Ratio Cell *versus* Number of Control Volumes in x Direction (d=6.40 mm).

Cell Aspect Ratio	Number of c.v.'s	10	15	20	25	30	35	40	45
40	heat flux	104.70	106.10	106.83	107.26	107.56	107.76	107.91	108.03
	error	3.38	2.09	1.42	1.02	0.74	0.47	0.42	0.30
	number of cells	0	0	0	0	0	0	0	0
20	heat flux	105.17	106.42	107.05	107.42	107.68	107.85	107.99	108.09
	error	2.94	1.80	1.22	0.87	0.63	0.44	0.35	0.25
	number of cells	0	0	0	0	0	0	0	0
10	heat flux	105.41	106.55	107.13	107.48	107.70	107.93	108.11	108.27
	error	2.72	1.67	1.14	0.82	0.62	0.40	0.24	0.09
	number of cells	0	0	0	0	0	9	11	11
5	heat flux	105.51	106.57	107.15	107.56	107.87	108.09	108.25	108.37
	error	2.63	1.65	1.13	0.74	0.45	0.25	0.11	0.00
	number of cells	0	0	0	9	11	11	12	12

note: heat flux [W/(m^2°C)]
error [%]
number of cell = the number of secondary cells found

Table 6.2: Heat Flux for Aspect Ratio Cell *versus* Number of Control Volumes in x Direction (d=12.70 mm).

Cell Aspect Ratio	Number of c.v.'s	10	15	20	25	30	35	40	45
40	heat flux	102.90	104.75	105.73	106.28	106.65	106.94	107.13	107.24
	error	4.16	2.44	1.53	1.01	0.67	0.40	0.22	0.12
	number of cells	0	0	0	0	0	0	0	2
20	heat flux	103.55	105.15	105.98	106.41	106.72	106.94	107.15	107.25
	error	3.56	2.07	1.29	0.89	0.60	0.40	0.20	0.11
	number of cells	0	0	0	2	3	4	4	4
10	heat flux	103.83	105.28	105.99	106.44	106.73	106.97	107.17	107.37
	error	3.30	1.95	1.29	0.87	0.59	0.37	0.19	0.00
	number of cells	0	0	3	4	5	5	5	5
5	heat flux	103.94	105.32	105.99	106.45	106.79	107.01	107.20	107.37
	error	3.19	1.91	1.29	0.86	0.54	0.34	0.16	0.00
	number of cells	0	3	5	5	5	5	5	5

note: heat flux [W/(m^2°C)]
error [%]
number of cell = the number of secondary cells found

Table 6.3: Heat Flux for Aspect Ratio Cell *versus* Number of Control Volumes in x Direction (d=19.05 mm).

Figure 6.2 shows temperature profiles, Figure 6.3 isotherms, and Figure 6.4 streamlines for an IGU of width 19.05 mm, for four cases: 1) only conduction in the IGU; 2) conduction and convection; 3) conduction , convection and radiation before cell generation; and 4) conduction, convection and radiation after cell generation. In Figure 6.2 the horizontal axis represents the vertical distance. It can be observed that the presence of radiation augments the heat transfer, increasing the number of cells from four to five and decreasing the surface temperature in the warm side.

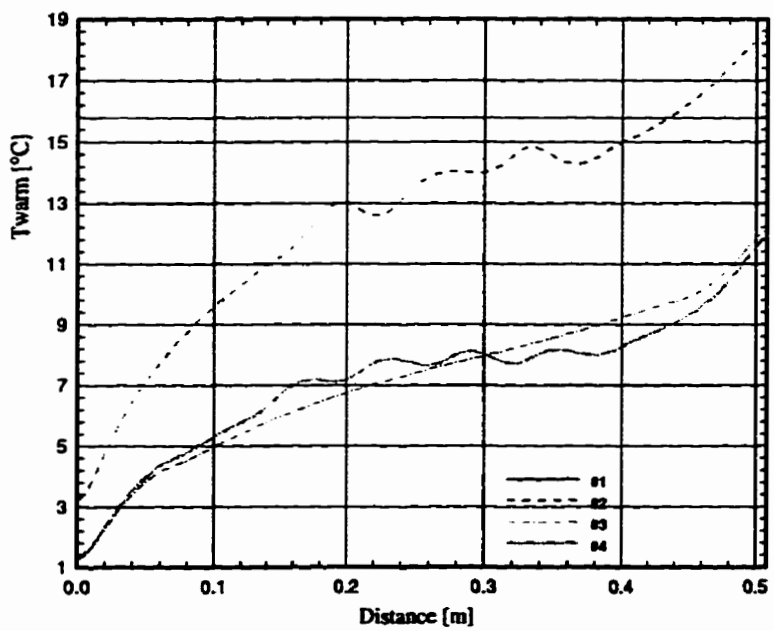

Figure 6.2: IGU Surface Temperature Profiles in the Warm Side for d = 19.05 mm.

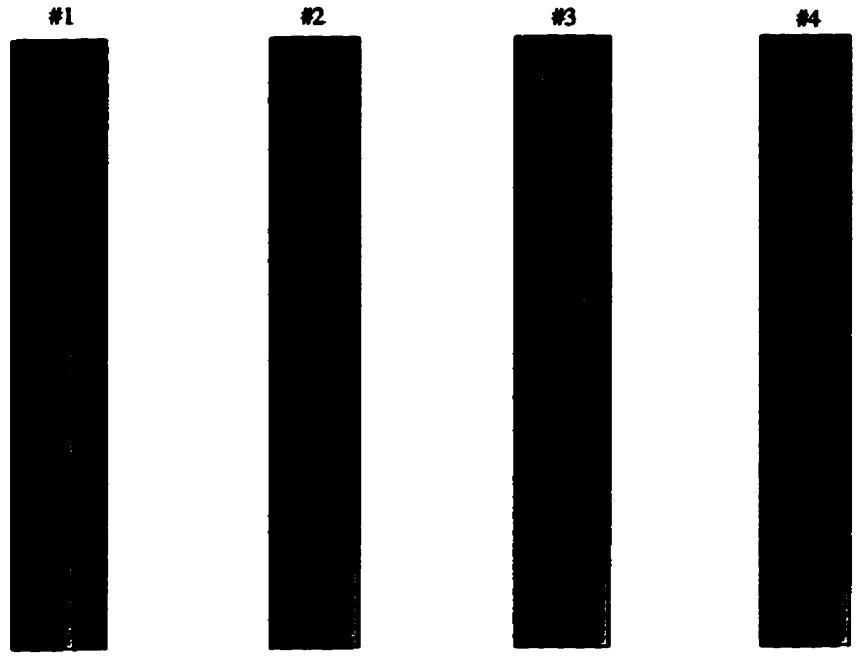

Figure 6.3: Isotherms Across the Cavity of Width d = 19.05 mm for an IGU of Height 508 mm.

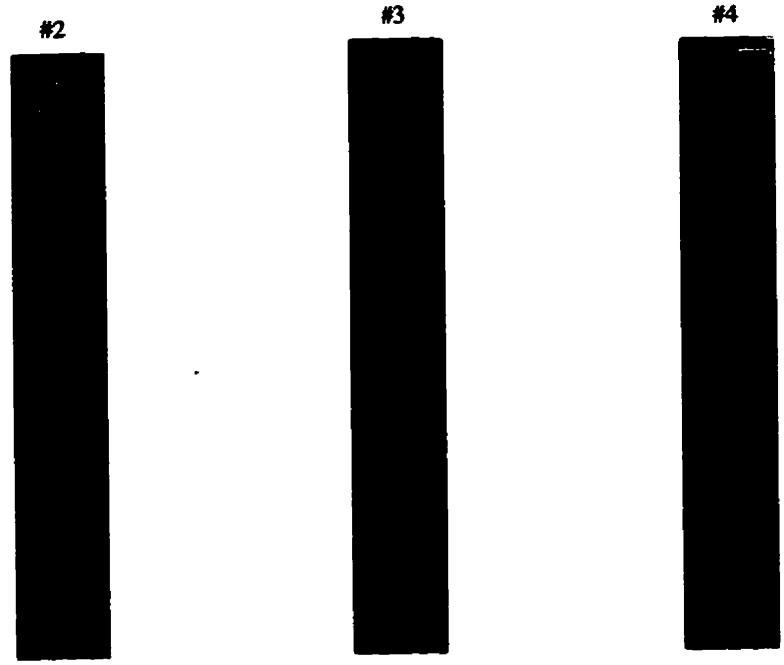

Figure 6.4: Streamlines Across the Cavity of Width d = 19.05 mm for an IGU of Height 508 mm.

6.1.2 Convergence

The convergence criterion is applied for the complete IGU system (glass, seal, and cavity) in three steps, in each iteration loop. Convergence is assumed if

1. the difference between each variable (temperature, velocities and pressure) is less than 10^{-4} in two consecutive iterations of the ADI solver;
2. the heat flux, q_h, of the fenestration system, . is equal the heat flux out, q_c, with error within 10^{-4} , i.e., the error for heat flux $[(q_h-q_c)/q_c]\cdot 100 \leq 10^{-4}$ %, and
3. the difference between heat fluxes in, q_h, are less than 10^{-4} for at least five consecutive iterations, i.e. $[(q_h^{n-1}-q_h^n)/q_h^n]\cdot 100 \leq 10^{-4}$ %.

6.1.3 Observations

It is worth while to note that the time step is calculated using an explicit time step formula and it is multiplied by a factor n to accelerate convergence, or even guarantee it. With the change in grid size, frequently n had to be changed to ensure convergence. For example, for a very coarse grid using EDS the value of n could not be taken smaller than 50. This fact required a search for the range of n where the buoyancy term could balance the derivative of pressure in the control volumes and hence guarantee convergence. The range of n is also dependent upon the relaxation factors used in the solver. For the grid chosen, the

best choice was n=50 for the EDS scheme and n=0.95 for the CDS scheme with the relaxation factor 1.8 for the solution of all equations in the ADI solver.

It is also interesting to note that secondary cells are generated spontaneously for certain $Ra > Ra_c$, but in most of the cases run the number of cells was smaller, and the heat transfer lower than when the cells were perturbed. To maintain the perturbed cells using EDS the grid in most cases has to have a cell aspect ratio smaller than 5, increasing time and storage requirements. Therefore, only the first 30 iterations are done using EDS to approach a "near converged" solution and "smooth the flow". Subsequently, the scheme is switched to CDS and perturbed after 3 iterations. The code then stops upon reaching convergence criteria or 6000 iterations, whichever comes first. If the run reaches 6000 iterations, the error for the heat flux is lower than 10^{-2}, and the error for all variables between consecutive iterations is lower than 10^{-3}, it is considered satisfactory, and stopped. If not, more iterations are run. For certain values of *Ra* CDS failed if EDS had not been run before hand; this is the meaning of the "smooth the flow" term used above.

The established condition (Shyy *et al.*, 1992) for CDS stability, i.e., cell Reynolds number $Re_{\Delta u} = (\Delta u \cdot \Delta x)/\nu \leq 2$, seems not to be valid in buoyancy driven flows, since, for IGU's, the CDS stable $Re_{\Delta u}$ at the top or bottom edge of the window cavity is observed to be greater than 4. As pointed out by Shyy *et al.* (1992) $Re_{\Delta u}$ seems not to be a reliable indicator

of performance for CDS, hence the non-observance of wiggles for $R_{\Delta u}$ greater than 2 is not surprising.

In the course of the grid refinement studies another observation made is that the Peclet number, Pe, is greater than ten for a large number of the flow field control volumes leading to a fully upwinded EDS formulation in this region, and leading to the appearance of false diffusion, which in turn precludes the appearance of secondary cell flows. This fact requires further investigation to improve EDS for buoyancy driven cavity flows (i.e., change the range of Pe).

6.2 A Qualitative Comparison of Surface Temperature Profiles for Four Insulated Glazing Units: BRAVO vs. Thermographic Profiles

This section presents an early attempt to compare thermographic measurement and simulation of surface temperature profiles. The four glazing units modeled are identified in Table 6.4. First a composite graph of results for the set of vertical surface temperature profiles for the four IGU's is presented. Also, this set of temperatures profiles is compared with measured thermography temperature.

IGU#	Glass Description	Pane Spacing(s), d	Total Pane Spacing	Fill Gas	Spacer(s)
1	Low-E double-glazed	19.050 mm	19.050 mm	argon	Foam
2	Clear Triple-glazed	15.875 mm	31.750 mm	air	Foam
3	Clear triple-glazed	9.525 mm	19.050 mm	argon	Foam
4	Clear triple-glazed	4.763 mm	9.525 mm	krypton	Foam

Table 6.4: Description of Glazing Units.

6.2.1 Glazing Unit Details and Mounting Configuration

The double glazed unit identified in Table 6.4 involving the foam spacer is modeled as shown in Figure 6.5. The triple-glazed units are modeled similarly. The pane spacing, d, is given in Table 6.4. The numbering scheme given in Table 6.4 will be used throughout this section to identify the different glazing units.

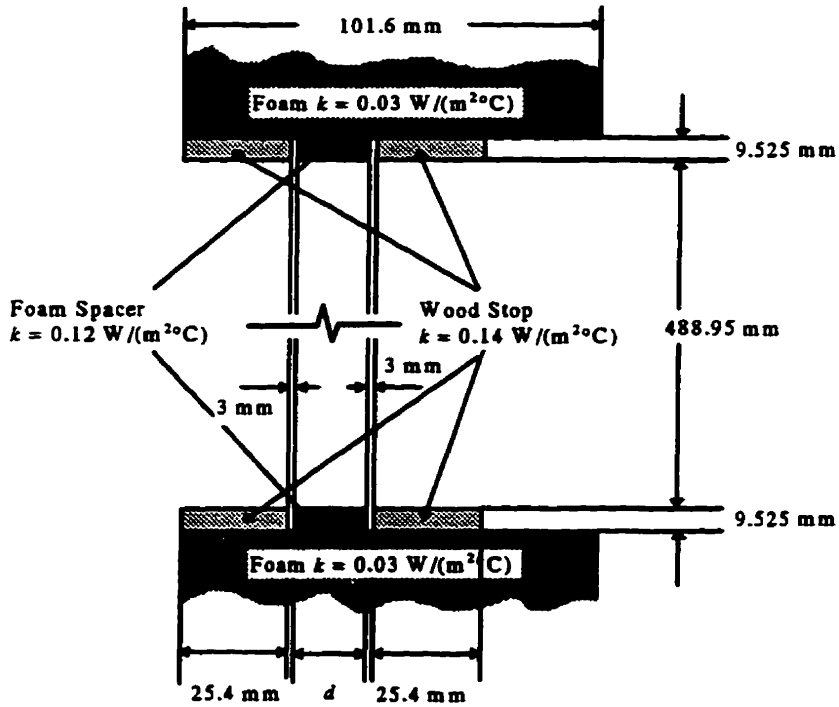

Figure 6.5: Glazing Unit and Mask Wall Geometry for the Double Glazed Unit.

IGU #1 has a low emissivity coating (emissivity ≈ 0.2) on the indoor facing surface of the outdoor glazing. The emissivity of the glass is taken as 0.84.

It is worth noting that the test samples are IGU's mounted in a mask wall without sash or frame. In the experiment to fasten the glazing in place and to prevent infiltration a wood stop is used to cover the length of the edge-seal.

6.2.2 Simulation Conditions

The boundary conditions used for computer simulation are listed in Table 6.5. The heat transfer coefficients include both long wave radiation and convective effects. No solar radiation is present. The boundary conditions approximate natural convection on the warm side. Measurements of the magnitude of the forced convection on the cold side were not performed. It is known that on the cold side there were two oscillating fans blowing air on the surface in order to create a uniform and reproducible heat transfer coefficient through forced convection.

Therefore, the convection heat transfer on the cold side, h_{co}, is modeled as constant (i.e., independent of position along the exposed glazing surface). The convection heat transfer on the warm side, h_{ci}, is simulated for a non-isothermal flat plate: see equation 6.1 below.

This is known to be in error, particularly on the indoor side where local effects due to stagnation flow near the head and sill are present.

Indoor Temp T_i	Indoor Convective Heat Transfer Coefficient h_{ci}	Outdoor Temp T_o	Outdoor Convective Heat Transfer Coefficient h_{co}
17.5 °C	non-isothermal flat plate	-10.0 °C	15.74 W/m^{2}K

Note: the radiation heat transfer coefficient, h_r, is evaluated using equation 6.2.

Table 6.5: Glazing Unit Boundary Conditions.

The h_{ci} equation for a non-isothermal flat plate, calculated using the method derived by Raithby and Hollands (1975) and modified by Yeoh *et al.* (1989) is

$$h_{ci}(y) = kC\left(\frac{g\beta}{\nu\alpha}\right)^{\frac{1}{4}} \frac{(T(y)-T_i)^{\frac{2}{3}}}{\left(\int_0^y (T(y)-T_i)^{\frac{5}{3}}\right)^{\frac{1}{4}}} \tag{6.1}$$

where T_i is the room temperature, and g is the gravitational acceleration. β, k, $\nu = \frac{\mu}{k}$, and $\alpha = \frac{k}{\rho c_p}$ are properties of the interior (room) gas taken as air at atmospheric pressure. $T(y)$

is the temperature distribution along the surface with y measured from the start of the boundary layer. The Prandtl number function, C, is given by $C = \frac{0.563}{\left[1+\left(\frac{0.437}{\mathrm{Pr}}\right)^{\frac{9}{16}}\right]^{\frac{4}{9}}}$.

Throughout this work, when required to calculate the radiation component, h_r, for the outdoor (cold side) and indoor (warm side) surfaces, the room wall surfaces and outdoor environment are taken as black bodies at air temperature.

$$q_r = \sigma\varepsilon\left(T_s^4 - T_r^4\right) \tag{6.2}$$

where T_s is the surface temperature, T_r is T_i (indoor) or T_o (outdoor), σ is the Stefan-Boltzman constant, and ε is the emissivity of the surface.

The great difficulty in using these measured surface temperature thermographic profiles for comparison are the unknown heat transfer coefficients (Sargent 1992). These thermographic experiments for measurement of the surface temperature profiles were in an early stage of development where heat fluxes were not quantified. The experiments were carefully and precisely performed, and were very reproducible. However, at this time the laboratory did not have the capability to determine the magnitude of the unknown but reproducible cold side and warm side heat transfer coefficients. Therefore, quantitative comparison is not possible. An early attempt at a qualitative comparison was done by

estimating the indoor heat transfer coefficient as constant, 8.3 W/(m^2°C) and a fan wind speed of 2 m/s on the cold side yielding a constant outdoor heat transfer coefficient of 15.74 W/(m^2°C). A warm side temperature of 20°C was used. The resulting temperature profile presented a similar trend but was shifted by about 2.5°C in the center glass region. The experimental profile was shifted to match the simulated center temperature with good agreement now between center glass temperatures. A slightly flatter slope was observed for the simulation profile. After shifting, the temperatures at top and bottom of the IGU were observed to differ by more than 2 °C. Even given these discrepancies in the bottom and top ends of the glazing, and the difference in center-glass temperature profile slope, the qualitative agreement may still be considered very satisfactory given the erroneous assumption of a constant convection heat transfer coefficient, e.g., a poor assumption at the ends due to flow stagnation.

As this thesis work neared completion two new data sets of experimental results became available (Griffith *et al.*, 1996 and Elmahdy, 1996). This data is compared with BRAVO simulations in Sullivan *et al.* (1996). The agreement obtained between simulated and measured surface temperatures profiles for the center glass is now very satisfactory, without any adjustment. The differences in center glass temperature are less than 1°C for a constant heat transfer coefficient. When the configuration reported by Sullivan *et al.*(1996) uses heat transfer coefficient on the warm side estimated by a non-isothermal flat plate correlation , e.g., locally varying heat transfer coefficient, the simulated and the experimental surface

temperature profiles on the warm side matched in the center glass region (see Section 6.6.1.1).

Reconsider the IGU's of Table 6.4. Afterwards, Sargent (1994) reported that the temperature on the warm side was in error: presumably less than assumed 20°C. Therefore a new attempt was made to compare the simulated surface temperature profiles without shifting the experimental profile. First the convection heat transfer coefficient at the cold side, h_{co}, was adjusted, to get agreement with the center glass temperature. It was noticed that a change of 1m/s in calculating h_{co} (calculated using Ito and Kimura's, 1972, 6th floor correlation) did not change the center glass temperature by more than 0.1°C. The thermal resistance of the IGU's was high enough such that changes on h_{co} did not result in noticeable temperature changes. The temperature on the warm side was then shifted down to 17.5°C. For all units this temperature was kept fixed and the h_{ci} was estimated by a non-isothermal flat plate correlation (Equation 6.1).

6.2.3 Simulation Results

The graphical presentation of the simulation results is similar for all the glazing units (see Figure 6.6 for example). The horizontal axis represents vertical distance with zero corresponding to the bottom sight line of the glazing unit, with the top sight line at 488.95 mm. The horizontal axis runs from -0.1 m to +0.6 m so that 100 mm of the foam mask wall plus wood stop is shown both below and above the glazing unit. The vertical axis records the

temperature profile in degrees Celsius on the warm side (room side) of the glazing unit. This temperature profile represents any vertical profile along the glazing unit as long as the "side effects" of the spacer and sealant, etc. are not influencing the temperature. The glazing units tested and simulated are 356 mm by 508 mm, and the IR thermographic images presented by Sargent (1992) indicate that a major portion of the glazing unit can be expected to be free of side effects (e.g., corner effects are confined to a relatively small region in the vicinity of the corners). In the comparison with experimental data, simulated temperature profiles are compared with the vertical temperature profiles along the center-line of the glazing units. All figures showing experimental data *versus* simulated results have the horizontal axis running from 0.0 m (bottom sight line) to 0.488 m (top sight line).

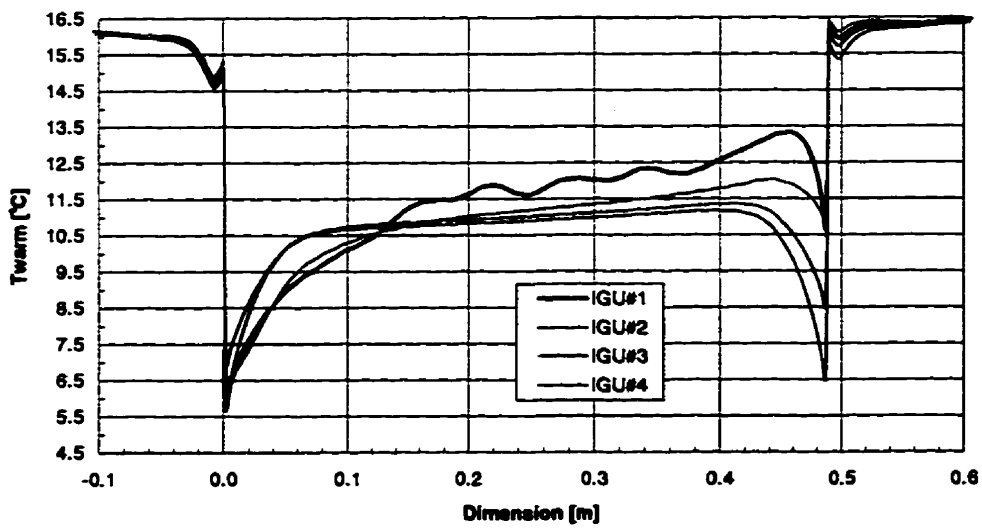

Figure 6.6: Simulated Warm Side Temperature Profile for all Four Glazing Units.

6.2.3.1 Reference Glazing Unit

IGU #1, the low-E double-glazed unit, with a 19.05 mm argon cavity and a foam edge-seal is considered the reference unit. The remaining three glazing units are clear triple glazed systems with air, argon and krypton fill gases, respectively; see Table 6.4.

6.2.3.2 Composite Results

Figure 6.6 is a composite plot showing the temperature profiles for all four glazing units. Based on the center-glass heat transfer characteristics, in the mid-part of the graph, away from the top and bottom edge effects, the lowest performing unit is the triple IGU #4 filled with krypton, and the best performing is the double IGU #1 filled with argon. It is noteworthy that the low-E double glazed filled with argon, IGU #1, has a similar center-glass performance to the conventional clear triple glazed filled with air, IGU #2. Also, similar center glass performance was observed for the clear triple glazed filled with argon, IGU #3 and for the clear triple glazed filled with krypton, IGU #4. In these cases it is difficult to use intuition to rank the IGU's because they have different widths and different fill gases. It is instructive to note that the best window based on center-glass heat transfer characteristics, IGU #1, is not the best for condensation resistance, which is likely to occur in the lower part of the IGU, i.e., near y=0 m.

Table 6.6 shows the thermal performance characteristics for the four glazing units.

IGU	*U-factor* [W/(m^2 °C)]	*R-value* [(m^2 °C)/W]	Temperature [°C] Center-Glass	Bottom
#1	1.685	0.593	11.16	5.72
#2	1.706	0.586	11.12	6.43
#3	1.716	0.583	11.10	6.89
#4	1.758	0.569	11.09	5.74

Table 6.6: Thermal Performance Characteristics of the Glazing Units.

By looking at the total width of the spacers it could be expected that the widest spacer, IGU #2, should yield offer the most resistance to condensation while the narrowest spacer, IGU #4, offers the least. This not true as see in the Table 6.6 and Figure 6.6. Ranking the IGU's, the best performance is seen in IGU #3, followed by IGU #2, IGU # 4 and then IGU #1. IGU #1 is worse than unit #4 due to stronger convection effects. The same is observed for IGU #2 (worse) and IGU #3 (better). Although IGU #4 has the smallest convection effect (small cavity width) which decreases the heat flux at the bottom, it is dominated by the smaller conduction path length that increases heat transfer, hence it is ranked second last instead of the best. If only the convection effects are taken into account then IGU #4 would be expected to perform best.

6.2.4 Comparison of Thermographic Measurements and 2-D Simulation

Figures 6.7 through 6.10 compare the measured and simulated results for each of the four IGU's, respectively. Each figure shows two vertical profiles of surface temperature, one for the measured results and the other for the simulated.

Recall that the warm side temperature is adjusted from 20°C to 17.5°C making the center glass temperature of the simulated IGU #1 nearly equal to the center glass surface temperature of the measured IGU #1. Besides this, curves are all plotted without any other adjustment.

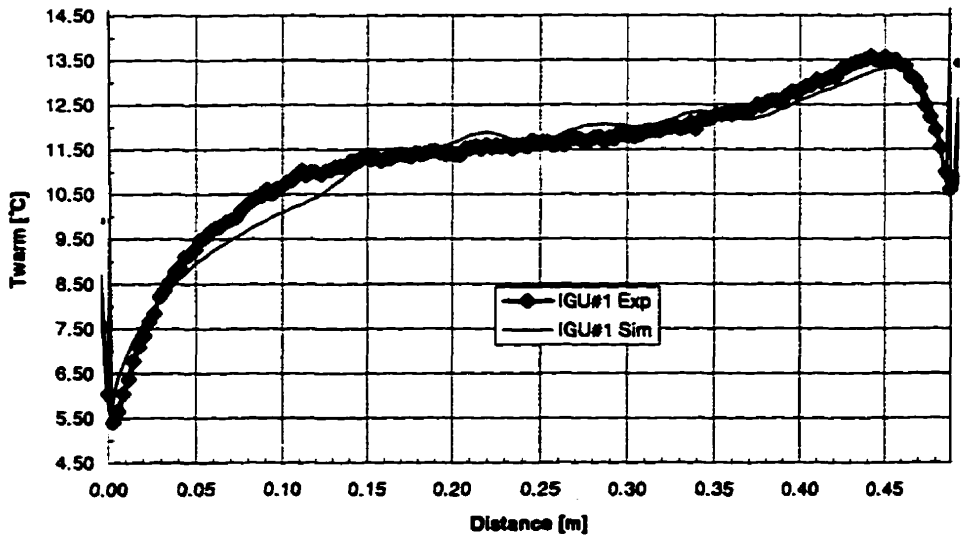

Figure 6.7: Temperature Profiles for IGU #1, Argon Filled, Low-E Double Glazed.

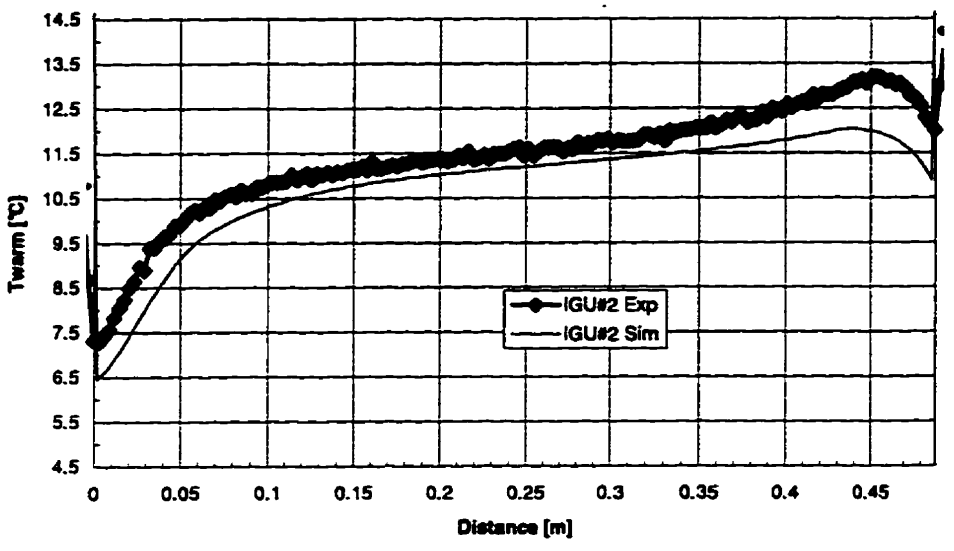

Figure 6.8: Temperature Profiles for IGU #2, Air Filled, Clear Triple Glazed.

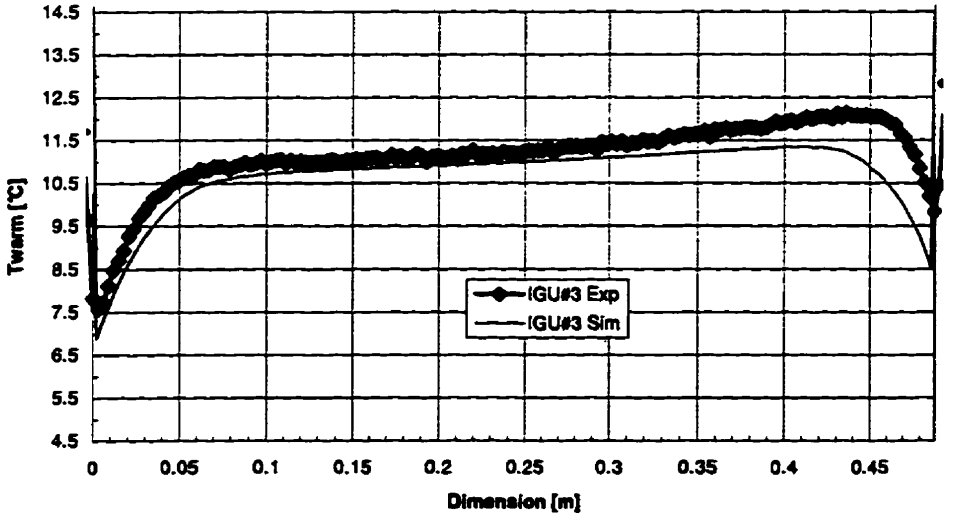

Figure 6.9: Temperature Profiles for IGU #3, Argon Filled, Clear Triple Glazed.

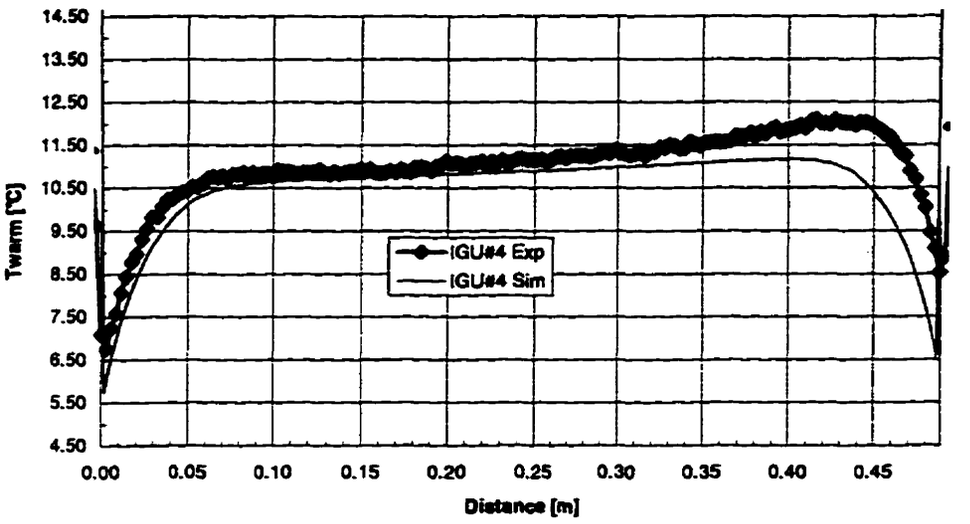

Figure 6.10: Temperature Profiles for IGU #4, Krypton Filled, Clear Triple Glazed.

All of the data sets presented in Figures 6.7 through 6.10 show qualitatively very good agreement. In all four IGU's the centre-glass temperature of the simulated units are lower than the corresponding temperatures of the measured units. This is consistent with the adjustment made, in which the simulated temperature of the IGU #1 was slightly lower than the measured one. Each curve shows a local minimum at, or very near, the top and bottom sight lines.

Figure 6.11, shows the comparison for IGU #1 of two simulated temperature profiles, a constant h_{ci} and a locally varying h_{ci} (non-isothermal flate plate), and for the measured profile. The warm side temperature is adjusted to 17.5°C in both simulation cases.

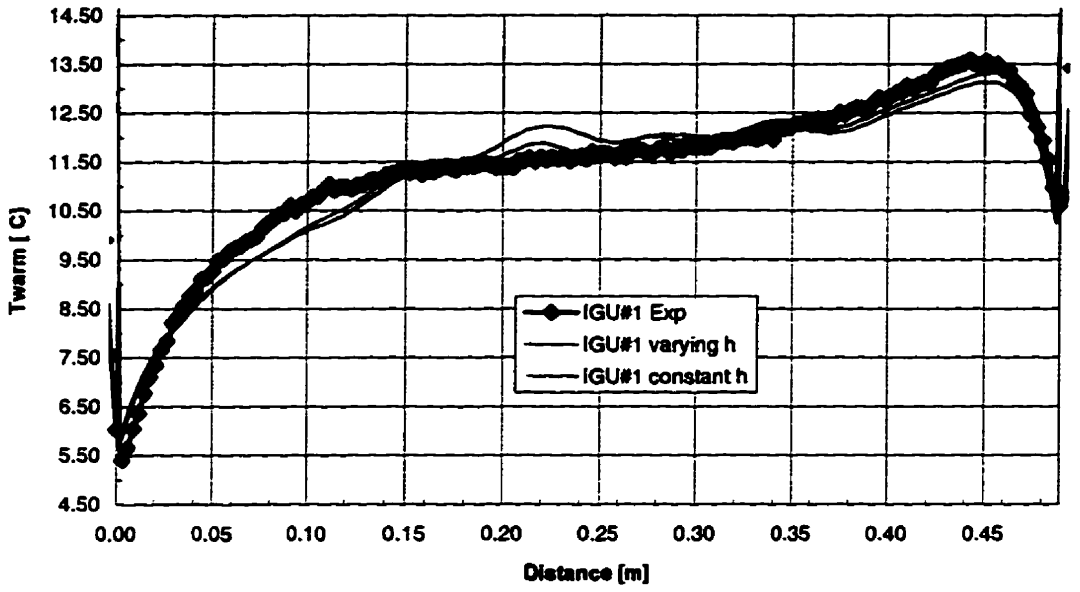

Figure 6.11: Warm side Temperature Profile Comparison: Measured *versus* Simulated for Constant and Locally Varying h_{ci}.

Although there are still discrepancies in the top and bottom sight line temperatures for both simulated temperature profiles in comparison to that measured, it is observed in Figure 6.11 that the experimental and simulated temperature profiles have similar slopes over the entire IGU. A similarity in temperature profiles for both heat transfer coefficients (constant and for the non-isothermal flat plate) is as expected due to the high thermal resistance of the IGU.

6.3 A Whole Window Modeled: Wood Frame

In this Section an entire window, including sash and frame elements, is simulated. The frame design investigated is a wood frame casement window manufactured by Pella. Pella is a large wood frame window manufacturer in the U.S. The reason for this choice of window is that it enables a direct comparison with the simulation results using a modified commercial code (Curcija, 1992) to be made. The results are presented as surface temperature distributions on the warm window surface. Additionally the overall U-factor is also given.

6.3.1 Window Details and Mounting Configuration

Figure 6.12 details the window cross-section and Table 6.7 presents the thermal conductivities and emissivities for the window materials as reported by Curcija (1992).

Material	Conductivity [W/(m^2°C)]	Emissivity
Wood	0.14	0.84
Glass	1.00	0.84
Butyl	0.24	N/A*
PIB	0.24	N/A
Polysulphide	0.19	N/A
Aluminum	236	0.10
Air	0.024	N/A

*N/A = Not applicable

Table 6.7: Thermal Conductivity and Emissivity of the Materials.

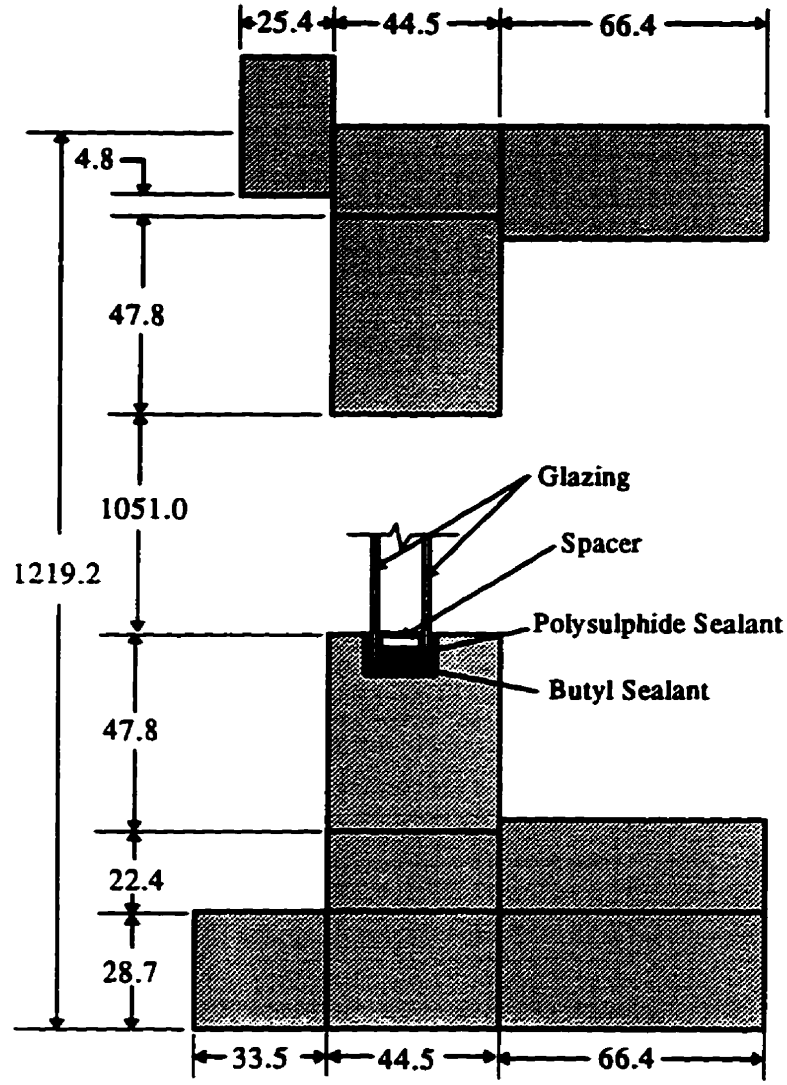

Figure 6.12: Cross Section of the Pella Window (Curcija, 1992). Units are in mm.

6.3.2 Simulation Conditions

First a grid independence study is conducted. The IGU mesh is uniform with 30 control volumes in the x direction with cell aspect ratio of 10. The glass sheets have 3 control

volumes in the x direction. The spacer cavity has 10 control volumes and the spacer sealant 6 control volumes in the y direction. The wood components have a relatively coarse mesh.

Three sets of boundary conditions are considered in evaluating the thermal performance of the window. The first two sets of surface heat transfer coefficients (warm side, h_i, and on the cold side, h_o) were obtained from Curcija (1992). They are estimated using the correlations for laminar natural convection and perpendicular forced convection over a flat plate (case Correlations), and the variable convective heat transfer coefficients obtained from numerical simulation for isothermal boundaries (case Simulations #1). The last set of surface convective heat transfer coefficients are obtained from Equations (6.1)to (6.6), case Simulations #2. These sets of boundary conditions are summarized in Table 6.8.

Case	h_i [W/(m^2°C)]	h_o [W/(m^2°C)]
Correlations	7.34	18.78
Simulations #1*	simulated	simulated
Simulations #2*	non-isothermal flat plate with corrections	15.52

*The radiative component of the film coefficients is estimated using Equation (6.2).

Table 6.8: Summary of Boundary Conditions for Pella Window (T_i=21.1°C and T_o=-17.8°C).

In using the Simulations #1 Curcija (1992) simulated the warm side as being at a constant temperature using a laminar natural convection model. To estimate the local

distribution of the heat transfer on the cold side, h_o, he modeled the wind as blowing perpendicular to the glazing surface using a forced convection model.

In using the Simulations #2 boundary conditions the local convection heat transfer coefficient, h_{ci}, was evaluated using Equation (6.1) for a non-isothermal flat plate and the radiation component, h_r, was estimated use equation (6.2). To account for the convective effect caused by the stagnating and recirculating regions on the warm side, the correlations suggested by Curcija and Goss (1993) are used.

On the vertical surfaces where the flow recirculates and stagnates due to the frame steps a linear variation in the convection heat transfer coefficient over an averaged length of 0.05 m was taken. Outside this region the non-isothermal flat plate profile is used (Curcija and Goss (1993) have suggested using an isothermal flat plate profile). For the horizontal regions of the frame members

$$h_{u_x} = 0.1 + 2.5\left(\frac{x}{x_1}\right)^{\frac{1}{3}} \quad \text{upper step} \tag{6.3}$$

$$h_{l_x} = 0.1 + 1.75\left(\frac{x}{x_1}\right)^{\frac{1}{3}} \quad \text{lower step} \tag{6.4}$$

where h_u and h_l are the convection heat transfer coefficients for the upper and lowers steps respectively, and, $x_1 = D - 0.00635$. The horizontal distance, x, is measured from the beginning of each step. D is the step length.

For the end region of the horizontal surfaces (6.40 mm long) the following set is recommended by Curcija and Goss (1993)

$$h_{u_x} = 2.5 + 945(x - x_1)^2 \tag{6.5}$$

$$h_{l_x} = 1.75 + 945(x - x_1)^2 \tag{6.6}$$

6.3.3 Results

As in Section 6.2.3, the graphics in this section have the horizontal axis representing the vertical distance with zero corresponding to the bottom of the window. The vertical axis records the temperature profile in degrees Kelvin on the warm side (room side) of the window.

A comparison between the *U-factors* obtained using the modified commercial code (Curcija, 1992) and BRAVO is given in Table 6.9. Very good agreement is obtained for the Correlations boundary condition yielding a discrepancy of 0.38%. The Simulations B.C.'s (each program used its correlation) yielded a discrepancy of 1.65%.

	BRAVO Correlations	BRAVO Simulations #2	Curcija (1992) Correlations	Curcija (1992) Simulations #1
U	2.59	2.39	2.58	2.43

Table 6.9: Comparison of *U-Factors* [W/(m^2°C)].

Figure 6.13 reproduces the local temperature distribution reported by Curcija (1992) while Figure 6.14 shows the corresponding local temperature profile from BRAVO. Note that although the horizontal axis scale for the window frame region in Figure 6.13 from Curcija (1992) does not correspond to the cross section shown in Figure 6.12, from the same reference, the region between the sight lines is scaled correctly, which permits a comparison between Figure 6.13 and Figure 6.14 in the glazing region. They clearly show an increase in the maximum temperature in the top of the IGU and a decrease in the temperature in the bottom of the IGU when using a variable heat transfer coefficient. Therefore, it is evident that to evaluate the local temperature distribution, i.e., surface temperature profile, a better estimation of the local heat transfer coefficients is required.

The agreement between the modified commercial code (Curcija, 1992) and BRAVO for the same correlations boundary conditions, case #1, is excellent over all the surface temperature profile. The differences using different boundary conditions are such that BRAVO predicted a higher temperature in the top region and a colder temperature in the bottom region.

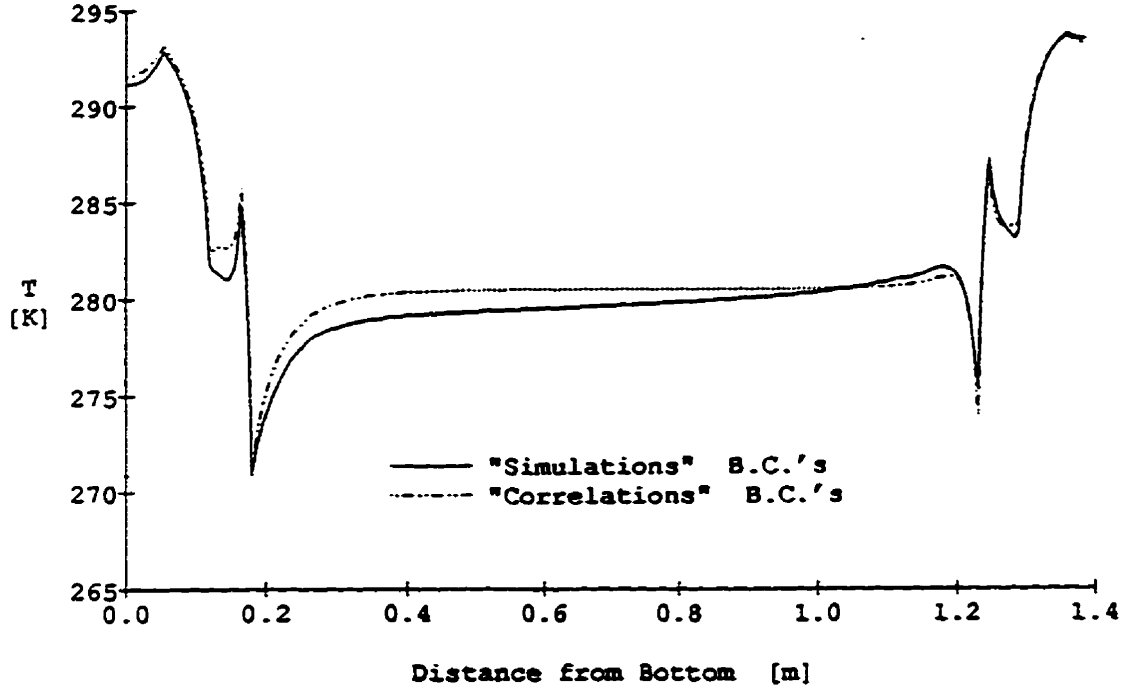

Figure 6.13: Temperature Distribution on the Warm Side of Modified Commercial Code (Curcija, 1992), "Correlations" and "Simulations #1" B.C.'s.

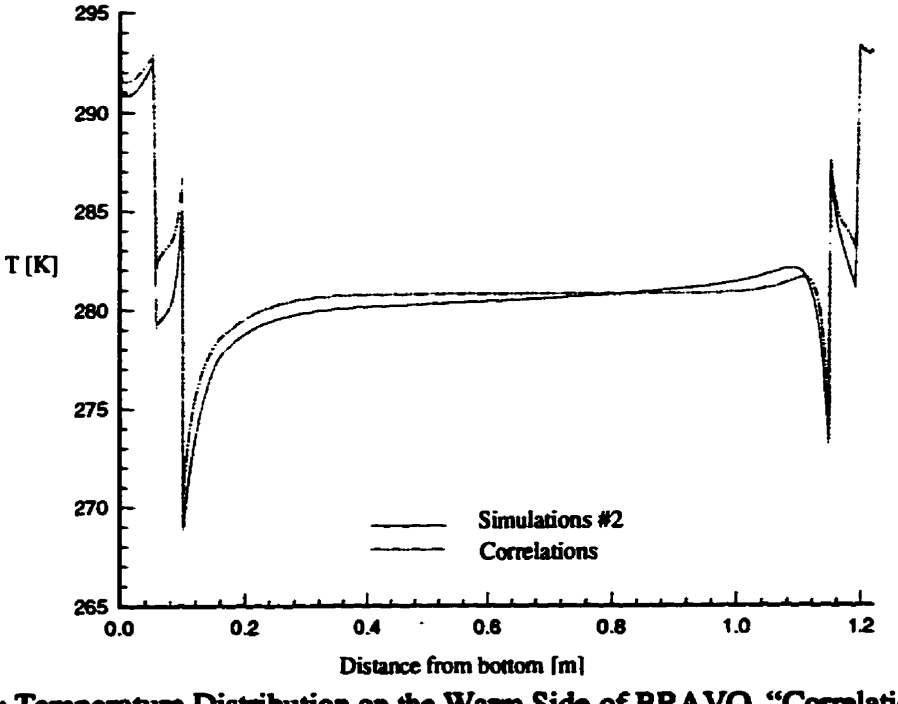

Figure 6.14: Temperature Distribution on the Warm Side of BRAVO, "Correlations" and "Simulations #2" B.C.'s.

6.4 Comparison of Surface Temperature Profiles from Thermographic Measurement and 2-D Simulation - A Blind Collaborative Research Study

This section describes a collaborative research project, including both measurement and simulation studies, aimed at determining the surface temperature of a set of insulated glazing units (IGU's). Duplicate sets of glazing units were provided to two measurement laboratories and their construction details were given to two simulation laboratories, one of which is the research group that the author is a part of. All participants in the study were asked to perform their portion of the research without knowledge of the results of the other investigators, i.e., a "blind study". A complete description of this collaboration among four laboratories is given in Sullivan *et al.* (1996).

There are two main parts in this section. The first part, reported in Section 6.4.3, focuses on determining by simulation *a priori* vertical surface temperature profiles (i.e., before any corresponding computational or experimental data were available) of the seven air-filled glazing units identified in Table 6.10. The second part, described in Section 6.4.4, presents the results of the collaborative research mentioned for all seven air filled units (Table 6.10).

The numbering scheme shown in Table 6.10 will be used throughout this section to identify the glazing units. The design options incorporated in these glazing units were

selected to cover a range of edge-seal type, pane spacing, low-E coating, number of glazings that would reasonably test both the measurement and simulation techniques. These design options are of interest because each one is expected to affect the indoor surface temperature profile.

6.4.1 Glazing Units Details and Mounting Configuration

The double glazed units identified in Table 6.10 involving the foam spacer are modeled as shown in Figure 6.15, insert a. The triple-glazed units are modeled similarly. The pane spacing, d, shown but not given in Figure 6.15 is given in Table 6.10.

IGU#	Glass Description	Pane Spacing(s), d	Spacer(s)
1	Clear double-glazed	12.7 mm	Foam
2	Clear double-glazed	12.7 mm	Aluminum
3	Clear double-glazed	6.4 mm	Foam
4	Clear double-glazed	19.1 mm	Foam
5	Low e double-glazed	12.7 mm	Foam
6	Clear triple-glazed	12.7 mm	Foam
7	Clear triple-glazed	6.4 mm	Foam

Table 6.10: Description of Blind Test Glazing Units.

Details regarding the metal-spacer glazing are shown in Figure 6.15, insert b. The metal is aluminum. A 50 μm air gap is used to simulate the solid-solid thermal contact resistance that exists between the glazing and the aluminum spacer (Fraser *et al.*, 1993). The spacer model is a simplification of the true spacer geometry with the thickness of the

aluminum preserved. Fraser *et al.* (1993) showed that it is the metal thickness and not the spacer's shape that dominates edge-seal thermal performance.

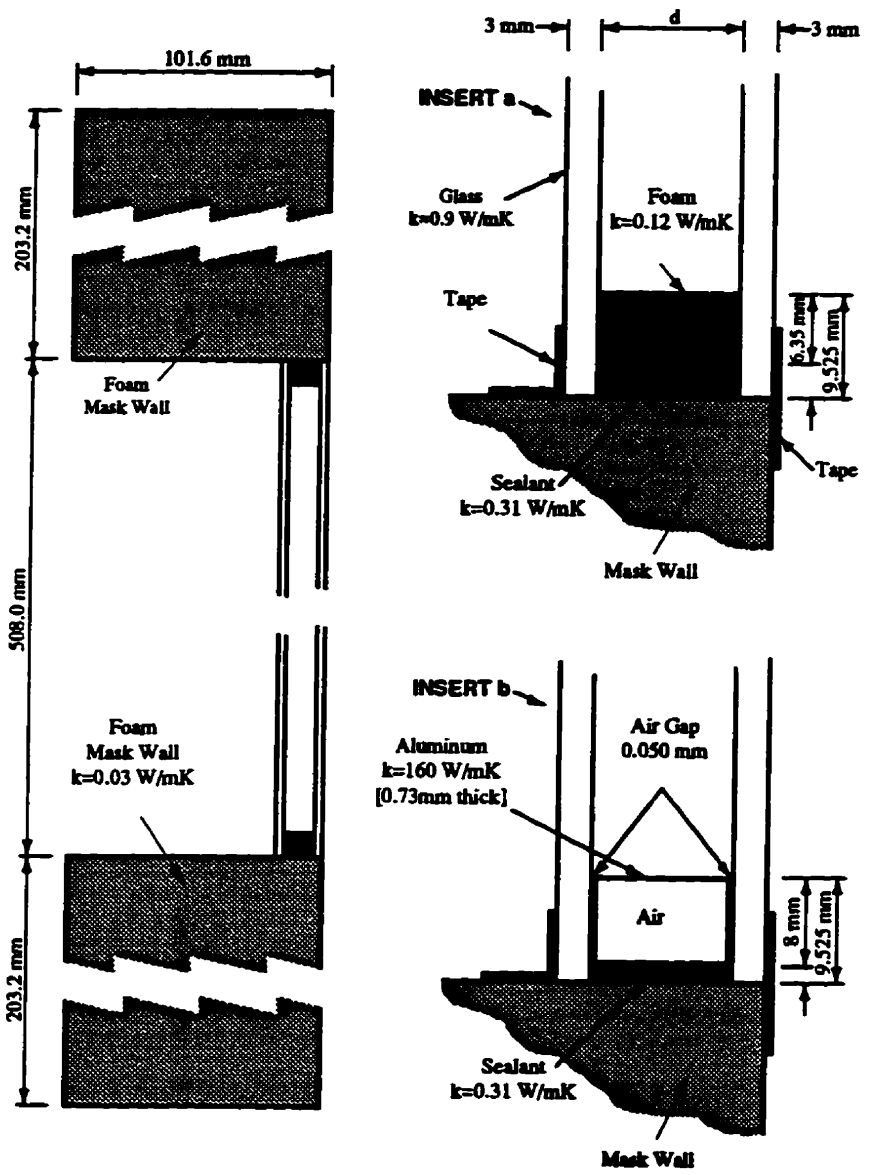

Figure 6.15: Blind Test Glazing Unit and Mask Wall Geometry.

IGU #5 has a low emissivity coating (emissivity = 0.2) on the indoor facing surface of the outdoor glazing. The emissivity of the glass is taken as 0.84.

Note that the test samples are IGU's mounted in a mask wall without sash or frame. The advantage of this simple arrangement is the removal of complicating factors. The disadvantage, however, is that the reader must keep in mind, for instance, that sensitivities to edge-seal structure may be magnified. In particular, the edge-seals of the glazing units studied account for a greater percentage of the heat loss than they would were a sash present.

The tape shown in Figure 6.15, insert a, was necessary in the experiment to fasten the glazing in place and to prevent infiltration. The tape, however, was not modeled because it was felt that its presence would not alter the heat transfer appreciably. In addition its thermal properties are unknown.

6.4.2 Simulation and Test Conditions

The boundary conditions used in the simulations are given in Table 6.11. The heat transfer coefficients include both long wave radiation and convective effects. No solar radiation is present. These boundary conditions approximate the ASHRAE winter design condition with a 6.7 m/s wind on the cold side and natural convection on the warm side but were chosen with the expectation that they would also approximate the conditions in the measurement laboratories. A sensitivity study to variations in the magnitudes of these

coefficients is reported in Section 6.6.1. This sensitivity information is important to consider when comparing computational and experimental results.

Indoor Temp T_i	Indoor Heat Transfer Coefficient h_i	Outdoor Temp T_o	Outdoor Heat Transfer Coefficient h_o
21.1°C	8.3 W/(m^2°C)	-17.8°C	30 W/(m^2°C)

Table 6.11: Blind Test Glazing Unit Boundary Conditions.

Note that h_o and h_i were modeled as constants (i.e., independent of position along the exposed glazing surface). This is known to be in error, particularly on the indoor side where local effects are present due to peculiarities in the boundary layer flow near the head and sill. In this study the test units are mounted flush on the warm side to minimize associated errors.

6.4.3 Simulation Results

The horizontal axis is vertical distance with zero corresponding to the bottom edge of the glazing unit and the top edge at 508 mm. The horizontal axis runs from -100 mm to +600 mm so that 100 mm and 92 mm of the foam mask wall is shown below and above the glazing unit, respectively. The vertical axis records the temperature profile in degrees Celsius on the warm side (room side) of the glazing unit. This temperature profile represents any vertical

profile along the glazing unit as long as the "side effects", i.e., 3-D effects, of the spacer, sealant, etc. are not influencing the temperature.

6.4.3.1 Reference Glazing Unit

Glazing unit #1, a clear double glazed unit with a 12.5 mm air cavity and a foam edge-seal, is considered to be the reference unit. The remaining six glazing units contain a number of variations from this reference configuration and the presentation of the simulation results will typically contrast the effects of these physical variations on the temperature profile of the glazing unit in question relative to the reference glazing unit.

6.4.3.2 Composite Results

Figure 6.16 is a composite plot showing the temperature profiles for all seven glazing units. Most figures are plotted to the same temperature scale to facilitate both qualitative and quantitative comparisons.

In Figure 6.16 it is relatively easy to sort out the different temperature profiles on the basis of their center-glass heat transfer characteristics. For example, in the mid-part of the graph, away from the top and bottom edge effects, the lowest performing unit is the double glazed 6.35 mm unit, and the best performing units are the clear triple unit with the largest

spacings (two 12.7 mm air cavities) and the 12.7 mm low-E unit. The remaining units occupy a position consistent with intuition.

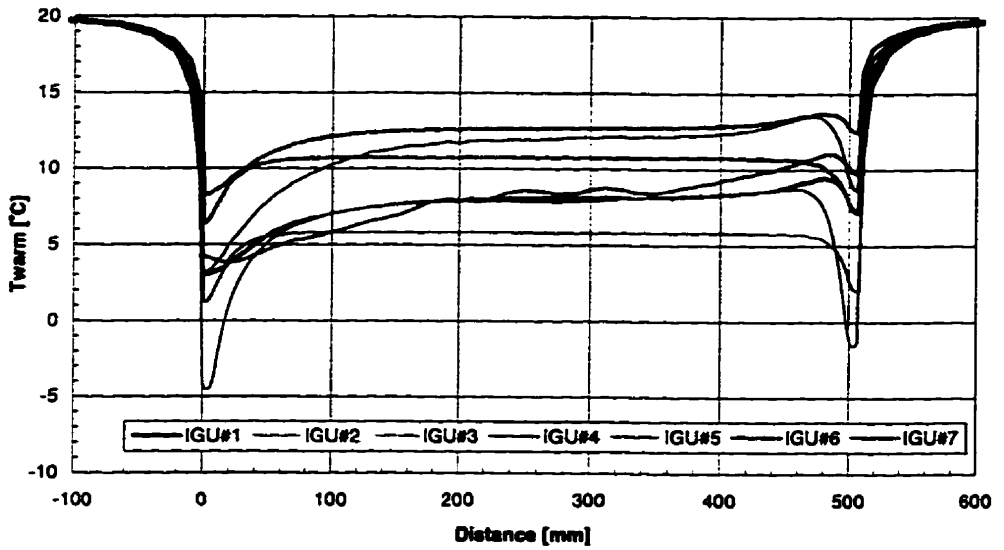

Figure 6.16: Warm Side Temperature Profile for All Seven Blind Test Glazing Units.

Figure 6.17 is a comparison of the temperature profiles for two glazing units identical except the spacer. IGU #1 has a 12.7 mm foam spacer and IGU #2 has a 12.7 mm conventional aluminum spacer bar. Both units have been modeled with appropriate amounts of sealant material. The model used for the aluminum spacer bar configuration incorporates a very narrow air gap (50 microns) to simulate the effects of the contact resistance which occurs at the glass-metal interface. For details about edge-seal modeling the reader is referred to

Fraser *et al.* (1993) and Wright *et al.* (1994) where a detailed comparison of spacer simulation models and experimental measurements is carried out. As expected, the unit with the aluminum spacer bar shows significantly lower temperatures than the unit with the foam spacer at both the head and sill regions. Across the center of the glazing unit the temperature profiles are essentially identical. The region of departure from the temperature profile of the reference unit IGU #1 is of order 50 mm at the top and 75 mm near the bottom.

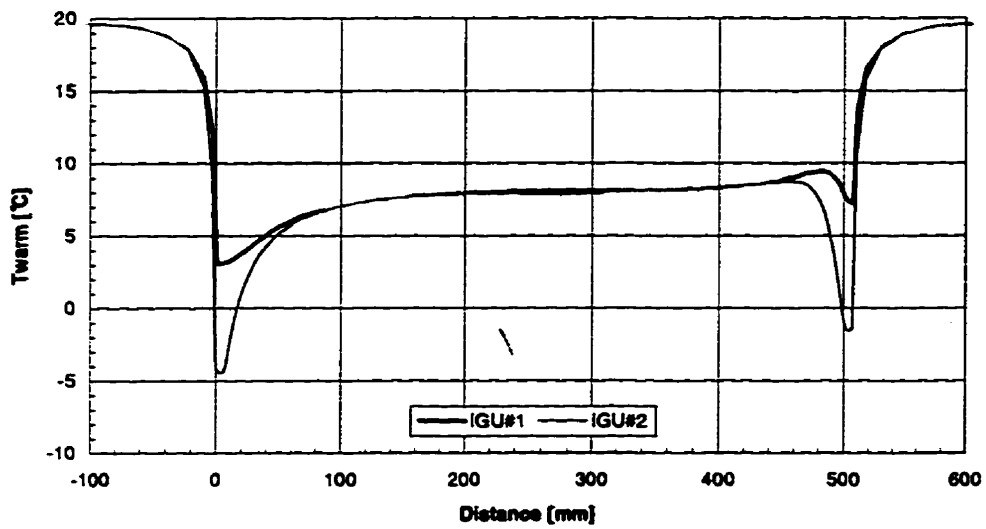

Figure 6.17: Effect of Spacer Material, Foam *versus* Metal, IGU's #1 and #2.

Since most attention is usually focused for condensation reasons on the sill portion near the lower sight line, an enlarged plot of this region for all seven glazing units is shown in

Figure 6.17. Again, the qualitative features illustrated in this figure can be easily explained. The coldest temperature is for the metal spacer, with the next coldest the narrow-gap 6.75 mm foam spacer.

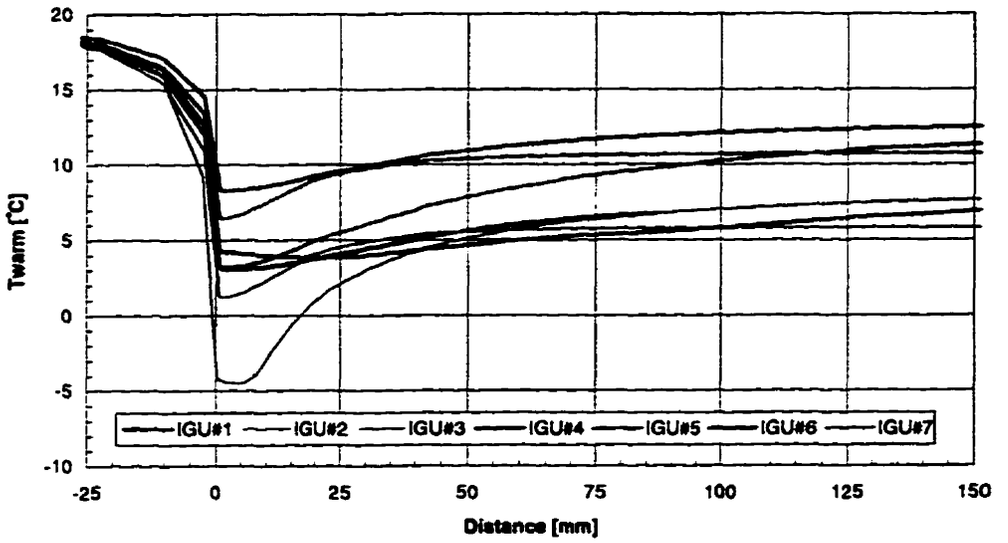

Figure 6.18: Enlarged Plot of Temperature Profiles Near Bottom Edge.

The two units with 12.7 mm foam show incremental improvement as does the unit with the 19.1 mm foam spacer. Both triple glazed units show the increased benefits of the longer path lengths through the foam spacer constituting the thermal bridge as well as the

incremental resistance provided by the additional pane of glass. Because all of these units are glazing units only, without a sash or frame, the reader is cautioned not to generalize these results to complete windows.

6.4.3.3 Effect of Pane Spacing

Figure 6.19 shows the temperature profiles for IGU samples #1, #3 and #4. These three glazing units are identical except for the thickness of the air cavity (and the corresponding foam spacer). The three spacings represented are 6.4, 12.7 and 19.1 mm. The temperature profile for IGU #3 is significantly "flatter" across the center-glass region.

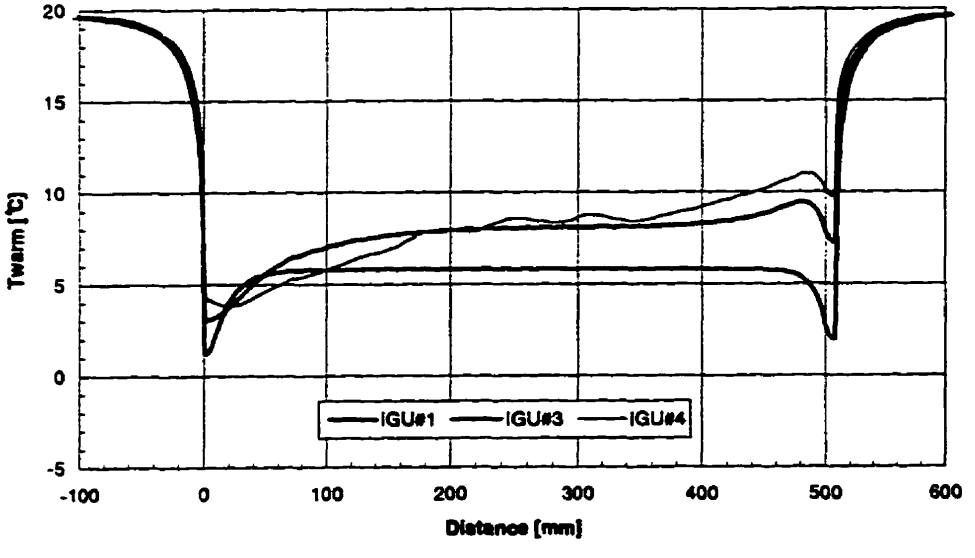

Figure 6.19: Effect of Pane Spacing IGU's #1, #3, and #4.

Although the mid-point temperatures for both units #1 and #4 are similar (an expected result since we know that beyond a spacing of 12.7 mm there is little additional benefit to going to larger spacings (Wright, 1989), these two temperature profiles have different characteristic shapes. The 19.1 mm profile is affected by the presence of secondary cells not noticeable in the other cases. The slope changes progressively from the 6.75 mm to the 12.5 mm and finally the 19.1 mm unit because of the changing convective flow in the cavity. The mechanism of convective heat transfer shifts from conduction to boundary layer transport as the aspect ratio of the glazing cavity increases. The temperature profile for IGU #4 also, as mentioned, exhibits characteristics of the secondary flow, "cat's eye cells" (Wright and Sullivan, 1989a, 1994).

6.4.3.4 Effect of Low-E

Figure 6.20 shows the temperature profiles for IGU samples #1 and #5, two glazing units identical in all respects except for the presence of a low-E coating (modeled with an emissivity of 0.20) on the cavity side of the outdoor or cold-side pane of IGU #5. The main observation to be made is that the presence of a low-E coating reduces the overall heat transfer through the glazing unit resulting in significantly warmer temperatures on the warm side except near the edges of the two glazing, where the glazing units have identical 12.7 mm foam spacers. Clearly, the effect of higher center-glass thermal resistance does not extend to

the edge of glass region. Improved spacer designs must accompany enhanced center-glass features.

The effect of the thermal bridging superimposed on convective effects persists for a significant distance away from the lower edge, up to as much as 150 mm. At the top the "edge effect" appears to be present for a dimension of order 100 mm.

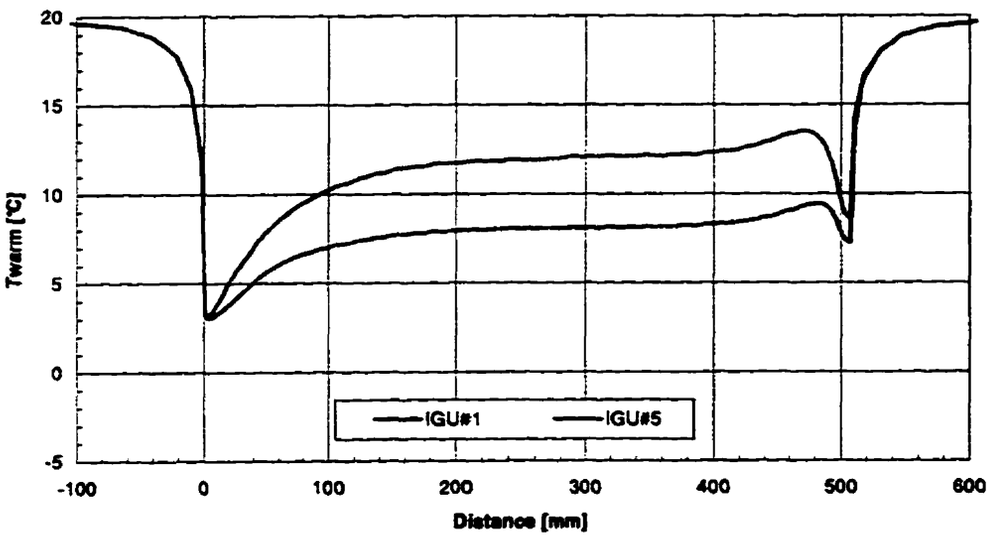

Figure 6.20: Effect of Low-E Coating, IGU's #1 and #5.

6.4.3.5 Triple Glazed Units

Figure 6.21 shows the temperature profiles for the two triple glazed units (IGU #6 with two 12.7 mm cavities, and IGU # 7 with two 6.75 mm cavities). In Figure 6.21 it can be seen that profile shapes through the center-glass differ because of the difference in cavity aspect ratios. The unit with the higher aspect ratio (i.e., narrower pane spacing) has a flatter curve. The same observation was made regarding the various double glazed units.

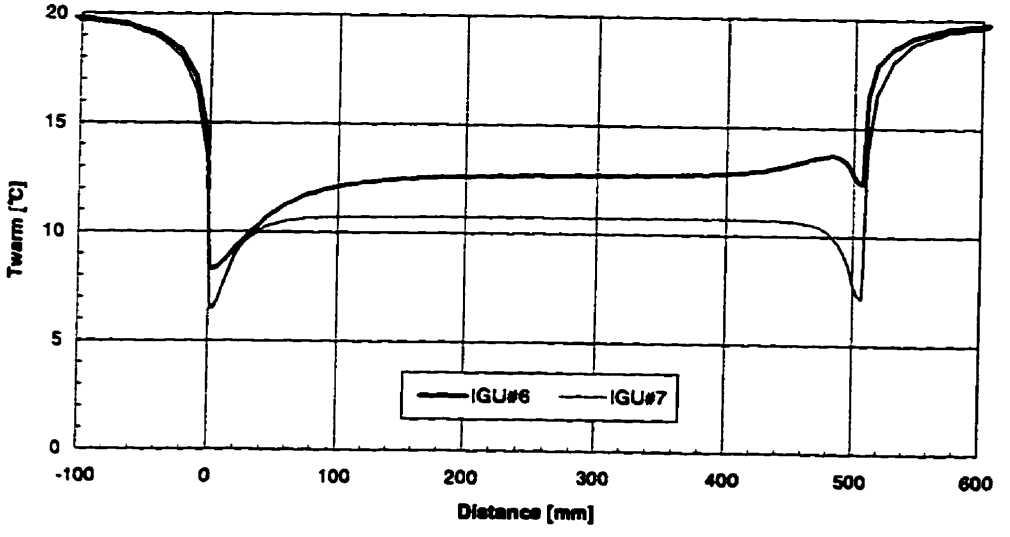

Figure 6.21: Comparison of Triple Glazed Units #6 and #7.

Another observation from Figure 6.21 is, as expected, that IGU #6 has a higher edge-glass temperature than IGU #7 because of the longer thermal path through the thicker spacers.

A variety of interesting observations can be made by comparing the bottom edge temperatures of the triple glazed units *versus* IGU #5 - the double glazed low-E unit with 12.7 mm (1/2 inch) pane spacing. The center-glass temperatures of these three units are similar but the bottom edge-temperatures of the triple glazed units are higher because of the additional conduction path length and because the intermediate pane segments the convective fill-gas flow.

6.4.4 Comparison of Thermographic Measurements and 2-D Simulation

This section reproduces part of the paper by Sullivan *et al.* (1996). The text below retains most of its original content and is changed only where appropriate. This collaborative research study reported surface temperatures for a series of insulated glazing units (IGU's). The research groups involved included two simulation laboratories and two thermographic measurement laboratories. Each group was required to obtain their data without knowledge of the results of the other groups. A manufacturer of commercial edge-seal products assembled multiple sets of glazing units having the characteristics listed in Table 6.10. Two laboratories with the capability of making thermographic measurements were supplied with sample sets.

One laboratory (LAB #1) constructed an apparatus consisting of two environmental chambers; the cold chamber is a modified commercial food freezer and the warm chamber incorporates an adjustable bellows to admit infrared (IR) thermography (Griffith *et al.*, 1996). The second laboratory (LAB #2) uses a guarded hot box with modifications to facilitate the IR camera (Elmahdy, 1996). Each laboratory was required to report cold-side and warm-side heat transfer coefficients.

The first simulation laboratory (SIMUL #1) corresponds to the research group of which the author is a part and used the BRAVO code. The second simulation laboratory (SIMUL #2) used a commercial finite element code to complete 2-D simulations (Zhao *et al.*, 1996).

The test laboratories were asked to impose test conditions similar to the ASHRAE winter design condition (i.e., 6.7 m/s wind on the cold side and natural convection on the warm side). Since the actual laboratory warm and cold side heat transfer coefficients were not known *a priori*, the simulation laboratories used the conditions shown in Table 6.11 (h_i = 8.3 W/(m^2°C) and h_o = 30 W/(m^2°C)). When the test results were available it was found that LAB #1 reported an average indoor side heat transfer coefficient of 7.6 W/m^{2}C and an outdoor side coefficient of 28.9 W/m^{2}C. The corresponding values from LAB #2 were 7.3 W/m^{2}C and 30.0 W/m^{2}C. A sensitivity study to heat transfer coefficient is given in section

6.6.1. Note that the heat transfer coefficients (film coefficients) mentioned above account for both convective and radiative heat transfer.

6.4.4.1 Comparison Results

Figures 6.22 through 6.28 represent a compilation of the results for each of the seven IGU's, respectively. Each figure shows four vertical profiles of surface temperature - one from each of the research groups. In each figure two curves represent simulation results and two curves represent measured data. The horizontal axis corresponds to vertical distance ranging from zero at the bottom edge of the IGU to 508 mm at the top of the IGU. The vertical axis shows the temperature scale which ranges from -6°C to 16°C except where results are shown for IGU #2 (the only unit with aluminum spacer bar) where the scale is shifted down by 2°C due to the lower temperature in the botton of the IGU.

It should be noted that the surface temperature curves are plotted without adjustment even though each one corresponds to a specific film coefficient as discussed earlier. Differences caused by the differences in film coefficients are not large (estimated to be of order 1°C). It is important to recognize that simulations were performed using a uniform warm side film coefficient. In other words, a constant value of h_i was applied at each location over the surface of the IGU. In contrast, h_i is not expected to have been constant over the height of the glazing units that were tested. Indoor air moves downward over the face of the IGU and mask wall forming thermal and velocity boundary layers. As a result the local value

of h_i is expected to be higher near the top of the IGU decreasing with distance downward. This trend in h_i would, in itself, have caused warmer surface temperatures near the top of the IGU. Since the fill gas motion causes a similar trend it is difficult to distinguish between the two effects. However, some portion of the difference between simulation and measurement can be explained by the modeling assumption of constant h_i. It should be pointed out that the mounting configuration selected for this study (i.e., IGU mounted flush with mask wall on the warm side) was intended to minimize local variations in h_i. The more usual situation of an IGU recessed in a sash and frame is known to have local pockets of flow recirculation/stagnation in the edges where detailed information is of interest but also where h_i is expected to be minimum

All of the data sets presented in Figures 6.22 through 6.28 show good agreement. It can be seen, even without adjustment, that each set of curves falls within a band typically no wider than ±1°C. Exceptions occur in the vicinity of steep temperature gradients as seen near the top and bottom of the glazings where the observed temperature band can be as large as ±3°C. However, these discrepancies are misleading knowing that some spatial uncertainty exists regarding the location of measured profiles - a topic which is discussed in more detail in Sullivan *et al.* (1996).

Although the sample sets include units with a wide variety of parameter variations (e.g., pane spacing, edge-seal type) all of the surface temperature profiles have a common

characteristic shape. Differences in detail can be seen from one curve to the next depending primarily upon differences in the mechanisms of conductive and convective heat transfer.

In all seven IGU's the thermal resistance of the edge-seal is less than the corresponding resistance of the centre-glass area. This thermal bridge causes higher heat flux and colder warm-side surface temperatures at the perimeter of the IGU. Each curve shows a local minimum at, or very near, the top and bottom of the glazing.

The effect of edge-seal conduction is seen at both the top and bottom. Fill gas motion provides additional cooling at the bottom edge and reduced cooling at the upper edge. Therefore, the combined effect of the edge-seal conduction and the fill gas convection consistently places the coldest temperature near the bottom edge. For this reason condensation resistance studies focus on this region of the window.

If one focuses on the centre-glass portion of the profiles a change in slope can be seen as a function of pane spacing. This characteristic is a result of the different aspect ratios of the glazing cavities. Glazing systems with narrow pane spacings (IGU's #3 and #7) have the flattest temperature profiles through the center-glass area and the narrowest region where edge-glass effects can be seen. Wider pane spacings are accompanied by a more pronounced slope in the center-glass temperature profile and edge-effects that extend further from the sight line.

In addition, at the widest pane spacing (IGU #4) the simulations show evidence of secondary cells in the fill gas flow resulting in ripples on the surface temperature profile. The laboratory data do not show these ripples. This discrepancy is likely caused by the fact that the Rayleigh number of the cavity (Ra » 2.2 x 10^4) is high enough (i.e., pane spacing and temperature difference are high enough) not only to exceed the critical value of Ra for secondary cells to form (Ra_c » 6.85 x 10^3) but also for a time-unsteady fill gas flow to exist (Wright and Sullivan, 1989a, 1994). Consequently, the local effect of individual cells would not be apparent in the glass temperature as the cell locations constantly change. In contrast, the numerical calculation generates a steady solution with stationary cells and their effect is then seen in the temperature of the glass.

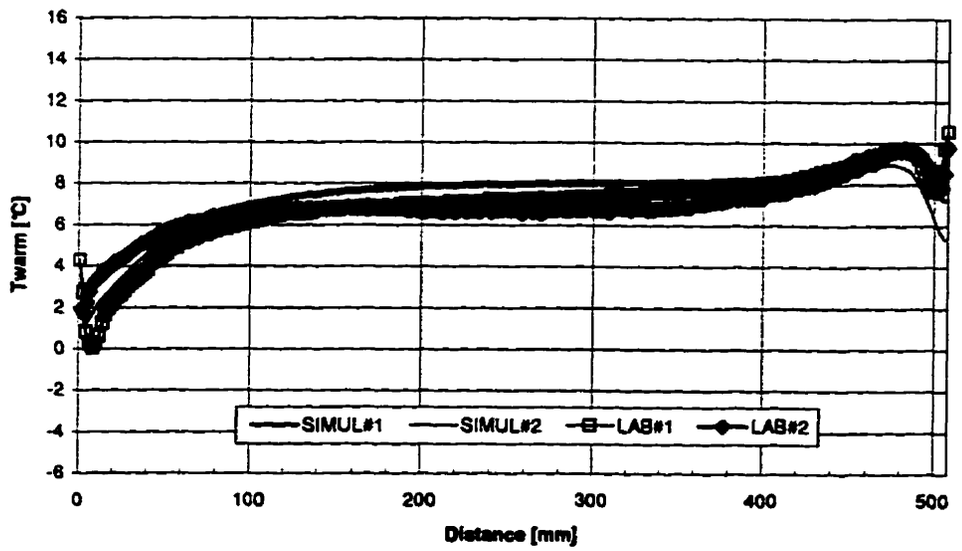

Figure 6.22: Temperature Profiles, IGU #1, Clear Double 12.7 mm Foam Spacer.

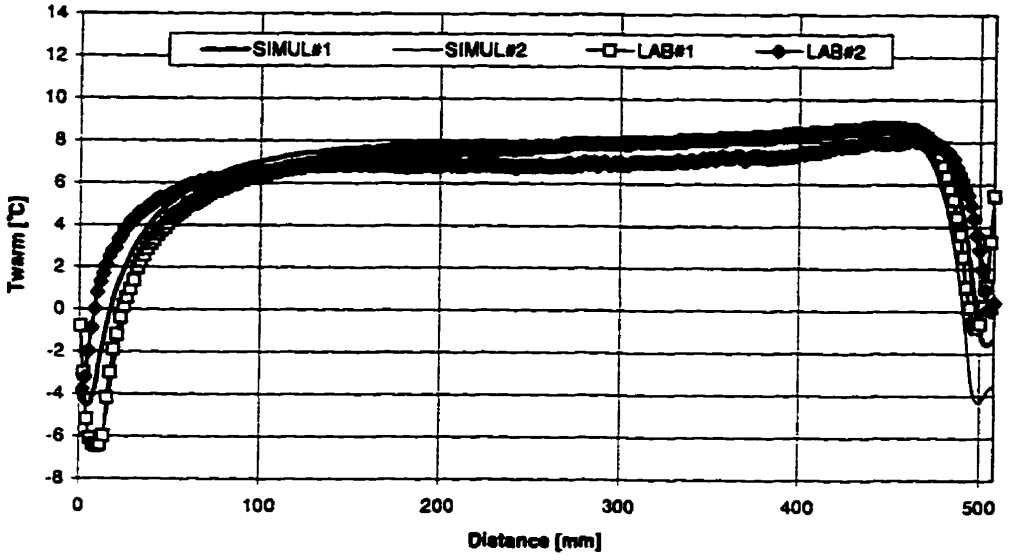

Figure 6.23: Temperature Profiles, IGU #2, Clear Double 12.7 mm Aluminum Spacer.

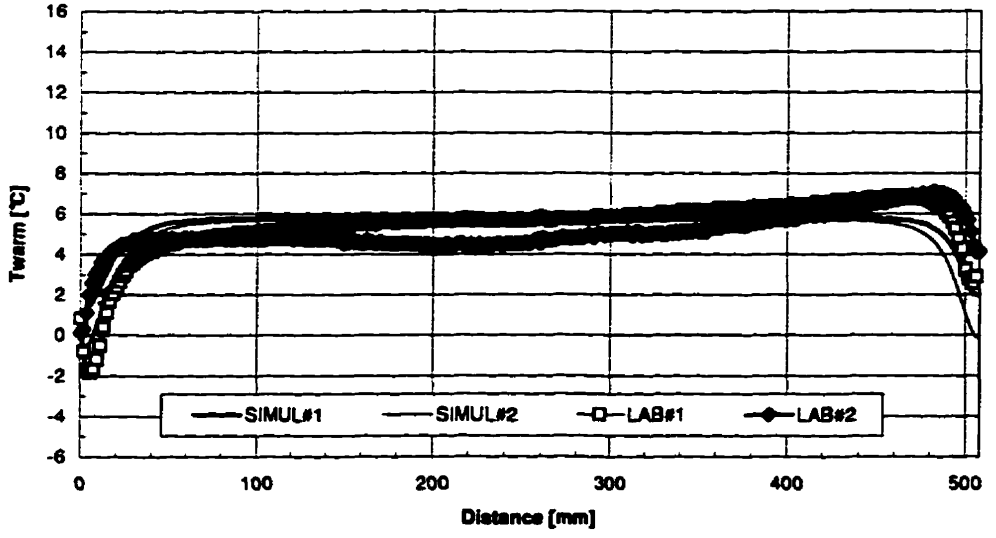

Figure 6.24: Temperature Profiles, IGU #3, Clear Double 6.4 mm Foam Spacer.

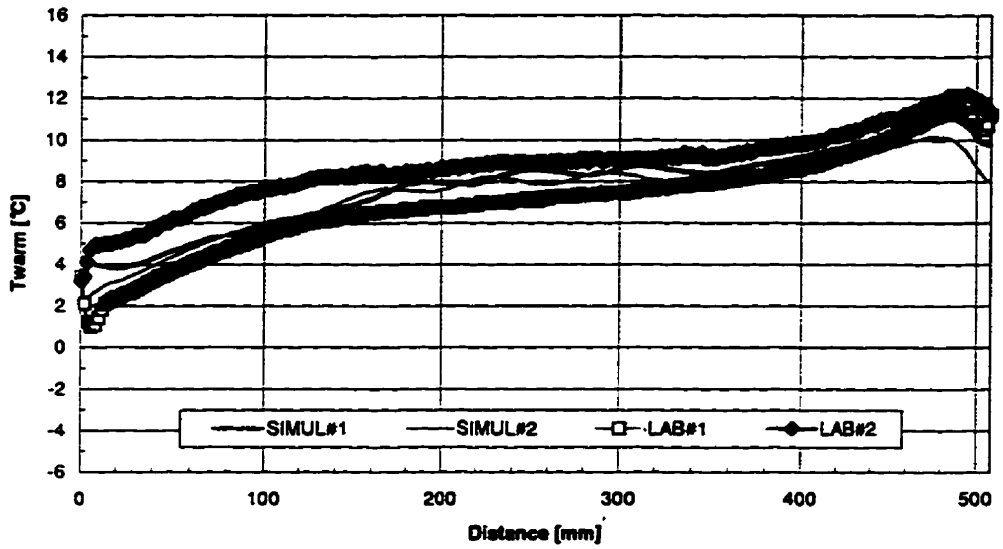

Figure 6.25: Temperature Profiles, IGU #4. Clear Double 19.1 mm Foam Spacer.

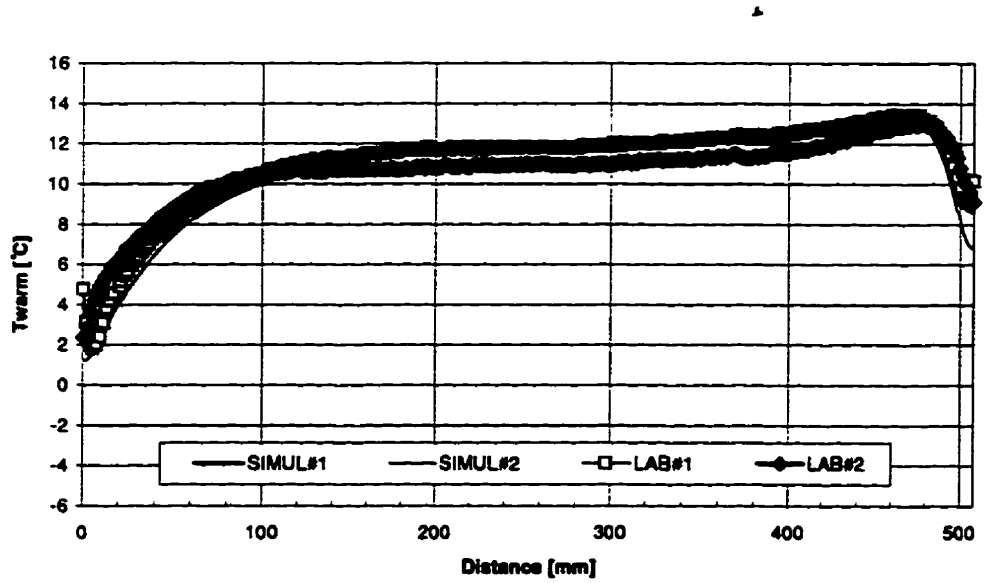

Figure 6.26: Temperature Profiles, IGU #5, Low-E Double 12.7 mm Foam Spacer.

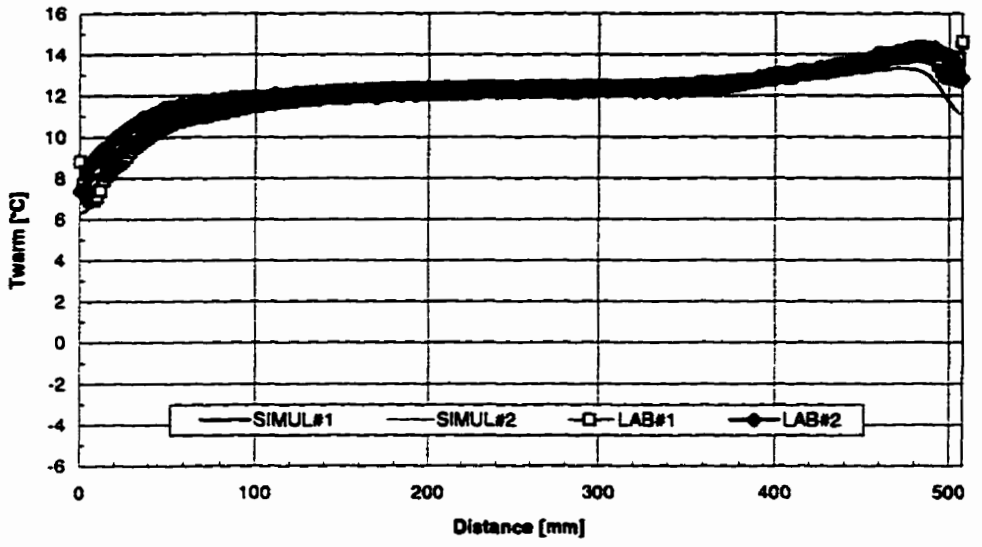

Figure 6.27: Temperature Profiles, IGU #6, Clear Triple 12.7 mm Foam Spacer.

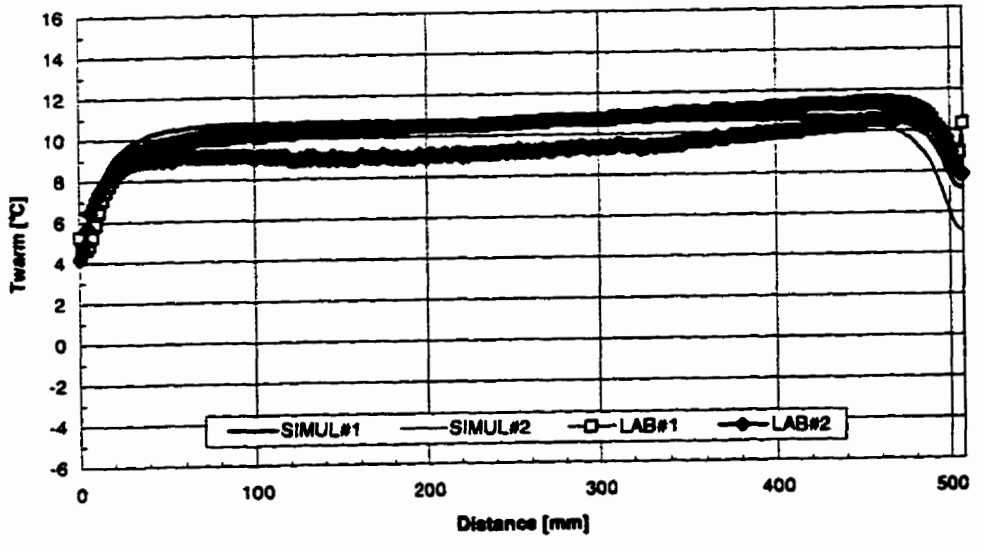

Figure 6.28: Temperature Profiles, IGU #7, Clear Triple 6.4 mm Foam Spacer.

6.5 Deflected Windows: Sensitivity Analysis

This section presents a sensitivity analysis to study the effects of glazing deflection on heat transfer and fluid flow in an IGU when the fill gas pressure changes. Difference in pressure between the IGU cavity and surrounding environment will deflect the IGU glass panes. This pressure difference may be caused either by a change in altitude, i.e., the window is transported to a higher elevation, or *vice-versa*, or by changes in temperature as occur during normal temperature variations. The simulation results are presented as streamlines, surface temperature profiles, and local Nusselt number distribution.

6.5.1 Glazing Units Details and Mounting Configuration

The double glazed unit involving a 12.7 mm foam spacer is modeled as shown in Figure 6.29. The clear double glazed IGU, 12.7 mm foam spacer, was chosen to provide a source of comparison with the experimental data of Beck *et al.* (1995).

It is worth noting, again, that the IGU is mounted in a mask wall without sash or frame. The advantage of this simple arrangement is the removal of complicating factors. The disadvantage, however, is that the reader must keep in mind, for instance, that sensitivities to edge-seal structure may be magnified. In particular, the edge-seals of these glazing units studied account for a greater percentage of the heat loss than they would be a sash present.

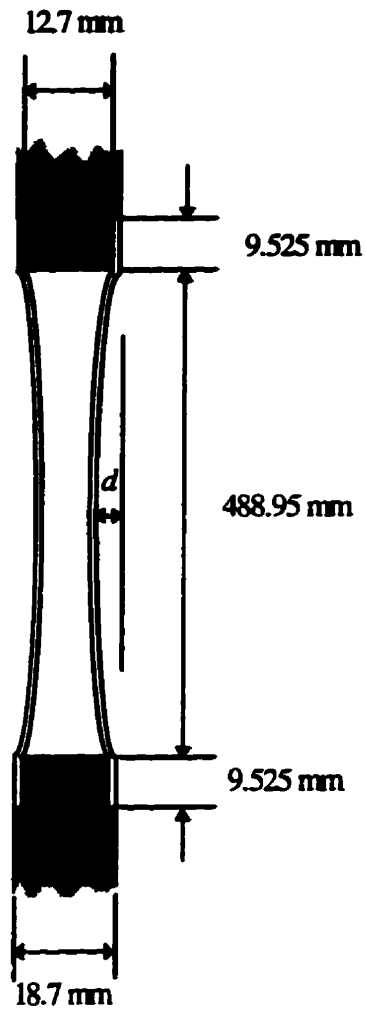

Figure 6.29: Deflected Window - Glazing Unit and Mask Wall Geometry.

6.5.2 Simulation and Test Conditions

The glass panes of a clear double glazed IGU, 12.7 mm spacer, filled with air is deflected in increments of 1 mm on each side to a maximum of 5 mm. The results are

evaluated only qualitatively because the actual deflection in the experiments of Beck *et al.* (1995) is not reported. Five cases are simulated with deflections of 1, 2 ,3, 4 and 5 mm on each side of the IGU.

The boundary conditions used are listed in Table 6.12. The heat transfer coefficients include both long wave radiation and convective effects. No solar radiation is present. These are the boundary conditions reported by Beck *et al.* (1995).

Indoor Temp T_i	Indoor Heat Transfer Coefficient h_i	Outdoor Temp T_o	Outdoor Heat Transfer Coefficient h_o
21.1°C	8.4 W/(m^2°C)	-17.8°C	20 W/(m^2°C)

Table 6.12: Deflected Window - Glazing Unit Boundary Conditions.

6.5.3 Simulation Results

Streamlines are shown in Figure 6.30, local Nusselt number distribution on the warm side of the cavity in Figure 6.31, and temperature profiles in Figure 6 32.

In Figure 6.30 it is observed that with a 1 mm deflection, two weak recirculation cells appear at the bottom and top of the IGU, and gain strength as the deflection is increased. A unicellular motion around the IGU walls still exists in all cases.

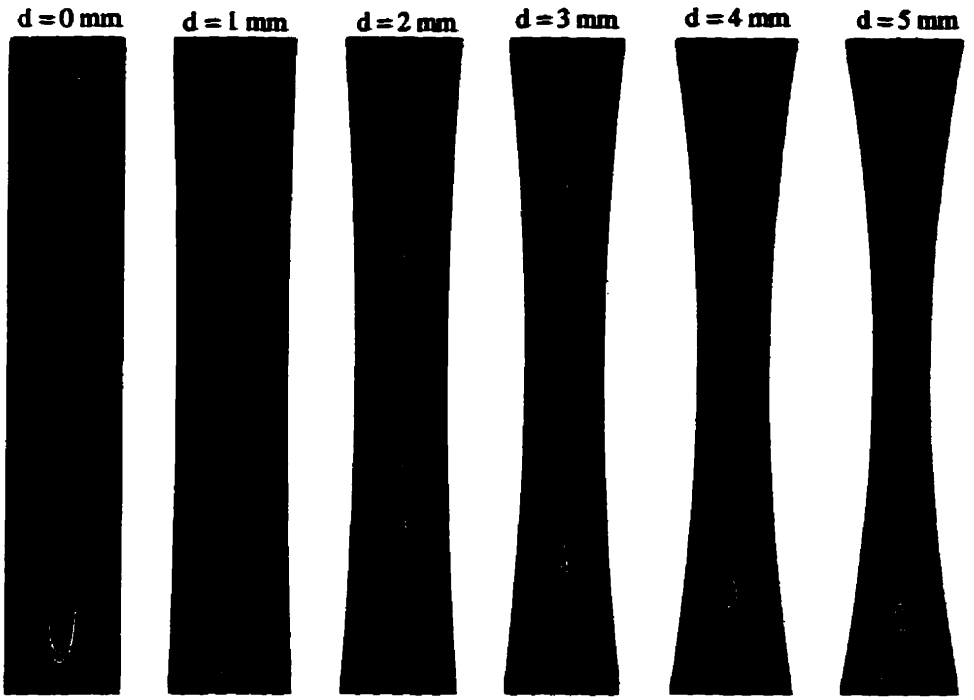

Figure 6.30: Deflected Window - Stream lines.

It is interesting to note in Figure 6.31 that the heat flux at the top and bottom of the cavity and at the center is augmented as the deflection increases until d = 3 mm. At d = 4 mm heat flux begins to decrease sharply at the bottom and slightly at the top, with a continuous increase at the center of the cavity. This increase in the heat flow at the top and bottom of the cavity until d=4 mm is due to the formation of the cells. The center increase is due to a decreasing conduction path.

Figure 6.32 shows the warm surface temperature profiles for the five deflected IGU's and the IGU without deflection. It can be seen that, with increasing IGU deformation, the center temperature decreases and is no longer uniform.

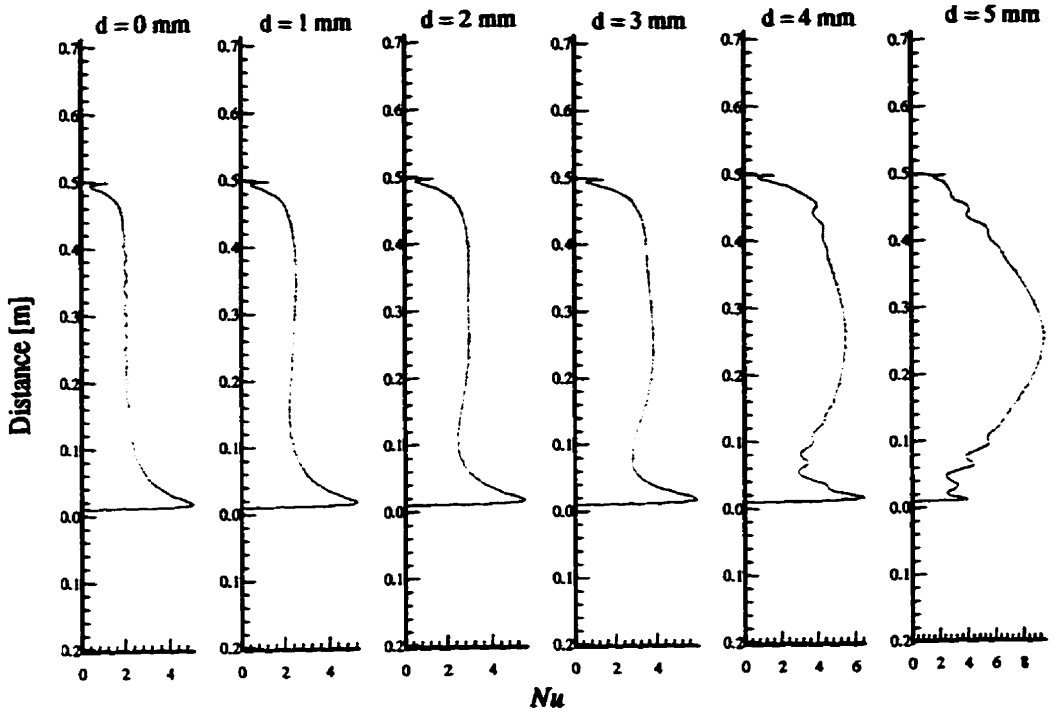

Figure 6.31: Deflected Window - Local Nusselt Number Distribution.

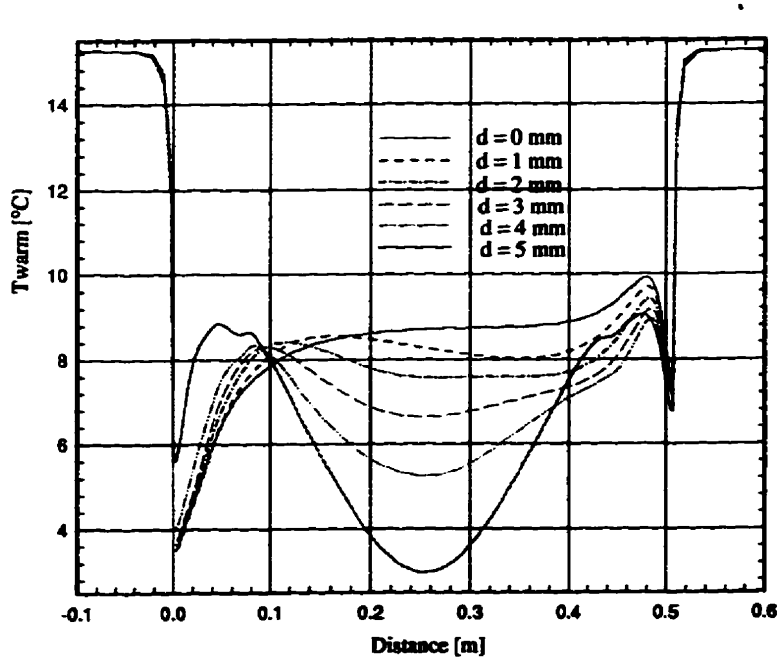

Figure 6.32: Deflected Window - Warm Side Surface Temperature Profiles.

Table 6.13 shows the heat flux, overall heat transfer coefficient, *U-factor*, and the resistance, *R*, for the IGU without deflection and for the deflected cases. As expected, it can be noticed that increasing the deflection increases the heat transfer.

Deflection, d [mm]	Heat Flux, q [W/m^2]	Overall Heat Transfer Coefficient, U-Factor [W/(m^2°C)]	Resistance, R [(m^2°C)/W]
0	109.01	2.79	0.36
1	110.77	2.85	0.35
2	113.47	2.92	0.34
3	117.29	3.02	0.33
4	123.15	3.16	0.32
5	133.18	3.42	0.29

Table 6.13: Deflected Window - Heat Flux, Overall Heat Transfer Coefficient and Resistance.

A comparison is made with the warm surface temperature profile reported by Beck *et al.* (1995) and it is found that the best agreement for the center glass temperature corresponds to the case of 2 mm deflection. However the temperatures differ about 1.25°C at the top, 0.65°C at the bottom and 0.25°C at the center glass

6.6 Sensitivity Analysis

In this Section to test the effects of outside and inside heat transfer coefficients a sensitivity analysis is made. These results are particularly applicable when analyzing the results of Section 6.4 where attempts were made to compare simulations with measurements in two laboratories from a "blind study" in which actual test conditions are unknown *a priori*.

At the outset of Section 6.4 it was clear that although several laboratories would attempt to test identical sets of glazing units at the **same test conditions**, physical differences in the laboratories would invariably lead to different boundary conditions. For example, one laboratory uses a perpendicular wind direction whereas the other laboratory uses a parallel wind direction on the cold side. In addition, there are differences associated with the presence or absence of constant temperature radiation baffles. These differences are expected to influence the cold side and warm side film coefficients. When simulating a given configuration the geometries of the test chamber differ, which in turn may have an impact. Also, the laboratories were testing similarly constructed windows, not the same windows, thus minor differences in material properties and geometries also exist.

6.6.1 Effects of Heat Transfer Coefficients.

In the literature review, Section 2.2.1.6, it is shown that heat transfer coefficients are an important issue in window thermal performance. It is known that with an increase of the thermal resistance of windows the external heat transfer coefficient does not become unimportant until the window reaches a thermal resistance in the range 1.4-1.8 (m^2K/W (Yazdanian and Klems, 1994). It is not known how changes in heat transfer coefficients affect the surface temperature of the window. The purpose here is to vary the heat transfer coefficient and observe its impact in the surface temperature of the IGU on the warm side.

Although the simulations, in most of the cases presented in Sections 6.2 to 6.5, are performed with constant outside and inside heat transfer coefficients, the test conditions and the real world installation geometry (sash and frame components, sills, recessed windows etc.) are not likely to yield uniform film coefficients. This invariably will lead to differences between simulations and measurements, the extent of which can only be determined by data comparison.

First a sensitivity analysis of a flush mounted window (on the warm side) is made. Second a recessed window is used to investigate the impact of the stagnant air pockets at the edges of the glass pane.

6.6.1.1 Flush Mounted Insulating Glazing Units

To relate the findings of this Section with Section 6.4 a clear double-glazed unit, with a 12.5 mm air cavity and foam edge-seal is chosen for the sensitivity analysis. This is the configuration used as the reference glazing unit in Section 6.4, Figure 6.15 and Table 6.10. Figure 6.15, insert a, give details of this glazing unit and of the mask wall in which it is mounted.

The total heat transfer coefficients on the cold and warm sides, designated h_i and h_i, combine both the convective and radiative effect. The nominal test conditions are to reproduce forced convection of 6.7 m/s on the cold side and natural convection on the warm side. Typically this would result in coefficients for h_o of up to 34 W/(m^2°C) and for h_i of 8.3 W/(m^2°C). To have "simulation conditions" match "test conditions" (see section 6.4), these coefficients are fixed at 30 and 8.3 W/(m^2°C), respectively.

Figures 6.33 and 6.34 display the effect on the indoor surface temperature profile for the reference glazing to changes in h_i in increments of 1 (6, 7, 8 and 9 W/(m^2°C)) for a fixed h_o of 30 W/(m^2°C) and to changes in h_o in increments of 10 (10, 20, 30 and 40 W/(m^2°C)) for a fixed h_i of 8 W/(m^2°C).

Figure 6.33 shows that variations in h_i in the range 6 to 9 simply shift the profile but preserve the profile similarity. Figure 6.34 shows that beyond a value of h_o = 30 W/(m^2°C little additional effect is expected and that in the range from 10 to 30 the major qualitative effect is to shift the temperature profile with the profile shape remaining unchanged. The results in Figure 6.34 were also calculated using h_i = 8.3 W/(m^2°C) to correspond to Section 6.4, with no qualitative variation from Figure 6.34.

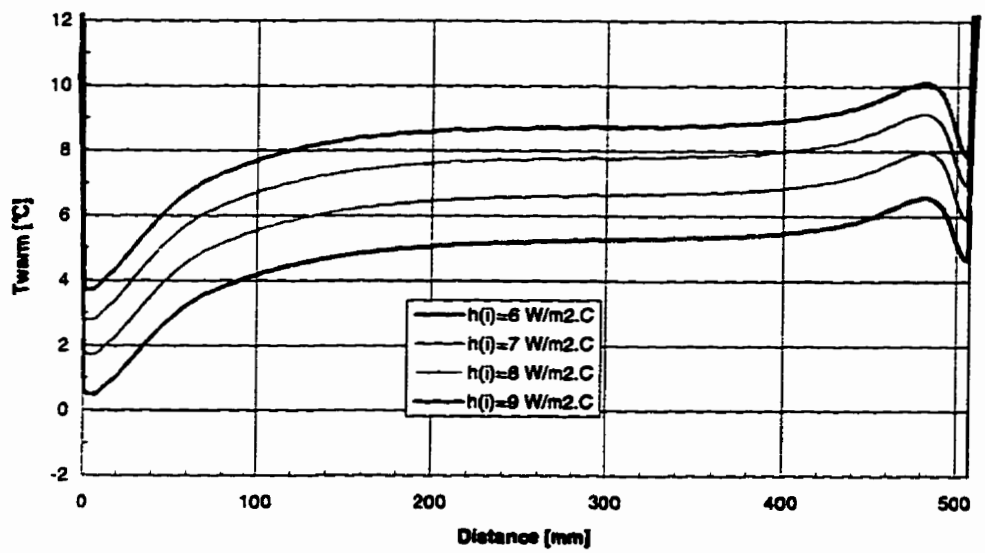

Figure 6.33: Effect of Changes in h_i with h_o fixed at 30 W/(m^2 °C).

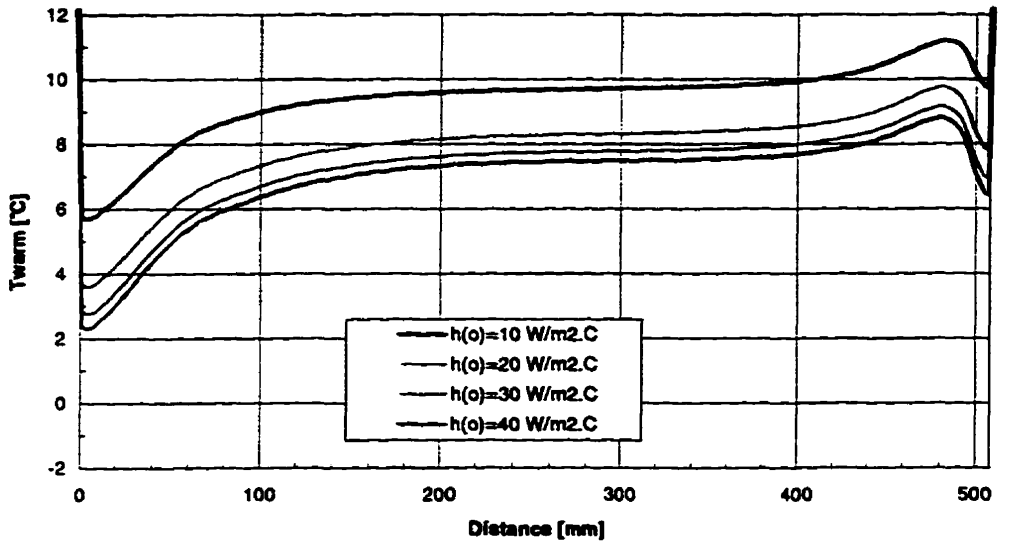

Figure 6.34: Effect of Changes in h_o with h_i fixed at 8 W/(m^2 °C).

6.6.1.1.1 Flush Mounted Insulating Glazing Units - Locally Varying Heat Transfer Coefficient

Although the actual local convection heat transfer profile is unknown, it is interesting to see how the surface temperature profile changes when a spatially varying heat transfer coefficient on the warm side (h_i) is used. The most reasonable assumption is to use h_i for a non-isothermal flat plate (Smith *et al.*, 1993). The problem in applying the flat plate profile is to determine where the boundary layer originates. This is complicated by the stagnation zone at the top edge of the room (ceiling - wall mask) and the large step change in temperature

between IGU and mask wall. Five starting location for the thermal boundary layer are simulated. The most convenient scenario is to place the first start point at the top of the IGU (spacer/mask wall), 508 mm from the bottom of the IGU. This is case #1. The subsequent starting points were located from the bottom of the IGU as follows: #2 at 538 mm, #3 at 629.6 mm, #4 at 720.8 mm and #5 at 812 mm. For simulation purposes the starting point is determined when the calculated window temperature profile becomes insensitive to the starting point, in particular, when the maximum local temperature difference between two starting points is less than 1%. Figures 6.35, 6.36 and 6.37 show the schematics for the mask wall and IGU, convective heat transfer, and the temperature distribution variation with the distance from the bottom of IGU, respectively.

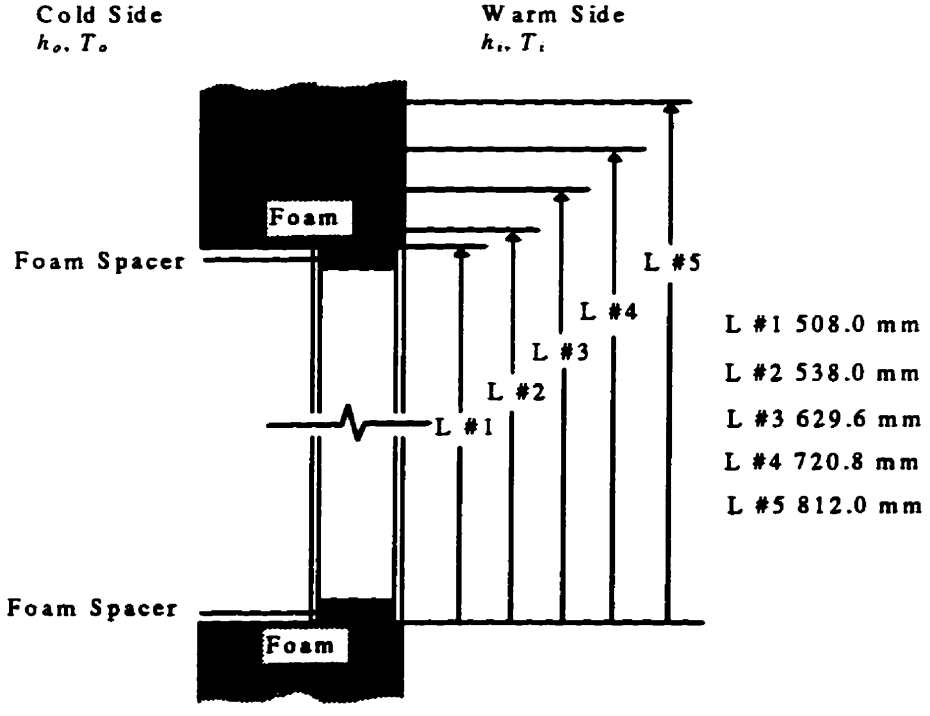

Figure 6.35: Schematic Configuration for Determination of Boundary Layer Starting Point.

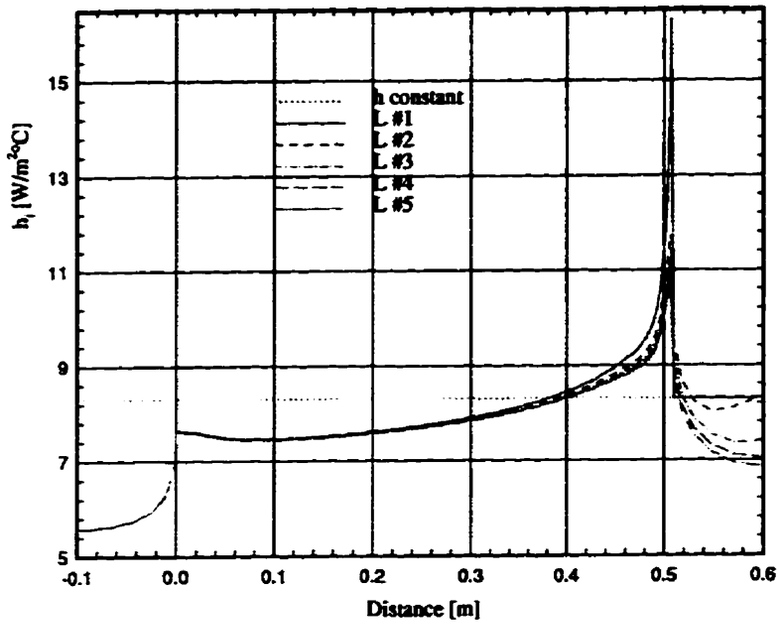

Figure 6.36: Heat Transfer Coefficient Distribution for Non-Isothermal Flat Plate for all Starting points.

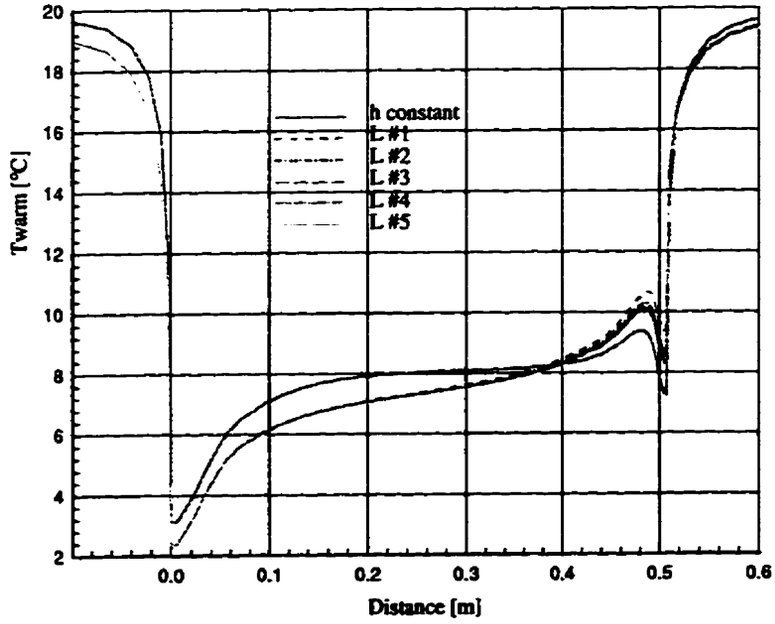

Figure 6.37: Temperature Distribution for a Non-Isothermal Flat Plate for all Starting Points.

From Figure 6.36 and 6.37, it can be seen that the starting point of the boundary layer has a substantial effect on the temperature profile at the top of the IGU. If the starting point of the boundary layer coincides with the top of the IGU, then h_{ci} is very high and there is an increase in temperature at the top of the IGU. It is observed that for an increasing distance from the top of the IGU (height of the boundary layer starting point), there was a decrease in the nominal value of h_{ci} that consequently decreases the temperature at the top of the IGU. It is worth noting, for these cases, that the temperatures at the bottom of the IGU are almost unaffected by variations in starting point height. This happened because the IGU is tall enough for the boundary layer to be well developed at the bottom hence it is much less dependent on the starting point of the boundary layer. This fact is important when the concern is the determination of a surface temperature profile to estimate condensation resistance, a bottom of the IGU concern. Recall that this is not a real window since it is not recessed in a frame. Frame effects are analyzed in Section 6.6.1.2.

Figures 6.38 and 6.39 show the heat transfer coefficient profiles, h_i, and the surface temperature profiles, respectively, for the four cases presented in Table 6.14.

In the Equations of Table 6.14 L is the height of the surface being considered, T_{surf} is the temperature of the surface, T_i is the room temperature, Ra_y is the Rayleigh number based on the distance y measured in the direction of the developing boundary layer, and k is the conductivity of the interior (room) gas, i.e. air at atmospheric pressure.

Cases	Warm Side Convective Heat Transfer Coefficient h_{ci} [W/(m^2°C)]
#1	Constant = 8.3
#2	Constant, based on the surface average temperature
	$h_{ci} = 1.42\left(\frac{T_{surf} - T_i}{L}\right)^{\frac{1}{4}}$ (6.7)
	ASHRAE equation for flat plate (ASHRAE, 1993)
#3	Isothermal flat plate (McAdams, 1956)
	$h_{ci}(y) = 0.4425\frac{k}{y}\left(Ra_y\right)^{\frac{1}{4}}$ (6.8)
#4	Non-Isothermal flat plate from Equation (6.1)

Table 6.14: Convective Film Coefficients for Sensitivity Analysis.

For the cases #2, #3 and #4, both components of h_i (convection and radiation) were updated continuously, i.e., estimated after each iteration. For cases #2 and #3 the surface temperature is based on the averaged window surface temperature. This gave similar results to those based on the glazing center temperature.

Figure 6.38 shows, as expected, that the local heat transfer coefficient value, h_i, for the flat plate, either isothermal or non-isothermal, goes from a higher value at the top decreasing to the bottom of the IGU. This is due to the downward movement of the air over the IGU face and mask wall, forming thermal and velocity boundary layers.

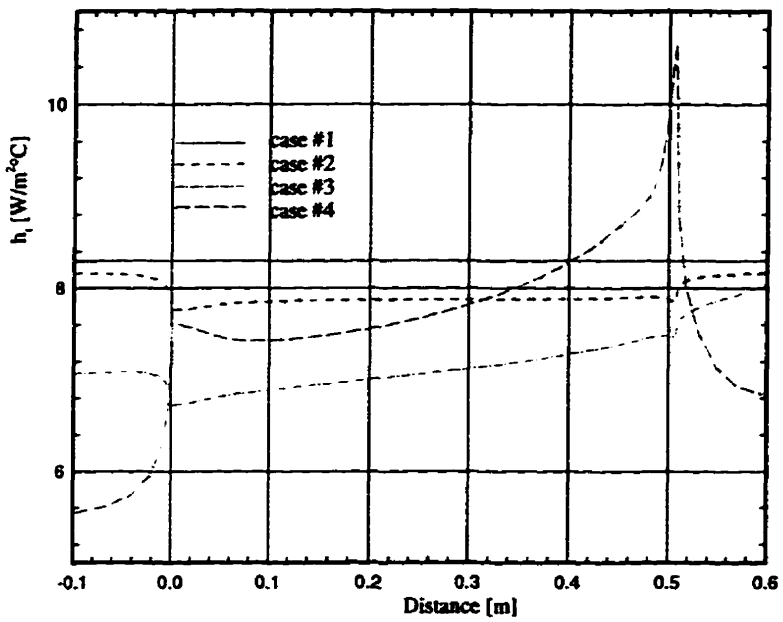

Figure 6.38: Heat Transfer Coefficient Distributions for cases #1, #2, #3 and #4.

The surface temperature profiles for these four cases are shown in Figure 6.39. The temperatures are warmer at the top and colder at the bottom for the non-isothermal flat plate case in comparison with the constant h_{ci} cases. The same pattern occurs for the non-isothermal flat plate in relation to the isothermal one. This is due to the higher heat transfer coefficient at the top that decreases towards the bottom in the case of the non-isothermal flat plate.

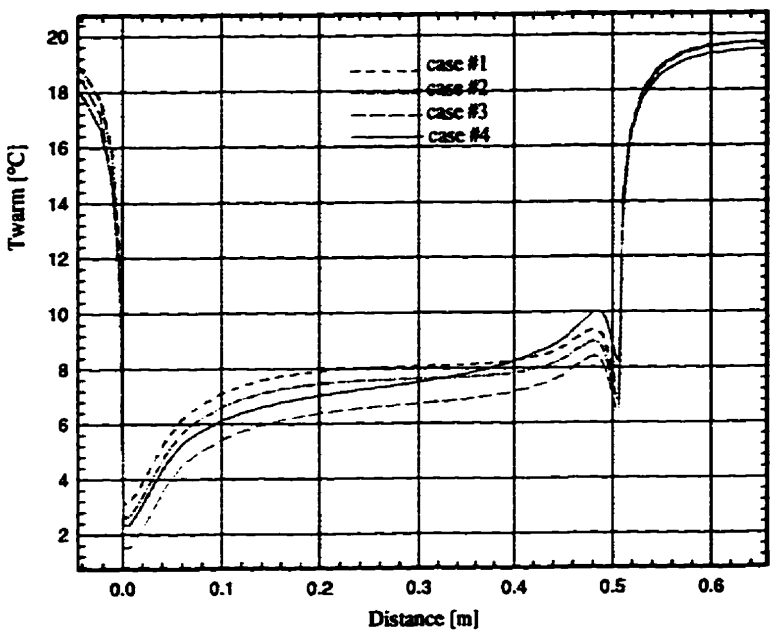

Figure 6.39: Temperature Profiles for Cases #1, #2, #3 and #4.

Figure 6.40 shows a comparison of surface temperature profiles for the four cases and the measured values from Griffith *et al.* (1996) presented in Section 6.4. It shows that the surface temperature for case #4 presents the best agreement with the measured temperatures. For case #4 the temperature profile practically superimposes the experimental one over the center glass region and departs from it at the top and bottom regions of the IGU. Note that there is greater measurement uncertainty (Sullivan *et al.*, 1996) at the top and bottom.

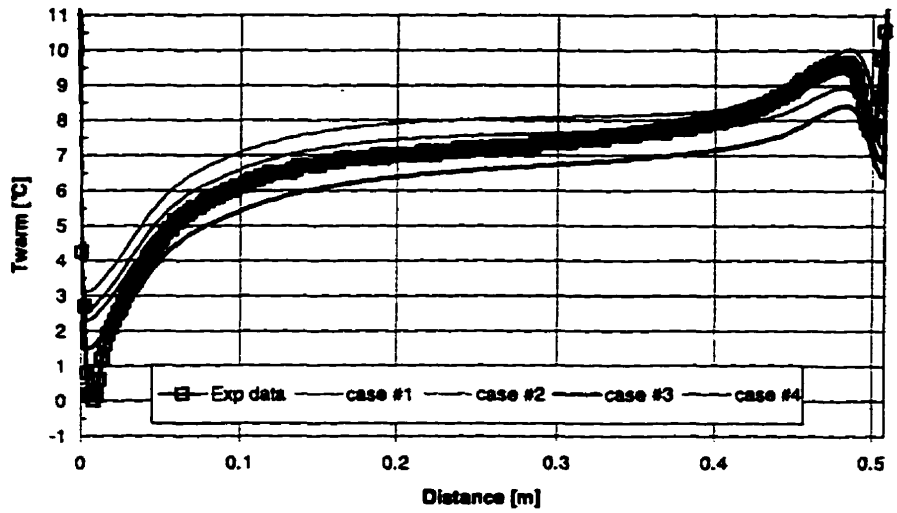

Figure 6.40: A Comparison of Four Simulated Surface Temperature Profiles *versus* a Measured Surface Temperature Profile.

6.6.1.2 Recessed Insulating Glazing Units

The common practice in heat transfer analysis in windows is to consider the inside heat transfer, h_i, constant. Clearly, from the previous section the convection heat transfer correlation for a flat plate provides a better approximation than a constant h_{ci}. For a recessed window, the effect of a step change is to locally reduce h_{ci}, due to the formation of air pockets (stagnation regions) at the top and bottom edges of the IGU (Curcija and Goss, 1993). There is also a change in h_{ci} caused by the radiation exchange between IGU, mask wall (step), and

room wall surfaces (in particular near the edge where the glazing surface sees the window sash and frame that are expected to be colder than the room surfaces).

In this section the effect of natural convection is verified with no radiation exchange between IGU surface and frame surfaces. To study convection effects five cases of h_{ci} boundary conditions are considered as follows:

case #1 - constant, using Equation (6.7);

case #2 - isothermal flat plate, utilizing Equation (6.8);

case #3 - non-isothermal flat plate, employing Equation (6.1);

case #4 - isothermal flat plate, Equation 6.(8), with correlations suggested by Curcija and Goss (1993), Equations (6.3) to (6.6);

case #5 - non-isothermal flat plate, Equation 6.(8), with correlations suggested by Curcija and Goss (1993), Equations (6.3) to (6.6).

For all cases above the radiation model uses the black body assumption for the room wall surfaces and air temperature outdoor environment. In the radiation model, no exchange among IGU and frame surfaces is considered, i.e. the IGU and frame surfaces "see" only the room walls. The radiation heat transfer coefficient is estimated using Equation (6.2).

Figure 6.41 shows the regions where the flow stagnates and recirculates in the IGU and mask wall. The flow stagnates at the top and bottom edges of the IGU, and recirculates at the upper edge of the vertical surface of the bottom mask wall. Details of the insulated

glazing unit and mask wall can be seen in Figure 6.5. The IGU is clear, air filled, with 19.05 mm foam spacer.

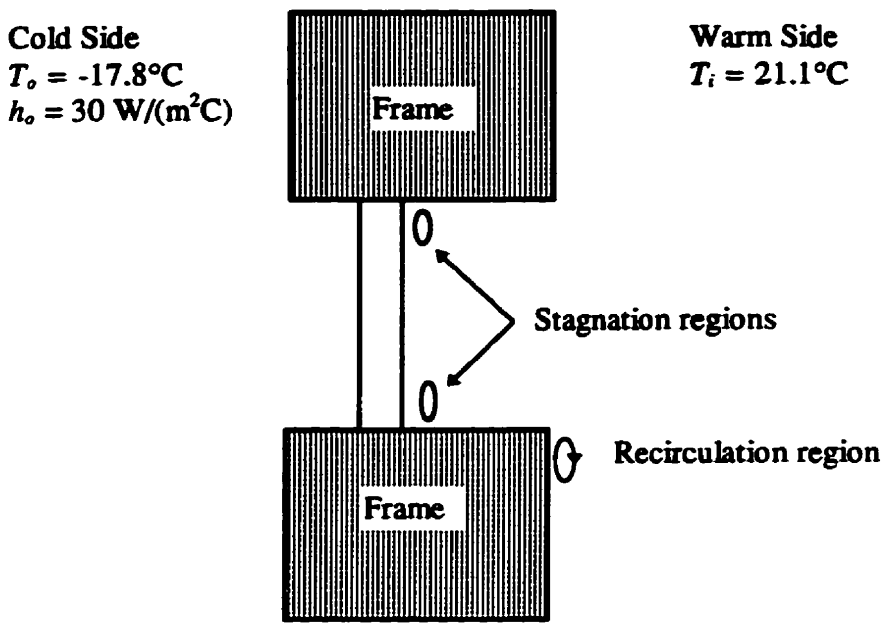

Figure 6.41: IGU and Mask Wall Geometry with the Regions of Stagnation and Recirculation.

Figure 6.42 shows the local heat transfer distribution on the warm side and Figure 6.43 presents the effect of the convection heat transfer in the surface temperature profile It is observed that the temperature profile for a constant h_i, case #1, presents a "flatter" center glass temperature profile, with colder temperatures at the top and warmer at the bottom of the IGU. The center glass temperature distribution for the cases where h_i is estimated using flat plate correlations, with or without correction, cases #2, #3, #4 and #5, have almost the same slope differing in the bottom and top temperatures, with the coldest temperature in the bottom for case #5 and warmest in the top for case #3.

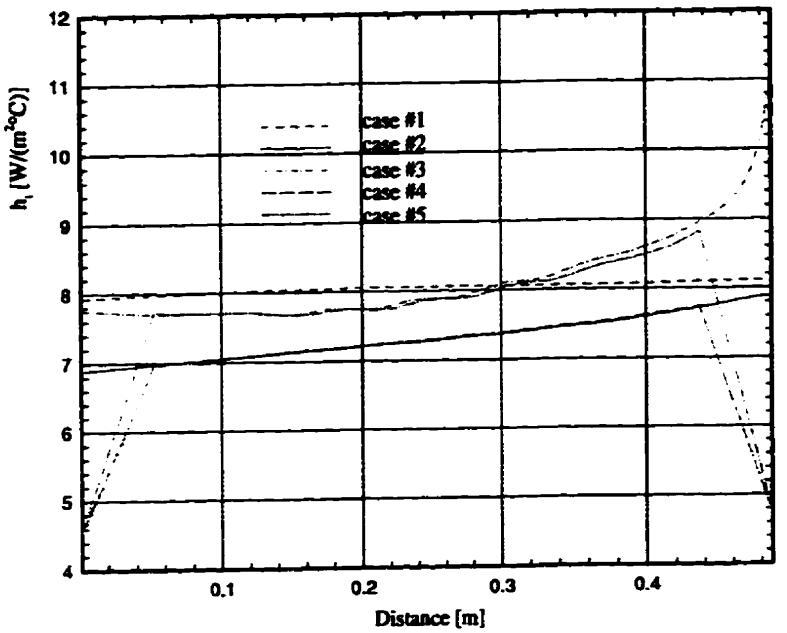

Figure 6.42: Local Heat Transfer Coefficient Distribution.

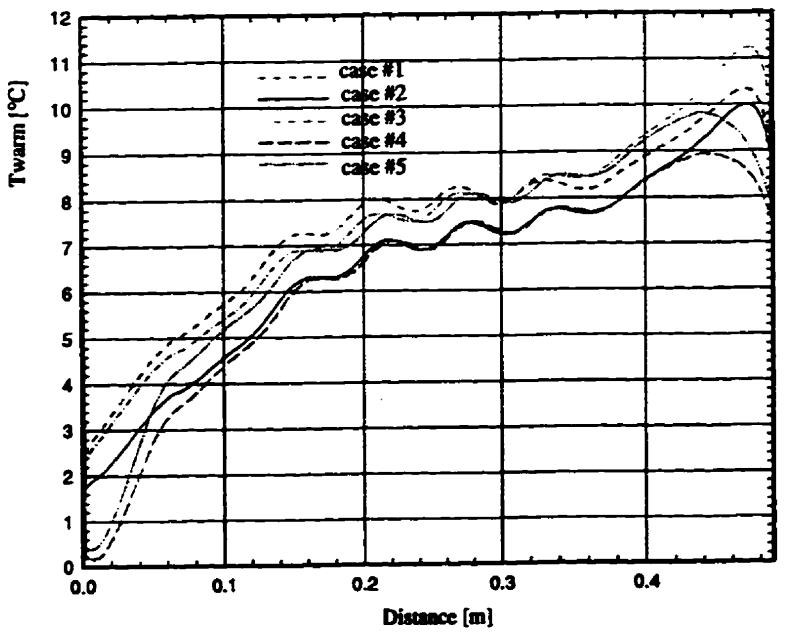

Figure 43: The effect of h_i in the Surface Temperature on the Warm Side.

6.7 Closure

In this Chapter the numerical code, BRAVO, is successfully applied to simulate realistic window problems. A summary of each application and major conclusions are given below:

1. In Section 6.1, a grid refinement study, the following observations are made:

   - the calculated explicit time step for the meshes studied are multiplied by a factor n=50 for EDS and n=0.95 for CDS;
   - although secondary cells could be generated spontaneously using EDS, they were in lower number then if they were perturbed when using CDS resulting in a lower total heat flux;
   - the established condition for CDS stability that the cells Reynolds number be ≤ 2, seems not be valid for buoyancy driven flows in a cavity as also reported by Shyy *et al.* (1992);

2. In Section 6.2, a qualitative comparison between a simulated recessed IGU and Sargent's (1992) corresponding thermographic measurements, shows very good agreement in the center glass region (same slope) when a convective heat transfer coefficient from a non-isothermal flat plate correlation is used;

3. In Section 6.3, an entire wood frame window is modeled. Excellent agreement between BRAVO and a modified commercial code when the same boundary conditions are applied is observed. The *U-factor* error is 0.38% while temperature differences over the entire surface are less than 0.5%;

4. In Section 6.4, a quantitative comparison with a set of thermographic measurements from Griffith *et al.* (1996) and Elmahdy (1996) are made for flush mounted IGU's. The agreement is satisfactory for the double glazed units, with the center glass temperatures differing by about 1°C, and very good for a triple glazed units, with the center glass temperatures differing by less than 0.25°C;

5. In Section 6.5, a sensitivity analysis for deflected IGU's is performed. A qualitative comparison with the results of Beck *et al.*(1995) shows the ability of BRAVO to model deflected windows;

6. In Section 6.6, a sensitivity analysis on the effects of heat transfer coefficient variations for flush and recessed mounted IGU's is performed. The importance of modeling a varying heat transfer coefficient is clearly demonstrated. When a convection heat transfer coefficient based on a non-isothermal flat plate correlation is used and compared with thermographic measurements for a flush mounted IGU the agreement in the center glass temperature profile is excellent.

All these observations lead to the conclusion that BRAVO is reliable and can be applied to the thermal and fluid flow analysis of a whole fenestration system within numerical and model limitations. The capabilities and limitations of BRAVO are briefly described in the next chapter along with the conclusions and recommendations.

7 CONCLUSION

The objective of this study was the numerical determination of the overall heat transfer coefficient (*U-Factor*) and the solar heat gain factor (*SHGF*) to evaluate the thermal performance, and surface temperature profiles to assist in the prediction of condensation on windows. It focused on the presence of natural convection, the radiation between panes, solar radiation, and the thermal effects of the frame.

At present, there is no computer program capable of providing data for the thermal analysis of a whole window (glazing systems and frames) with two or more panes in the presence of radiation (solar and thermal), with the ability to generate secondary cells near the critical *Ra* number, and the ability to handle deflected glazings and bar grills. Also, this code can model tertiary cells which, for the windows investigated in this work, are found not to exist. Therefore, this code provides a unique instrument for the thermal analysis of natural convection in tall cavities, in particular windows. This code is designed to run on a PC or compatible platform to permit portability and access by the research community and window manufacturers.

7.1 Conclusions

This work is divided in two major parts: the assessment of the numerical method and the application of the numerical code. The conclusions are presented in the same way.

7.1.1 Assessment of the Numerical Method

BRAVO's capability to model windows, with respect to accuracy, cost and reliability is examined in three stages:

1. Pure Natural Convection Problem in Enclosures

   - benchmark solutions comparison with the works of Vahl Davis (1983), Hortman *et al.* (1990) and Demirdzic *et al.* (1992) the errors were lower than 10^{-2}%;

   - BRAVO generated secondary cells near the critical Rayleigh number, *Ra*, with the calculated averaged Nusselt Number agreeing to within about 1% or less with the numerical results of Lee and Korpela (1983), Raithby and Wong (1981), and Wright (1989), and in about 1% and 5%, or less, with the measured data of Shewen (1986) and ElSherbiny *et al.* (1982a), respectively.

2. Conjugate Heat Transfer Problem

- a heat flux difference of less than 1% results for the heat flux in the hot wall of a cavity bounded by two sheets of glass and spacer bars when compared with the numerical results of Wright (1989);
- it is proven that BRAVO is capable of modeling new edge-seals designs.

3. Interaction of Conduction, Natural Convection and Radiation

- BRAVO's ability to tackle window system heat transfer problems (predicting the thermal and solar radiation heat transfer together with viscous fluid flow and conduction heat transfer) is proven;
- the heat flux agreement between BRAVO and the heater plate apparatus experimental results of Wright (1989) slightly exceeded the experimental error of 10% when only thermal radiation was considered;
- when solar radiation was added to the comparison of simulated solar heat gain factors with the solar calorimeter experimental results of Harrison and Wonderen (1994) good agreement is obtained for nine samples, with errors of 2.5% or less for seven samples, and with errors of 12% and 5% for the other two.

7.1.2 Application of the Numerical Method

The following observations are made when more realistic window problems, both geometrically and physically, are simulated with BRAVO:

1. in the grid refinement study, the observation made by Shyy *et al.* (1992) that the established cell Reynolds number based condition for CDS stability, i.e., $Re < 2$, seems invalid for buoyancy driven flows is verified;

2. in the qualitative comparison between a simulated recessed IGU and Sargent's (1992) thermographic measurements, very good agreement is shown for the center glass region (i.e., same slope) when non-isothermal flat plate heat transfer coefficients are used;

3. in modeling an entire wood frame window, excellent agreement is observed between BRAVO and a modified commercial code when the same boundary conditions are applied. The error in *U-factor* is 0.38% while the maximum surface temperature difference is less than 0.5%;

4. quantitative comparisons with a set of thermographic measurements from Griffiths *et al.* (1996) and Elmahady (1996) for a flush mounted IGU, yield satisfactory for the clear double glazed units, with the center glass temperature differing by about 1°C,

and very good agreement for the triple glazed units and the double low-E with the center glass temperature differing by less than 0.25°C;

5. a qualitative comparison between the results of Beck *et al.*(1995) and BRAVO for deflected IGU reveals the ability of BRAVO to model deflected windows;

6. the effects of heat transfer coefficients in flush and recessed mounted IGU's, clearly reveals the importance of modeling a locally varying heat transfer coefficient. When a convection heat transfer coefficient using a non-isothermal flat plate correlation is used, and results compared with thermographic measurements for the flush mounted IGU, the agreement between the center glass temperature profiles is excellent.

7.2 Contributions

Filling the void of information regarding energy flows within windows and temperature distributions in individual glazings and frame are reasons enough to justify the importance of this study. For example surface temperature distributions are relevant in the prediction of condensation problems and volume temperature distributions are relevant to evaluating thermal stress in glazings.

BRAVO is part of an effort by the University of Waterloo Advanced Glazing Laboratory to expand its modeling capabilities to systematically address window problems.

The major contributions of this work are as follows:

1. the formulation of a unique tool, BRAVO, for the thermal analysis and design of new windows;
2. the capability to simulate a whole window with multiple glazings, cavities in the frame, and exposure to solar radiation;
3. the demonstration of the need to model with a locally varying heat transfer coefficient as a warm side boundary condition;
4. the modeling of a deflected (bent) insulated glazing unit; and,
5. the ability of BRAVO to run on a PC or compatible platform thus permitting potential portability and access by the research community and window manufacturers.

7.3 Code Features and Limitations

BRAVO is a non-orthogonal grid, control-volume based, computational code developed specifically for the two-dimensional modelling of window. One strength of the code is its ability to model an entire window assembly (centre-glass, edge-glass, frame, and wall) simultaneously. This is in contrast to current industry practice of modelling the centre-glass region separately from the edge-glass/frame/wall region (EEL 1995, UW 1995, LBL

1994) as practised by the Canadian Standards Association's (CSA) window energy rating (ER) procedure (CSA 1993) and the National Fenestration Rating Council (NFRC 1995) procedure.

BRAVO incorporates much of the appropriate physics, it yields detailed surface temperature profiles, it provides flexible boundary condition capabilities, and it readily admits modification as refinements are developed. For example, no assumptions concerning the location of edge-glass demarcation is needed; a detailed vertical temperature profile along the entire window is available for comparison with thermographic measurements; specification of an indoor window surface temperature or heat transfer coefficient can be replaced with room air convection; and, different algorithms modelling specular reflection of solar radiation can be tested.

The ability of BRAVO to accurately determine local window temperatures makes it possible to be used to supplement experimental data in validating simpler, more user friendly, codes (EEL 1995, UW 1995).

7.3.1 BRAVO's Capabilities

There are seven features that together distinguish BRAVO from other computational fluid dynamics (CFD) codes. They are as follows:

1. it can model thermal radiation, convection, and conduction heat transfer in multiple cavities simultaneously. The governing equations conserving mass, momentum, and energy are all solved. It does not require, for instance, an effective conductivity or correlations inside cavities;
2. it can model the impact of solar radiation in a multiple glazed window without full or partial internal obstructions in the cavities;
3. boundary conditions and system boundaries can readily be changed. This includes the ability to input spatially varying boundary conditions;
4. it can model secondary flow (cat's eye cells) (Wright and Sullivan 1989, Lee and Korpela 1983) expected for many combinations of IGU design and indoor-outdoor temperature combinations;
5. it can model the specular reflection of solar radiation within rectangular cavities. This feature is needed to model the real life situation of incident solar radiation striking a window from an off-normal direction;
6. it can model non-orthogonal structures. This feature is useful for modeling frames or for modeling deflected glazings;
7. it can be run on a personal computer, operating on an 80386 processor or better, with 16Mb of memory.

7.3.1.1 BRAVO's Features

The code, BRAVO, models combined radiation, convection and conduction in a entire window with the following modeling features:

1. it is structured in such way that the user can change or create new modules to, for example,
   a) simulate transient problems,
   b) use more complex radiation (solar and thermal) models,
   c) input a new type of boundary condition,
   d) model infiltration;
2. it simulates multiple cavities in glazing and frame;
3. it accounts for solar radiation without partial obstruction inside any cavity for
   a) one to three pane windows, and for normal and off-normal solar radiation with either
      i) an one band model (i.e., short wave), or
      ii) a multi-band model (i.e., spectral),
   b) more than three pane window with normal solar radiation (for off-normal makes an approximation) with either

i) an one band model (i.e., short wave), or

ii) a multi-band model (i.e., spectral);

4. it estimates long-wave radiation (one band) (in cavities no obstructions are permitted except as outlined in 6);

5. it has the capability to model either conduction, surface radiation, or convection alone, or any combination of these three of heat transfer modes;

6. it models horizontal or vertical partitions without radiation, i.e., venetian blinds, grills, muntin bars, etc., and can model with radiation either one partial vertical or one partial horizontal partition (the edges of the partition must be separated from the cavity walls), for example, one muntin bar inside a glazing cavity;

7. it determines the properties for fill gases or mixtures in the inter-pane spaces;

8. it provides necessary information for a heat transfer analyses:

   a) it calculates the overall heat transfer coefficient, *U-factor*, of the whole window or center glass, edge-seal, and frame;

   b) it estimates solar heat gain factor, *SHGF*; and,

   c) it provides surface temperature profiles, isotherms and heat-flux , and

9. it provides velocity distributions and stream lines for a convective flow analyses.

7.3.1.2 BRAVO's Limitations

Current major limitations of BRAVO are as follows:

1. it is a research tool not readily adapted for widespread commercial use by the window industry, i.e. it lacks a user-friendly interface;
2. it is a two dimensional model, i.e. it does not account for three dimensional effects;
3. it is not a robust code, i.e., for each configuration a new mesh requires a search for the range of time steps which guarantee convergence;
4. it does not model radiation with obstructions inside cavities except as mentioned in Section 7.2.1.1, item 6;
5. it does not account for turbulence;
6. it cannot model a full room problem;
7. it is not able to model honeycombs or similar convection suppresser structures; and
8. it calculates solar radiation in a window without full or partial internal obstructions in the cavities.

7.4 Future Research

The first area for future research is an effort to improve the heat transfer modeling capabilities of the code by

1. incorporating a turbulence model suitable for confined flows,
2. devising better solar and thermal radiation models to account for full or partial obstructions inside cavities,
3. improving the radiation model for external surfaces to account for radiation between glass surfaces and frame, and
4. modeling natural convection inside the room and forced convection outside the room.

Other areas for code improvement include

1. making it user friendly by improving the pre-processing (grid generation),
2. determining the range of time steps for a set of representative IGU's currently on the market with a fixed grid, thus making the code robust for these configurations,
3. introducing a more complex solar radiation model for either one band or multi-band calculations, and

4. implementing forced convection (i.e. adding infiltration and calculation of outdoor convection) and natural convection in a full room (considering thermal plumes) velocity boundary conditions.

REFERENCES

Abu-Mulaweh, H.I., B.F. Armaly and T.S. Chen, 1993. "Measurements in Buoyancy-Assisting Laminar Boundary Layer Flow Over a Vertical Backward-Facing Step – Uniform Wall Heat Flux Case", International Journal of Experimental Heat Transfer, Thermodynamics, and Fluid Mechanics, vol. 7(1), pp. 39-48.

Abu-Mulaweh, H.I., B.F. Armaly and T.S. Chen, 1994. "Measurements in Buoyancy-Opposing Laminar Flow Over a Vertical Backward-Facing Step", Journal of Heat Transfer, vol. 116(1), pp. 247-250.

Acharya, S. and C.H. Tsang, 1985. "Natural Convection in a Fully Partitioned, Inclined Enclosure", Numerical Heat Transfer, vol. 8(4), pp. 407-428.

Acharya, S. and R. Jetli, 1990. "Heat Transfer Due to Buoyancy in a Partially Divided Square Box", International Journal of Heat and Mass Transfer, vol. 33(5), pp. 931-942

AGSL, 1995. "VISION5 Glazing System Thermal Analysis - Computer Program", Advanced Glazing System Laboratory, Department of Mechanical Engineering, University of Waterloo.

Anderson, R. and A. Bejan, 1981. "Heat Transfer Through Single and Double Vertical Walls in a Natural Convection: Theory and Experiment", International Journal of Heat and Mass Transfer, vol. 24(4), pp. 1611-1620.

Arasteh, D., S.E. Selkowitz and J. Wolfe, 1988. "The Design and Testing of a Highly Insulating Glazing System for Use with Conventional Window Systems", Lawrence Berkeley Laboratory, report LBL-24903.

Arasteh, D. and J. Wolfe, 1989. "An Analysis of Frame and Edge Heat Transfer in Residential Windows", Lawrence Berkeley Laboratory, report LBL-26068, pp. 1-23.

Arasteh, D.K. and S.M. Reilly, 1989. "A Versatile Procedure for Calculating Heat Transfer through Windows", ASHRAE, vol. 95(2), pp. 755-765.

Arasteh, D.K., E. Finlayson., M.D. Rubin and J. Sadlier, 1995. "Recent Technical Improvements to the WINDOW Computer Program", Proceedings of the Window Innovations '95 Conference, Toronto, pp. 400-405.

Asako, Y. and H. Nakamura, 1982. "Heat Transfer Across a Parallelogram Shaped Enclosure". Bulletin of JSME, vol. 25, pp. 1412-1424.

ASHRAE, 1993. "ASHRAE Handbook - Fundamentals", American Society of Heating Refrigerating and Air Conditioning Engineers, Inc., chap. 27, pp. 27.1-27.38.

Bajorek, S.M. and J.R. Lloyd, 1982. "Experimental Investigation of Natural Convection in Partitioned Enclosures", ASME Journal of Heat Transfer, vol. 104, pp. 527-532.

Balaji, C. and S.P. Venkateshan, 1993. "Interaction of Surface Radiation with Free Convection in a Square Cavity", International Journal of Heat and Fluid Flow, vol. 14(3), pp. 260-267.

Balaji, C. and S.P. Venkateshan, 1994a. "Combined Surface Radiation and Free Convection in Cavities", Journal of Thermophysics and Heat Transfer, vol. 8(2), pp. 373-376.

Balaji, C. and S.P. Venkateshan, 1994b. "Correlations for Free Convection and Surface Radiation in a Square Cavity", International Journal of Heat and Fluid Flow, vol. 15(3), pp. 249-251.

Balaji, C. and S.P. Venkateshan, 1995. "Combined Conduction, Convection and Radiation in a Slot", International Journal of Heat and Fluid Flow, vol. 16(2), pp. 139-144.

Ballinger, J.A and P.R. Lyons, 1993. "Identification & Definition of Key Glazing Performance Parameters", Report T18/A1/WD1/93, International Energy Agency, Sydney, Australia.

Barry, C.J., 1995. "Thermal Stress in High Performance Glazing", Proceedings of the Window Innovations '95 Conference, Toronto, pp. 115-122.

Batchelor, G.K., 1954. "Heat Transfer by Free Convection Across a Closed Cavity Between Vertical Boundary Vertical Boundaries at Different Temperatures", Quarterly of Applied Mathematics, vol. 12(3), pp. 209-233.

Beck, F.A., B.T Griffith, D. Turler, and D. Arasteh, 1995. "Using Infrared Thermography for the Creation of a Window Surface Temperature Database to Validate Computer Heat Transfer Models", Proceedings of the Window Innovations '95 Conference, Toronto, pp. 280-290.

Bejan, A., 1979. "Note on Gill's Solution for Free Convection in a Vertical Enclosure", Journal of Fluid Mechanics, vol. 1979, pp. 561-568.

Bejan, A., 1982. "Natural Convection Heat Transfer in Porous Layer with Internal Flow Obstructions", International Journal of Heat and Mass Transfer, vol. 24, pp. 815-822.

Bejan, A., 1984. "Convection Heat Transfer", John Willey and Sons.

Behnia, M., J.A. Reizes and G. de Vahl Davis, 1985a. "Natural Convection in a Cavity with a Window", AIAA paper No. 1073.

Behnia, M., J.A. Reizes and G. de Vahl Davis, 1985b. "Natural Convection in a Rectangular Slot with Convective-Radiative Boundaries", ASME paper No. 85-HT-35.

Behnia, M., J.A. Reizes and G. de Vahl Davis, 1990. "Combined Radiation and Natural Convection in a Rectangular Cavity with a Transparent Wall and Containing a Non-Participating Fluid", International Journal for Numerical Methods in Fluids, vol. 10, pp. 305-325.

Bergholz, R. F., 1978. "Instability of Steady Natural Convection in a Vertical Fluid Layer", Journal of Fluid Mechanics, vol. 84(4), pp. 743-768.

Bilski S.M., J.R. Lloyd and K.T. Yang, 1986. "An Experimental Investigation of the Laminar Natural Convection Velocity Field in a Square and Partitioned Enclosures", in Proceedings of 8th International heat Transfer Conference, San Francisco, vol. 4, pp. 1513-1518.

Birikh, R.V., G.Z. Gershuni, E.M. Zhukhovitskii and R.N. Rudakov, 1968. "Hydrodynamic and Thermal Instability of a Steady Convective Flow", Prikl. Mat. Meckh., vol. 32(2), pp. 256-263.

Blomberg, T., 1995. "HEAT2 Update of Manual Version 2.5 including HEAT2W Version 1.0", Department of Building Physics, Lund University, Sweden.

Brown, W.C. and K. Ruberg, 1988. "Window Performance Factors", Window Performance and New Technology, Proceedings of Building Science Insight '88, NRC, Ottawa, pp. 17-28.

Carpenter, S., 1991. "Window Energy Standards Have Arrived", Glass Canada, pp. 18-20, October.

Catton, I., 1976. "Natural Convection in Enclosures", Proceedings of the 6th Heat Transfer Conference, Toronto, Ontario, Canada, vol. 6, pp. 13-31, August 7-11.

Caroutas, C.A. and A.T. Kirkpatrick, 1991. "Natural Convection Heat Transfer in Rectangular Partitioned Enclosures", in Proceedings of Solar World Congress, Denver, vol. 3(II), pp. 3191-3196.

Castellano, L., S. Pasini and E. Sani, 1992. "Comparison of Numerical Models for Combined Convection and Radiation in Three-Dimensional Complex Enclosures Containing Participating Gases", Developments in Radiative Heat Transfer, ASME, HTD-vol. 203, pp. 245-251.

Chai, J.C., H.S. Lee and S.V. Patankar, 1994a. "Improved Treatment of Scattering Using the Discrete-Ordinates Method". Journal of Heat Transfer, vol. 116, pp. 260-263.

Chai, J.C., H.S. Lee and S.V. Patankar, 1994b. "Treatment of Irregular Geometries Using a Cartesian Co-ordinates Finite-Volume Radiation Heat Transfer Procedure". Numerical Heat Transfer, vol. 26(2), part B, pp. 225-235.

Chai, J.C., H.S. Lee and S.V. Patankar, 1994c. "Finite Volume Method Radiation Heat Transfer". Journal of Thermophysics and Heat Transfer, vol. 8(3), pp. 140-144.

Chai, J.C., S.V. Patankar and H.S. Lee, 1994d. "Evaluation of Spatial Differencing Practices for the Discrete-Ordinates Method". Journal of Thermophysics and Heat Transfer, vol. 8(1), pp. 140-144.

Chait, A. and S.A. Korpela, 1989. "The Secondary Flow and Its Stability for Natural Convection in a Tall Vertical Enclosure", Journal of Fluid Mechanics, vol. 200, pp. 189-216.

Chang, L.C., J.R. Lloyd and K.T. Yang, 1982. "A Finite Difference Study of Natural Convection in Complex Enclosures", in Proceedings of 7th International Heat Transfer Conference, Munich, pp. 183-188.

Chen, K.S. and P.W. Ko, 1991. "Natural Convection in a Partially Divided Rectangular Enclosure with an Opening in the Partition Plate and Isoflux Side Walls", International Journal of Heat and Mass Transfer, vol. 34(1), pp. 237-246.

Chen, C.F. and S. Thangam, 1985. "Convective Stability of a Variable Viscosity Fluid in a Vertical Slot", Journal of Fluid Mechanics, vol. 161, pp. 161-173.

Chikhaoui, A., J.F. Marcillat and R.L. Sani, 1988a. "Successive Transitions in Thermal Convection within a Vertical Enclosure", in: *Natural Convection in Enclosures*, ASME HTD, vol. 99, pp 29-35.

Chikhaoui, A., M.K. Maslanik and R.L. Sani, 1988b "Steady Three-Dimensional Thermal Convection in a Vertical Rectangular Enclosure", Communication in Applied Numerical Methods, vol. 4, pp. 825-834.

Choi, I.G. and S.A. Korpela, 1980. "Stability of the Conduction Regime of Natural Convection in a Tall Vertical Annulus", Journal of Fluid Mechanics, vol. 99(4), pp. 725-738.

Chung, I.K., J.Y. Kim and H.J. Lee, 1991. "The Oscillatory Natural Convective Flow in Square Enclosure with Lower Heated Wall and a Horizontal Partition", Journal of Inst. of Industrial Technology, Yeugnam University, vol. 19, n.1, pp. 55-62.

Chung, I.K, D.J. Song and J.Y. Kim 1994. "The Natural Convective Flow and Heat Transfer in Square Enclosure with a Horizontal Partition", Proceedings of 10th International Heat Transfer Conference, vol. 7, pp. 19-24.

Chung, I.K, D.J. Song and J.Y. Kim 1995. "A Natural Convective Flow in Square Enclosure with Partition", Proceedings of ASME/JSME Thermal Engineering Conference, vol. 1, pp. 233-241.

Ciafalo, M. and T.G. Karayiannis, 1990. "Natural Convective Heat Transfer in a Vertical Cavity with Partitions at the Ends", in Proceedings of 9th International Heat Transfer Conference, pp. 297-303.

Ciafalo, M. and T.G. Karayiannis, 1991. "Natural Convection Heat Transfer in a Partially – or Completely – Partitioned Vertical Rectangular Enclosure", International Journal of Heat and Mass Transfer, vol. 34, pp. 167-179

Clever, R.M. and F.H. Busse, 1977. "Instabilities of Longitudinal Convection Rolls in an Inclined Layer", Journal of Fluid Mechanics, vol. 81(1), pp. 107-127.

CSA, 1993. "CSA A440.2-M1993 - Energy Performance Evaluation of Windows and Sliding Glass Doors", Canadian Standards Association, Ontario, Canada.

Curcija, D., 1992. "Three-Dimensional Finite Element Model of Overall, Night Time Heat Transfer Through Fenestration Systems", Ph.D. Thesis, Department of Mechanical Engineering, University of Massachusetts.

Curcija D. And W.P. Goss, 1993. "Two-Dimensional Natural Convection Over the Isothermal Indoor Fenestration Surface – Finite Element Numerical Solution", ASHRAE Transactions, vol. 99(1), pp. 274-287.

Curcija D. And W.P. Goss, 1994. "Two-Dimensional Finite-Element Model of Heat Transfer in Complete Fenestration Systems", ASHRAE Transactions, vol. 100(2), pp. 1207-1220

Curcija D. And W.P. Goss, 1995a. "Three-Dimensional Finite-Element Model of Heat Transfer in Complete Fenestration Systems", Proceedings of the Window Innovations '95 Conference, Toronto, pp. 406-420.

Curcija D. And W.P. Goss, 1995b. "Two-Dimensional Forced Convection Perpendicular to the Outdoor Fenestration Surface – FEM Solution", ASHRAE Transactions, vol. 101(1), pp. 201-209.

de Abreu, P.F., R..A. Fraser, H.F. Sullivan, and J.L. Wright, 1996. "A Study of Insulated Glazing Unit Surface Temperature Profiles Using Two-Dimensional Computer Simulation". ASHRAE Transactions, vol. 102(2).

de Vahl Davis, G., 1983. "Natural Convection of Air in a Square Cavity: A Bench Mark Numerical Solution". International Journal for Numerical Methods in Fluids, vol. 3, pp. 249-264.

de Vahl Davis, G., 1986. "Finite Difference Methods for Natural Convection and Mixed Convection in Enclosures". In Proceedings of the 8th International Heat Transfer Conference, San Francisco, Hemisphere Publishing Corporation, vol. 1, pp. 101-109.

de Vahl Davis, G. and I.P. Jones, 1983. "Natural Convection in a Square Cavity: A Comparison Exercise". International Journal for Numerical Methods in Fluids, vol. 3, pp. 227-248.

de Vahl Davis, G. and I.P. Jones, 1984. "The Effect of Vertical Temperature Gradients on Multi-Cellular Flows in High Aspect Ratio Cavities". In Proceedings of the Conference on Liquid Metal Technology in Energy Production, Oxford, April 9-13.

de Vahl Davis, G. and G.P Mallison, 1975. "A note on Natural Convection in a Vertical Slot", Journal of Fluid Mechanics, vol. 72(1), pp. 87-93.

Demirdzic I., Z. Lileck and M Peric, 1992. "Fluid Flow and Heat Transfer Test Problems for Non-Orthogonal Grids: Bench-Mark Solutions", International Journal for Numerical Methods in Fluids, vol. 15, 329-354.

Draoui, A., J.P. Simoneau and F. Allard, 1988. "Combined Radiation and Convection in Gray Fluids Enclosed in Two-Dimensional Cavities", Proceedings of the Winter Annual Meeting of the ASME, HTD-vol. 104, Chicago, Illinois, USA, pp. 141-146, November 27 - December 2.

Draoui, A., F. Allard and C. Berghein, 1991. "Numerical Analysis of Heat Transfer by Convection and Radiation in Participating Fluids Enclosed in Square Cavities", Numerical Heat Transfer, vol. 20, part A, 253-261.

Drummond, J.E., A.J. Yovichin and J.P. Mckee, 1991. "The Effect of Upwind Formulations on Secondary Flows in a Thermally Driven Cavity", Proceedings of the ASME/JSME Thermal Engineering Joint Conference, Nevada, USA, pp. 147-154.

Duffie, A.J. and W.A. Beckman, 1991. "Solar Engineering of Thermal Process", John Willey & Sons, 2nd edition, New York.

Eckert, E.R.G. and W.O. Carlson, 1961. "Natural Convection in an Air Layer Enclosed Between Two Vertical Plates with Different Temperatures", International Journal of Heat and Mass Transfer, vol. 2, pp. 106-120.

Ede, A.J., 1967. "Advances in Free Convection", Advances in Heat Transfer, ed. H.P. Hartnett and T.F. Irvine, vol. 4, Academic Press.

Edwards, D.K., 1977. "Solar Absorption by Each Element in an Absorber-Coverglass Array", Solar Energy, vol. 19, pp. 401-402.

Ehlert, J.R. and T.F. Smith, 1994. "Surface Radiation for Rectangular Enclosures Using the Discrete-Ordinates Method". Journal of Thermophysics and Heat Transfer, vol. 8(3), pp. 628-631.

Elder, J.W., 1965a. "Laminar Free Convection in a Vertical Slot", Journal of Fluid Mechanics, vol. 23(1), pp. 77-98.

Elder, J.W., 1965b. "Turbulent Free Convection in a Vertical Slot", Journal of Fluid Mechanics, vol. 23(1), pp. 99-111.

Elgelman, M., and M.-A. Jamnia, 1991. "Grey-Body Surface radiation Coupled with Conduction and Convection for General Geometries", International Journal for Numerical Methods in Fluids, vol. 13, pp. 1029-1053.

Elmahdy, H., 1996. "Surface Temperature Measurement of Insulating Glass Units Using Infrared Thermography", ASHRAE Transactions, vol. 102(2).

ElSherbiny, S.M., G.D. Raithby and K.G.T. Hollands, 1982a. "Heat Transfer by Natural Convection Across Vertical and Inclined Air Layers", Journal of Heat Transfer, vol. 104, pp. 96-102.

ElSherbiny, S.M., K.G.T. Hollands and G.D. Raithby, 1982b. "Effect of Thermal Boundary Conditions on Natural Convection in Vertical and Inclined Air Layers", Journal of Heat Transfer, vol. 104, pp. 515-520.

Emery, A.F., 1963. "The Effect of a Magnetic Field upon the Free Convection of Conducting Fluid", Journal of Heat Transfer, Series C, vol. 85, pp. 119-124, May.

Emery, A.F., 1969. "Exploratory Studies of Free Convection Heat Transfer through an Enclosed Vertical Liquid Layer with a Vertical Baffle", ASME Journal of Heat Transfer, vol. 91, pp. 163-165.

Enermodal, 1992. "FRAME 3.0: A Computer Program to Evaluate Thermal Performance of Window Frame Systems", Enermodal Engineering Limited.

Enermodal, 1995. "FRAME 4.0: A Computer Program to Evaluate Thermal Performance of Window Frame Systems", Enermodal Engineering Limited.

Fant, D.B. and D.C. Jarman, 1991. "Multicellular Natural Convection in a Vertical Slot", ASME/JSME Thermal Engineering Joint Conference 1991, vol. 1, pp. 131-140.

Ferguson, J.E. and. J.L. Wright, 1984. "Computer Simulation of the Thermal Performance of Super Windows", Proceedings of the 1984 SESCI conference.

Fiveland W.A. and J.P. Jessee, 1994. "Finite Element Formulation of the Discrete-Ordinates Method for Multidimensional Geometries". Journal of Thermophysics and Heat Transfer, vol. 8(3), pp. 426-433.

Fiveland W.A. and J.P. Jessee, 1995. "Comparisons of Discrete-Ordinate Formulations for Radiative Heat Transfer in Multidimensional Geometries". Journal of Thermophysics and Heat Transfer, vol. 8(3), pp. 426-433.

Fraser, R.A., P.F. de Abreu, J.L. Wright, H.F. Sullivan and Y. Huafo, 1993. "Critical Issues in comparing Edge-Seal Performance: Modelling Versus Experiment", ASHRAE Transactions, vol. 99(1), pp. 923-938.

Frederick, R.L., 1989. "Natural Convection in an Inclined Square Enclosure with a Partition attached to its Cold Wall". International Journal of Heat and Mass Transfer, vol. 32(1), pp. 87-94

Frederick, R.L. and A. Valencia, 1989. "Heat Transfer in Square Cavity with a Conduction Partition on its Cold Wall". International Communication of Heat and Mass Transfer, vol. 16, pp. 347-354

Fu, W.S, J.C. Perng and W.J. Shieh, 1989. "Transient Laminar Natural Convection in an Enclosure Partitioned by an Adiabatic Baffle, Numerical Heat Transfer, Part A, vol. 16, pp. 325-350.

Furler, R., P. Williams, F.K. Kneubuhl. 1988. "Experimental and Theoretical Study on Energy Balance of Windows", Ph.D. Thesis 8580, ETH Zurich, Switzerland, NEFF report 177.1.

Fusegi, T. and B. Farouk, 1989. "Laminar and Turbulent Natural Convection-Radiation Interactions in a Square Enclosure Filled with a Nongray Gas", Numerical Heat Transfer, vol. 15, part A, pp. 303-322.

Fusegi, T. and B. Farouk, 1990. "A Computational and Experimental Study of Natural Convection and Surface/Gas Radiation Interactions in a Square Cavity", Journal of Heat Transfer, vol. 112, pp. 802-804.

Fusegi, T., K. Ishii, B. Farouk and K. Kuwahara, 1991. "Natural Convection-Radiation Interactions in a Cube Filled with a Nongray Gas", Numerical Heat Transfer, vol. 15, part A, pp. 207-217.

Fusegi, T. And J.M. Hyun, 1994. "Laminar and Transitional Natural Convection in an Enclosure with Complex and Realistic Conditions", International Journal of Heat and Fluid Flow, vol. 15(4), August.

Gill, A.E., 1966. "The Boundary-Layer Regime for Convection in a Rectangular Cavity", Journal of Fluid Mechanics, vol. 26(3), pp. 515-536.

Gill, A.E, and A. Davey, 1968. "Instabilities of a Buoyancy-Driven System", Journal of Fluid Mechanics, vol. 35(4), pp. 775-798.

Gill, A.E. and C.C. Kirkhan, 1970. "A Note on Stability of Convection in a Vertical Slot", Journal of Fluid Mechanics, vol. 42, (1), pp. 125-127.

Gilmore, V.E., 1986. "Superwindows", Popular Science, March, pp. 76-77.

Goss, W.P. and D. Curcija, 1989. "Fenestration Performance Research - Progress/Trip Report", Mechanical Engineering Department, University of Massachusetts, November.

Graebel, W.P., 1981. "The Influence of Prandtl Number on Free Convection in a Rectangular Cavity", International Journal of Heat and Mass Transfer, vol. 24, pp. 125-131.

Griffith, B.T., D. Turler, and D. Arasteh, 1996. "Surface Temperature of Insulated Glazing Units: Infrared Thermography Laboratory Measurements", ASHRAE Transactions, vol. 102(2).

Haidekker, A., A. Charette and Y.S. Kocaefe, 1994. "Applications of the Hybrid Zone/Monte Carlo Method to 3-D Curvilinear Grids in Radiative Heat Transfer". International Journal for Numerical Methods in Engineering, vol. 37(2), pp. 203-216.

Han, B.J., D.W. Yarbrough and S.M. Han, 1986. "Thermal Resistance of Wall Cavities Containing Reflective Insulation", Journal of Solar Energy Engineering, vol. 108(4), pp. 338-341.

Harrison, S.J. and S.J. Wonderen, 1994. "A Test Method for the Determination of Window Solar Heat Gain Coefficient", ASHRAE Transaction, vol. 100(1), pp. 1057-1064.

Hart, J.E., 1971. "Stability of the Flow in a Differentially Heated Inclined Box", Journal of Fluid Mechanics, vol. 47(3), pp. 547-576.

Hogan, J., 1995. "The Use of NFRC Ratings in U.S. Energy Codes", Proceedings of the Window Innovations '95 Conference, Toronto, pp. 309-324.

Hollands, K.G.T. and L. Konick, 1973. "Experimental Study of the Stability of Differentially Heated Inclined Air Layers", International Journal of Heat and Mass Transfer, vol. 16, pp. 1467-1476.

Hortmann, M., M. Peric, and G. Scheuerer, 1990. "Finite Volume Multigrid Prediction of Laminar Natural Convection: Bench-Mark Solutions". International Journal for Numerical Methods in Fluids, vol. 11, pp. 189-207.

Hutchins, M.G., 1995. "The Optical and Thermal Performance of Advanced Glazing Materials", Proceedings of the Window Innovations '95 Conference, Toronto, pp. 2-12.

Hutchinson, B.R. and G.D. Raithby, 1986. "A Multigrid Method Based on the Additive Correction Strategy", Numerical Heat Transfer, vol. 9, pp. 511-537.

Hutchinson, B.R. and G.R. Stefurak, 1995. "Prediction of Radiative, Convective and Conductive Heat transfer Using the Hemi-Cube Method". In Proceedings of Third Annual Conference of the CFD Society of Canada, Banff, Alberta, Canada.

IEA, 1987. Energy Conservation in Buildings and Community Systems Programme, "Annex XII, Windows and Fenestration, Step 2 - Thermal and Solar Properties of Windows (Expert Guide)", International Energy Agency, December.

Ito, N. and K. Kimura, 1972 "A Field Experiment Study on the Convective Heat Transfer Coefficient on the Exterior Surface of a Building", ASHRAE Transactions 78(1), pp. 184-185.

Jetli, R. and S. Achary, 1988. "End Wall Effects on Thermal Stratification and Heat transfer in a Vertical Enclosure with Offset Partitions", Canadian Journal of Chemical Engineering, vol. 66, pp. 563-571.

Jones, I.P., 1980. "Numerical Predictions from the IOTA2 Code for Natural Convection in Vertical Cavities", American Society of Mechanical Engineers Paper 82-HT-70.

Jonsson, B., 1985. "Heat Transfer through Windows During the Hours of Darkness with Effect of Infiltration Ignored", Swedish Council for Building Research, document D13:1985, March.

Kangni, A., P. Vasseur and E. Bilgen, 01995. "Natural Convection in Inclined Enclosures with Multiple conducting Partitions", Journal of Thermophysics and Heat Transfer, vol. 9(2), pp. 270-277.

Kangni, A., R. Ben Yedder and E. Bilgen, 1991. "Natural convection and Conduction in Enclosures with Multiple Vertical Partitions", International Journal of Heat and Mass Transfer, vol. 34(11), pp. 2819-2825.

Kelkar, K.M. and S.V. Patankar, 1990. "Numerical Prediction of Natural Convection in Square Partitioned Enclosures", Numerical Heat Transfer, Part A, vol. 17(3), pp. 269-285.

Kim, J.S., I.K. Chung and D.J. Song, 1992. "The Oscillatory Natural Convective Flow in Square Enclosure with a Horizontal Partition", JSME Journal, vol. 16, n. 10, pp. 1963-1970

Kim D.M. and R. Viskanta, 1984. "Heat Transfer by Conduction, Natural Convection and Radiation Across a Rectangular Cellular Structure", International Journal of Heat and Fluid Flow, vol. 5(4), pp. 205-213.

Kim D.M. and R. Viskanta, 1985. "Effect of Wall Heat Conduction on Natural Convection Heat Transfer in a Square Enclosure", Journal of Heat Transfer, vol. 107, pp. 139-146.

Kimura, K., 1977. "Scientific Basis of Air Conditioning", Applied Science Publishers Ltd., London, U.K..

Korpela, S.A., 1974. "A Study on the Effect of Prandtl Number on the Stability of the Conduction Regime of Natural Convection in an Inclined Slot", International Journal of Heat and Mass Transfer, vol. 17, pp. 215-222.

Korpela, S.A., D. Gözüm and C.B. Baxi, 1973. "On the Stability of the Conduction Regime of Natural Convection in a Vertical Slot", International Journal of Heat and Mass Transfer, vol. 16, pp. 1683-1690.

Korpela, S.A., Y. Lee and J.E. Drummond, 1982. "Heat Transfer Through a Double Pane Window", Journal of Heat Transfer, vol. 104, pp. 539-544.

Lampert, C.M., 1995. "Chromogenic Switchable Glazing: Towards the Development of the Smart Window", Proceedings of the Window Innovations '95 Conference, Toronto, pp. 348-364.

Larson D.W and R. Viskanta, 1976. "Transient Combined Laminar Free Convection and Radiation in a Rectangular Enclosure", Journal of Fluid Mechanics, vol. 78, pp. 68-85.

Lauriat, G., 1980. "Numerical Study of Natural Convection in a Narrow Cavity: an Examination of High Order Accurate Schemes," ASME paper No. 80-HTD-90.

Lauriat, G. and G. Desrayaud, 1985a. "Natural Convection in Air-Filled Cavities of High Aspect Ratios: Discrepancies Between Experimental and Theoretical Results", presented at the National Heat Transfer Conference, ASME, Denver, Colorado, August 4-7.

Lauriat, G. and G. Desrayaud, 1985b. "Influences of the Boundary Conditions and Linearization on the Stability of a Radiating Fluid in a Vertical Layer", International Journal of Heat and Mass Transfer, vol. 28, pp. 1613-1617.

LBL, 1994. "WINDOW 4.1: A PC Program for Analysing Window Thermal Performance in Accordance with Standard NFRC Procedures - Program Description", Lawrence Berkeley Laboratory, Berkeley, California, USA.

Le Queré, P., 1990. "A Note on Multiple and Unsteady Solutions in Two-Dimensional Convection in Tall Cavity", Journal of Heat Transfer, vol. 112, pp. 965-974.

Lee, Y. and S.A. Korpela, 1983. "Multicellular Natural Convection in a Vertical Slot", Journal of Fluid Mechanics, vol. 126, pp. 91-121.

Leonard, E., J.A. Reizes, 1979, "Natural Convection in Compressible Fluids with Variable Properties", Proceedings of the 1st Conference on Numerical Methods in Thermal Problems, pp. 297-306.

Liakopoulos, A. and P.A. Blythe, 1990. "Convective Flows in Tall Cavities", Presented at the Winter Annual Meeting of the ASME, Dallas, Texas, USA, vol. 157-HTD, November 25-30.

Lin, N.N. and A. Bejan, 1983. "Natural Convection in a Partially Divided Enclosure", International Journal of Heat and Mass Transfer, vol. 26, n. 12, pp. 1867-1878.

Lobo, M. and A.F. Emery, 1992. "The Discrete Maximum Principle in Finite Element Thermal Radiation Analysis". Developments in Radiative Heat Transfer, HTD-203, pp. 169-177.

Lobo, M. and A.F. Emery, 1993. "The Use of the Discrete Maximum Principle in Finite Element Analysis of Combined Conduction and Radiation in Non-Participating Media". General Papers in Radiative Heat Transfer, HTD-257, pp. 11-23.

Lokmanhekim, M., 1975. "Procedure for Determining Heating and Cooling Loads for Computerised Energy Calculations; Algorithms for Building heat Transfer Subroutines", ASHRAE, New York, USA.

Maliska, R.M., 1995. "Transferência de Calor e Mecânica dos Fluidos Computational", LCT-Livros Técnicos e Científicos Editora S.A., Rio de Janeiro, Brazil.

Mallinson, G.D. and G. de Vahl Davis, 1973. "The Method of False Transient for the Solution of Coupled Elliptic Equations", Journal of Computational Physics, vol. 12, 436-461.

Marballi, V.M., S.A. Korpela, Y. Lee, and S. Nakamura, 1984. "Heat Transfer Through a Vertical Enclosure with Convective Boundary Conditions". International Journal of Heat and Mass Transfer, vol. 27(12), pp. 2431-2434.

Markatos, N.C. and K.A. Pericleous, 1984. "Laminar and Turbulent Natural Convection in a Enclosed Cavity", International Journal of Heat and Mass Transfer, vol. 27, pp. 755-772.

Martin, B.W., 1984. "An Appreciation of Advances in Natural Convection and Radiation Along an Isothermal Vertical Surface", International Journal of Heat and Mass Transfer, vol. 27(9), pp. 1583-1586.

Maryama, S. and T. Aihara, 1995. "Radiation Heat Transfer of Arbitrary 3-D Participating Media and Surfaces Using Radiation Element Method by Ray Emission Model (REM2)". In Proceedings of the ASME/JSME Thermal Engineering Joint Conference, Maui, Hawaii, vol. 3, pp. 235-242.

McAdams, W.H., 1956. "Heat Transmission", McGraw-Hill Book Company Inc., New York, 3rd ed.

McCabe, M.E. and W.P. Goss, 1987. "Interim Procedure to Measure the Thermal Performance of Window Systems", National Bureau of Standards, report No. NBSIR 87-3569, June.

McCabe, M.E., 1989. "Origins of ASHRAE Window U-Value Data and Revisions for the 1989 Handbook of Fundamentals", Proceedings of the 15th Annual Conference of Solar Energy Society of Canada, Penticton, BC, pp. 237-277, June 19-21.

McGowan, A.G., 1995. "Numerical Prediction of Window Condensation Potential", ASHRAE Transactions, vol. 101(1), pp. 832-837.

Menart J.A. and H.S. Lee, 1993. "Nongray Gas Layer Analyses for Reflecting Walls Utilising a Flux Technique". Journal of Heat Transfer, vol. 115(3), pp. 645-652.

Menart J.A., H.S. Lee and T-K Kim, 1993. "Discrete Ordinates Solutions of Nongray Radiative Transfer with Diffusely Reflecting Walls". Journal of Heat Transfer, vol. 115(1), pp. 184-193.

Min, T.C. et al., 1956. "Natural Convection and Radiation in a Panel-Heated Room", ASHRAE Transaction, vol. 62, pp. 337-358.

Modest, M.F., 1993. Radiative Heat Transfer, McGraw-Hill, New York.

Nagata, M. and F.H. Busse, 1983. "Three-Dimensional Tertiary Motions in a Plane Shear Layer", Journal of Fluid Mechanics, vol. 135, pp. 1-26.

Nakamura, H., Y. Asaka and T. Hirata, 1984. "Natural Convection and Thermal Radiation in Enclosures with a Partition Plate", Transactions of the Japanese Society of Mechanical Engineers, vol. B50, pp. 2647-2654.

Nansteel, M.W. and R. Greif, 1981, "Natural Convection in Undivided and Partially Divided Rectangular Enclosure", ASME Journal of Heat Transfer, vol. 103, pp. 623-629.

Nansteel, M.W. and R. Greif, 1983, "Natural Convection Heat Transfer in Complex Enclosures at Large Prandtl Number", ASME Journal of Heat Transfer, vol. 105, pp. 912-915.

Nansteel, M.W. and R. Greif, 1984, "An Investigation of Natural Convection in Enclosures with Two- and Three- Dimensional Partitions", International Journal of Heat and Mass Transfer, vol. 27, pp. 561-571.

Naraghi, M.H.N. and M. Kassemi, 1988. "Radiative Transfer in Rectangular Enclosures: A Discretized Exchange Factor Solution", Proceedings of ASME National Heat Transfer Conference, vol. 1, pp. 259-267, July 24-27.

Nishimura, T., M. Shiraishi and Y. Kawamura, 1987a. "Analysis of Natural Convection Heat Transfer in Enclosures Divided by a Vertical Partition", in Proceedings of the International Symposium on Heat Transfer, Peking, China, pp. 129-137.

Nishimura, T., M. Shiraishi and Y. Kawamura, 1987b. "Natural Convection Heat transfer in Enclosures with an Off-Center Partition", International Journal of Heat and Mass Transfer, vol. 30(8), pp. 1756-1758.

Nishimura, T., M. Shiraishi, F. Nagasawa and Y. Kawamura, 1989. "Natural Convection Heat transfer in Enclosures with Multiple Partitions", International Journal of Heat and Mass Transfer, vol.31(8), pp. 1679-1686.

Nishimura, T., F. Nagasawa and Y. Kawamura, 1990. "Natural Convection Heat transfer in Inclined Enclosures with/without Partitions", in Proceedings of the 9th International Heat Transfer Conference, vol. 2, Jerusalem, Israel, August 19-24.

Nowak, E.S. and H. Novak, 1994. "Vertical Partitions in Slender Rectangular Cavities", International Journal of Heat and Fluid Flow, vol. 15(2), pp. 104-110.

Oñate E. and S.R. Idelsohn, 1992. "A Comparison Between Finite Element and Finite Volume Methods in CFD", Computational Fluid Dynamics, vol. 1, pp. 93-100.

Ostrach S., 1952. "An Analysis of Laminar Free-Convection Flow and Heat Transfer About a Flat Plate Parallel to the direction of the Generating Body Force", NACA TN 2635.

Ostrach, S., 1972. Natural Convection in Enclosures, "Advances in Heat Transfer", vol. 8, pp. 161-227.

Ostrach, S.,1988. "Natural Convection in Enclosures", Journal of Heat Transfer, vol. 110, pp. 1175-1190, November.

Parmalee, G.V., 1947. "Heat Transmission Through Glass", ASHVE, Research Bulletin, vol. 53(1).

Patankar, S.V., 1980. "Numerical Heat Transfer and Fluid Flow", Hemisphere Publishing Corp.

Peck, R.E., W.S. Fagan and P.P. Werlein, 1951. "Heat Transfer Through Gases at Low Pressures", Transactions of ASME, vol. 73, pp. 281-287, April.

Peric, M. R. Kessler and G. Scheuerer, 1988. " Comparison of Finite-Volume Numerical Methods with Staggered and Collocated Grids", Computer & Fluids, vol. 16(4), pp. 389-403.

Peterson, Jr., C.O., 987. "How Is Low-E Performance Criteria Determined?", Glass Digest, pp. 70-76, January 15.

Pignatel, J.F., and J.F. Marcillat, 1986. "Transition to Time-Dependent Free Convection in an Inclined Air Layer", International Journal of Heat and Fluid Flow, vol. 7, pp. 169-178.

Platzer, W.J. and P.O. Braun, 1995. "Transparent Insulation Technology for Buildings — A Review", Proceedings of the Window Innovations '95 Conference, Toronto, pp. 588-597.

Probert, S.D. and Ward J., 1974." Improvements in the Thermal Resistance of Vertical, Air-Filled, Enclosed Cavities", in Proceedings of the 5th international Heat Transfer Conference, Tokyo, Japan, vol. 3.

Raithby, G.D. and H.H. Wong, 1981. "Heat Transfer by Natural Convection Across Vertical Air Layers", Numerical Heat Transfer, vol. 4, pp. 447-457.

Raithby, G.D. and K.G.T. Hollands, 1975. "A General Method of Obtaining Approximate Solutions to Laminar and Turbulent Free Convection Problems", in Advances in Heat transfer, ed. T.F. Irvine and J.P. Hartnett, Academic Press, New York, vol. 11, pp. 1121-1128.

Raithby, G.D. and K.G.T. Hollands, 1985. Natural Convection, "Handbook of Heat Transfer Fundamentals", eds. Rohsenow, W.M., J.P. Hartnett and N. Ganiæ, chapter 6, McGraw-Hill, New York, 1985.

Raithby G.D. and K.E. Torrance, 1974. "Upstream-Weighted Differencing Schemes and their Application to Elliptic Problems Involving Fluid Flow", Computer & Fluids, vol. 2, pp. 191-206.

Raithby, G.D., K.G.T. Hollands and T.E. Unny, 1977. "Analysis of Heat Transfer by Natural Convection Across Vertical Fluid Layers", Journal of Heat Transfer, vol. 99, No. 2, pp. 287-293.

Ramanan, N. and Korpela, S.A., 1989. "Multigrid Solution of Natural Convection in a Vertical Slot", Numerical Heat Transfer, vol. 15(3), part A, pp. 323-339.

Rhie, C.M., 1981. "A Numerical Study of the Flow Past an Isolated Aerofoil with Separation", Ph.D. Thesis, University of Illinois, Champaign, Urbana, chap. 4, pp. 22-35.

Rousseau, M.Z., 1988. "Windows: Overview of Issues", Window Performance and New Technology, Proceedings of Building Science Insight '88, NRC, Ottawa, pp. 1-15.

Roux, B., J-C. Grondin and P. Bontoux, 1979. "Natural Convection in Inclined Rectangular Cavities", Proceedings of the 1st International Conference on Numerical Methods in Thermal Problems, pp. 423-432, July 2-6.

Roux, B., J. Grondin, P. Bontoux and G. de Vahl Davis, 1980. " Reverse Transition from Multicellular to Monocellular Motion in Vertical Fluid Layer", Proceedings of Physics Chemistry Hydrodynamics, vol. 3F, pp. 292-297.

Rowley, F.B. and W.A. Eckley, 1932. ASHVE Transactions 38:33.

Rubin, M.D., 1982. "Calculating Heat Transfer through Windows", International Journal of Energy Research, vol. 6, pp. 341-349.

Sabatiuk, P., 1983. "Review of Gas-Filled Window Technology: Summary Report", ASHRAE Transactions, pp. 643-653.

Sánchez A. and T.F Smith, 1992. "Surface Radiation Exchange for Two-Dimensional Rectangular Enclosures Using the Discrete-Ordinate Method". Journal of Heat Transfer, vol. 114, pp. 465-472.

Sánchez A., T.F Smith and W.F. Krajewski, 1994. "Dimensionality Issues in Modelling with the Discrete-Ordinate Method". Journal of Heat Transfer, vol. 116(1), pp. 257-260.

Sargent, D., 1992. Personal Communication.

Sargent, D., 1994. Personal Communication.

Schlichting, H., 1979. "Boundary-Layer Theory", McGraw-Hill Publishing Company.

Schmidt, F.M., 1976. "The Window Book." Season-All industries Inc., Pennsylvania.Seki, N., S. Fukusako and H. Inaba, 1978a. "Visual Observation of Natural Convective Flow in a Narrow Vertical Slot", Journal of Fluid Mechanics, vol. 84(4), pp. 695-704.

Seki, N., S. Fukusako and H. Inaba, 1978b. "Heat Transfer of Natural Convection in a Rectangular Cavity with Vertical Walls of Different Temperatures", Bulletin of the JSME, vol. 21, pp. 246-253.

Selkowitz, S.E., S.U. Choi, D.L. DiBartolomeo, R.L. Johnson, J.D. Kessel, J.H. Klems, C.M. Lampert, M. Nawab, E. Ne'eman, M.D. Rubin, J. Ryan and G.M. Wilde, 1982. "Window and

Daylighting", Chapter from FY 1982 Annual Report - Energy Efficient Buildings Program, Lawrence Berkeley Laboratory, report W/L-17.

Shaw, H.J., C.K. Chen and J.W. Cleaver, 1987. "Cubic Spline Numerical Solution Two- and Three- Dimensional Natural convection in a Partially Divided Enclosure", Numerical Heat Transfer, vol. 12, pp. 439-455.

Shawn, P. B., J.R. Howell and D.E. Klein, 1994. "Assessment of the Swartz-Wendroff Finite Element Formulation for Combined Mode Heat Transfer". Radiative Heat Transfer: Current Research, HTD-vol. 276, pp. 1-7.

Shewen, E.C., 1986. "A Peltier-Effect Technique for Natural Convection Heat Flux Measurement Applied to the Rectangular Open Cavity", Ph.D. Thesis, Department of Mechanical Engineering, University of Waterloo.

Shyy, W., S. Thakur and J. Wright, 1992. "Second Order Upwind and Central Difference Schemes for Recirculating Flow Computation", AIAA Journal, vol.30(4), pp. 923-932.

Siegel, R. and R..J. Howell, 1981. "Thermal Radiation Heat Transfer", Hemisphere Publishing Corporation.

Siegel, R. and C.M. Spuckler, 1993. "Refractive Index Effects on Radiation in an Absorbing, Emitting, and Scattering Laminated Layer". Journal of Heat Transfer, vol. 115(1), pp. 194-200.

Simko, T.M., R.E. Collins, A.C. Fischer-Cripps and J.D. Garrison, 1995. "An Overview of the Technology of Vacuum Glazing", Proceedings of the Window Innovations '95 Conference, Toronto, pp. 578-587.

Smith, G.B, S. Dligatch and M.W. Ng, 1995. "Optimising Daylighting and Thermal Performance of Windows with Angular Selectivity", Proceedings of the Window Innovations '95 Conference, Toronto, pp. 598-605.

Smith, T. D., C. Beckermann and C.C. Adams, 1993. "A Numerical Simulation Model for Studying the Thermal Performance of Windows", ASHRAE Transactions, vol. 99(2), pp. 585-596.

Sparrow, E.M. and C. Prakash, 1981. "Interaction Between Internal Natural Convection in an Enclosure and an External Natural Convection Boundary-layer Flow", International Journal of Heat and Mass Transfer, vol. 24(5), pp. 895-907.

Standaert, P., 1986. "KOBRU86 Computer program to Calculate Two-Dimensional Steady State Heat Transfer in Objects, Described in a Rectangular Grid, Using the Energy Balance Technique. Alphanumerical Input, Alphanumerical and Graphical Output", Information Brochure, June.

Stubley, G., 1990. "Finite Volume Methods for Fluid Flow and Heat Transfer Calculations", Notes on ME780, University of Waterloo.

Sullivan, H.F., J.L. Wright, and R.A. Fraser, 1996. "Overview of a Project to Determine the Surface Temperatures of Insulated Glazing Units: Thermographic Measurement and Two-Dimensional Simulation.", ASHRAE Transactions, vol. 102(2).

Tan, Z. and R. Howell, 1991. " Combined Radiation and Natural Convection in a Two-Dimensional Participating Square Medium", International Journal of Heat and Mass Transfer, vol. 34(3), pp. 785-793

Thangam, S. and C. F. Chen, 1986. " Stability Analysis on the Convection of a Variable Viscosity Fluid in an Infinite Vertical Slot", vol. 29, pp. 1367-1372.

The, J.L., 1993. "A Time Implicit Method for the Solution of Fluid Flow Problems with Moving Boundaries", Ph.D. Thesis, Department of Mechanical Engineering, University of Waterloo.

Thomas, F. and H. Mühlebach., 1987. "Coefficient de Transmission Thermique des Fenêtres", Taken from an article in Ingenieurs et Architetes Suisse, pp. 7-9.

Tong, T. W. and F.M. Gerner, 1986. "Natural Convection in Partitioned Air-Filled Enclosures", International Communications in Heat and Mass Transfer, vol. 13, 99-108.

Tsang, C. and S. Acharya, 1984. "Natural Convection in an Inclined Enclosure with an Off-Center, Complete Partition"', in Proceedings of the Winter Annual Meeting of the American Society of Mechanical Engineers, New Orleans, Louisiana, ASME HTD, vol. 39, pp. 55-62.

Unny, T.E., 1972. "Thermal Instability in Differentially Heated Inclined Fluid Layers", Journal of Applied Mechanics, vol. 39, pp. 41-46.

Varapaev, V.N., 1987. "Convection and Heat Transfer in a Vertical Layer with Allowance for Radiation from Non-Isothermal Walls". Fluid Dynamics, vol. 22(1), pp. 19-24.

Vest, M.C. and V.S. Arpaci, 1969. "Stability of Natural Convection in a Vertical Slot", Journal of Fluid Mechanics, vol. 36(1), pp. 1-15.

Viskanta, R. and M.P. Menguc, 1987. "Radiation Heat Transfer in Combustion Systems", Progress in Energy and Combustion Science, vol. 13(2), pp. 97-160.

Wakitani, S., 1994. "Experiments on Convective Instability of Large Prandtl Number Fluids in a Vertical Slot", Journal of Heat Transfer, vol. 116(1), pp. 120-126.

Webb, B.W. and R. Viskanta, 1987a. "Radiation-Induced Buoyancy-Driven Flow in Rectangular Enclosures: Experiment and Analysis", Journal of Heat Transfer, vol. 109, pp. 427-433.

Webb, B.W. and R. Viskanta, 1987b. "Analysis of Radiation-Induced Natural Convection in Rectangular Enclosures", Journal of Thermophysics and Heat Transfer, vol. 1(2), pp. 146-153.

Wilkes, G.B. and C.M.F. Peterson, 1938. "Radiation and Convection from Surfaces in Various Positions", ASHRAE Transactions, vol. 44(1), pp. 513-522.

Winters, K.H., 1982. "The effect of Conducting Divisions on the Natural Convection of Air in a Rectangular Cavity with Heated Side Walls", ASME Paper, 82-HT-69.

Winters, K.H., 1988. "Laminar Natural Convection in a Partially Divided Rectangular Cavity at High Rayleigh Number", International Journal of Numerical Methods in Fluids, vol. 8, pp. 247-281.

Wright, J.L., 1989. "The Measurement and Computer Simulation of Heat Transfer in Glazing Systems," Ph.D. Thesis, Department of Mechanical Engineering, University of Waterloo.

Wright, J.L., 1995. "A Simplified Method for the Numerical Condensation Resistance Analysis of Windows", Proceedings of the Window Innovations '95 Conference, Toronto, pp. 439-444.

Wright, J.L. and H.F. Sullivan, 1989a. "Natural Convection in Sealed Glazing Units: A Review", ASHRAE Transactions, vol. 95(1).

Wright, J.L. and H.F. Sullivan, 1989b. "Thermal Resistance Measurement of Glazing System Edge-Seals and Seal Materials Using a Guarded Heater Plate Apparatus", ASHRAE Transactions, vol. 95(2).

Wright, J.L., P.F. de Abreu, R.A Fraser and H.F. Sullivan, 1994. "Heat Transfer in Glazing System Edge-Seals: Calculations Regarding Various Design Options", ASHRAE Transactions, vol. 100(1).

Wright, J.L., and H.F. Sullivan, 1994. "A 2-D Numerical Model for Natural Convection in a Vertical, Rectangular Window Cavity", ASHRAE Transactions, vol. 100(2).

Wright, J.L., and H.F. Sullivan, 1995. "A Two-Dimensional Numerical Model for Glazing System Thermal Analysis", ASHRAE Transactions, vol. 101(1), pp. 819-831.

Yang, K.T., 1986. "Numerical Modelling of Natural Convection-Radiation Interactions in Enclosures", Proceedings of the 8th International Heat Transfer Conference, San Francisco, California, USA, vol. 1, pp. 131-140, August, 17-22.

Yang, K.T., 1987. Natural Convection in Enclosures, "Handbook of Single-Phase Convective Heat Transfer", eds. Kakaç, S., R.K. Shah and W. Aung, chap. 13, Wiley-Interscience, pp. 13.1-13.51.

Yang, M., W.Q. Tao and Z.Q. Chen, 1990. "Solution Comparison of Three Coupled Fluid Flow and Heat Transfer Problems with Staggered and Collocated Grids", Advanced Computational Methods in Heat Flow, eds. Wrobel, L.C., C.A. Brebbia and A.J. Newak, vol. 2, pp. 207-218.

Yazdanian M and J.H. Klems, 1994. "Measurement of the Exterior Convective Film Coefficient for Windows in Low-Rise Buildings", ASHRAE Transactions, vol. 100(1), pp. 1087-1096.

Yeoh, G.H., G. de Vahl Davis and E. Leonardi, 1989. "Heat Transfer Across a Double-Glazed Window with Convective Boundary Conditions", in proceedings of Numerical Methods in Thermal Problems VI(1), pp. 355-365.

Yin, S.H., T.Y. Wung and K. Chen, 1978. "Natural Convection in an Air Layer Enclosed within Rectangular Cavities", International Journal of Heat and Mass Transfer, vol. 21, pp. 307-315.

Yücel, A., 1989. "Analysis of Coupled Conduction and Radiation in Partitioned Enclosures", Proceedings of the Winter Annual Meeting of the ASME, HTD-vol. 104, San Francisco, California, USA, pp. 91-97, December 10-15.

Yücel, A., S. Acharya and M.L. Williams, 1989. "Natural Convection and Radiation in a Square Enclosure", Numerical Heat Transfer, vol. 15, part A, pp. 261-278.

Zenouzi M. and Y. Yener, 1992. "Simultaneous Radiation and Natural Convection in Vertical Slots", Developments Irradiation Heat Transfer, ASME, HTD-vol. 203, pp. 179-185.

Zhang, Z., A. Bejan and J.L. Lage, 1991. "Natural Convection in a Vertical Enclosure with Internal Permeable Screen". Journal of Heat Transfer, vol. 113(2), pp. 377-383.

Zhao, Y., D. Curcija, and W.P. Goss, 1996. "Condensation Resistance Validation Project - Detailed Computer Simulations Using Finite-Element Methods", ASHRAE Transactions, vol. 102(2).

Zhong, Z.H., J.R. Lloyd., and K.T. Yang, K.T., 1983. Variable-Property Natural Convection in Tilted Square Cavities, " Numerical Methods in Thermal Problems", eds. Lewis, R.W., Johnson, J.A., and Smith, W.R., Pineridge Press, Swansea, UK, pp. 968-979.

Zhong, Z.Y., J.R. Lloyd., and K.T. Yang, K.T., 1987. "A Total Slice Band Absortance Model for Nongray Gas-Natural Convection Interaction in a Two-Dimensional Square Enclosure" Proceedings of the International Symposium of Heat Transfer, Peking, China.

Zimmerman, E. And S. Acharya, 1987. "Free Convection Heat Transfer in a Partially Divided Enclosures with Conducting End Walls", International Journal of Heat and Mass Transfer, vol. 30(2), pp. 319-331.

APPENDIX A

The Discretization of the Non-Orthogonal Terms

In this appendix the collocated approach, due to Rhie (1981), to obtain the pressure-velocity coupling within a single control volume (i.e., scalar variables and velocities share the same control volume) is used to discretize the governing equations for a non-orthogonal grid in an arbitrary bounded geometry domain. To avoid the calculation of extremely grid sensitive curvature terms (Peric, 1984) cartesian velocity components are used as dependent variables on a non-orthogonal grid. Velocity components, for the node and faces of a non-orthogonal control volume, can be seen in Figure A1, where node P in the control volume is surrounded by four neighbouring nodes (East=E, West=W, North=N and South=S). The discrete equations for each variable relates to values at P to values at these neighbouring nodes. For the 2-D problems considered in this thesis, the grid is defined by the location of the North-East corner of every control volume. The following subsection describes how all parameters of the grid can be found from this information.

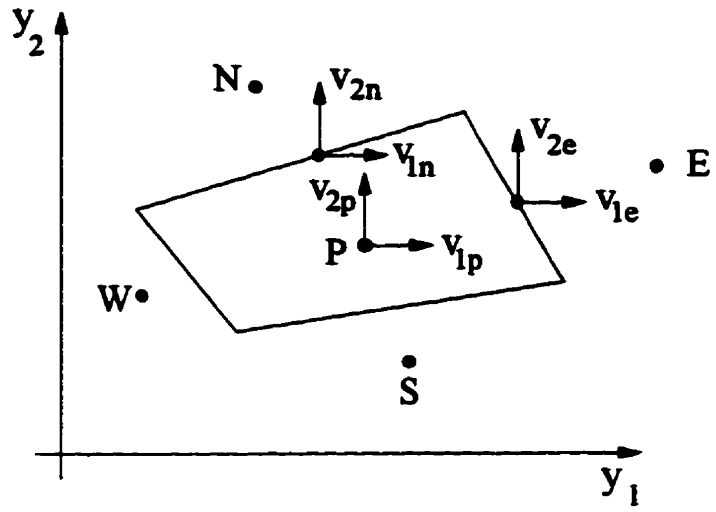

Figure A1: Non-Orthogonal Grid with Cartesian Velocity Components.

Grid Layout

This section describes how the location of the node within the control volume, the location of the integration points, and all the direction vectors on the faces of the control volumes are found. Figure A2 contains the notation for these parameters.

Each face is defined by two corner points[1] and contains an integration point. Only values for variables in the north and east faces are stored. The other two faces have their values stored in surrounding control volumes[2]. Integration points lie at the midpoint of their

[1] An integration point is the location where values crossing the face of a control volume are calculated. Corner points are the locations where two faces of the control volume intersect.

[2] In this method, the south face values are stored in the north face of the south control volume and the west face values are stored on the east face of the west control volume.

respective faces (i.e., midpoint between the corner points that define the face). The control volume node, denoted by *P* in Figure A2, lies at the center of the control volume. The location of node *P* is defined by the intersection point of the main diagonals in the control volume. Four subquadrant distances, shown in Figure A3, are required. Nodal point distances are necessary to complete the geometric description of the grid, since they are used in the calculation of gradients. Figure A4 presents the definition for the nodal point distances.

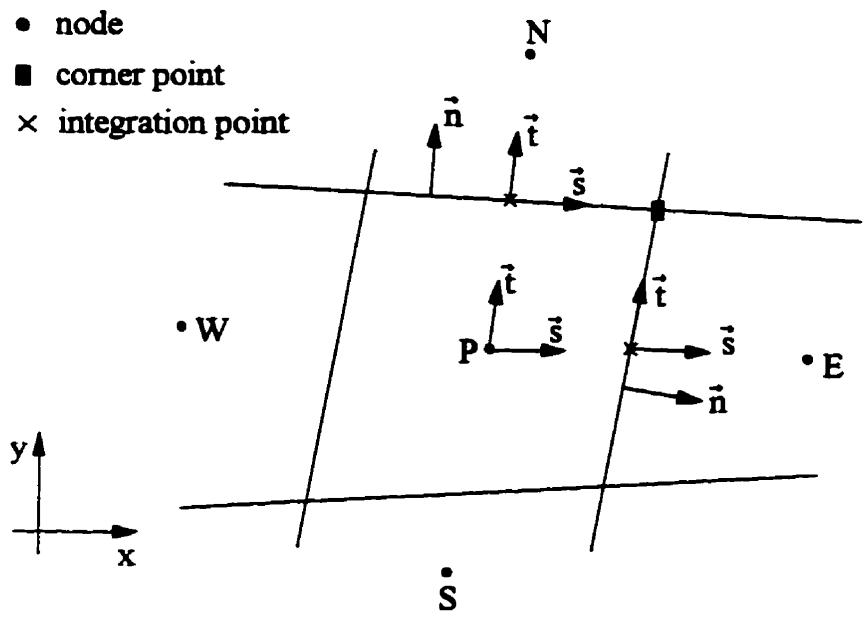

Figure A2: Notation for Integration Points and Direction Vectors.

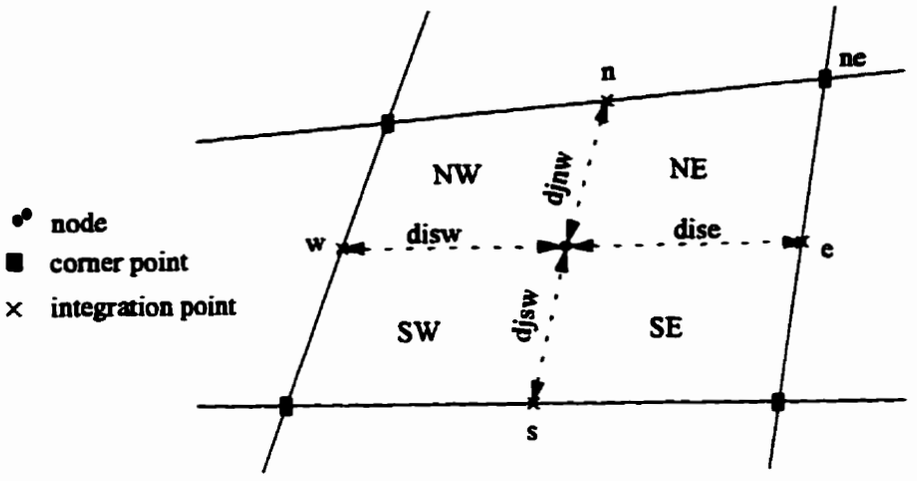

Figure A3: Sub-Quadrant Distances in Non-Orthogonal Control Volume.

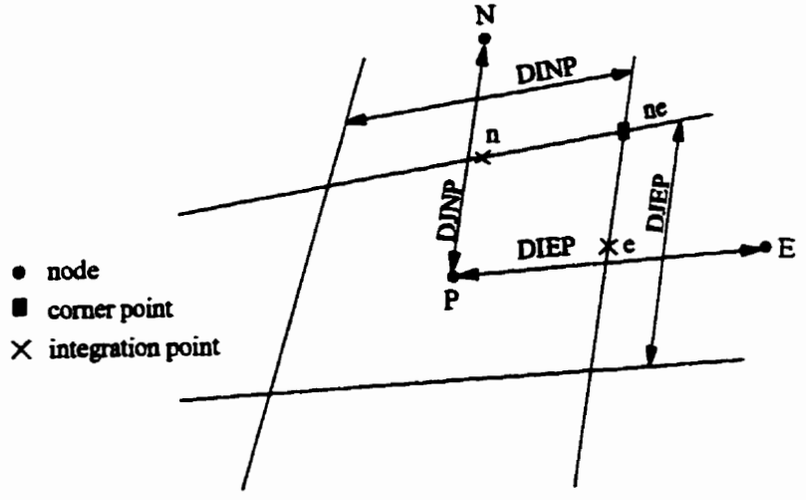

Figure A4: Nodal Point Distances in the Non-Orthogonal Grid.

Boundary nodes are necessary for the application of boundary conditions and are placed on the same location as the integration point of the control volume face exposed to a boundary.

Algebraic Equation for the General Scalar Variable ϕ

To simplify the explanation of the discretization procedures employed in this work, the discretization of the general scalar variable ϕ equation is presented first. This is useful since the same procedure is applied to conservation of mass, momentum and energy. This equation for ϕ, in differential form, is expressed as

$$\frac{\partial}{\partial t}(\rho\phi) + \frac{\partial}{\partial x_j}(\rho u_j\phi) = \frac{\partial}{\partial x_j}\left(\Gamma\frac{\partial\phi}{\partial x_j}\right) + S^{\phi} \qquad \text{A.1}$$

Each term will now be treated individually. The first term on the L.H.S. of Equation (A1), the rate of change, is discretized as follows

$$\int_{\forall}\rho\frac{\partial\phi}{\partial t}d\forall = \frac{(\rho\forall\phi)^n - (\rho\forall\phi)^o}{\Delta t} \qquad \text{A.2}$$

where superscript n represents new value (active or value being calculated) and superscript o indicates old values (from previous time step). The second term on the L.H.S. of Equation

(A2), which represents the convection of ϕ, is integrated over the four control volume faces to produce

$$\int_s \rho u_j \phi n_j dS = \rho A_e u_{ex} n_{ex} \phi_e + \rho A_e u_{ey} n_{ey} \phi_e - \rho A_w u_{wx} n_{wx} \phi_w - \rho A_w u_{wy} n_{wy} \phi_w + \rho A_n u_{nx} n_{nx} \phi_n + \rho A_n u_{ny} n_{ny} \phi_n - \rho A_s u_{sx} n_{sx} \phi_s - \rho A_s u_{sy} n_{sy} \phi_s \quad \text{A.3}$$

where n_j is the normal vector of area element dS, n_{ex} and n_{ey} are Cartesian components of the normal vector at the east face, $(\rho A_{facex} u_{facex} n_{facex} + \rho A_{facey} u_{facey} n_{facey})$ is the mass flux across a face, and ϕ_{face} is interpolated from nodal values. The first term on the R.H.S. of Equation (A2) is discretized as follows

$$\int_s \Gamma \frac{\partial \phi}{\partial x_j} n_j dS = (\Gamma A \frac{\partial \phi}{\partial x_j} n_j)_e - (\Gamma A \frac{\partial \phi}{\partial x_j} n_j)_w + (\Gamma A \frac{\partial \phi}{\partial x_j} n_j)_n - (\Gamma A \frac{\partial \phi}{\partial x_j} n)_s \quad \text{A.4}$$

Since the control volume is non-orthogonal and the velocity components are Cartesian, the terms in the last equation require more work. Discretization of the terms in Equation (A4) is carried out in the next subsection.

Treatment of Diffusive Terms in Non-Orthogonal Grids

From calculus, the normal gradient at a face contained in Equation (A4), can be expressed as

$$\frac{\partial \phi}{\partial x_j} n_j = \Delta\phi \bullet \vec{n} = \frac{\partial \phi}{\partial n} = \frac{\partial \phi}{\partial x} n_x + \frac{\partial \phi}{\partial y} n_y \qquad \text{A.5}$$

In Equation (A5) the unknowns are $\partial\phi / \partial x$ and $\partial\phi / \partial y$.

The normal gradient at the east face can be expressed as follows,

$$\frac{\partial \phi}{\partial n}\Big/_e = \Delta\phi_e \bullet \vec{n}_e = \frac{\partial \phi}{\partial x}\Big/_e \bullet n_{ex} + \frac{\partial \phi}{\partial y}\Big/_e \bullet n_{ey} \qquad \text{A.6}$$

Since one wants to have the equations in terms of cartesian velocity components, Equation (A6) should be made explicit in the gradients of ϕ in both cartesian directions.

The first step is to express the gradient of ϕ along $\vec{s}$ and $\vec{t}$. These two gradients are easily expressed in terms of surrounding nodes and corner locations, and can be expressed as,

$$\begin{aligned} \left.\frac{\partial \phi}{\partial s}\right|_e &= \left.\frac{\partial \phi}{\partial x}\right|_e \bullet s_{xe} + \left.\frac{\partial \phi}{\partial y}\right|_e \bullet s_{ye} \\ \left.\frac{\partial \phi}{\partial t}\right|_e &= \left.\frac{\partial \phi}{\partial x}\right|_e \bullet t_{xe} + \left.\frac{\partial \phi}{\partial y}\right|_e \bullet t_{ye} \end{aligned} \qquad \text{A.7}$$

where,

$$\begin{aligned} \left.\frac{\partial \phi}{\partial s}\right|_e &= \frac{\phi_E - \phi_P}{DIEP} \\ \left.\frac{\partial \phi}{\partial t}\right|_e &= \frac{\phi_{ne} - \phi_{se}}{DJEP} \end{aligned} \qquad \text{A.8}$$

and ϕ_{ne} is calculated by interpolation from the surrounding nodes. DIEP and DJEP are nodal point distances presented in Figure (A4). One can now make gradients, of the cartesian components, explicit. These equations are

$$\frac{\partial \phi}{\partial x}\Big|_e = \frac{1}{s_{xe}}\left[\frac{\partial \phi}{\partial s} - \frac{\partial \phi}{\partial y} s_{ye}\right]_e \qquad \text{A.9}$$

and

$$\frac{\partial \phi}{\partial y}\Big|_e = \frac{1}{t_{ye}}\left[\frac{\partial \phi}{\partial t} - \frac{\partial \phi}{\partial x} t_{xe}\right]_e \qquad \text{A.10}$$

Substituting Equation (A9) into equation (A10), to obtain an expression for $\partial\phi / \partial x|_e$ yields

$$\frac{\partial \phi}{\partial x}\Big|_e = \left(\frac{\partial \phi}{\partial s} t_{ye} - \frac{\partial \phi}{\partial t} s_{ye}\right)\frac{1}{|\vec{s} x \vec{t}|_e} \qquad \text{A.11}$$

where $|\vec{s} x \vec{t}|_e = (s_{xe} \bullet t_{ye} - s_{ye} \bullet t_{xe})$. In the same way,

$$\frac{\partial \phi}{\partial y}\Big|_e = \left(\frac{\partial \phi}{\partial t} s_{xe} - \frac{\partial \phi}{\partial s} t_{xe}\right)\frac{1}{|\vec{s} x \vec{t}|_e} \qquad \text{A.12}$$

Therefore, the cartesian gradient components, of Equation (A6), are described for the east face as

$$\frac{\partial \phi}{\partial x}\Big|_e = \left(\frac{\partial \phi}{\partial s} t_{ye} - \frac{\partial \phi}{\partial t} s_{ye}\right)_e \frac{1}{|\vec{s} x \vec{t}|_e} \qquad \text{A.13}$$

$$\frac{\partial \phi}{\partial y}\Big|_e = \left(\frac{\partial \phi}{\partial t} s_{xe} - \frac{\partial \phi}{\partial s} t_{xe}\right)_e \frac{1}{|\vec{s} x \vec{t}|_e}$$

where $|\vec{s} x \vec{t}| = (s_x t_y - s_y t_x)$ and the local gradients $\partial\phi/\partial s$ and $\partial\phi/\partial t$ are expressed by

$$\frac{\partial \phi}{\partial s}\Big|_e = \frac{\phi_E - \phi_P}{DIEP} \qquad \text{A.14}$$

$$\frac{\partial \phi}{\partial t}\Big|_e = \frac{\phi_{ne} - \phi_{se}}{DJEP}$$

where DIEP and DJEP are nodal point distances presented in Figure (A4), ϕ_E and ϕ_P are nodal values of ϕ, and ϕ_{ne} and ϕ_{se} are corner point values.